Université d'Ottawa · University of Ottawa

The large-scale structure of uniformly sheared turbulence and its distortion by a solid wall at rest or in motion

by

Benoit C. Kislich-Lemyre

B.A.Sc.(University of Ottawa) 1993

Submitted in partial satisfaction of the
requirements for the degree of
Doctor of Philosophy

in

Mechanical Engineering

in the

Department of Mechanical Engineering
of the
University of Ottawa
Ottawa-Carleton Institute for Mechanical and Aerospace Engineering

July 2002

Abstract

The large-scale structure of sheared turbulence has been documented with the use of flow visualization and laser-Doppler velocimetry. The study includes nominally unbounded uniformly sheared flow (USF), turbulent boundary layers, used as reference, and the effects of stationary and moving walls on USF.

USF with statistical properties comparable to those in earlier wind-tunnel studies was succesfully generated in a water tunnel. Horseshoe-type structures, generally considered as one of many typical eddies in turbulent boundary layers and also observed in jets, wakes and mixing layers, have been observed in USF, for the first time experimentally. This indicates that the presence of a wall is not required for such structures to develop. These structures evolved by being stretched and rotated by the velocity gradient. The dominant large-scale structures in USF were observed to be similar to those found in the outer layer of a turbulent boundary layer, albeit much less organized. No evidence of streaks was found in the core USF, while streaks were clearly visible near the wall in the reference turbulent boundary layer study. The energetic bursting of horseshoe structures that has been observed in boundary layers was not observed in USF, however the heads of the horseshoe structures were often noticed to travel in the transverse direction.

The study of USF in the vicinity of a wall moving at the local mean speed has been the first of its kind, as previous studies with a moving wall were conducted in uniform flow. The present research has demonstrated that shear associated with friction with the wall (no-slip condition) is the major factor in the production of turbulence, and that the physical barrier (no-penetration condition) of the wall acts as a suppressant to oncoming

turbulence structures and provides organization to their development. The moving wall studies were extended to cases with the wall moving faster than the local mean velocity and the wall moving in a direction opposite to that of the local mean velocity. These studies provided interesting information on the interaction of turbulence with the mean shear and the effects of the wall.

Acknowledgment

The author would like to acknowledge the support and supervision of Dr. Stavros Tavoularis in all aspects of the research and writing of this thesis. The construction of the water tunnel facility could not have been completed without the support of the University of Ottawa Mechanical Engineering Machine Shop and its technicians, as well as Alexander Metal Products for the forming of the large, complex metal components. I must also mention the assistance and partnering of work with Sebastien Marineau-Mes, with whom the high speed USF was completed for both of our works. Most of all, I would like to acknowledge the support and encouragement from my wife and family.

Contents

List of Tables

List of Figures

Nomenclature

b_{ij} turbulence anisotropies

C_f skin friction coefficient ($C_f = \frac{2\tau_w}{\rho U_e^2}$)

h half-height of channel (0.21 m)

k kinetic energy growth exponent

k_s flow generator constant

L integral lengthscale

P static pressure

P_r production rate of turbulent kinetic energy

q_r turbulent kinetic energy reference value

Re_x Reynolds number based on streamwise distance ($Re_x = \frac{xU_e}{\nu}$)

Re_θ Reynolds number based on momentum thickness ($Re_\theta = \frac{\theta U_e}{\nu}$)

R_λ Reynolds number based on Taylor microscale ($Re_\lambda = \frac{\lambda u_1'}{\nu}$)

t time

U_c centerline mean velocity

U_e free stream mean velocity

U_i velocity

$\overline{U}_i$ mean velocity

u_i velocity fluctuation

u_1' root-mean squared velocity fluctuation

U_o mean velocity of USF extrapolated to the wall

U_r USF-wall flow reference velocity

U_w moving wall velocity

u^* friction velocity ($u^* = \sqrt{\tau_w/\rho}$)

u^+ dimensionless velocity

w half-width of the channel (0.27 m)

x_i position vector (x_1 : streamwise direction; x_2 : transverse direction; x_3 : spanwise direction)

y distance from the wall ($y = -x_2 + h$)

y^+ dimensionless distance from the wall ($y^+ = \frac{yu^*}{\nu}$)

δ Boundary layer thickness (based on $U_1 = 0.99U_e$)

δ_r boundary layer reference thickness in USF-wall flow

ϵ turbulent kinetic energy dissipation rate

η Kolmogorov microscale

θ momentum thickness ($\theta = \int_0^\infty \frac{U_1}{U_e}\left(1 - \frac{U_1}{U_e}\right) dy$)

λ Taylor microscale

μ viscosity ($\mu = 1.0 \times 10^{-3}$ kg/m/s for water)

ν kinematic viscosity ($\nu = 1.0 \times 10^{-6}$ m^2/s for water)

ρ density ($\rho = 1.0 \times 10^3$ kg/m^3 for water)

τ total strain ($\tau = \frac{x_1}{U_c}\frac{d\overline{U_1}}{dx_2}$)

τ_w wall shear stress

Chapter 1

Introduction

1.1 Motivation for the Present Study and the Methodology Used

Observing patterns in a fluid in motion can generate some very significant insight about that flow. Flow patterns are frequently observed in everyday life: the swirling of rain behind a fast moving vehicle; the gentle rise of smoke from a cigarette that eventually transforms to a chaotic pattern; the slow pouring of milk in a cup of tea that we stir into a swirling motion. In the study of fluid mechanics, flow visualization has been an essential tool. One of the more popular visual scientific experiments in fluid mechanics was conducted by Reynolds (1883), who observed the shape of a streak of dye injected in water flow through a glass tube. Reynolds distinguished between two distinct types of motion: laminar flow, identified by a thin, steady streak of dye, and turbulent flow (which Reynolds called "sinuous"), identified by a wavering, dispersed and highly mixed appearance of the

dye. Flow visualization of turbulent flows has since become a highly sophisticated scientific field, encompassing a great variety of techniques. It will be used as a main experimental tool in the present study.

Turbulence arises in most systems that contain a fluid. A laminar flow will generally become turbulent under certain conditions. Whether turbulence is useful or detrimental in a certain technological system depends on the specific application. Turbulence control, including generation, enhancement or suppression of turbulence, has been the focus of much research. The prediction and control of turbulence are essential in applications involving mixing of fluids, chemical reactions, heat and mass transfer, and aerodynamic forces on immersed bodies in relative motion with a fluid. Many researchers have studied turbulence using mathematical analysis, the development of empirical relations, numerical simulations and a variety of experimental techniques, including flow visualization. Despite intense efforts, the full understanding and prediction of turbulent flows has not yet been achieved. Although an appropriate statistical formulation of the governing equations has been known for a long time, a solution cannot be devised, because the number of dependent variables exceeds the number of available equations ("closure problem"). Turbulent flows contain distinct, large-scale, patterns of motion, known as "coherent structures", whose interactions among themselves and with the small-scale, non-coherent motions determine the macroscopic structure and evolution of the flow. Much research has been oriented toward the understanding of the origins and interactions of coherent structures and their contribution to the turbulent flow field as a whole.

Although the structure and properties of turbulent flows vary widely depending on

the geometrical and dynamic conditions, all turbulent flows contain some common features, which are best understood in relatively simple and well-controlled environments. It seems a plausible hypothesis that the insight accumulated from the study of relatively simple types of flow, which are reproducible in a scientific laboratory, may be used as a starting point for the description of more complex, practical cases. In general, turbulent flows may be classified as either free or bounded, depending on whether their properties are influenced by solid boundaries. A fundamental type of bounded flow is the turbulent boundary layer, which has been studied extensively and still remains a subject of research. The simplest case of free turbulence is that of homogeneous and isotropic turbulence, in which turbulence statistics are independent of location and orientation of the coordinate axes. Although almost never observed in practical applications, isotropic turbulence has been studied for the insight that it provides into the general processes of turbulent mixing and kinetic energy dissipation. Isotropic turbulence differs from most other turbulent flows in an essential element, that it contains no mechanism of turbulence energy production. In contrast, shear flows are capable of generating turbulence by shearing actions, namely by non-uniformities in their mean velocity distributions. A configuration that is more representative of practical flows is the uniformly sheared flow (USF), which is approximately homogeneous, yet possesses a mean velocity gradient, and thus turbulence production. Results from studying USF have been successfully applied to the study of a variety of turbulent shear flows.

The structure of USF generated in wind-tunnels has been studied by several authors, however, it has not yet been documented visually. Although it has been stated that USF contain coherent structures, their shapes and possible relationships to coherent struc-

tures in boundary layers and other shear flows have not been adequately studied. A case of interest that has not yet been addressed is the interaction of USF with a still or moving wall. In particular, a solid wall is known to have two distinct effects on the flow. First, it generates turbulence due to the imposed shearing, as necessitated by the application of the dynamic constraint of the no-slip condition. And second, it imposes a kinematic constraint on the structure of oncoming turbulence, as a result of the no-penetration condition. In boundary layers, both effects are present simultaneously and cannot be separated. The combination of free USF and a wall creates the opportunity to examine a number of interesting problems. One such problem is to examine how turbulent eddies which are generated by shearing actions away from the wall would behave if brought to the vicinity of a stationary or moving wall. Another interesting problem is to match the wall speed and the local speed of USF and consider the turbulent structure near a wall that creates no shear.

Statistical measurements of a flow at one or more fixed locations have traditionally been obtained with hot-wire/hot-film anemometers (HWA) and laser-Doppler velocimeters (LDV). Such methods have an excellent temporal resolution but cannot easily describe the properties of large structures. Particle Image Velocimetry (PIV) has been established as the method of choice to obtain simultaneous velocities over a plane section of a flow field, but its temporal resolution has not been sufficient to capture the time development of a structure in motion. A powerful method for flow visualization in liquids is laser induced fluorescence (LIF) in combination with laser-sheet illumination. This method allows one to visualize a cross-section of a flow and observe flow patterns both still and in motion. After consideration of the available methods, it was realized that the use of LIF/laser sheet

illumination combined with digital videography would be the most appropriate, as well as relatively simple, method for documenting the formation and development of flow patterns in low-speed turbulent flows.

1.2 Objectives of this Research

The objective of this research is to obtain a better understanding of the structure of the energy containing motions in uniformly sheared turbulence, and, by implication, in other turbulent shear flows. The first task will be to document the USF structure away from boundaries and compare it to those of inhomogeneous flows, primarily turbulent boundary layers. This comparison will provide some insight into possible differences between the mechanisms of turbulence production by shear present in an unbounded flow and shear created by a solid wall. The second task will be to distinguish between the kinematic and dynamic effects of the wall, by performing studies of USF with a wall moving at different speeds in relation to the flow. This will include different combinations of shearing actions with the wall effect enhancing or counteracting the free-shear effect.

1.3 Outline of the Thesis

Following the general introduction to the thesis, presented as Chapter 1, Chapter 2 provides some background material of the topics covered, while Chapter 3 contains a survey of the relevant results available in the literature. A brief description of the experimental facility, instrumentation and procedures used in this study will be presented in Chapter 4, while some details of the construction of the facility and its features will be relegated

to the Appendix. LDV measurements will be presented in Chapter 5, followed by flow visualization results in Chapter 6. An interpretation of all the results and their relevance to this thesis will be discussed in Chapter 7. Finally, Chapter 8 will summarize the main conclusions of this work and will outline some recommendations for future extensions.

Chapter 2

Background

2.1 Turbulence and Methods of Study

Turbulence represents a random state of fluid motion and has properties which fluctuate in space and time; it is highly diffusive of momentum, mass and heat; it is rotational and three dimensional; and it is strongly dissipative, with the kinetic energy of fluctuations continuously being dissipated to internal energy, namely energy of random molecular motions. Due to their importance in technological applications and their intrinsic interest as a scientific problem, turbulent flows have been studied intensively by all available means, which include a great variety of theoretical, numerical and experimental methods.

The mathematical representation of turbulence has been developed by several different methods. A common approach is to average statistically the equations of motion (Reynolds-averaged Navier-Stokes equations - RANS). However, exact mathematical solutions of the averaged equations cannot be obtained because their number is less than the number of unknowns, which is referred to as the closure problem of turbulence. The

approximate solution of such equations has been achieved with the use of empirical relations, commonly referred to as turbulence models. Turbulence models have been partially successful in predicting the statistical properties of specific types of turbulent flows within limited ranges of conditions. In most cases, however, turbulence models contain only a crude, if at all, representation of the complex physical processes involved in turbulence and cannot be applied to turbulence as a whole. Following the advent of more and more powerful computers, an alternative approach emerged, called direct numerical simulation (DNS), which bypasses the closure problem by ensemble averaging the repeated solutions of non-averaged equations, subjected to random initial conditions. DNS have been performed on a variety of flows and are currently being extended to include additional complexities, such as chemical reactions. There is a substantial volume of DNS-generated information on the structure of turbulence, particularly on isotropic turbulence and USF, however, this information is limited to relatively low turbulence Reynolds numbers, of ranges typical to the lower end of laboratory experiments. A third approach, also numerical, is large eddy simulation (LES). LES attempts to resolve the relatively large-scale, energetic motions in a flow, while modelling the effects of the smaller eddies which are assumed to have universal properties. LES have produced many useful results, but they are, by definition, lacking the ability to describe precisely the fine structure and the important effects that it has on turbulent mixing.

Although the computational work has significantly contributed to the understanding of turbulence processes, experimental approaches remain an essential tool for the study of this complex subject. Moreover, experimental results are also necessary for validating

theories and simulations. Much of the experimental database on turbulence consists of time-averaged measurements, obtained by methods such as HWA and LDV. It is obvious that such results cannot identify the developing structure of a flow and particularly the properties of recurring, large-scale flow patterns known as coherent structures. Coherent structures have usually been detected and documented with the use of phase-averaging and conditional sampling techniques. Such techniques employ specific criteria, the choice of which remains an important topic of research. A great deal of physical insight into turbulence has been accumulated through qualitative visual studies. For example, the visualization of flow patterns in the turbulent boundary layer has led to many insightful results for the mechanism of turbulence production and the effects of a solid wall on fluid motion.

2.2 Statistical Description of Turbulence

The following description will be based on the conventional Reynolds decomposition approach, which decomposes all fluctuating properties, for example the velocity vector $U_i, i = 1,2,3$, into a mean value, e.g. $\overline{U}_i$, and a zero-mean fluctuation, e.g. u_i. The root-mean-squared value of the fluctuations are denoted with a prime (e.g. u_i'). Cartesian tensor convention will be used, by which a repeated subscript implies summation. Reynolds-averaged equations have been established for the mean flow field and for the statistical moments of the fluctuations. Most useful are the mean continuity, mean momentum and turbulent kinetic energy equations. In these equations, x_i represents the position vector, t represents time, P is the static pressure, ρ is the fluid density and ν is the fluid kinematic viscosity. In the following, it will be assumed that the fluid is incompressible and Newtonian

with a constant kinematic viscosity. The equations of interest will first be presented for the general case of a turbulent flow, and then they will be simplified to the case of statistically stationary USF with a linear mean velocity $\overline{U}_1(x_2)$ pointing towards the positive x_1-axis, and a constant mean gradient $\frac{\partial \overline{U}_1}{\partial x_2}$. It will be assumed that the statistical moments of this flow are uniform on the (x_2, x_3) plane, but allowed to vary along the x_1-axis. For USF, and other flows with a dominant mean velocity gradient that is normal to the mean velocity direction, the axes x_1, x_2 and $x_3$will be referred to as the streamwise, transverse and spanwise directions, respectively.

Mean Continuity Equation:

$$\frac{\partial \overline{U}_i}{\partial x_i} = 0 \tag{2.1}$$

The continuity equation expresses the law of conservation of mass. In USF this equation degenerates to a trivial equality.

Mean Momentum Equation:

$$\frac{\partial \overline{U}_i}{\partial t} + \overline{U}_j \frac{\partial \overline{U}_i}{\partial x_j} = -\frac{1}{\rho}\frac{\partial \overline{P}}{\partial x_i} + \nu \frac{\partial^2 \overline{U}_i}{\partial x_j \partial x_j} - \frac{\partial \overline{u_i u_j}}{\partial x_j} \tag{2.2}$$

The momentum equation expresses Newton's second law of motion. In the simplified form presented here for the mean momentum, gravitational forces have been neglected. In USF, the three components of this equation become

$$-\frac{1}{\rho}\frac{\partial \overline{P}}{\partial x_1} - \frac{\partial \overline{u_1^2}}{\partial x_1} = 0 \tag{2.3}$$

$$-\frac{1}{\rho}\frac{\partial \overline{P}}{\partial x_2} - \frac{\partial \overline{u_1 u_2}}{\partial x_1} = 0 \tag{2.4}$$

$$-\frac{1}{\rho}\frac{\partial \overline{P}}{\partial x_3} = 0 \tag{2.5}$$

These equations are not very useful and, in fact, if they were taken to apply exactly, they would lead to some rather unrealistic conclusions concerning the mean pressure and Reynolds stress variations (Harris, Graham and Corrsin, 1977).

Turbulent Kinetic Energy Equation:

$$\frac{\partial {}^1/_2\overline{u_i u_i}}{\partial t} + \overline{U}_j\frac{\partial {}^1/_2\overline{u_i u_i}}{\partial x_j} = -\overline{u_i u_j}\frac{\partial \overline{U}_i}{\partial x_j} - \frac{\partial}{\partial x_j}\left[\overline{u_j\left(\frac{p}{\rho}+\frac{1}{2}u_i u_i\right)}\right] + \nu\overline{u_i\frac{\partial^2 u_i}{\partial x_j \partial x_j}} \tag{2.6}$$

The left hand side of this equation represents the total rate of change of the turbulent kinetic energy per unit mass, ${}^1/_2\overline{u_i u_i}$. The first term of the right hand side represents the production rate of turbulence by interactions of the velocity fluctuations with the mean shear. The second term on the right hand side represents the turbulent diffusion, or transport, of turbulent kinetic energy. The last term on the right hand side represents molecular motion effects, including the rate of dissipation $\epsilon = \nu\overline{\frac{\partial u_i}{\partial x_j}\left(\frac{\partial u_i}{\partial x_j}+\frac{\partial u_j}{\partial x_i}\right)}$ of turbulent kinetic energy by the application of viscous forces. The balance between the different terms on the right hand side of the turbulent kinetic energy equation determines whether the energy of turbulent flow will increase or decrease. Dissipation of energy by viscous forces is always present in turbulent flows and always reduces turbulent kinetic energy. The major contributor to the increase in turbulent kinetic energy for the cases being studied is the production of turbulence. Because it is related to the mean shear, it is obviously important in all shear flows, including USF. In USF, the turbulent kinetic energy equation is simplified to:

$$\overline{U_1}\frac{\partial {}^1/_2\overline{u_i u_i}}{\partial x_1} = -\overline{u_1 u_2}\frac{\partial \overline{U_1}}{\partial x_2} - \epsilon \tag{2.7}$$

The downstream growth or loss of turbulent kinetic energy is determined by the strength of the turbulent dissipation ϵ in comparison to the turbulence production $P_r = -\overline{u_1 u_2}\frac{d\overline{U_1}}{dx_2}$.

A note of caution is in order when dealing with the simplified USF equations. It is well known that the turbulent kinetic energy equation cannot be satisfied exactly by USF, neither is it Galilean invariant (namely invariant to any translation of the coordinate system; see, for example, Harris, Graham and Corrsin, 1977). Nevertheless, this equation describes fairly well the available experimental realizations of USF, for which it has been assumed that the transverse extent of the facility was small enough for a constant mean convection velocity U_c to apply approximately to the entire flow.

It is generally accepted that a turbulent flow is the conglomerate of identifiable entities, called "eddies", of varying sizes and shapes. An important scale of the flow is the integral lengthscale L, which represents the average distance over which fluctuating properties are correlated significantly. Most of the kinetic energy of the turbulence is contained in eddies of size comparable to the integral length scale ("energy containing eddies"). Through mutual interactions with other eddies in the flow, the energy containing eddies break apart into smaller ones. According to this process, eddies are generated at ever diminishing sizes, until a minimum size is reached at which viscous actions between eddies of that size smear out velocity differences and, thus, dissipate turbulence energy into internal energy (heat). The minimum size of dynamically significant turbulent eddies is the Kolmogorov microscale, η. Finally, an intermediate scale that is typical of the distance between regions in the flow with intense dissipation activity is the Taylor microscale, λ. The above described "energy

cascade" process represents a general model of energy transfer and dissipation. Turbulent eddies break down to smaller sizes, but can also combine to form larger eddies. The structure of different eddies and the corresponding lengthscales can also vary in different directions, in response to the orientation of the mean strain rate or other overall characteristics of the flow.

2.3 Turbulent Flows of Interest

2.3.1 Homogeneous and Isotropic Turbulence

A fruitful configuration in the study of turbulence has been the relatively simple case of homogeneous and isotropic flow. Turbulence is called homogeneous if its statistical properties are independent of translations of the coordinate axes. A homogeneous turbulent flow is considered isotropic if its statistical properties are also independent of the orientation of the axes chosen. An ideal homogeneous and isotropic flow must be unbounded and have zero mean velocity. Turbulent flows that are approximately homogeneous and isotropic in a frame of reference moving with the mean flow speed have been produced in wind tunnels using periodic obstructions, such as grids, screens or perforated plates. The characteristics of grid turbulence depend on the shape and size of the obstruction elements and the solidity of the obstruction. The nearly homogeneous and isotropic region is limited to the core of the test section, away from the walls and from the turbulence producing obstruction. Although homogeneous and isotropic flows are rarely encountered in nature and industry, they have been studied extensively because they provide good insight into several fundamental mechanisms of turbulence, notably the mechanism of energy dissipation.

2.3.2 Uniformly Sheared Flows (USF)

USF represents the simplest turbulent flow that has an active production mechanism. Its turbulence structure is assumed to be homogeneous, at least on a transverse plane, but it is strongly anisotropic. Thus, this flow differs greatly from the case of homogeneous and isotropic turbulence, in which turbulence decays. USF have been produced in wind- and water-tunnels using obstructions of varying solidity ("shear generators"). Although close to the shear generator the turbulence consists mainly of inhomogeneous eddies produced by the obstruction, as distance from it increases, the initial turbulence decays and homogeneous turbulence is produced by the mean shear.

Ideally, USF should be unbounded, in which case it has no externally imposed length or velocity scale and it can only be characterized by the timescale $\left(\frac{d\overline{U}_1}{dx_2}\right)^{-1}$. Experimental USF has an initial lengthscale imposed by the shear generating apparatus, which, however, is free to evolve downstream. Another relevant parameter is the centerline velocity U_c, which represents the average convection speed of the turbulence. Then, at downstream distance x_1 from its origin, the turbulence in USF will have been exposed to the mean shear over a dimensionless development time $\tau = \frac{x_1}{U_c}\frac{d\overline{U}_1}{dx_2}$. The same parameter τ also represents the total strain imposed on the turbulence. It is implicitly assumed that the transverse extent of the facility is sufficiently narrow for the centerline velocity to be representative of the mean velocity in the entire test section. Otherwise, the total strain would change considerably across the flow.

2.3.3 Free Shear Flows

Free shear flows are turbulent flows with non-uniform velocity, but essentially unaffected by solid boundaries. Classical examples of free shear flows include jets issuing from nozzles, mixing layers between two streams with different speeds and wakes behind objects. Such flows are subjected to a nonuniform mean strain rate and have turbulence statistics which are inhomogeneous and anisotropic. They have a mechanism of production of turbulence as velocity fluctuations interact with the mean velocity gradient.

2.3.4 Turbulent Boundary Layers

Bounded shear flows are turbulent flows which are subjected to the direct effects of solid walls. Classical examples include pipe, duct and channel flows, which are surrounded by solid walls, and boundary layers, which are bounded by a wall on one side but are free on the other. Friction between a solid wall and the fluid in contact with it eliminates their relative velocity (no-slip condition). Subsequent layers of fluid are also subjected to shear stresses originally generated at the wall and, thus, the entire fluid in the vicinity of the wall is strained and mean shear is generated. The turbulent boundary layer is one of the most common flows in a variety of applications and has been a very popular topic of turbulence research. The simplest case is the turbulent boundary layer generated over a plane wall in a semi-infinite flow field with uniform velocity and pressure. An important parameter of this flow is the wall shear stress τ_w. This parameter is of great interest in technological applications, because it is directly related to the drag on the wall. The generation of wall shear stress is intimately related with the phenomenon of turbulence production, in general,

and particularly with the generation of coherent structures.

The two important effects of an immersed solid wall on the surrounding fluid are, first, the reduction of the relative tangential velocity by friction, and, second, the physical inhibition of the relative flow velocity normal to the wall. Thus, a solid wall is said to impose both a "no-slip" and a "no-penetration" boundary condition on the fluid. In conventional boundary layers and other common bounded flows, both effects are applied simultaneously and it is difficult, if not impossible, to distinguish their individual effects on the turbulence structure.

The boundary layer can be divided into an inner layer, where viscous stresses are important, and an outer layer, where direct viscous stresses are small compared to the turbulent stresses. The inner layer may be further subdivided into the viscous sublayer, which is in direct contact with the wall and where viscous stresses dominate, the buffer sublayer, where turbulent stresses and viscous stresses are comparable in magnitude, and the logarithmic or inertial sublayer. In the inner layer, the important scales are the kinematic viscosity, ν, and the wall shear stress, τ_w,which allow one to define a friction velocity $u^* = \sqrt{\tau_w/\rho}$. This leads to a dimensionless velocity parameter $u^+ = \frac{\overline{U}_1}{u^*}$ and the dimensionless distance $y^+ = \frac{yu^*}{\nu}$,where y is the distance from the wall. The viscous sublayer is generally assumed to extend in the range $0 < y^+ < 5$, the buffer sublayer in the range $5 < y^+ < 30$, and the logarithmic region in the range $30 < y^+ < y^+_{l\,\max}$, with the upper limit $y^+_{l\,\max}$ increasing with increasing Reynolds number and typically taking values of the order of 100. The outer layer, which includes part of the logarithmic region according to some researchers, has relatively small turbulence production and is characterized by entrainment

of free-stream fluid and the associated intermittency.

2.4 Coherent Structures

Turbulent shear flows contain recurring elements with distinct features, called coherent structures. These usually appear in the form of connected, large-scale turbulent fluid masses with a phase-correlated vorticity over their spatial extent. Coherent structures coexist with smaller scale random turbulence. In many turbulent flows, the coherent structures play an important part in the development of turbulence and are essential to developing an understanding of many processes at work. Specific types of coherent structures that have been observed in various flows and the associated terminology will be discussed in the literature review in Chapter 3.

In the turbulent boundary layer, the dominant type of coherent structures is the "hairpin" or "horseshoe" vortex. It consists of the "legs", which are a pair of counter-rotating vortices with essentially streamwise vorticity, which lift up away from the wall and join together at the "head", which has essentially spanwise vorticity. Asymmetrical hairpins with a single leg of streamwise vorticity that lifts up to a head of spanwise vorticity have also been observed. The hairpin vortex has been identified as the major contributor in the production of turbulence. Chains of hairpin vortices have been observed, with one hairpin vortex inducing the generation of another. Another type of coherent structure, which occurs in the inner sublayer, is called a "streak". These have been described as alternating regions of low and high speed fluid, and have been associated with the legs of hairpin vortices or to the flow ejected between them. The generation of both hairpin and streaky structures have

also been detected in USF by DNS (see Chapter 3).

The generation, evolution and mutual interactions of coherent structures is of major importance to the understanding of the mechanisms that produce turbulence, particularly in turbulent boundary layers. In the turbulent kinetic energy equation, the term that represents production of turbulent kinetic energy in a boundary layer with conventional axes orientation will be positive when the Reynolds stress $\overline{u_1 u_2}$ is negative. This process requires a dominance of motions involving high-speed fluid moving towards the wall or low-speed fluid moving away from the wall. The first type of motions are widely described as "sweeps", while the second type are generally known as "ejections" or "bursts". An ejection event refers to the motion of fluid with low streamwise velocity and low kinetic energy from the inner layer up to the outer layer. This has been associated with the upward flow induced between the legs of a hairpin. The exact mechanism of the "bursting" process remains unclear, thus necessitating the need for further research.

Chapter 3

Literature Review

Since the pioneering study of transition to turbulence in pipe flow by O. Reynolds (1883) more than a century ago, the study of turbulent flows has attracted considerable attention. Reviews of the voluminous results on turbulent flows can be found in the books by Monin and Yaglom (1972), Tennekes and Lumley (1972), Hinze (1976) and Pope (2000), among many others. In the following, we shall summarize the relevant literature on three topics of specific interest: uniformly sheared flow, the turbulent boundary layer and studies involving moving boundaries.

3.1 Uniformly Sheared Flows (USF)

3.1.1 Experimental Studies

Homogeneous, unbounded, sheared turbulence was conceived by von Kàrmàn (1937) as a simplified model of free shear flows. Experimentally, this idealized flow has been approximated by the core regions of turbulent flows in wind- and water-tunnels having a

uniform shear generated by adjustable transverse obstructions. The first such experiments were performed by Rose (1966) and utilized a series of bars of varying spacing but suffered from significant non-uniformity of lengthscales. Champagne, Harris & Corrsin (1970) utilized a shear generator consisting of an array of evenly spaced parallel plates with screens of varying resistance between them. This resulted in uniform lengthscales across the flow and reasonable turbulence homogeneity. Similar shear generators or variations of the concept of evenly spaced parallel channels have been used by several other researchers, including Mulhearn & Luxton (1975), Harris, Graham & Corrsin (1977), Tavoularis & Corrsin (1981, a & b), Rohr et al (1988), Tavoularis & Karnik (1989) and Ferchichi & Tavoularis (2000).

The earliest studies of nearly homogeneous USF, including those by Rose (1966), Champagne, Harris & Corrsin (1970) and Mulhearn & Luxton (1975), used relatively low values of mean shear and found that the kinetic energy did not grow within the available test section, although the integral lengthscales and the Taylor microscales grew. Harris, Graham & Corrsin (1977) introduced higher shear values and achieved larger values of the total strain. They noticed that the turbulence produced initially by the shear generator decayed, but, further downstream, all turbulence stresses increased monotonically; they also found that the integral lengthscales also increased, while the Taylor microscale remained nearly constant. Tavoularis (1985) and Tavoularis & Karnik (1989) further investigated sheared flows to even larger development times and obtained exponential growths of the components of the kinetic energy. This result was also confirmed by Rohr et al (1988).

In summary, all high-shear USF having total dimensionless development times τ greater than about 5 were found to have comparable values of the corresponding turbulence

anisotropies $b_{ij} = \overline{u_i u_j}/\overline{u_k u_k} - \delta_{ij}/3$ (δ_{ij} is Krönecker's delta; $\delta_{ij} = 1$, if $i = j$, and 0, otherwise) and essentially equal growth rates of all turbulent stresses and the turbulent kinetic energy. The integral lengthscales were found to increase continuously as the flows developed, while the Taylor microscales appeared to reach essentially constant levels and the Kolmogorov microscales were shown to decrease monotonically, although at a slow pace. In a later study, De Souza, Nguyen and Tavoularis (1995) produced USF with higher values of shear and found a shear stress anisotropy that was somewhat lower than that in previous experiments, in conformity with results in inner boundary layers and DNS of high-shear USF.

3.1.2 Direct Numerical Simulations

Rogers and Moin (1987) first revealed the presence of hairpin vortices in DNS of temporally evolving homogeneous shear flows. Their results show that vorticity vectors tend to orient themselves in a plane at 45°to the flow, along the expansive strain direction, but, as shear rates increased, the vectors became stretched to lower angles, between 22°and 40°. The same authors detected no hairpin vortices in strained flows without mean shear, but found vortical structures formed in the planes of primary strain.

Lee, Kim & Moin (1990) performed DNS of homogeneous shear flows at very high shear rates. They demonstrated that, under such conditions, USF show patterns of high- and low-speed streaks, similar to those found in the inner boundary layer. They suggested that the streaks may be the result of strong shearing and not necessarily linked to the physical presence of a wall.

In another study, Kida & Tanaka (1992 and 1994) performed DNS of USF and

presented vorticity and Reynolds stress contours. They observed tube-like structures with longitudinal vorticity that became inclined at an angle of 15°-30°with respect to the flow direction as they developed. They also observed transverse tube-like structures with spanwise vorticity. They also noted a decrease in inclination angle as the rate of shear increased.

3.2 Turbulent Boundary Layers

3.2.1 Experimental Studies

The first thorough experimental investigation of a turbulent boundary layer was conducted by Klebanoff (1954), who reported mean velocity profiles, turbulence levels, spectra, intermittency factors and energy balances. He found that the streamwise velocity fluctuations peaked in the buffer sublayer, at around $y^+ = 15$, and very high levels of turbulence production as well as dissipation were concentrated in this region.

Visual studies of turbulent boundary layers have established a link between coherent structures and the production process. Kline et al (1967) used the hydrogen-bubble technique to reveal the formation of alternating high- and low-speed streaks in the viscous sublayer. The location of streaks seemed to form a random pattern, approaching a uniform distribution (Schraub et al, 1965). Runstadler et al (1963), Schraub et al (1965), Bakewell & Lumley (1967) and others have used both hot-wire anemometry and visual signatures to measure the mean spanwise spacing between streaks; a typical value of this spacing is approximately $100\nu/u^*$.

Kim, Kline & Reynolds (1971) later expanded on this research using two perpendicular hydrogen bubble wires introducing combined time-streak markers. They showed that

the low-speed streaks lift up from the inner boundary layer and related this phenomenon to the production of turbulence through a dynamical process referred to as bursting. They concluded that this process occurs in three stages: i) lifting of the low-speed streaks away from the wall, ii) growth of an oscillatory motion due to the instability of the low-speed streaks, and iii) breakup of the oscillatory motion into a chaotic behavior with return of the low-speed streak to the wall. They showed that the production of turbulence was directly related to the bursting process by observing production values with bursting times. They also showed that large peaks in the turbulent kinetic energy were found at frequencies matching that of the oscillations of the low speed streaks. Finally, they determined that the bursting cycle was intermittent but with a well-defined frequency.

Lu & Willmarth (1973) studied the relation between bursting and turbulence using a four-quadrant burst detection method. Data from the u_1u_2 signal were plotted on a u_1 vs u_2 graph, forming four quadrants with data representing positive and negative values of each velocity fluctuation. The contribution to production from motions in the second quadrant ($u_1 < 0$, $u_2 > 0$), corresponding to bursts, was found to provide 77% of the shear stress, while the fourth quadrant ($u_1 > 0$, $u_2 < 0$), corresponding to sweeps, provided 55% of the shear stress, with the excess 32% attributed to the small positive stress produced during events corresponding to the other two quadrants. Bursts were noticed to occur when the streamwise velocity at the wall was small and decreasing, whereas sweeps required the wall velocity to be high and increasing. The bursts were noticed to provide a larger contribution to the shear stress very close to the wall.

Ueda & Hinze (1975) provided further insight into the fine-scale turbulence near

the wall using very fine hot wire measuring techniques. They measured spectra of streamwise velocity fluctuations and their first and second derivatives, which indicated that the peak of the turbulent kinetic energy was at about $y^+ = 15$. They also concluded that the viscous sublayer was affected by inrushes, whereas the rest of the boundary layer was affected by both inrushes and ejections.

Falco (1977) used a combination of hot-wire anemometry and flow visualization to distinguish small-scale coherent motions which were large contributors to the Reynolds shear stress and which he called "typical eddies". These typical eddies were most active as part of large-scale motions in the outer boundary layer. They often formed in the shape of mushrooms and indicated an outward motion from the wall layer.

Head and Bandyopadhyay (1981) presented extensive visual evidence supporting the presence in the boundary layer of many hairpin vortices inclined by an angle of approximately 40°with the wall, as had been earlier conjectured by Theodorsen (1952) and others. Using laser sheets inclined by 45°to the wall, they showed details of hairpin vortices and an elongation of these vortices as the Reynolds number was increased (Figure 3.1 and 3.2). They also produced films which indicated that the tips of the hairpin vortices curved upstream, presumably because the hairpin vortex approached a region of low shear.

Acarlar & Smith (1987) studied dye injected through a surface slot in a laminar boundary layer, which initially formed a streaky structure. They concluded that external forcing of the flow created a three-dimensional shear-layer instability that led to the formation of hairpin vortices, which they observed using simultaneous imaging from three different views and found to grow into larger, more complex structures.

Although the production of turbulence has been linked to coherent structures, there is still no positive conclusion as to how the whole process evolves. A review of the role of coherent structures in the production process has been made by Robinson (1991). As researchers attempted to classify and generalize their work, the description of the different types of coherent structures and processes has generated a large nomenclature that is not always consistently used. Robinson (1991) summarizes much of the work concerning coherent structures in low-Reynolds number turbulent boundary layers and includes a condensed nomenclature. The terms "sweep" and "ejection" were introduced by Wallace et al (1972) and by Willmarth & Lu (1972) and refer to the motion of high speed fluid toward the wall and the motion of low speed fluid away from the wall respectively. High and low speed "streaks" have been reported by many researchers and refer to regions of fluid observed in the inner sublayer with velocity faster or slower, respectively, than the local mean. Head and Bandyopadhyay (1981) conjectured vortical structures in the form of a loop inclined upward into the flow with both ends originating at the wall. At low Reynolds numbers, the loops were very wide and were called "arch" or "horseshoe" structures, whereas, at high Reynolds numbers, the legs of the arch moved inward and resembled hairpins, hence named "hairpin" structures. Another term popularly used is "quasi-streamwise vortices", referring to vortical structures with streamwise vorticity that are elongated in the streamwise direction but are often slanted in the spanwise and/or transverse directions.

Smith et al (1991) have described a complete physical process for the production and generation of turbulence in a high Reynolds number boundary layer and proposed the hairpin vortex as the primary flow structure. They investigated the interaction of a hairpin

vortex, either symmetric or asymmetric, with the wall surface, the shear flow and other hairpin structures to form a complete model that was in good agreement with experimental and DNS studies. These authors observed an eruption of fluid from the wall-region flow induced by the streamwise vorticity of the hairpin legs. The generation of hairpin vortices was observed to occur in a field of strong vorticity, as well as by interaction with the wall. The bursting of the flow from the wall due to the presence of a hairpin vortex was also demonstrated. Finally, Smith at al (1991) showed that, in general, hairpin vortices began forming in a symmetric form, but they could rapidly develop to asymmetric shapes.

Haidari & Smith (1994) studied the generation and growth of single hairpin vortices created by controlled surface fluid injection in a laminar boundary layer. The formation of low-speed streaks and turbulent pockets of fluid was evidenced by the passage of a hairpin. An increase of Reynolds number indicated a regeneration process of hairpin structures above a critical level, both by lateral deformation of the initial vortex lines as well as by the interaction of the hairpin vortex entraining an ejection of surface fluid.

Adrian et al (2000) used Particle Image Velocimetry to investigate a conventional turbulent boundary layer. They determined that, in the outer layer, structures representative of hairpin vortices occurred in streamwise-aligned packets that grew upwards in the streamwise direction. They also observed packets of vortical structures in the near-wall region, as well as interactions, entrainment and over-running of different packets and vortical structures of different size in the logarithmic region.

In the following, the term hairpin is taken to represent cane, hairpin, horseshoe or omega-shaped vortices and deformed versions thereof, recognizing that these patterns are

variations of a common basic flow structure at different stages of evolution and with varying size, age, aspect ratio and degree of symmetry. The signature pattern of the hairpin consists of a spanwise vortex core located above a region of strong second-quadrant fluctuations ($u_1 < 0$ and $u_2 > 0$) that occur on a locus inclined at 30°to 60°to the wall (Adrian et al, 2000).

3.2.2 Direct Numerical Simulations

Kim, Moin & Moser (1987) developed a numerical database of detailed statistics of fully developed turbulent channel flow, completing previous studies that targeted specific regions of the turbulent flow field. Statistics in the boundary layer agree reasonably well with experimental results. This database provided an excellent reference source for comparisons with subsequent studies and has been used to provide starting conditions for DNS of more complex systems. The same database has also been used in conjunction with conditional sampling techniques to provide values of u_1u_2 in the different quadrants. The DNS, in agreement with the experimental evidence, have demonstrated that, very near the wall, $\overline{u_1u_2}$ contributions from sweeps dominate, whereas further from the wall, contributions from ejections dominate.

In another DNS study, Jimenez & Moin (1991) showed that turbulence could not be sustained for flows for which the spanwise dimension was lower than a certain value, which they found to correlate well with the mean spanwise spacing between streaks, namely $100\nu/u^*$. Hamilton, Kim and Waleffe (1995) expanded on this issue by performing DNS on plane Couette flows to determine the effect of spanwise spacing on the turbulence regeneration cycle. They determined that the spanwise spacing affected the whole cycle and not

simply one component of the cycle. They concluded that the spacing of the streaks was likely determined by the turbulence regeneration, and, if the spanwise dimension were limited, turbulence regeneration would not take place. The turbulence regeneration cycle, as described by Hamilton, Kim & Waleffe (1995) consists of a three-step, continuous process: first streamwise vortices form streaks through linear advection, then these streaks breakdown due to instabilities, and, finally, this breakdown regenerates the streamwise vortices through non-linear interactions.

Jeong et al (1996) performed conditional sampling to educe coherent structures from numerically simulated channel flow in the near-wall region, for $y^+ < 60$. They observed that the dominant structures were quasi-streamwise vortices, inclined by 9°to the wall, and tilted alternately at +4°and -4°in the spanwise direction. The endpoints of these vortices were seen to roll up above the starting points of other vortices of the opposite sign. The same authors reproduced the formation of high and low speed streaks and internal shear layers in the inner boundary layer and confirmed the dominance of sweeps over bursts near the wall. They did not detect the presence of hairpin vortices, although they noted that some of the streamwise vortices that rose upward toward the outer layer could be presumed to form the long legs of hairpin vortices, which could not be resolved due to smearing of data above $y^+ = 50$. The observed structures provided a possible explanation for the energy transfer near the wall from transverse fluctuations to fluctuations tangential to the wall, a process that involves the pressure-strain covariance.

More recently, Jimenez & Pinelli (1999) defined a turbulence regeneration cycle in the inner layer that was essentially independent of outer layer effects. They showed

that streamwise vortices extracted energy from the mean flow to create streaks, which in turn, most likely as the result of inflectional instability, created streamwise vortices. They proposed this process to be one of several mechanisms of turbulence production in the boundary layer.

Finally, Zhou et al (1999) performed DNS of an initially specified hairpin vortex structure in a turbulent flow field. They observed an induction of new hairpins, both downstream and upstream of the primary hairpin structure, for initial hairpin vortices with sufficiently strong vorticity. The hairpin structures seemed to form more often in packets and not as singular structures.

3.3 Moving Wall Studies

3.3.1 Experimental Studies

Uzkan & Reynolds (1967) distinguished wall-turbulence interactions by passing grid-generated turbulence over a wall moving at the mean speed of the flow. The mean velocity gradient at the wall was zero and the production of turbulence by shearing was eliminated. In these experiments, the sharp peak in streamwise turbulence intensity normally found near a stationary wall was no longer present. Uzkan & Reynolds (1967) also described an inhomogeneity layer, created by the disturbance of the wall, and its effect on the flow. The experimental work of Thomas and Hancock (1977), in conjunction with the analytical solutions of Hunt & Graham (1978), described this inhomogeneity layer as comprising two separate layers: an inner viscous region, affecting the fluctuations tangential to the wall, and an outer kinematic region, characterized by the length scale of the external

turbulence and which inhibits velocity fluctuations normal to the wall.

The results obtained by Thomas & Hancock (1977) on the variation of streamwise Reynolds stress toward the wall followed the theory of Hunt and Graham but did not match the results of Uzkan & Reynolds (1967). The turbulent fluctuations smoothly dropped to zero at the wall for the Uzkan & Reynolds experiments, whereas an increase was observed by Thomas & Hancock. This can be explained by a significant difference in the grid Reynolds numbers for the two experiments. The theory of Hunt and Graham assumes large Reynolds number and the study of Uzkan & Reynolds would indicate that the effect of the viscous layer would extend farther into the kinematic boundary layer. These differences would be points of concern for similar research in the future.

The effect of mismatching wall velocity with that of the flow was demonstrated by both Uzkan & Reynolds (1967) and Thomas and Hancock (1976). Thomas and Hancock showed that streamwise and transverse turbulence intensities did not change if wall and flow speeds were within 5% of each other, except in regions of significant shear, so that the moving wall was not causing other disturbances that could alter the results.

The presence of streaks near a stationary wall for a turbulent boundary layer was confirmed by Uzkan & Reynolds (1967) in their water tunnel facility. The streaks slowly disappeared as the velocity of the wall was increased to match the mean flow velocity, supporting the theory that streaks and their breakup are directly related to the presence of shear.

Uzkan & Reynolds (1967) showed, using spectral analysis, that the presence of the wall affected the larger eddies more than the smaller ones, and persisted over larger

distances from the wall. They also showed that, in the inhomogeneity layer, the integral lengthscale decreased toward the wall, which implied the presence of smaller eddies near the wall, while, at the same time, the integral timescale increased toward the wall, which implied that the turbulent motions were slowed down.

More recently, Aronson et al (1997) furthered these earlier moving wall studies with decaying turbulence and determined that the effect of the wall can be associated with two different lengthscales. A larger lengthscale was associated with the wall-normal velocity component, whereas a smaller scale was associated with the velocities tangential to the wall.

3.3.2 Direct Numerical Simulations

Perot & Moin (1995a & b) performed DNS in box turbulence with different boundary conditions to provide further insight into the effects of the wall on the turbulence structure. They studied a case with an idealized permeable wall, through which the fluid could pass in the normal direction, yet subjected to viscous effects on the flow velocity tangential to the wall, thus separating the kinematic from the viscous effects. In another case, they imposed an idealized free surface, at which the normal velocities vanished, while viscous effects were removed by assuming this surface to be a stress-free boundary. They observed the formation of fluid entities approaching or leaving the boundary, which they identified as "splats" and "antisplats" respectively. They also observed intercomponent energy transfer, which was controlled by the viscous, and not the kinematic, effects of the wall, and further showed that all terms in the turbulent kinetic energy equation should be fully investigated near a boundary, because their contribution may not be insignificant, as sometimes has been assumed.

3.4 Summary

Although a great deal of knowledge has been accumulated on turbulence, there remains much more to be investigated and understood. The hairpin vortex has been found to be a primary factor in the generation of turbulence in boundary layers, and is conjectured to be a dominant structure in USF as well. "Streaks" have also been observed in turbulent boundary layers and numerically in highly sheared USF, and are also an important structure to study. The use of a moving wall to remove shear near a wall has presented insights into wall effects, however, information on the interaction of coherent structures with a wall is not available. The experimental visualization of coherent structures in USF is a research topic that needs further investigation. Finally, the interaction of coherent structures with a wall is another topic that deserves attention, but has not yet been studied.

Chapter 4

Experimental Facilities and Procedures

4.1 Water Tunnel Facility

All experiments were conducted in the water tunnel facility of the Department of Mechanical Engineering at the University of Ottawa. The water tunnel was designed to provide a high quality, low turbulence flow for both visual and quantitative studies for a wide variety of possible experiments. The author was responsible for its design and the supervision of its construction.

4.1.1 Water Tunnel

The water tunnel is a closed loop system with a free-surface water level that can be varied, providing different heights of the flow in the test section. The water is recirculated by an axial flow pump, manufactured by Cascade Inc., Santa Fe Springs, California, USA,

having a diameter of 0.305 m and located directly under the settling chamber. The pump was driven by an electric motor, manufactured by General Electric, having a nominal power of 5.6 kW and controlled by a speed controller (Siemens Relcon Q2000). Water was pumped through a vertical perforated cylinder into a large settling tank with several high-solidity perforated plates and foam sheets for flow conditioning. The settling tank was connected to the test section through a three-way contraction, that was 1.52 m high and 2.44 m wide, providing a minimum contraction ratio of 9.2 at full water height, or higher when the water level was lowered. The test section was 0.75 m high, 0.54 m wide and about 4.0 m long, and consisted of three sections, all enclosed on the bottom and the two sides by tempered glass sheets (see figures 4.1, 4.2 and 4.3). The top of the test section could be left open for free-surface flow, covered by plane, transparent covers or fitted, in its central section, by the moving wall (see below).

A filtration and chlorination system was installed to maintain clarity of the water. Following relatively long periods of inactivity or after dye injection at large volumes, the water became cloudy and was replaced partly or entirely. The water temperature was kept at roughly 19°C.

4.1.2 Traversing Systems

The water tunnel is equipped with a two-dimensional traversing system, consisting of a set of rails for manual traverse along the side of the entire test section and a motorized vertical leadscrew. A still camera, video camera, laser sheet lens or LDV probe could be mounted on the vertical traverse to cover almost any location of the flow, except where structural supports interrupted direct view of the test section. A right-angle bracket could

be connected to the side traverse, thus enabling laser-sheet/video camera traversing underneath the tunnel, along a central section that was 1.8 m long. A separate pair of traversing rails also run along the top of the test section, permitting the mounting and traversing of components from the top.

4.1.3 Shear Generator

USF was generated using a shear generator and a flow separator located at the entrance of the test section. The shear generator was a perforated aluminium plate with a linearly varying resistance to the flow. It was 3 mm thick and had a total height of 0.457 m. It was divided to 16 levels, each containing a set of holes and/or slots (see figure 4.4) with solidities decreasing by 5% at each level, from 75 % to 0%, with the two top levels at 0%.

The flow separator serves the purpose of producing a uniform distribution of initial length scales. It consisted of 16 sheets of tempered glass, 1.6 mm thick, mounted at their ends on two vertical supports, made of PVC (see figure 4.5). The distance between consecutive sheets, centre-to-centre, was 28.2 mm, thus forming 16 parallel channels, which were aligned with the perforations of the shear generator.

4.1.4 Moving Wall Apparatus

The moving wall apparatus (see figures 4.6 and 4.7) comprises a continuous belt, three drums on a mounting frame, a motor and a controller. The belt is a Habasit HNB-5E, 1.3 mm thick and 0.53mm wide, with a smooth polyurethane surface on the water side and an impregnated polyrurethane fabric on the drum side. A dark green colour was the darkest

available to minimize any light reflections for visual studies, and the belt was joined at the factory using a Flexproof system that provided high tensile strength and flexibility while maintaining a smooth belt surface. The three drums are made of PVC pipe and are 0.15 m in diameter. Two of these drums were mounted, through sealed stainless steel bearings (6304-2RSR), on aluminum shafts. The shafts were 1.8 m apart and were supported on a frame made of aluminium sheets 3 mm in thickness. The third drum was driven by a 93 W (1/8 hp) reversible DC motor with a variable speed controller. The third drum and motor were mounted on a carriage running on traversing rails so that the belt tension could be adjusted. The drive drum was cross-knurled to minimize slippage. Felt padding was installed near the drums to wipe water droplets off the belt. A UHMW polyethylene sheet served as a backplate for the belt, providing an even surface for the belt to run along as it came in contact with the free surface of the water. The frame of the apparatus could be lowered to the desired depth in the water.

4.2 Flow Visualization Equipment

Visual data for this research were obtained using digital videography of fluorescent dyes excited by a laser light sheet.

4.2.1 Dye Injection

Several dyes were tested in the facility, including regular water based dyes, shear-thickening dyes and finally fluorescent dyes, the latter being the one used for this research. Fluorescein, in a powder state used at 10 mg per litre of water, fluoresced a green colour

when injected in the flow and passed through the argon-ion laser sheet. Because the dye is heavily diluted and insoluble in water, the physical properties of the dye/water mixture are assumed to be very similar to those of water and thus the dye has little influence on the flow structure. Diffusion of the dye in the flow did occur at a slow rate for low-speed tests of the water tunnel, and obviously increased with turbulence, providing a good indication of highly turbulent regions.

The dye was contained in canisters, located alongside the water tunnel, and forced through the flexible tubing with the use of compressed air. The flexible tubing connected the dye from the canisters to the dye injection system in the tunnel. This consisted of a rigid tube with a streamlined profile with a chord length of 6.7 mm and a maximum height of 3.1 mm, which could be positioned at most locations in the flow. The airfoil contained a round tube, 3.1 mm outer diameter and 2.5 mm inner diameter, projecting perpendicularly from the trailing edge of the airfoil near its bottom end. The airfoil tube of the dye injection system provided a rigid mechanism for injecting dye at most locations in the tunnel while minimizing the wake and induced vibrations on the tube.

The flow rate was controlled using valves but was not measured or monitored except by visual observation of the dye entering the flow. The dye injection system did not appear to vibrate at the flow rates tested, although earlier studies with a round injection tube did indicate minor vibrations. LDV measurements of the flow at x_1=1.83, 2.70 and 3.29 m across the channel height showed no effect on the statistical measurements with and without the dye injection system in place at x_1=2.2 m. LDV measurements with dye injected into the flow at a properly adjusted rate also showed no effect on the statistical

measurements. Observation of the dye released into the flow was the main method used to control its release. The flow rate could be controlled to create a strong jet of fluid, down to an unsteady drip. The dye flow rate was optimized for good visibility while creating a minimum disturbance to the flow when the dye was observed to leave the tube in a laminar fashion. The flow rate of the dye did decline slowly over an experimental test, however, one canister could contain approximately two hours of dye for testing, and the pressure in the canisters was adjusted periodically to maintain a continuous rate of dye release. In most cases, dye was injected in significant amounts far upstream of the region of interest, to permit viewing of a wide region of the overall flow structure, and to permit the dye to develop with the turbulence structures.

The location of the dye injection tube in the flow varied depending on the region of study. For all studies centering on the core flow, the dye was released at a downstream location of $x_1 = 1.25$ m at the centre height of the channel. For wall studies, the dye was released at $x_1 = 1.25$ m, and tests were performed at wall-normal distances of 0, 3 and 30 mm, to investigate differences that may occur depending on the origin of the dye. These were determined to be negligible regarding the observed structures in the flow.

Tests with a second dye, Rhodamine 6G, which fluoresced yellow, were performed with the two dyes injected in the flow at different locations, but were not an essential element of this thesis. Tests using an injection tube rake, with multiple dye ports were also performed, and although the disturbance to the flow was found to be minimal, this arrangement did not provide more benefit to the visualization of the flow.

4.2.2 Laser Light Sheet Illumination

A laser beam, produced by a 5W Ar-Ion laser, operated at a continuous power of 0.95 W, was passed through a fibre optic cable and then a Powell lens, which expanded it into a triangular sheet of light of uniform intensity, with a thickness of approximately 1 mm. The light sheet could be oriented normal or inclined to the flow direction and, due to the flexibility of the optical fibre and the small size of the lens, could be also traversed along or across the flow.

4.2.3 Image Recording

During preliminary testing, 35 mm photographic cameras (Minolta and Nikon professional cameras) were used with various lens attachments. The majority of the visual recording in the present experiments was performed using a Sony DCR-VX1000, 3CCD NTSC digital video camera. This camera provided sufficient resolution, frame rates and light sensitivity. The room was kept dark to minimize reflections and glare from light sources other than the excited fluorescent dye. The camera iris was set to automatic and was often at its widest position. Depth of field was not a concern because the illuminated image of the flow was essentially planar. Shutter speeds were kept at or above 1/500 s, depending on the light intensity. The video camera could be placed on the side, rear or underside of the test section. Size references for visual studies were usually made by videotaping a known reference object positioned on the plane of interest.

4.2.4 Image Processing

Video was recorded on miniDV format tapes and later transferred to computer via a IEEE 1394 connection using a SPARK DPS video capture board and a Microsoft WDM Capture Board. This provided a high bandwidth transfer of video to the computer, allowing resolutions of 720×480 pixels in 24-bit colour at 30 frames per second to be stored on a computer. Non-linear video editing was then performed to organize the images and provide snapshots or short segments of the video of most interest. Adobe Premiere 4.2 and MGI Videowave II software packages were used on high-end personal computers, mainly a PC with AMD Athlon K7 processor with 128Mb RAM and a 15Gb hard drive. Several hours of video were recorded and processed during the research. Managing the storage of the data was very critical considering that 1 min of video in AVI format requires roughly 250 Mb of memory. Video clip files of 10-15 s duration were created to better manage the information. These files are available in AVI file format for post-processing of all the original information, as well as in MPEG-2 format, which maintains the high resolution information of the video clip while compressing down to almost 20% of the original size. The only drawback of MPEG-2 compression is that viewing of the video clips requires that the original compression-decompression files be installed on the viewing PC, making it more difficult to share.

4.3 Laser-Doppler Velocimetry

4.3.1 Instrumentation

LDV measurements were obtained using a Dantec two-component, two–colour LDV system with a beam splitter, Bragg cell, laser head probe and two 57X08 photo-multiplier tubes. The system was powered by a 5 W Ar-Ion laser, operated for the most part at 0.95 W due to the power limitation of the optical fibre cable that transmitted the beam to the laser optics. The system used green and blue peaks of the spectrum, having wavelengths of 514.5 nm and 488 nm. A Pentium 486-66 personal computer running Floware 3.2 software, supplied by Dantec Inc., was used to process the data. The laser itself was located on a shelf on the side and above the water tunnel facility, while the rest of the equipment was situated on a shelf alongside and below the test section.

In order to collect data in the very near wall region of the flow, the LDV probe head was rotated slightly in both x_1 and x_2 directions, allowing the corner beam to pass through the glass wall perpendicularly, while the two edge beams crossed the inspection point at a slight angle. Thus, following the application of appropriate corrections, the LDV system could be used to obtain u_1 and u_2 data all the way up to the wall, limited only by the beam diameter and probe volume. Verification of the data obtained with the rotated LDV probe was achieved by using the probe in the usual orientation with only a single velocity component measured, u_1. This allowed measurement of the streamwise velocity component all the way to the wall, with values matching those obtained from the rotated probe configuration.

4.3.2 Calibration and Settings

The settings and components of the LDV system were optimized for the range of experiments being conducted. A lens with a focal distance of 243 mm was used, as it provided the lowest focal distance of the lenses available, while permitting measurements on the centreplane of the water tunnel. The laser beam diameter was 1.4 mm, the beam separation was 26.87 mm, while the probe volume dimensions are given in Table 4.1.

A Bragg cell with a frequency shift of -40 MHz was used to allow for negative velocity readings and a higher resolution. The LDV was triggered on the streamwise component U_1, which generally had a much higher value than the other component measured, U_2 or U_3, which provided higher data rates and validity of the results. The bandwidth was set to 0.12 MHz for both U_1 and U_2, which provided the highest possible resolution while capturing the full range of velocities present in the flow. Validation was set to +2 dB, which was determined through various tests to be a reliable gain that improved the signal while causing minimal error. This applies similarly to the fringe count of 16 to 46.0955 (the latter determined by the LDV), which provided the best validation of the data at a reasonably high data rate. The high voltage setting was set to the highest value permitted by the software, usually at 2000 V, to provide the best signal strength, while making sure that the photomultiplier tubes did not overload.

Data and validation rates were improved by seeding the water with silicon carbide particles of maximum diameter of 5 μm . These particles were mixed with a small volume of water to ensure proper dispersion, and then released into the tunnel at the pump inlet. Even distribution of the particles would take up to half an hour to be achieved, but provided

much higher data rates than without the seeding. Each addition of seeds provided good quality data for 2 to 3 days, following which more seeds had to be added.

	Δx_1	Δx_2	Δx_3
U_1	0.1138	0.1137	2.0597
U_2	0.1080	0.1078	1.9536

Table 4.1. Probe volume dimensions in mm

4.3.3 Uncertainty Estimates

Tests were performed to determine whether the pump motor and controller operation affected the LDV measurements as well as to determine the electronic noise of the LDV system. These tests were performed by turning the LDV system on while the pump controller was operating, with and without flow in the tunnel. The LDV probe was mounted on the frame of the tunnel to test for vibration effects. Then the beams were focused at a point in the inside corner of a structural member that was painted white. Settings in the LDV software were varied to determine any possible influence for the different cases studied. Triggering of the LDV had to be changed to a set frequency. The laser was set to a power of 400 mW and the high voltage to 648 V (any higher values would have overloaded and damaged the PMTs). The maximum noise determined in the system was 0.0002 m/s.

The relative velocities of both the natural seeds and the silicon carbide particles were estimated to be negligible, compared to the resolution to the LDV system.

For LDV measurements on the spanwise components of velocity, an error can be associated to the length of the control volume crossing the velocity gradient. For a typical gradient of 0.4 s^{-1}, the error over the 2 mm length of the probe volume was estimated as 0.0004 m/s.

The relatively low resolution of the available LDV system was the greatest contributor to the experimental uncertainty. The processor had a 8-bit output, which corresponds to a resolution of 1/256 of the full range. For the velocity ranges of 0.56 m/s for U_1 and 0.53 m/s for U_2, used in the present measurements, the velocity resolution should have, ideally, been 0.0022 m/s. From the data history, however, the actual resolution was found to be 0.0029 m/s. The effect of the resolution limitation was reduced by taking average values over very long periods of time, but, nonetheless, did limit the accuracy of the LDV data for statistical measurements at very low speeds, such as near the wall.

Chapter 5

Measurements

The coordinate system and basic dimensions of the test section are shown in Figure 5.1. The channel width was $2w = 0.54$ m, while the water height was maintained at $2h = 0.42$ m. The origin of the co-ordinate system (x_1, x_2, x_3) was positioned on the centreline of the flow, at the exit of the flow separator. When dealing with the near-wall region, the transverse coordinate will be referred to as y, measured as the distance from the top wall downwards, namely $y = -x_2 + h$. The moving wall apparatus formed an upper boundary over the region 1.35 m $< x_1 <$ 3.15 m, while the majority of measurements and visualization results were taken in the region between 2.6 m$< x_1 <$ 2.7 m. The water tunnel was operated in a high-speed mode and a low-speed mode, corresponding to flow rates of 0.031 m^3/s and 0.017 m^3/s, or centreline mean velocities of 0.136 m/s and 0.073 m/s. Repeatability was excellent as long as the water level was maintained accurately at 0.42 m, corresponding to a contraction ratio of 16:1 from the settling tank to the test section.

Originally the study was planned to be conducted at the high speed mode alone,

which provided a higher turbulence Reynolds number and a reasonable resolution of the LDV system. A detailed study of USF in the test section was made under these conditions, which included LDV measurements of the streamwise, transverse and spanwise variations of turbulence statistics. Sharp and clear still images of the flow structure could be easily obtained using 35mm photographic film, high quality lenses and appropriate film speeds. It turned out, however, that the motion in the high-speed flow was too fast to allow clear, sharp images with the available digital video camera. Furthermore, the interlaced effect of NTSC video created some blurring when capturing 60 fields combined together to make 30 frames per second. In addition, the relatively large distance travelled by the fluid particles during the 1/30 s that separated two consecutive frames limited the resolution of the video sequence. Another limitation was the velocity range of the moving wall system. In order to match the local flow speed for the high-speed mode, the wall velocity would have to be adjusted to a value that was beyond its range of stable operation. For these reasons, most visual studies were conducted in the low-speed mode, while LDV measurements for this case were confined to the main region of interest, at $x_1 = 2.7$ m.

Major consideration for the moving wall apparatus included tension and sagging in the belt. With the belt tensioned at its highest possible limit which allowed the motor to maintain a constant speed through a full cycle of the belt, the belt sagged 3 mm at the centre of its lower span of 1.5 m. This indicated that the belt did not run along the back-plate of the apparatus at all. The motor was able to perform continuously for at least 2 hours without showing any overheating effects, and the belt maintained its tension, with no slippage occuring and no straining or heating of the belt noticeable. The belt never

appeared to flap or change its shape in the water, which lets us assume that the flexible wall material was representative of a solid wall. There is a slight curvature of the wall, however this should have little effect on the flow, because the radius of curvature was vastly greater than the boundary layer thickness. The belt speed was measured by timing the motion of a reference point. This was repeated five times for every LDV run and its was found that the belt speed essentially remained constant throughout the experiment, with the flow speed varying by less than 0.5%.

The orientations of the USF velocity profiles were different for the two modes of operation. A positive mean velocity gradient (velocity increasing upwards) was used for the high-speed studies, while a negative gradient was used for most of the low-speed studies. The USF case with a negative gradient corresponds to the orientation of the boundary layer on the top wall. Reversal of the profile was achieved by inverting the shear generator plate. Some measurements were repeated for the low-speed case with both positive and negative mean velocity gradients and indicated no significant differences in the turbulence structure. Other studies that were briefly performed but are not an essential part of this research include flow visualization using two fluorescent dyes released at different locations and investigations of side wall and free surface effects.

5.1 Core USF Studies

Figure 5.2 presents profiles of the streamwise velocity. In all cases, the gradient was reasonably uniform over most of the channel height. The mean velocity gradient $d\overline{U_1}/dx_2$ was measured at an average of 0.405 s^{-1} for the high-speed case, and -0.25 s^{-1}, for the

low-speed case.

Figure 5.3 presents the streamwise turbulent stress variation across the channel height at three downstream locations. It can be seen that this parameter grew downstream and that its growth rate varied in the transverse direction, growing faster in the low-speed region of the flow. Figure 5.4 shows the variation of the transverse turbulent stress; this stress grew very little in the downstream direction, except in the low-speed region where its growth rate was comparable to that of the streamwise turbulent stress. Finally, Figure 5.5 shows the transverse variation of the shear stress correlation coefficient $\overline{u_1 u_2}/u_1' u_2'$. The values of this coefficient were approximately -0.45 in the low-speed region of the flow, but of measurably lower magnitude in the high-speed region. In summary, the turbulence in the present USF deviated somewhat from the assumption of transverse homogeneity and was in better conformity with previous wind tunnel USF (Tavoularis and Corrsin, 1981a & b; Tavoularis and Karnik, 1989) in its low-speed rather than the high-speed region. A possible explanation for this observation is that the turbulence in the low-speed region had a longer development time (higher total strain) than that in the high-speed region. On the other hand, it is also possible that these differences were due to differences in the initial turbulence intensity and length scales produced by different parts of the shear generator. In the low-speed region, the shear generator had perforated circular holes, whereas, in the high-speed region, it had perforated slots.

Figure 5.6 presents the downstream development of the Reynolds stresses along the centreline of the test section. As in previous wind-tunnel studies of USF, one may observe an initial region where the turbulence produced by the shear generator/flow sepa-

rator obstructions decayed. Beyond a certain distance, however, which was approximately at $\tau = 5$, turbulence produced by the mean shear dominated and an exponential growth of the turbulence stresses may be observed. Similarly to previous studies, the largest normal stress was the streamwise one, with the spanwise stress being second and the transverse stress being the smallest. The values of $\overline{u_1^2}/\overline{U_1}^2$ measured from data taken from the side of the tunnel and from below the tunnel matched quite well, indicating reproducibility of the results.

The spanwise variation of the flow was investigated within a limited range and indicated no problems in this respect. The mean streamwise velocity was generally within 1% of the average value (Figure 5.7), while the mean spanwise velocity (Figure 5.8) appeared to be slightly negative, which could be caused by a slight misalignment in the LDV system or unevenness in the lower glass wall. The spanwise shear stress correlation coefficient $\overline{u_1 u_3}/u_1' u_3'$ (Figure 5.9) was slightly positive with typical values near 0.05, which could also be attributed to slight misalignments. Figure 5.10 presents the spanwise variations of the streamwise and spanwise stresses; both were nearly uniform within a significant part of the core and increased slightly towards the side walls. For the present purposes, the spanwise variation of all parameters is considered sufficiently small to be neglected.

5.1.1 Comparison with Previous Studies

Results obtained from the USF study are in general agreement with previous research. As in previous studies, initial turbulence generated by the shear generator was observed to decay, while sufficiently downstream, the shear generated turbulence grew exponentially. The rates of growth of the different Reynolds stresses were very close to each

other and to the growth rate of the turbulent kinetic energy q^2 (Figure 5.6). Spectra measurements were taken and indicate a downstream increase of energy, along with inferred integral lengthscales. The spectra information is introductory at this point and the accuracy of results needs greater improvement. As it is not an essential element of this thesis, spectra information is presented in appendix B.

An important indicator of the state of development of USF is the shear stress correlation coefficient. Typical values of this coefficient in fully developed USF have been around -0.45. The present flow had values near -0.45 over a considerable region of its low-speed side. However, on the high-speed side, values as low as -0.25 were observed, indicating that the flow was still developing towards its asymptotic structure at these locations. A positive indication was that, as the flow developed downstream, the shear stress correlation coefficient on the high-speed side also approached values closer to -0.45. It is reminded that, as far as the studies of interaction of USF with the wall are concerned, the previous discrepancy is not of much concern, because it is the low-speed side that was closer to the wall.

For comparison with other flows, certain parameters have been measured at $x_1 =$ 2.6 m, which is the downstream location where most of the visual experiments were performed. Table 5.1 summarizes these results, where available, as well corresponding results of Tavoularis & Corrsin (1981a, TC), Rohr et al (1988; R case S2) and Tavoularis & Karnik (1989, TK case D). In this table, the flow generator constant is defined as $k_s = \frac{1}{U_c}\frac{d\overline{U_1}}{dx_2}$, and k is the exponential growth factor of turbulent kinetic energy in $q^2 = q_r^2 e^{k(x_1 - x_r)}$, where q_r and x_r are reference values. The values of k_s and k, along with the centreline mean velocity

U_c and the mean velocity gradient $\frac{d\overline{U_1}}{dx_2}$, were calculated directly from measurements. The production term P_r was also computed from measurements, while the dissipation term ϵ was computed as the balance of the other two terms in the simplified turbulent kinetic energy equation. The integral lengthscale L_{11} was estimated using the empirical expression $L_{11} = \frac{0.24q^3}{\epsilon}$ and the Taylor microscale using $\lambda_{11} = \sqrt{\frac{B\nu q^2}{\epsilon}}$, where $B = 12$ for USF (De Souza et al, 1995). R_λ was determined as $R_\lambda = \frac{u_1'\lambda_{11}}{\nu}$.

	U_c	k_s	ϵ/P_r	k	L_{11}	λ_{11}	$\frac{dU_1}{dx_2}$	R_λ
	$[m/s]$	$[m^{-1}]$	$[-]$	$[m^{-1}]$	$[m]$	$[m]$	$[s^{-1}]$	$[-]$
high-speed	0.136	3.0	0.47	0.389	0.05	0.023	0.405	150
low-speed	0.073	3.4			0.05		0.25	
TK - case D	13	3.0	0.61	0.39	0.05	0.0064	38.4	360
R - case S2	0.20	4.8	0.68	0.49	0.05	0.010	0.96	124
TC	12.4	3.8	0.57	0.46	0.05	0.0058	46.8	245

Table 5.1 Selected USF results in the present and some previous studies.

5.2 Turbulent Boundary Layer Studies

LDV measurements were taken for the high and low speed cases at $x_1 = 2.6\,\text{m}$, which represented a distance of 1.25 m along the top wall. The very near wall region, down to $y^+ = 2.4$, was measured using a single component LDV system, and down to $y^+ = 3.4$ using the modified two-component arrangement, described in 4.3.1 above; with the correction applied to the latter method to correct for the angle shift of the beams, the results of the two methods were found to be very close to each other. The exact distance from the wall was estimated by observation of the beam intersection with the wall and had an uncertainty of about 0.5 mm. However, the uncertainty of relative distances between measurement points was much smaller, as it corresponded to the uncertainty of

the vertical traversing screw (approximately 0.05mm). Figure 5.11 shows measurements of the mean velocity, while Figures 5.12 and 5.13 show the streamwise and transverse rms turbulent fluctuations, respectively. A peak in the streamwise rms fluctuations was observed at approximately $y^+ = 15$. The shear stress correlation coefficient, shown in Figure 5.14, was nearly constant at about -0.45 in the lower half of the boundary layer, where the flow sees a sustained region of mean shear. A logarithmic region was obtained in the range between approximately $y^+ = 30$ to $y^+ = 100$ (Figure 5.15). Results from DNS studies at a comparable Reynolds number (Re_θ=300 and Re_θ=670, Spalart, 1988) are included for comparison and compare very closely to the present high-speed results. On the other hand, the low-speed boundary layer, although resembling a turbulent boundary layer, may not have been fully developed, as can be seen in the following analysis and will be later noted in the visual observations. An indication of this fact is that the shear stress correlation coefficient did not maintain its peak value of -0.45 in the outer layer.

Table 5.2 presents various characteristics of interest for the two turbulent boundary layers studied. The boundary layer thickness δ was defined as the distance from the wall at which the mean velocity was 99% of that in the free stream. The mean velocity profile for the high speed case was well described by Prandtl's 1/7th power-law, which resulted in δ = 0.036 m. However, in the low-speed case, the data indicated a boundary layer thickness of δ = 0.064 m, which was much larger than the estimated value of 0.039, based on a commonly used empirical relation for fully-turbulent boundary layers. This agrees with the assumption that the boundary layer in the low-speed case did not reach a fully turbulent state. The wall shear stress was estimated from the definition $\tau_w = \mu \frac{d\overline{U}}{dy}|_{y=0}$,

with the slope determined using the five data points nearest the wall. For the high-speed case, the measured value $\tau_w = 0.042$ N/m^2 compared well to that obtained using the empirical relation $C_f \approx \frac{0.027}{\mathrm{Re}_x^{1/7}}$, which provided $\tau_w = \frac{C_f \rho U_e^2}{2} = 0.046$ N/m^2. The low-speed value of $\tau_w = 0.0065$ N/m^2 was much smaller than the empirical $\tau_w = 0.014$ N/m^2. The momentum thickness was calculated from its definition $\theta = \int_0^\infty \frac{U_1}{U_e}(1 - \frac{U_1}{U_e})dy$, and the Reynolds number based on momentum thickness was defined as $\mathrm{Re}_\theta = \frac{\theta U_e}{\nu}$. The friction velocity was computed from $u^* = \sqrt{\tau_w/\rho}$.

		high-speed	low-speed
x_1	[m]	1.25	1.25
U_e	[m/s]	0.138	0.073
Re_{x_1}	[-]	172500	91250
δ	[m]	0.038	0.064
τ_w	[N/m^2]	0.042	0.0065
θ	[m]	0.0048	0.0051
Re_θ	[-]	662	372
u^*	[m/s]	0.0065	0.0025
$100\nu/u^*$	[m]	0.015	0.04

Table 5.2 Turbulent boundary layer results.

5.3 Moving Wall Studies

5.3.1 Definition of Scales and Summary of Results

As indicated earlier, the moving wall studies were performed for the low-speed case only because of limitations imposed by the belt and the speed of the motor. As well, only the case with the velocity increasing away from the wall ($dU/dy > 0$) was studied, because of its direct relevance to boundary layers and, also, the limitation of the motor speed. The flow studied represents a combination of USF and wall-bounded flow. Away from the wall

(core flow region) the flow structure is that of USF. Four different types of wall motion were considered:

- stationary wall (MW0);
- wall moving at a speed equal to the local mean flow velocity (MWE);
- wall moving in the opposite direction of the local mean flow (MWN);
- and wall moving at a speed higher than the local mean flow velocity (MWP).

Because this appears to be the first study of its kind, it has been necessary to devise new approaches for analyzing the measurements and comparing the different cases. In particular, the choice of velocity and length scales for non-dimensionalization of the flow variables in the boundary layer was not obvious. The boundary layer thickness cannot be defined as clearly as that in the conventional boundary layer, because the "free stream" has a varying velocity and is also fully turbulent, so that there is no turbulent/non-turbulent interface. From observation of the LDV data however, it was noted that the mean velocity profiles of the core flow for the three different cases coincided up to approximately the same distance δ_r from the wall, while, closer to the wall, these profiles diverged. This distance was chosen as a reference length, representative of the boundary layer thickness.

In addition, there appear to be several different relevant characteristic velocities:

- the absolute velocity of the wall U_w;
- the hypothetical USF mean velocity at the wall $\overline{U}_o$, namely the velocity obtained by extrapolating the core USF profile to the wall;

- the relative velocity of the wall $U_w - \overline{U}_o$;
- the friction velocity u^*, related to the actual wall shear stress $\tau_w = \mu\frac{\partial\overline{U}}{\partial y}$ as $u^* = \sqrt{|\tau_w|/\rho}$;
- the centerline velocity U_c;
- the flow velocity U_τ at the edge of the boundary layer, i.e. at $y = \delta_\tau$, representative of the free stream velocity.

Table 5.3 presents a summary of some relevant results in the moving wall studies, with $|\tau_w| = \left|\mu\frac{\partial\overline{U}}{\partial y}\right|_{y=0}$ measured from the data near the wall.

		MWE	MWN	MWP
U_w	[m/s]	0.025	−0.030	0.082
δ_τ	[m]	0.060	0.060	0.060
U_τ	[m/s]	0.041	0.041	0.041
$\|\tau_w\|$	[N/m^2]	0.0016	0.0108	0.0047
u^*	[m/s]	0.0013	0.0033	0.0021
$100\nu/u^*$	[m]	0.077	0.030	0.048

Table 5.3 Values of parameters for the moving wall studies

Because of the wall obstruction, LDV measurements near the wall were taken for the streamwise velocity only. Figure 5.16 shows the transverse variation of the mean streamwise velocity for the three cases studied. It illustrates the fact that the wall motion had an effect on the flow near it, but left the core flow essentially unaffected. Figure 5.17 indicates that the streamwise velocity fluctuations were also unaffected by the moving wall in the core USF. These measurements are sufficient reassurance that the USF in the core region would have the same structure as the reference case of nominally unbounded USF. By oversight, LDV measurements for the MW0 case were unfortunately not taken. As a

result, comparison of stationary-wall turbulent boundary layers in uniform flow and those in USF could not be made. This omission is not considered to be essential for the present purposes. For comparison with the moving wall studies, results from the low speed turbulent boundary layer case have been included instead (Figure 5.18a and 5.19a).

5.3.2 Wall Speed Equal to Local Flow Speed

Among the cases studied, the case with the moving wall speed equal to the extrapolated USF mean flow speed (case MWE) is probably the most useful for separating the kinematic from the dynamic effects of the wall. It has not been possible to attain a perfectly constant mean velocity gradient all the way to the wall (Figure 5.18b). Even so, the velocity fluctuations near the wall (Figure 5.19b) were significantly lower than those observed in a conventional turbulent boundary layer, and lacked the characteristic peak that is present in the latter (Figure 5.19a). The magnitude of the shear stress correlation coefficient in the wall region was substantially lower than that in a TBL and even lower than the value in the core USF.

It is interesting to note that the wall velocity for the MWE case was actually higher than the velocity of USF extrapolated linearly to the wall. This should not cause significant problems in regards to the validity of this study. The goal of the moving wall apparatus was to create a wall speed that would be equal to the USF speed extrapolated to the wall. An ideal USF, unbounded on all other sides, should have been unaffected by the presence of a wall, at rest or in motion. In practice, however, local velocity variation due to the wall caused a rearrangement of the flow in the entire channel, such that the total flow rate would be preserved. The core USF was adjusted with the tunnel flow having a free surface rather

than a wall cover. When a stationary wall was put in place, a boundary layer formed near it, creating streamline displacement and a deficit in the local mass flow rate. As the wall speed was increased, this deficit diminished, effectively allowing more fluid to pass near the wall. This can be seen in Figure 5.18b, in which the velocity profile for MWE was linear in the core of the flow, but, as the wall was approached, the velocity increased slightly above the extrapolated values before decreasing again towards the wall. This odd shape of the profile could possibly be corrected by modifying the shear generator slightly, but this would have been a long complicated process without guarantee of success, and would probably create non-uniformities in the core flow. After considering the available options, time limitations and the pioneering nature of this study, it was decided not to attempt further changes in the oncoming USF profile.

5.3.3 Wall Motion Opposing Local Flow

Reverse wall motion (MWN) created a narrow reverse flow zone near the wall (Figure 5.18c). Velocity fluctuations were quite high in the direct vicinity of the wall corresponding to the increased shear levels present (Figure 5.19c). The peak in velocity fluctuations seems to be greater than that found in the conventional TBL case, if one uses the reference velocity U_r as a free stream velocity.

5.3.4 Wall Motion Faster Than Local Flow Speed

With the wall moving faster than the local flow (MWP), the near-wall flow was drawn forward due to friction with the wall. The mean velocity profile had a minimum (zero-shear point), between regions of negative and positive shear (Figure 5.18d). This

complication created significant changes in the velocity fluctuations, as seen in Figure 5.19d. The level of velocity fluctuations was directly related to the magnitude of the local mean velocity gradient, irrespective of its direction. Starting from the core flow and moving towards the wall, the mean velocity gradient decreased, first linearly and then non-linearly, till it reached its minimum, around which the velocity fluctuations also diminished to a minimum. On the other side of the minimum, the mean velocity increased with decreasing distance from the wall, and the velocity fluctuations increased until a peak was reached at some point near the wall. As the wall was further approached, velocity fluctuation levels dropped again. The drop in velocity fluctuations from their peak towards the wall is especially important to note, considering that the shear in the flow remained fairly constant up to the wall. This decrease could be attributed to the kinematic effects of the wall, which impeded fluid motions and velocity fluctuations.

5.3.5 Comparison of Moving Wall Studies

The differences in flow behaviour for the cases studied are apparent when comparing the corresponding LDV measurements. The mean shear created by the no-slip condition at the wall and the relative wall velocity had a great impact on the flow and the turbulence activity as the turbulence intensity seemed to be directly affected by the local mean velocity gradient.

The present results may also be used for testing the universality of the law of the wall. This requires normalization of the results by wall variables. The dimensionless velocity deficit was defined as $u^+ = \left|\overline{U}_1 - U_w\right| / u^*$, so that it was always positive, even in the MWP case, where $U_w > \overline{U}_1$. The present measurements are summarized in Figure 5.20. It may

be seen that the velocity deficit in the MWN case followed very closely the logarithmic law in the range $30 < y^+ < 100$. In the MWP case, the velocity deficit overlapped with the logarithmic law only in a narrow range. In contrast, in the MWE case, this deficit did not follow the logarithmic law at all; this seems to be consistent with the expectation that removal of the shearing effect of the wall would completely alter the local turbulence production process and, thus, the turbulence structure.

Chapter 6

Visual Studies

6.1 Interpretation of the Observed Images and Arrangement of Optical Components

The interpretation of the visual images obtained is an important aspect of this research. Depending on the orientation of the laser-sheet, different views of the patterns present in the flow were obtained. Based on these views, one may attempt to reconstruct the 3-D features of these patterns at a fixed time. Furthermore, by following these patterns through a sequence of videotaped images, one may describe their evolution in time.

Unfortunately, the extraction of flow characteristics from dye concentration patterns is not always easy. The dye was injected from thin tubes, initially forming continuous streaks. Thus, a circular dye pattern indicates a vortical motion present in the flow, with vorticity normal to the plane of the laser-sheet. The strength of the vorticity can be inferred, albeit in a qualitative sense, from the intensity of relative motion in the video.

Pairs of counter-rotating circular dye patterns represent pairs of counter-rotating vortices. These may be interpreted as the legs of a curved coherent structure, but the nature of such structure depends on the shape and orientation of the vortex pair, the distance between the two vortices and the dye patterns in the regions between and surrounding the pair. Thus, vortex pairs that are far spread apart with a single streak of dye connecting them represent a type of structure different from a mushroom-shaped, closely spaced pair of vortices.

Long streaks of dye are suggestive of elongated structures or the flow between structures, and were often useful in determining overall rotation in a flow and relative motion of structures. The motion of structures along the laser-sheet from one edge to another provided information on the development of the structure on the plane of the laser-sheet. Relative velocities within the structure or between neighbouring structures could also be inferred from the video.

The appearance or disappearance of a region of dye on the observation plane indicates motion through the plane of the laser-sheet. An indication of the 3-D dimensions and shape of a structure can also be determined as the dye pattern grows or shrinks in size and moves along the plane.

Images were taken near the downstream location $x_1 = 2.6$ m, unless otherwise indicated. Images for the core flow were taken around the centreline of the flow, while images for the wall flows were taken near the belt, located on the upper side of the flow. The video camera could be mounted on a tripod and positioned underneath the tunnel or facing the window at the downstream end of the tunnel or on the traversing system on the

side of the tunnel. The laser-sheet lens was either mounted on the traversing system on the side of the tunnel or fastened on a support underneath the tunnel. To illuminate the flow at an inclination of 45°to the flow direction, the laser-sheet lens was mounted on the side of the tunnel and rotated around the x_3 axis. In this case, the camera was positioned either directly below the laser sheet, giving a skewed view of the sheet, or perpendicular to the sheet, creating some slight distortion effects that did not hamper visualizing the flow. No mirrors were used in the processes of illumination or recording and the flow was not disturbed in any way. Reflections of the laser sheet by the belt were sometimes present in the images and should be ignored.

In order to provide an approximate size reference, the width of the laser-sheet intersection with the belt, when the light was projected from below, was measured to be 0.23 m. For most other images in which the top wall was not visible, the width of the laser sheet in the center of the image could be used; this was found to be approximately 0.18 m. The laser-sheet lens and camera could also be traversed in the downstream direction in order to provide the development of flow patterns in a moving frame. An approximate convection speed and the downstream location of each frame were determined from the time lapse in the video in reference to two tape marks located at the top of the glass wall, 1.50 m apart. Traversing in the transverse (vertical) direction was also possible with the use of a double threaded screw driven by a stepper motor. Typical traverse speeds in this direction were about 5 mm/s, extending over the total height of 70 mm. Manual traversing in the spanwise direction was also attempted in some cases to reveal the spanwise extent of the observed flow patterns.

In the frame sequence images shown, transformations to the images have been applied to make them more presentable. The original image was a frame grabbed from the original digital video recording. This consists of two fields (or half-frames) of interlaced video, each taking even or odd lines of the image and putting them together. There can be a slight shift seen in the image due to this process, but it is generally negligible at lower speeds. The images were then converted from 24-bit RGB colour to 8-bit black and white grayscale for ease of printing, without loss of information, if one considers that the information consisted primarily of a black background and one colour of fluoresced dye. In most cases, the images were adjusted further to remove what would be considered as visual "noise", essentially attempting to minimize the appearance of the laser sheet itself in order to define more clearly any dye patterns that were present. This was simply done by adjusting the brightness, contrast and intensity of the images. "Before" and "after" images were compared to ensure that no essential information was lost or distorted, and that the "after" images were indeed more clear.

6.2 Core USF Studies

For the high speed case of USF, video recordings were made simultaneously with still camera pictures, in conjunction with the work of Sebastien Marineau-Mes (2002, thesis in preparation). This case did not permit the capturing of clear video images and is not included in this thesis, although some observations were used in comparisons with those of the low speed case. Low speed USF was documented visually for both orientations of the mean velocity gradient, with most emphasis on the case with the positive gradient, due to

its relevance to the boundary layer configuration.

6.2.1 Observations

Frame sequence 6.1 represents a side view of structures in low speed USF, with the camera moving at the local speed of the flow, or approximately $0.07m/s$. The structure observed in the centre of the image could very likely represent a hairpin-type vortex that moves spanwise, crossing the plane of the laser sheet. In Frame 6.1a, the central vortical structure has a fairly rounded shape, with other structures upstream and downstream of it. The fore and aft structures could be induced by other structures as well as inducing hairpin structures themselves. More interesting, however, is to follow the central pattern (marked as A) in Frames 6.1b-e, where it can be easily observed to stretch and rise, while losing the vortical appearance. The most likely explanation is that Frames 6.1d-e show the legs of the hairpin, which has crossed the laser sheet in the spanwise direction.

Frame sequence 6.2 represents core USF with less dye injected in the flow, compared to Frame sequence 6.1. This sequence clearly defines a pair of vortical structures, marked A & B, which form at almost the same time, and have comparable sizes and angular velocities. Of note is the fact that, in both Frames 6.1 and 6.2, the observed vortical patterns generally moved toward the higher velocity region, although the two frame sequences corresponding to opposite directions of shear. Another interesting observation in Frame sequence 6.2 is the similarity of the structures observed in core USF to the dominant coherent structures that have been observed in two-dimensional mixing layers. It appears that USF contains localized mixing layers between two masses of fluid moving at different speeds, which generate chains of vortices rotating from the high speed towards the low speed

regions as they move downstream. Such chains of vortices were actually observed in the present flow, although not particularly frequently.

Frame sequence 6.3 represents a situation where dye was introduced in larger amounts to mark a wider region of the flow. In the video, dye patterns can be observed to move in all directions, but, on the average, one may notice a general rolling of the high-speed fluid into the low-speed fluid. Near the top of these images, a vortical structure (marked in a square) can be observed to travel toward the higher speed fluid relatively fast. This high speed motion of vortical structures in the transverse direction is of great interest, because it may relate to the growth process of vortical structures in a shear flow and, thus, to turbulence production.

Frame sequence 6.4 shows the core USF viewed from below with the laser sheet parallel to the $x_1 - x_3$ plane. Many vortical patterns can be observed, with rotation in both directions, indicating structures with transverse vorticity. Observed patterns include: mushroom shaped pairs of counter-rotating vortices (Frame 6.4a), a singular vortical structure with a long streak connecting it to the bulk of the dye (Frame 6.4b), dye streaks forming long and wavy lines (Frame 6.4c), and vortical patterns in interconnected chains with random direction of vorticity (Frame 6.4d). In the video, structures of dye could also be observed to cross the laser sheet indicating motion of structures in the transverse direction.

Rear viewing of the core USF was not very successful as it resulted in unclear images that travelled very quickly across the laser sheet. Instead, spanwise visualization of the core USF was best observed with the laser sheet at a 45°angle. In Frame sequence

6.5, the laser sheet was inclined at 45°with respect to the $x_1 - x_2$ plane and such that it agreed with the sense of the mean velocity profile. The dye was observed to cross the laser sheet very rapidly, creating traces that appeared and disappeared very quickly. The dye crossing the laser sheet rarely formed recognizable patterns and did not travel along the sheet, which implies that the coherent structures in the flow were elongated and inclined by angles near 45°with respect to the flow direction. Small vortical structures were observed very infrequently and were not typical events in the flow.

With the laser sheet inclined at 45°with respect to the $x_1 - x_2$ plane, but in a sense opposite to the mean velocity profile (Frame sequence 6.6), the observed patterns were very different from those in the previous case. The dye was observed to cross the sheet and travel along it for a long distance. This observation is consistent with the concept that coherent structures were inclined with respect to the flow direction. The structures that were observed in this sequence were especially interesting because they most often consisted of pairs or chains of counter-rotating vortices, originating in the same region of dye. These pairs were not aligned, but instead spread out spanwise from one another as they travelled in the plane of the laser sheet. This does not necessarily indicate motion in the spanwise direction, but that these structures had shapes that stretched in the spanwise direction, revealing themselves gradually as they crossed the laser sheet. The dye patterns seen from this angle changed very quickly, especially with spanwise motion, but they consistently started at the upstream edge of the laser sheet and travelled along it in the streamwise direction, with a streak of dye being easily tracked as it flowed downstream. At least three different structures, marked A, B & C, can be followed in Frame sequence 6.6 as they

travelled along the laser sheet in very short time intervals. Frame sequence 6.7 shows similar results as those in Frame sequence 6.6, although the two frame sequences correspond to USF with opposite mean shears. In Frame sequence 6.7, the vortical structures could again be tracked as they travelled downstream. Pattern A consists of a pair of counter-rotating vortices, one of which eventually evolved into a new pair of counter-rotating structures. Structure B shows the spanwise extent of a wide structure of fluid.

6.2.2 Comparisons with Previous Studies

Viewed from the side, USF was found to contain several different types of structures. The most recognizable ones were vortical structures of very strong spanwise vorticity, with axes parallel to the mean vorticity axis. The other major observation made was the stretching and elongation of the regions of dye in the direction of the velocity gradient. Along with the stretching, regions of higher and lower speed fluid could be easily distinguished, sliding over and around each other. The regions of high vorticity clearly defined coherent structures and could represent the heads of hairpin-type or similar vortices. Of equal interest was the stretching and rolling of the entire flow. The higher velocity region continually seemed to be pulling ahead of the lower velocity region, and generally rolling over and into it, in a manner similar to that observed in two-dimensional mixing layers. The coherent vortical structures seemed generally to tilt at a forward angle, not always approximately equal to 45°. Some structures moved quickly in the streamwise direction, or more commonly in the transverse direction toward the higher speed flow. The transverse motion of the vortical structures is of great interest because it can help in the understanding of the bursting process of spanwise vortical structures in the boundary layer as they leave

the inner layer. The transverse motion could be caused by the Magnus effect, due to the fluid rotation (such as at the head of a hairpin), or just as likely caused by the upward motion of fluid induced between the legs of a hairpin. There could also be a relation between adjacent vortical structures, as they were on occasion noticed to be present in pairs or organized patterns. The dye streaks that formed the vortical structures had trailing edges that indicated the turning of the structures away from the dye origin; in contrast, their leading edges were typically drawn into a helical motion towards the interior of the vortical structure. These leading and trailing edges could be considered to represent the legs of a hairpin, or the shear layer formed behind a hairpin vortex, but no conclusive observation can be made.

6.3 Turbulent Boundary Layer Studies

Visualization of the boundary layer was performed for the high speed case only from views with the camera to the side of and underneath the flow. The greatest detail of information can probably be found from the view below the tunnel, in which cross-sections of the flow at various distances from the wall could be seen. Streaks, regions of concentrated dye, counter rotating vortices and hairpin-type structures were all observed in these two views. Viewing structures from the rear of the tunnel or at a 45°angle were not very clear because of the relatively high speed and small size of the structures as well as the large number of structures present in the boundary layer.

For the high speed case, visualization clearly indicated a fully turbulent boundary layer. In the low speed case, however, the boundary layer was observed to grow from a

transitional state and may or may not have become fully developed at the location of study, which agrees with measurements taken of this flow. The flow patterns observed during transition were very interesting but were not included in the present study whose subject was the structure of fully developed turbulence. It is worth mentioning at this point that, when the free stream was turbulent, the near wall flow also appeared to be fully turbulent, even in the low speed USF case (MW0).

6.3.1 Observations from the Side

Visualization of the turbulent boundary layer from the side, shown in Frame sequence 6.8, identified vortical structures of spanwise vorticity, which were found both in the near wall region and the outer boundary layer. The most commonly observed vortical structures had a negative spanwise vorticity and were produced in the boundary layer. In the near wall region, they appeared as masses of fluid spinning very rapidly along the wall with nearby dye at the wall being drawn in or around them. Occasionally, they disappeared from the image, and at other times they lifted away from the wall to the outer region, with a trail of dye forming behind them. The structures formed near the boundary layer edge were clearly observed as they entrained free-stream, dye-free fluid into the boundary layer. In general, these structures had comparable sizes, speeds of rotation and overall motions and growth rates. Larger vortical structures sometimes appeared, often consuming or entraining smaller ones, and creating a complex image of interacting vortical motions. Independent vortical structures with positive spanwise vorticity were also occasionally present, but these were quickly entrained into another structure.

A distinct type of structures that were often observed was mushroom shaped struc-

tures, with a slight rearward or forward inclination. These comprised a pair of counter-rotating vortices, connected and in motion together, with a shear layer formed at their front. These structures could represent a burst of fluid ejected away from the wall region, which has been identified as a positive contributor to the production of turbulence. Such structures have been observed to start with an initial rearward orientation, but, as they move away from the wall and enter a higher streamwise velocity region, the mushroom head would be rotated toward the downstream direction. Often, one half of the mushroom would get absorbed into another vortical structure having the same direction of vorticity.

Although following these structures over the short wall length was difficult, they were often seen to leave the wall region only to be dragged back inward to the wall by another structure. In fact, it would seem that the entire boundary layer region frequently rolled back into itself, with only the exceptional vortical structure managing to escape into the core flow to entrain free stream fluid into the boundary layer.

The structures and activity in the inner layer can easily be observed with the use of a laser sheet and dye, whereas other flow visualization methods often obscure the inner layer region. However, the scale of the structures observed is still limited by the camera lenses, the dispersion of dye, and the ability to capture a wide region of flow. A thin layer of dye seems to hug along the wall over most of its length. This thin layer seems to often form waves that shrink and grow, and often the wave head ends up leaving this thin layer to start a vortical structure. This all occurs in a region separate from the outer boundary layer where larger vortical structures dominate, and could possibly be a defining region for an inner boundary layer region. Although "inner" structures were clearly seen to migrate to

the outer layer, it was not clear in the present study whether the "inner" structures related to the "outer" structures and, if so, how.

6.3.2 Observations from Below

The changes in the boundary layer structure as the distance from the wall increased were seen very clearly when viewed with the laser sheet parallel to the wall (Frame sequence 6.9).

In the viscous sublayer (Frames 6.9a-b at $y^+ \approx 1$ and 7, respectively), streaks of slower moving dye formed between regions of highly turbulent fluid. The low-speed streaks appeared to be recirculating backward as the faster and more turbulent structures interacted with the wall. The streaks formed were generally much longer than the individual turbulent structures. In general, the streaks were inactive and tended to be interconnected, almost as if they formed a sheet of slow dye along the wall, penetrated by the turbulent structures. The streaks seemed to be the regions of dye where turbulent structures were not present and they tended to align themselves in the streamwise direction. This statement appears to be a novel interpretation of the terms high- and low-speed streaks, which is not necessarily inconsistent with previous interpretations, but which clarifies the type of fluid in the high- and low-speed regions. A streak has been defined by a fluid marker, whether it be hydrogen bubbles, dye, or other marker, which more likely collects in the low-speed region of a flow. Any low-speed region must be near a region that has relatively higher speed. In this research, the term streak is used to represent the low-speed fluid because it has a smooth, laminar-like appearance, whereas the high-speed region was formed by a variety of structures of higher speed.

As an indication of the relative spanwise spacing between streaks, the length scale $100\nu/u^* = 0.015$ m has been indicated on the frames. Although the spanwise spacing of the streaks varied quite a bit over their length, it was generally comparable to this length scale. The spacing between streaks and the size of the majority of the turbulent structures were also of comparable magnitudes.

As the laser sheet was moved further away from the wall (Frames 6.9c-e at $y^+ \approx 27, 68$ and 136, respectively), a different type of structure, having transverse vorticity, appeared. It was difficult to assign a specific pattern to these vortical structures, except that they often appeared in counter-rotating pairs or were connected together in a chain, and were offset in the streamwise and spanwise directions. This indicates that the spanwise extent and intermingling patterns of the structures were important.

Finally, as the laser sheet passed to the outer region of the boundary layer (Frame 6.9f at $y/\delta \approx 0.83$ and Frames 6.9g-i $y/\delta \approx 1.1$) the flow intermittency became apparent. The heads of turbulent structures were clearly defined as pairs of counter-rotating vortices with a mushroom shape facing upstream. Tails formed behind the mushroom heads, which would seem to indicate the origin of the structure.

6.3.3 Comparison of Studies

In summary, the present observations were in good agreement with previous work. The observed coherent structures included mushroom shaped structures similar to those that Falco (1977) described as typical eddies which are responsible for turbulence production. The viscous sublayer was seen to be dominated by the presence of streaks, as observed by many previous researchers. Along with the presence of streaks, the use of LIF has allowed

us to observe the presence of structures impacting with the wall in the viscous sublayer, not normally viewable with other visualization techniques. When comparing the appearance of boundary layer structures with those seen in USF, one may conclude that structural similarities exist between the outer boundary layer region and unbounded USF.

6.4 Moving Wall Studies

As explained earlier, flow visualization with the moving wall was performed only for the low speed USF core flow ($U_c = 0.073$ m/s). These studies focussed mostly on the wall region and its interaction with the core USF, which seemed to be unaffected by the wall presence or motion.

Viewed from the side, the appearances of the flows corresponding to the four cases of moving wall speed were quite distinct from each other. The characteristics that are of interest in this work are the shapes of typical eddies that are formed, the motion of these eddies, the growth rate of the region affected by the wall and the wall effects on the core USF, if any. Observations are based on dye patterns. It is assumed that dye streaks that remain together for long durations indicate low turbulence activity. Dye patterns that appear as highly diffused and spread widely indicate high turbulence level in the flow.

6.4.1 Stationary Wall

For the case with stationary wall (case MW0), structures similar to those in the conventional boundary layer case were observed, taking into account the fact that this flow had a lower Reynolds number than the reference turbulent boundary layer. When

viewing this flow from the side (Frame sequence 6.10), one could observe dye that tended to concentrate in the near wall region and vortical structures forming near the wall and extending away from it into the core region. The boundary layer grew downstream and the number of observable structures increased. However, a narrow region near the wall seemed to maintain itself without much downstream growth, but continuously producing vortical structures that eventually left the wall region. The wall flow was often observed to be slowed down, as if by an obstruction in its path, and redirecting some of the near-wall fluid away from the wall. This can be possibly attributed to the approach of a coherent structure, which either originated in the core USF, or more likely originated in the boundary layer, left the wall region and returned towards the wall again.

When viewed from below (Frame sequence 6.11), the flow structure was similar, but of much lower intensity, to that in the high speed boundary layer case. Low-speed streaks were observed in the very near wall region with dye forming patterns of large spots between the streaks, presumably structures impacting with the wall. An estimate of the spanwise streak spacing $100\nu/u^* = 0.040$ m (inferred from LDV measurements for the MWN case, because such measurements for the MW0 case were not available) has been included in Frames 6.11a and b, and seems to be comparable with the spacing between streaks. As the distance from the wall increased, the streaks disappeared and vortical structures appeared in the flow. At sufficiently large distances, the flow appearance became similar to that in the core USF.

Focussing now in the inner region more closely (Frame sequence 6.12) one may observe a turbulent blob with slower moving fluid around in the form of streaks. The

turbulent blob seems to represent an entity of fluid impacting on the wall and most likely breaking up into smaller structures. The impacting of an external structure would also seem to be the cause for the slower inner layer fluid to collect together, forming a streaky pattern. The origin of this external structure cannot be determined from this view, but the effect of the wall on physically breaking up the structure and organizing the slow inner fluid into streaks seems to be of major significance.

From the rear of the tunnel, the laser sheet clearly defined a planar cross-section of the flow. However, the patterns observed in this view were rather difficult to interpret, due to the speed by which the dye crossed the sheet as well as the loss of clarity due to the considerable amount of dye in the fluid between the observation plane and the camera. Frames 6.13 show a region of dye that maintained itself close to the wall, often forming peaks of dye at the wall. In the core flow, structures were difficult to discern, but generally indicated streamwise vorticity and interconnection with other structures.

Frame sequence 6.14 provides a planar view of the wall flow at a 45°angle with the wall, in the opposite direction of the velocity profile slope. It is difficult to discern information from the very near wall region, however the development of structures originating from the wall is clearly seen. Vortical patterns can be observed, indicating structures with streamwise and/or transverse vorticity. The structures generally originated in the wall region, as can be seen by the trails of dye behind the structures that led down to the wall. In these frames, a centerline of the frame has been drawn as a reference for the relative motion of the structures. Structure A, which seemed to originate away from the wall, had a slight motion toward the wall as the frames progressed. Structure B, on the other hand,

which in the first frame seemed to originate from the same mass of fluid as structure A, as the frames progressed, can be seen to originate from the wall region and seems to be related to a separate counter-rotating vortex (structure D) in Frame 6.14c. Structure C seems to be a streamwise vortex that stayed in essentially the same relative position throughout this sequence of frames and did not lift away from the wall. By observation of the full video sequence, one may identify a definite motion of vortical structures along the laser sheet plane toward the wall region, as well as a slowing down of this motion as the wall was approached. This would indicate that the structures were elongated in the downstream direction away from the wall, and had a relatively long residence in the near wall region before they were lifted away from the wall.

6.4.2 Wall Motion with Speed Equal to the Local Flow Speed

The near-wall region with the wall moving at the local flow speed (case MWE) had a distinct appearance. Frame sequence 6.15 presents a side view of this region, which appears relatively free of dye and without the typical vortical structures observed in the stationary wall case. Some relatively weak structures were sometimes identifiable, but these could be caused by the imperfect matching of the wall velocity to the local mean flow, and, in any case, they were not a strong feature in the flow. Structure A in Frames 6.15c-d, for example, was a vortical structure with vorticity direction in the negative spanwise direction, which was slowly being rotated by the flow that had a positive mean spanwise vorticity, and eventually disappeared (the disappearance has not been shown in the presented frames but could be seen on the full video sequence). Structures from the core region of the flow did not seem to be influenced by the wall. Regions of fluid marked by strands of dye were

seen to approach the wall region, with no distinct result or effect to the flow.

Frame sequence 6.16 presents a view from below. These images show streaks near the wall similar to those in the stationary wall study. Similarly to the MW0 case, as the laser sheet was moved away from the wall, these streaks disappeared and structures similar to those in core USF appeared. It is difficult to determine whether and how the MWE and MW0 cases differed when viewed from below, possibly due to the low turbulence levels, or possibly because the kinematic effects of the wall were similar in both cases. In Frames 6.16a and b, the typical spanwise spacing of streaks did not seem to match very well with the scale $100\nu/u^*$. This is consistent with the fact that the MWE case was quite different from conventional turbulent boundary layers to which this scale applies.

When viewed from the rear (Frames 6.17) the structure of the MWE case looked very similar to that in the MW0 case, with a little bit less dye remaining near the wall. A mushroom-shaped structure can be clearly observed in Frame 6.17c. This structure remained in the same region for a long time, indicating that it was not moving away from the wall area.

When the laser sheet was inclined at a 45°angle with respect to the wall and in a sense opposite to the slope of the mean velocity profile (Frame sequence 6.18), fewer and less organized structures could be observed. As the sequence progressed, these structures appeared to move toward the wall, which indicates that they were elongated and inclined in the same direction as the mean velocity profile. Occasionally, a structure seemed to originate near the wall, similarly to observations in the MW0 case, but such events were much less frequent and did not extend as far away from the wall as those in MW0. Fluid from the

core flow seemed to reach all the way to the wall, although there was very little interaction or activity there. Although the wall presented a physical barrier that the structures could not cross, it otherwise affected the structures very little until they came really close to it, where they gradually disappeared.

6.4.3 Wall Motion Opposite to the Local Flow Direction

In the case of wall motion opposite to the local flow direction (case MWN), the near wall region was exposed to higher levels of shear than any other case. When viewed from the side (Frame sequence 6.19), the flow was seen to contain vortical structures which were much more dominant than those in the other cases. Furthermore, the boundary layer in the MWN case seemed to grow further into the flow. Recirculation of flow near the wall could also be observed. The dye diffused rapidly downstream, which indicated a stronger turbulence activity than in the other cases. Structures originating in the core USF were often seen to interacted with the outer region of the boundary layer, but, because of the high turbulent diffusion of dye near the wall, it was difficult to observe details inside the boundary layer.

The side view of the wall region was investigated in more detail to obtain information on the spanwise extents and shapes of the vortical structures leaving the wall region. This was accomplished by a quick traverse of the laser sheet in the spanwise direction, while video recording from the side. A sample of such results is shown in Frame sequence 6.20, which shows two vortical structures (indicated by arrows), most likely hairpin vortices captured in three dimensions. The total spanwise distance traversed for this sequence was approximately 50 mm and the centreline of the frame has been drawn as a reference. The

head of the hairpin was formed by a vortical structure in the outer region of the boundary layer, with a trail of dye indicating its origin near the wall. As the laser sheet was moved in the spanwise direction, the visible part of the structure maintained a similar shape, except that the head of the hairpin was moving toward the wall. This pattern continued for the entire 50 mm span covered.

Viewed from below (Frame sequence 6.21), the structure of the MWN flow was difficult to discern, as the dye was highly diffuse. Even so, this structure seemed to be similar to that in the high speed boundary layer case, with streaks interspersed with active turbulent structures. As distance from the wall was increased, a highly turbulent region was observed, similar to that in the high speed TBL, but with the dye more highly diffused and no regions of intermittency. Although it was difficult to discern the streaks, their typical spanwise spacing seemed to fit the scaling of $100\nu/u^*$.

>From the rear (Frame sequence 6.22), case MWN can be seen to contain structures with streamwise vorticity, often appearing in counter-rotating pairs and moving toward the wall as they crossed the laser sheet. This is consistent with the side view observations that the structures were inclined in the direction of the velocity profile. At the wall, a small layer of dye was formed from the structures in the flow that originated near the wall. This layer changed thickness in the spanwise direction and appeared to be the origin of structures which originated in the inner layer and lifted up into the flow. This statement, however, cannot be definitely proved by the presented information and would require simultaneous recording of two views of the flow for a more reliable evidence. It can be mentioned at this point that the MWN case provided the most information on the flow from the rear view,

due to the large spread and diffusion of dye being clearly picked up by the video camera.

With the laser sheet inclined at a 45°angle with respect to the wall, and in a sense opposite to the slope of the mean velocity profile (Frame sequence 6.23), one could see the formation of structures similar to those in the MW0 case but with a larger extent into the core USF. Vortical structures with components of streamwise and/or transverse vorticity could be observed, generally linked in pairs or in chains of counter-rotating vortices. These structures travelled along the laser sheet from the core USF to the wall (see Structures A, B & C), which indicated an inclination in the direction of the USF velocity profile, and covered a wide spanwise region.

6.4.4 Wall Motion with Speed Higher than the Local Flow Speed

When the wall velocity was greater than the local flow speed (case MWP), the mean shear changed direction at some point in the flow. A side view of this flow (Frame sequence 6.24) shows two regions with distinct structures. In the region closest to the wall, which has a shear opposite to that of the core USF, dye streaks were inclined at opposite inclinations as dye streaks in the core USF. In this region, there seems to be a tendency towards relaminarization of the flow, as indicated by the dye forming very smooth streaks, stretched forward by the wall motion. However, some vortices did form on occasion in this region and appeared to be very similar in shape to the vortical structures produced in the stationary wall case (MW0), although at a much lower frequency and oriented in the opposite direction (Frames 6.24e-f). These vortices tended to grow away from the wall, but their growth was arrested in the zero-shear region between the wall flow and core USF. This is a very important observation because it indicates that the formation and growth of

vortical structures in the wall region depends on the shear direction and not the direction of the streamwise velocity. The growth of the structures away from the wall is also very important, because it was opposite to the behaviour of many vortical structures observed which tended to move toward regions of higher streamwise velocity. Another feature of the MWP case was the low-shear region between the wall flow and the core USF flow. In this region, there seemed to be little evidence of vortical structures and no stretching of the dye in the flow. Vortical structures generated in the core USF were sometimes observed to approach the no-shear region but only rarely to cross it. The energy of these structures was generally diminished in the low-shear region.

With the laser sheet parallel to the wall, viewed from below, Frame sequence 6.25, streaks are found in the inner wall region very similar to the MW0 case. Turbulent structures begin to appear as the laser sheet travels away from the wall. Exact correlation to the structures and which region of the flow they are in (negative shear, no-shear, positive shear) is not necessarily very reliable. From the video it can be seen that at a certain height, structures are present but not as active and probably relate to the no-shear region, of which Frame 6.25c may be a good representation. Also of interest is the spanwise streak spacing which appears to follow the general guideline of $100\nu/u^*$, indicating a similar behaviour in this boundary layer to conventional turbulent boundary layers, even though the wall is inducing a forward motion in the flow.

When viewed from the rear, Frames 6.26, structures are observed in the wall and core USF regions. In the core USF, the structures cover a large spanwise width, and generally first appear in the laser sheet first toward the core, and move downward toward,

but not to, the wall as the flow passes the sheet. In the wall region, dye usually first appears at the wall, and as the flow passes across the sheet, seems to form structures that grow away from the wall. This confirms that the structures that originate from the wall are lifted away from the wall in the upstream direction. The two different types of structures meet at a point which would relate to the zero-shear region of the flow, where the structures tend to vanish across the sheet. Of note for the MWP case is that the structures were observed to travel in the spanwise direction more than in the other cases, with unknown explanation.

With the laser sheet inclined at a 45°angle with respect to the wall, and in a sense opposite to the slope of the core mean velocity profile (Frame sequence 6.27; the centreline of the frame has been added to the image as a reference for relative motion), the MWP case was also clearly seen to contain two regions of opposing shear separated by a low-shear region. The structures in the core USF appeared to move toward the region of zero-shear, indicating an inclination of structures along the slope of the core USF velocity profile (Structure A). Conversely, the structures that originated at the wall appeared to move outward toward the core USF, with an inclination opposite to that of the core USF structures (Structure B). Structures from the two regions sometimes met in the low-shear region, where they usually tended to disappear, or sometimes to join together.

6.4.5 Comparisons of Wall Studies

The observations made for the different cases of wall motion may be combined to provide the following conclusions. The MW0 case represents a bounded wall flow in which the effect of wall-induced shear was not as pronounced compared to a conventional boundary layer. In both cases, the mean shear was maximum at the wall. However, in the

conventional TBL case, it decreased gradually to zero at the free-stream, which is a more severe change than that in the MW0 case, in which the mean shear gradually matched the core USF value. The structures observed in the MW0 case showed a smooth growth away from the wall and were slowly drawn forward by the core USF, unlike the conventional boundary layer in which structures that reached the free-stream were abruptly changed. On the other hand, a stationary wall exposed to either a uniform stream or USF seems to have similar effects on the fluid in its near vicinity. The immediate slowing down of the fluid at the wall, the formation of streaks and structures impacting the wall were clearly observed in both cases. The structures that were formed in the near wall region appeared to be similar, but their departures from the wall region varied due to the difference in the shearing away from the wall.

When viewed from below, all four cases indicated the presence of streaks very near the wall. This would seem to indicate that the wall has a limiting affect on fluctuations very close to its surface regardless of its relative motion to the flow. This would conform to the "no-slip condition" applying to the fluctuations of the velocity. Comparison of the mean spanwise spacings between streaks indicated that the scale of $100\nu/u^*$ would appear to apply to all the cases except MWE. If we consider that the streaks represent low turbulence, near-wall fluid pushed aside as coherent structures impacted with the surface, and that structures from the inner region of the boundary layer have been viewed to impact with the wall, it would seem plausible that the streak spacing would most likely scale with wall variables. This would agree with our findings, considering that the MWE case is the only one where no structures were created near the wall, and the only structures that approached the wall

had originated in the USF core. The streaks in the MWE case were much less distinct and frequent, which agrees with the fact that structures from the USF generally moved toward higher velocity regions rather than towards the wall. This motion of structures of spanwise vorticity toward regions of higher streamwise velocity also supports the idea that it was the structures from the wall region that were most often impacting with the wall, and not those from the outer region. All this considered, the spanwise spacing of streaks would also provide a lengthscale for the turbulent structures produced at the wall, namely $100\nu/u^*$.

Further away from the wall, the view from below provided little more information on the individual character of each case due to similarities in the flow and the low frequency of appearance of patterns that could be used for comparison.

The rear view of the flow was difficult to extract clear information from. The turbulence activity in the flow, measured by the diffusion of dye, was definitely the highest for the MWN case and the lowest for the MWE case. Flow observation from the rear of the tunnel revealed structures crossing the laser sheet and was expected to provide three-dimensional information on these structures; unfortunately, the structures crossed the sheet too fast for the video camera to properly identify them.

Views obtained with the laser sheet inclined at a 45°angle, provided a clearer observation of the spanwise dimension of the structures than the rear view could provide, while taking advantage of an assumed elongation of the structures to better describe their shape. The MWN case, and to a limited extent the MW0 case, showed much more activity than the MWE and MWP cases, and the structures found in the former two cases seemed to be more complex and interconnected than those found in the latter two cases. The motion

of structures along the laser sheet clearly indicated the direction of elongation and origin of the structures. For the MWP case, this also provided a good comparison for the two shear regions. Although not shown in this thesis, images taken with the laser sheet inclined at a 45°angle in the same sense as the slope of the mean velocity profile were consistent with the assumed shape of the structures. However, the structures were difficult to observe as they quickly crossed the laser sheet and one could not extract any additional information from this view.

The reference boundary layer thickness, δ_r, has been included in Frame sequences 6.10, 6.15, 6.19 and 6.24. It can be seen for most cases that a wall flow region was formed within δ_r, while, beyond it, the flow behaved more typically like the core USF flow.

Chapter 7

Discussion

7.1 Core USF

7.1.1 Measurements

USF was studied with the goal of obtaining the first visual records of the large-scale structure of this type of flow. For meaningful comparisons with previous studies, it was first confirmed that the present flow had a nearly uniform mean velocity profile and that its Reynolds stresses were not severely inhomogeneous on the transverse plane. The development time, also referred to as total strain, was sufficiently long for the turbulence to reach its asymptotic development state, for both the high-speed and low-speed cases studied (the total strain at the centerline was up to $\tau = 10$, for the high speed case, and $\tau = 15$, for the low speed case). The Reynolds stresses developed similarly in both cases. In the high-speed case, an exponential growth region was clearly defined for $\tau > 5$, as $q^2 = q_\tau^2 e^{k\tau}$, where $q_\tau^2 = 0.0000361$ m^2/s^2 and $k = 0.389$ m^{-1}. In agreement with the USF results of

Tavoularis and Karnik (1989), the growth exponent k was related to the flow generator constant $k_s = (1/U_c)\left(d\overline{U}_1/dx_2\right)$ as $k \approx 0.1k_s$.

Closer inspection of Reynolds stress profiles indicated measurably larger magnitudes in the lower speed regions than in the higher speed regions. This was reinforced by the value of the coefficient $\overline{u_1 u_2}/\left(u_1' u_2'\right)$, which reached the conventional level of -0.45 only in the low-speed region of the flow. It would seem that the flow was better developed in the low speed region, where the total strain, based on the local (and not the centreline) mean velocity, was higher. This apparent inconsistency is a known limitation of USF (Champagne, Harris and Corrsin, 1970) but should not cause any significant problem for the present study. In any case, the present study of the interaction of USF and wall flows utilized mostly the low-speed part of USF, in which flow development was complete.

7.1.2 Flow Visualization

The large-scale turbulence structure of USF has been visualized in detail for the first time. The first observation noticed in the flow was a general rotation and stretching of the injected dye, caused by velocity differences across the flow. This was a direct result of the mean shear in the flow and affected the development of coherent structures as much as the relative motions of all fluid particles. The angle of inclination of the flow and its structures was not constant, with many structures stretching at almost a 45°angle, while others moved from a vertical orientation to a horizontal orientation. It would be difficult to determine from the video if there were any preferred angle of inclination, although this may be a subject of future research.

Another important observation was the frequent occurrence of organized motions

with identifiable rotation, which clearly qualified as coherent structures. Different views of the flow revealed the presence of fully three-dimensional structures with vorticity in the streamwise, spanwise or transverse directions. Structures with positive and negative streamwise vorticity occurred with roughly equal frequencies. Similarly, there seemed to be no preference of rotation in the positive or negative transverse directions. Structures with streamwise or transverse vorticity often appeared in combinations as counter-rotating pairs or chains of vortices. These structures had axes which, on the average, tended to be inclined with respect to the mean flow direction by an angle that was consistent with the shape of the mean velocity profile. On the other hand, structures with spanwise vorticity usually had the same sense as the mean vorticity of USF. Most structures observed appeared to be of a similar type. They were three-dimensional and had axes of rotation that were generally inclined with respect to the three axes of the water tunnel. Although the evidence of the present images is not entirely conclusive, one may plausibly infer that the typical structure in the present USF was a hairpin-type vortex, or portions thereof, as was expected to be seen from previous numerical research. The exact mechanisms of generation and development of these structures remain unclear, but their similarity to structures observed in the outer boundary layer would seem to imply that the presence of shear is a main contributing factor.

A final observation regarded fluid that was not part of the primary structures observed above, but was affected by them. One example would be the streaks of dye that formed outside of a vortical eddy. These streaks possibly connected this eddy to the location of its origin as well as to other nearby eddies. In some cases, the streaks were actually a part of the primary structure, possibly forming the shear layer that forms behind a hairpin-type

structure. Another observation in the fluid surrounding the primary structures was the formation of secondary flow patterns. Generally, these regions of dye were relatively small in size and short in lifespan and could not be classified in the same group as the primary coherent structures. These can be seen as dye entrained into a primary structure or as wake vortices created by the passage of a primary structure through slower fluid.

The formation of the observed pairs or chains of structures with spanwise vorticity is rather difficult to explain. In boundary layers, it has been hypothesized that hairpin structures induce other hairpin structures. Whether such a mechanism applies to core USF is quite unclear, if one considers the lack of organization of USF structures. A more likely explanation can be given by analogy to two-dimensional mixing layers, in which the shearing action generates a chain of well-organized structures with strong spanwise vorticity, all in the same sense (Brown and Roshko, 1971). Because in USF the shear regions are much less organized compared to those in mixing layers, and further distorted by the randomly oriented turbulence, the chains of spanwise vortices occur rather infrequently and are relatively short compared to observations in a mixing layer.

The transverse motion of the vortical structures is of particular interest because it occurs without the presence of a wall. The general motion of a vortical structure with spanwise vorticity towards a region of higher velocity may be attributed to the Magnus effect on rotating objects or on the induced motion of fluid between a pair of counter-rotating streamwise vortices, e.g. the legs of a hairpin vortex. The trail of dye formed behind a structure with transverse motion was suggestive of a shear layer, and supports the theory that the primary structures were of a hairpin-type shape. Transverse motion toward

higher velocity regions has been observed consistently for different orientations of mean shear. This motion also suggests a formation mechanism for hairpin-type structures. In a structure with variable spanwise vorticity, any part of the structure with higher vorticity would have a higher transverse force, thus causing part of the structure to move faster and deforming it into a hairpin or partial hairpin shape.

Based on the above observations and speculations, one could put together the following likely scenario for the generation of the typical, hairpin-type, structures in USF.

a) Initial mean shear as well as initial, inhomogeneous turbulence in the flow were generated by the shear generator and flow separator.

b) In a flow region near the exit of the flow separator, the initial turbulence decayed as well as becoming organized by the mean shear. At the same time, the initial, highly distorted, mean velocity profile developed towards a linear one.

c) Localized strong velocity differences between faster and slower fluid regions generated new vortical motions with spanwise vorticity, on the average aligned with and in the same sense as the mean flow vorticity. When sufficiently strong, these motions can be classified as coherent structures.

d) As these structures evolved, they became distorted, stretched and re-oriented by the turbulence. At the same time, they are subjected to a lifting force towards the high-velocity region, due to a Magnus effect or, as the flow develops, by induced motion betweem counter-rotating vortices. Depending on the history of turbulence distortion and influence of other nearby structures, some parts of these structures tended to be slimmer and to have a higher vorticity. These parts would lift further away, deforming the initially spanwise

vortex to a hairpin-type or similar shape. The general orientation and overall stretching of the structures as they further evolved were imposed by the mean velocity field.

e) The passage of a strong coherent structure would induce secondary vortical motions at all possible orientations, thus producing additional turbulence. All turbulent motions would, at all times, be subjected to dissipation and eventually decay or be integrated into other structures.

In the previous scenario, the production of coherent structures and overall turbulence is clearly independent of the presence of solid boundaries. It is associated with the effects of mean shear, which produces structures with spanwise vorticity, deforms them towards hairpin-type shapes and orients them preferentially with respect to the mean flow direction. This scenario does not necessarily contradict previous explanations for the generation of hairpin vortices in boundary layers, because the friction of fluid with the wall also creates mean shear and provides a preferential orientation. The similarities and differences between turbulence production in USF and in TBL certainly deserve closer and more detailed scrutiny than provided in the present work.

7.2 Turbulent Boundary Layer

7.2.1 Measurements

The boundary layer corresponding to a low-turbulence, uniform free stream was studied for both the high-speed case, which was determined to be fully turbulent in the entire length of the wall, and the low-speed case, which indicated possible transitional behaviour and may not have achieved a fully turbulent state at the region of study. The LDV probe

was positioned at an inclined orientation to enable two-component measurement very close to the wall, down to $y^+ = 3$ or even less. Measurements of the mean velocity and the Reynolds stresses were generally comparable with previous results in low Reynolds number TBL. A logarithmic region was identified and the typical peak in streamwise turbulence intensity near $y^+ = 15$ was noticed.

7.2.2 Flow Visualization

Flow visualization of the turbulent boundary layer resulted in observations that compared well with previous studies. When viewing the flow on planes parallel to the wall, one could clearly observe the formation of low-speed, streak-like structures in the near-wall region. These streaks seemed to form around disturbances that were most likely coherent structures impacting with the surface. When viewed from the side, the near-wall region appeared to consist primarily of slow moving fluid in a wavy motion. Occasionally, the oscillations grew to form an eddy of spanwise vorticity, which left behind it a trail of dye. These structures of high spanwise vorticity would often be drawn back into, and impact with, the wall, or otherwise would escape the near-wall region towards the outer layer.

>From the side view, it was difficult to determine the average distance from the wall at which these structures were formed, or where they were most active. According to LDV measurements, the turbulent kinetic energy production term $-\overline{u_1 u_2} d\overline{U}_1/dx_2$ and the streamwise turbulence stresses were highest at $y^+ = 15$ ($y = 2.3$ mm), but it was impossible to notice any special activity at this point because it was so close to the wall. From the bottom view, one could identify streaks as closely as at $y^+ = 7$, whereas, at $y^+ = 27$, no streaks were visible. At the latter position, coherent structures with transverse vorticity

started to appear; their extents in the streamwise and spanwise directions were comparable, unlike the streaks which were elongated in the streamwise direction. The above observations help to explain the statistical measurements of the turbulent stresses. Very close to the wall, friction formed a layer of slow-moving fluid and forced the turbulent stresses to drop, while, far away from the wall, the boundary layer merged with the free stream and the turbulence approached the free stream level. The high shear created by the friction of the wall assisted the production of turbulence, and it would appear that the peak turbulent activity occurred at a point where the slow moving fluid of the wall was no longer present. Simply explained, the wall-related shear caused the streamwise turbulent stress and the turbulent kinetic energy to increase as one moved from the free stream towards the wall, until they reached maxima at some position where regions of slow-moving fluid were found. The production of turbulence near the wall also caused an increase in the transverse turbulence intensity, however its maximum was reached further away from the wall than the maximum of the streamwise stress was; the reason for this difference is that the physical barrier of the wall had a far-extending reach on the structures that approach it.

The outer layer contained vortical structures with strong spanwise vorticity, whose outer edges defined the interface between the boundary layer and the free stream fluid. These structures were generally of similar orientations and extended further away from the wall as the boundary layer grew downstream at a nearly constant rate. They definitely originated in the wall region and grew outward towards the free-stream, as can be seen from side- as well as bottom views, in which the structures appeared to become smaller and eventually to disappear as the laser sheet was moved away from the wall. These structures

often entrained fluid from the free stream and induced the production of other vortical structures. A leading vortical structure created a shear layer behind it, which was easily defined by a trailing strand of dye that was not easily deformed by nearby structures. When viewed with the laser sheet parallel to the wall, these structures appeared as a mushroom-shaped, closely-spaced pair of counter-rotating vortices. These vortex pairs most likely represent the legs of a hairpin vortex, connected to its head that had lifted outward from the wall. The upstream side of the head of the hairpin formed a sharp, smooth curve, whereas the downstream side contained dye without a clear shape. This dye streak downstream of the vortex pair most likely represents a part of the hairpin vortex head, which was generally observed in the side view to form downstream with the legs and subsequent shear layer behind it.

In the outer layer, the side view provided some evidence of occasional violent ejections of fluid away from the wall. These appeared in the form of mushroom-shaped vortex pairs rising away from the wall and towards the upstream direction. Most often, the vortex pair split up, with the wall-side vortex being entrained back into the boundary layer, and the free-stream-side vortex forming a strong vortical structure at the edge of the boundary layer, similar to the hairpin-type structures observed above. Mushroom-shaped vortex pairs were also observed at the underside of a hairpin-type structure that would draw in fluid under the hairpin head, with part of the fluid entrained into the hairpin and the rest turning away from the underside of the shear layer. It would appear that the mushroom-shaped pair of counter-rotating vortices is a recurring structure in turbulent flows, and may be an essential element in the formation of hairpin-type vortices, as proposed by Falco

(1977).

In accordance with the observations in USF, it would appear that coherent structures with spanwise vorticity were formed in the near-wall region, due to the very high shear present there. These structures deformed and either rose outward into the outer layer, or were drawn back into the wall region. Those that rose outward appeared to assume a hairpin-type shape and contributed to the growth of the boundary layer.

7.3 Moving Wall Studies

7.3.1 Measurements

LDV results from the moving wall studies show dramatic differences in flow behaviour for the different wall motions only in a narrow region near the wall. The changes in the statistical properties of the flow caused by wall motion seemed to correlate well with the observed flow structure.

In the MWE case, the linearly extrapolated mean velocity profile nearly, but not precisely, matched the wall speed. In the MWN case, a region of reverse flow was created near the wall, whereas, in the MWP case, the flow was drawn forward by the wall, creating a layer of reverse shear. In the MWP case, the no-slip condition at the wall created a layer of nearly-laminar fluid with velocity close to the wall speed. The near-wall turbulence activity was greatly reduced for the MWE case and greatly increased for the MWN case. For the MWP case, the turbulence intensity seemed to depend on the magnitude of shear in the flow, and presented a peak similar to, but much smaller than, that for the MWN case. This peak seemed to form in a region of high shear near the wall, and then quickly diminished

toward zero. This same behaviour is noted in the MWN case as well as in the turbulent boundary layer study, where a drop in the streamwise turbulence intensity was found right at the wall, even though for the MWP case the shear was opposite in direction.

7.3.2 Flow Visualization

For the MW0 case, the structure of the wall region appeared to be very similar in nature to that found in conventional turbulent boundary layers, although less active. Streaks were clearly visible within a certain range of distances from the wall and coherent structures with strong spanwise vorticity were seen to form within that range and then grow and extend away from the wall into the outer layer. The relationship between the structures impacting with the wall, causing the formation of low-speed streaks, and the structures with spanwise vorticity was not easy to discern. The structures in the outer layer had strong vorticity in the streamwise and transverse directions, and were inclined with respect to the flow direction. When followed backward near the wall, these structures had portions with strong streamwise vorticity and were seen to lift away from the wall region. These portions most likely can be characterized as the legs of hairpin-type vortices.

With the wall moving at the local mean velocity (MWE), the structures in its vicinity resembled more closely those found in core USF than those in conventional boundary layers. No structures seemed to form in the near-wall region, and the wall acted as a barrier, suppressing approaching structures and the overall turbulence activity. This is corroborated by the measured variation of the turbulence intensities, which, up to some point, were comparable to those in the core flow and dropped as the wall was approached. The slightly streaky appearance of the flow structure in the very near wall region supports

the possible presence of a sublayer near the wall with relative motion matching that of the wall, regardless of the wall speed.

With the wall moving in the reverse direction (MWN), the mean streamwise velocity reversed direction near the wall where a layer of recirculating dye could be clearly observed. The turbulence intensity was relatively high in the near-wall region, which was seen in the images by the great diffusion of the dye and a more active formation of vortical structures with small and large sizes. Compared to the MW0 case, the MWN case had a thicker boundary layer and coherent structures that were more energetic and extended further away from the wall. Otherwise, observations in the two cases were quite similar.

With the wall moving faster than the flow (MWP), one could distinguish two regions of opposing shear separated by a low-shear region. Streaks of dye were clearly observed to stretch and rotate in accordance with the local direction of the mean shear. The structures in the near-wall region were quite distinct from the typical USF structures. The structures from the two regions were rarely seen to cross the no-shear region in between. Close to the wall, the flow appeared to almost relaminarize, although occasionally generating vortical structures which migrated from a region of higher streamwise velocity to a region of lower streamwise velocity, in contrast to the migration patterns of structures previously observed. This could indicate an effect of the physical presence of the wall to redirect flow away from the wall. From the rear and inclined views, it could be seen that the structures in the two regions were inclined in opposite directions, depending on the direction of the corresponding mean velocity gradient.

7.4 General Comments on the Structure of Turbulent Shear Flows

The USF results presented above have shown that production of hairpin-type vortices and growth of turbulence can occur in shear flows irrespective of the presence of a wall. In turbulent boundary layers, low-speed streaks were observed, but these seemed to be a result of interactions between vortical structures and the near-wall fluid and were possibly unrelated to any mechanism of generation of these vortical structures. More specifically, in cases with a stationary wall, the streaks seemed to simply be dye collected in the nearly stagnating, slow moving region of the inner boundary layer. In cases of wall motion, this region contained fluid with a speed nearly equal to the wall speed and also quasi-laminar. The streaky appearance could be attributed to the near-absence of relative motion and turbulence at the wall. The low-speed streaks were interspersed by regions of high-speed fluid, which were seen to be coherent structures that impacted on the wall. The spanwise spacing between low-speed streaks seemed to be about $100\nu/u^*$ for all cases except the MWE case. The no-slip condition imposed by the wall may be viewed as responsible for turbulence production by generating local, high-shear, mixing layers between fluid with a speed close to the wall speed and free-stream fluid. The turbulence production phase seemed to begin with the creation of roller-type vortical motions in these mixing layers. Thus, the inner boundary layer may be viewed as a region of inactive, quasi-laminar fluid, subject to the occasional generation or intrusion of a coherent structure. The turbulence in this region is intermittent, analogous to but quite distinct from, intermittency in the outer layer. The no-penetration condition imposed by the wall contributed to an organization

of the coherent structures into preferential orientations. In both core USF and the outer boundary layer, the coherent structures appeared to take hairpin-type shapes. Observations of their spanwise appearance clearly indicated a primary vortex on the downstream edge of the structure, followed by a trail of dye.

Chapter 8

Conclusions and Recommendations for Further Research

This research has provided new insight into the effects of free shear as well as the effects of a solid boundary, in motion or not, on the large-scale structure and the production mechanism of turbulence. The water tunnel testing facility was proved to be an excellent environment for both quantitative and visual studies of turbulent flows. The combination of laser-sheet illumination and laser-induced fluorescence provided great detail into the structure of turbulence. USF with properties conforming to those in previous popular studies was generated in the water tunnel, permitting its convenient flow visualization for the first time experimentally, with predicted results. The present moving wall apparatus also proved to be a reliable method for creating a variety of configurations suitable for studying wall-flow interactions.

From the results of the USF and moving wall studies, new ideas into the generation

and development of coherent structures have been introduced. It has been confirmed that shear in a flow, regardless of the presence of a solid wall, is the essential characteristic for the generation of vortical structures that have been associated with the production of turbulence. Earlier moving wall research has been limited to studies with a uniform flow and without mean shear in the boundary layer. The combination of a moving boundary and USF has provided new insight into the kinematic effects of a wall on the turbulence structure, without the removal of mean shear.

The "typical" coherent structures in both the core USF and the outer boundary layer were seen to have hairpin-type shapes. These structures were stretched and tilted by the mean shear in all flows studied. Low-speed streaks were found in the inner boundary layer, and the equivalent high-speed regions were observed to be formed of structures impacting with the wall, and not really having a streaky nature, other than being flanked by low-speed streaks.

The present study may be viewed as introductory. It resulted in a number of possible new concepts, which remain to be tested and applied to other cases as well as to be compared to earlier observations and hypotheses. Several extensions of the experiments and ideas presented in this thesis could be suggested for future research. For example, DNS of USF at very high shear rates (Lee, Kim & Moin, 1990) have documented the formation of streaky coherent structures, although no experimental evidence for such structures in USF yet exists. It is possible that, when subject to extremely high shear, a roller vortex would be stretched in a direction parallel rather than inclined to the flow direction so that its "legs" would have strong streamwise vorticity. It would be interesting to explore this

possibility by designing a proper high-shear experiment.

The present LDV measurements were both of limited scope and of limited resolution. Since this research was completed, a high resolution (16-bit rather than the present 8-bit) LDV system has become available to the fluid mechanics laboratory and should be used to repeat all measurements in more detail as well as to document the few missing cases. Measurements of the frequency spectra should be completed in more detail with the higher resolution LDV system as well. Further investigations into the transverse inhomogeneity of the flow should also be considered. Applying this study to different Reynolds number cases would obviously provide further insight into the Reynolds number effect of the turbulent structures. The variation of size and shape of hairpin structures with the Reynolds number of the flow has been observed in previous research. The inclination angle of the structures varying with the shear in the flow is another important topic, and shear and Reynolds number effects should be investigated concurrently.

Measurements of the near-wall region for the moving-wall studies should be performed with the two component LDV system to obtain more information on the Reynolds stresses, primarily the shear stress correlation coefficient. This will require an adjustment to the moving wall apparatus to draw the moving wall belt upward at the sides using tabs or similar devices.

Multiple-tube dye injection was performed in tests preliminary to this research and its results have not been included in this thesis. These provide useful information as to the origin of structures and should be further experimented with in both the transverse and spanwise directions.

Further analysis of the visual records to obtain statistical results could provide more insight into the production mechanism of the coherent structures. This would require larger visual records and should probably be performed for a wider range of Reynolds numbers. The frequency of occurrence, time and lengthscales and probability density function could all be measured. Measurements of concentration of the dye in the structures could also be conducted. These studies would require a much better controlled introduction of the dye into the flow field, whereas the present study focused primarily on the concepts and basic observations of the nature of the flow. The mean spanwise streak spacing has presented a scaling law that applies to situations that were probably not considered in its original concept, and should be further investigated.

One of the most interesting regions of the flow that needs further study is the inner boundary layer, where the viscous sublayer appears to behave in an intermittent, quasi-laminar fashion and the production of turbulence is strongest. The use of laser-induced fluorescence/laser-sheet videography has been shown to provide an excellent means of investigating this area. Another interesting study would be to analyze the instantaneous realizations of LDV measurements, taken simultaneously with visual images, to determine intermittency in the inner layer, if any.

Finally, a more complicated arrangement that could help provide more concrete evidence into the presence and shape of hairpin type vortices would be the use of a dual-camera/dual-laser-sheet system to observe a specific region of the flow from various angles simultaneously. Viewing structures from the side in conjunction with viewing them from the rear, or from underneath, preferably with an inclined laser-sheet, would further provide

an understanding of the perpendicular extent of the vortical structures observed in each plane. This configuration could be easily managed with the current water tunnel facility, which has been improved since the present study was completed. A streamwise traverse of the structures could also be obtained, providing insight into their streamwise development and interactions.

Bibliography

Acarlar, M.S. & Smith, C.R., 1987, A study of hairpin vortices in a laminar boundary layer. Part 2. Hairpin vortices generated by fluid injection, J Fluid Mech 175, 43-83.

Adrian, R. J., Meinhart, C. D. & Tomkins, C.D., 2000, Vortex organization in the outer region of the turbulent boundary layer, J Fluid Mech 422, 1-54.

Aronson, D., Johansson, A. V. & Lofdahl, L., 1997, Shear-free turbulence near a wall, J Fluid Mech 338, 363-385.

Bakewell, H. P. & Lumley, J. L., 1967, Viscous sublayer and adjacent wall region in turbulent pipe flow, Phys Fluids 10, 1880-1889.

Brown, G. V. & Roshko, A., 1971, Turbulent shear flows, AGARD-CP-93, 23.1.

Champagne, F. H., Harris, V. G & Corrsin, S., 1970, Experiments on nearly homogeneous shear flow, J Fluid Mech 41, 81-139.

De Souza, F. A., Nguyen, V. D. & Tavoularis, S., 1995, The structure of highly sheared turbulence, J Fluid Mech 303, 155-167.

Eidetics International, Inc., Sales brochure, gnm 8956.

Erickson, G. E., Peake, D. J., Del Frate, J., Skow, A. M. & Malcolm, G. N. Water, Nov 1986, Facilities in Retrospect and Prospect - an Illuminating Tool for Vehicle Design, NASA Technical Memo 89409.

Falco, R. E., 1977, Coherent motions in the outer region of turbulent boundary layers, Phys Fluids 20, 10, S124-S132.

Farell, C. & Youssef, S., 1996, Experiments in turbulence management using screens and honeycombs, J Fluids Eng Trans ASME 118, 26-32.

Ferchichi, M. & Tavoularis, S., 2000, Reynolds number effects on the fine structure of uniformly sheared turbulence, Phys Fluids 12, 11, 2942-2953.

Groth, J. & Johansson, A. V., 1988, Turbulence reduction by screens, J Fluid Mech 197, 139-155.

Haidari, A.H. & Smith, C.R., 1994, The generation and regeneration of single hairpin vortices, J Fluid Mech 277, 135-162.

Hamilton, J. M., Kim, J. & Waleffe, F., 1995, Regeneration mechanisms of near-wall turbulence structures, J Fluid Mech 297, 317-348.

Harris, V. G, Graham, J. A. & Corrsin, S., 1977, Further experiments in nearly homogeneous turbulent shear flow, J Fluid Mech 81, 657-687.

Head, M. R. & Bandyopadhyay, P., 1981, New aspects of turbulent boundary-layer structure, J Fluid Mech 107, 297-338.

Hinze, J. O., 1976, Turbulence, New York : McGraw-Hill.

Humphreys, W. W., 1988, An experimental study of the effect of streamwise vortices on unsteady turbulent boundary-layer separation, Stanford Univ, Dept of Mech Eng.

Hunt, J.C.R. & Graham, J.M.R., 1978, Free-stream turbulence near plane boundaries, J Fluid Mech 84, 209-235.

Jeong, J., Hussain, F., Schoppa, W. & Kim, J., 1996, Coherent structures near the wall in a turbulent channel flow, J Fluid Mech 332, 185-214.

Jimenez, J. & Moin, P., 1991, The minimal flow unit in near-wall turbulence, J Fluid Mech 225, 213-240.

Jimenez, J. & Pinelli, A., 1998, The autonomous cycle of near-wall turbulence, J

Fluid Mech 389, 335-359.

Karman, T. von, 1937, The fundamentals of the statistical theory of turbulence, J Aero Sci 4, 131.

Karnik, U. & Tavoularis, S., 1987, Generation and manipulation of uniform shear with the use of screens, Exper Fluids 5, 247-254.

Kida, S. & Tanaka, M., 1992, Reynolds stress and vortical structure in a uniformly sheared turbulence, J Phys Soc Japan 61, 12, 4400-4417.

Kida, S. & Tanaka, M., 1994, Dynamics of vortical structures in a homogeneous shear flow, J Fluid Mech 274, 43-68.

Kim, H. T., Kline, S. J.& Reynolds, W. C., 1971, The production of turbulence near a smooth wall in a turbulent boundary layer, J Fluid Mech 50, 133-160.

Kim, J., Moin, P. & Moser, R., 1987, Turbulence statistics in fully developed channel flow at low Reynolds number, J Fluid Mech 177, 133-166.

Klebanoff, P. S., 1954, Characteristics of turbulence in a boundary layer with zero pressure gradient, NACA Report 1247.

Kline, S. J., Reynolds, W. C., Schraub, F. A. & Runstadler, P. W., 1967, The structure of turbulent boundary layers, J Fluid Mech 30, 741-773.

Lee, M. J., Kim, J. & Moin, P., 1990, Structure of turbulence at high shear rate, J Fluid Mech 216, 561-583.

Lu, S. S. & Willmarth, W. W., 1973, Measurements of the structure of the Reynolds stress in a turbulent boundary layer, J Fluid Mech 60, 481-511.

Mikhail, M. N. & Rainbird, W. J., 1978, Optimum design of wind tunnel contrac-

tions, AIAA 78-819, 376-384.

Monin, A. S. & Yaglom, A. M., 1972, Statistical Fluid Mechanics, 2 vols., MIT Press, Cambridge, Mass.

Mulhearn, P. J. & Luxton, R. E., 1975, The development of turbulence structure in a uniform shear flow, J Fluid Mech 68, 577-590.

Perot, B. & Moin, P., 1995-a, Shear-free turbulent boundary layers. Part 1. Physical insights into near-wall turbulence, J Fluid Mech 295, 199-227.

Perot, B. & Moin, P., 1995-b, Shear-free turbulent boundary layers. Part 2. New concepts for Reynolds stress transport equation modelling of inhomogeneous flows, J Fluid Mech 295, 229-245.

Pope, S.B., 2000, Turbulent flows, Cambridge University Press.

Reynolds, O., 1883, An experimental investigation of the circumstances which determine whether the motion of water shall be direct or sinuous, and of the law of resistance in parallel channel. Phil Trans Roy Soc London 174, 935-982.

Robinson, S. K., 1991, Coherent motions in the turbulent boundary layer, Ann Rev Fluid Mech 23, 601-639.

Rogers, M. M. & Moin, P., 1987, The structure of the vorticity field in homogeneous turbulent flows, J Fluid Mech 176, 33-66.

Rohr, J. J., Itsweire, E. C., Helland, K. N. & Van Atta, C. W., 1988, An investigation of the growth of turbulence in a uniform-mean-shear flow, J Fluid Mech 187, 1-33.

Rose, W. G., 1966, Results of an attempt to generate a homogeneous turbulent

shear flow, J Fluid Mech 25, 97-120.

Runstadler, P. G., Kline, S. J. & Reynolds, W. C., 1963, An experimental investigation of flow structure of the turbulent boundary layer, Rep MD-8, Dept Mech Eng Stanford Univ.

Schraub, F. A., Kline, S. J., Henry, J., Runstadler, P. W. & Littell, A., 1965, Use of hydrogen bubbles for quantitative determination of time-dependent velocity field in low-speed water flows, ASME J Basic Eng 87, 429-444.

Smith, C.R., Walker, J.D.A., Haidari, A.H. & Sobrun, U., 1991, On the dynamics of near-wall turbulence, Phil Trans. R. Soc Lond. 336, 131-175.

Spalart, P. R., 1988, Direct simulation of a turbulent boundary layer up to Re =1410, J Fluid Mech 187, 61-98.

Tavoularis, S., 1985, Asymptotic laws for transversely homogeneous turbulent shear flows, Phys Fluids 28, 999-1001.

Tavoularis, S. & Corrsin, S., 1981-a, Experiments in a nearly homogeneous turbulent shear flow with a uniform mean temperature gradient, Part 1, J Fluid Mech 104, 311-347.

Tavoularis, S. & Corrsin, S., 1981-b, Experiments in a nearly homogeneous turbulent shear flow with a uniform mean temperature gradient, Part 2, J Fluid Mech 104, 349-367.

Tavoularis, S. & Karnik, U., 1989, Further experiments on the evolution of turbulent stresses and scales in uniformly sheared turbulence, J Fluid Mech 204, 457-478.

Tennekes, H. & Lumley, J. L., 1972, A first course in turbulence, MIT Press,

Cambridge, Mass.

Theodorsen, T., 1952, Mechanism of turbulence, In Proc. 2nd Midwestern Conf. On Fluid Mech. Ohio State University, Columbus, Ohio.

Thomas, N.H. & Hancock, 1977, P.E. Grid turbulence near a moving wall J Fluid Mech 82 481-496.

Ueda, H. & Hinze, J. O., 1975, Fine-structure turbulence in the wall region of a turbulent boundary layer, J Fluid Mech 67, 125-143.

Uzkan, T. & Reynolds, W.C., 1967, A shear-free turbulent boundary layer, J Fluid Mech 28, 803-821.

Wallace, J. M., Eckelmann, H., Brodkey, R. S., 1972, The wall region in turbulent shear flow, J Fluid Mech 54, 39-48.

Whitehead, L. G., Wu, L. Y. & Waters, M. H. L., 1951, Contracting ducts of finite length, Aero Quart 2, 254-271.

Willmarth, W.W. & Lu, S.S., 1972, Structure of the Reynolds stress near the wall, J Fluid Mech 55, 65-92.

Zhou, J., Adrian, R.J., Balachandar, S. & Kendall, T.M., 1999, Mechanisms for generating coherent packets of hairpin vortices in channel flow, J Fluid Mech 387, 353-396.

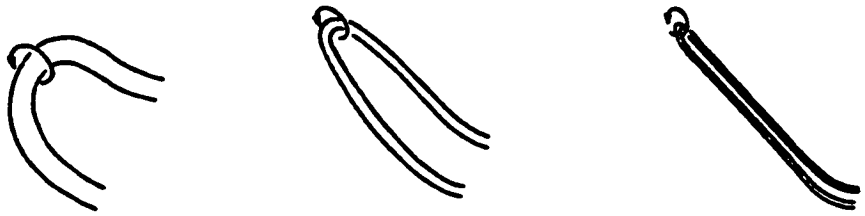

Figure 3.1 Description of a hairpin vortex with Reynolds number increasing from left to right. (Head and Bandyopadhyay, 1981)

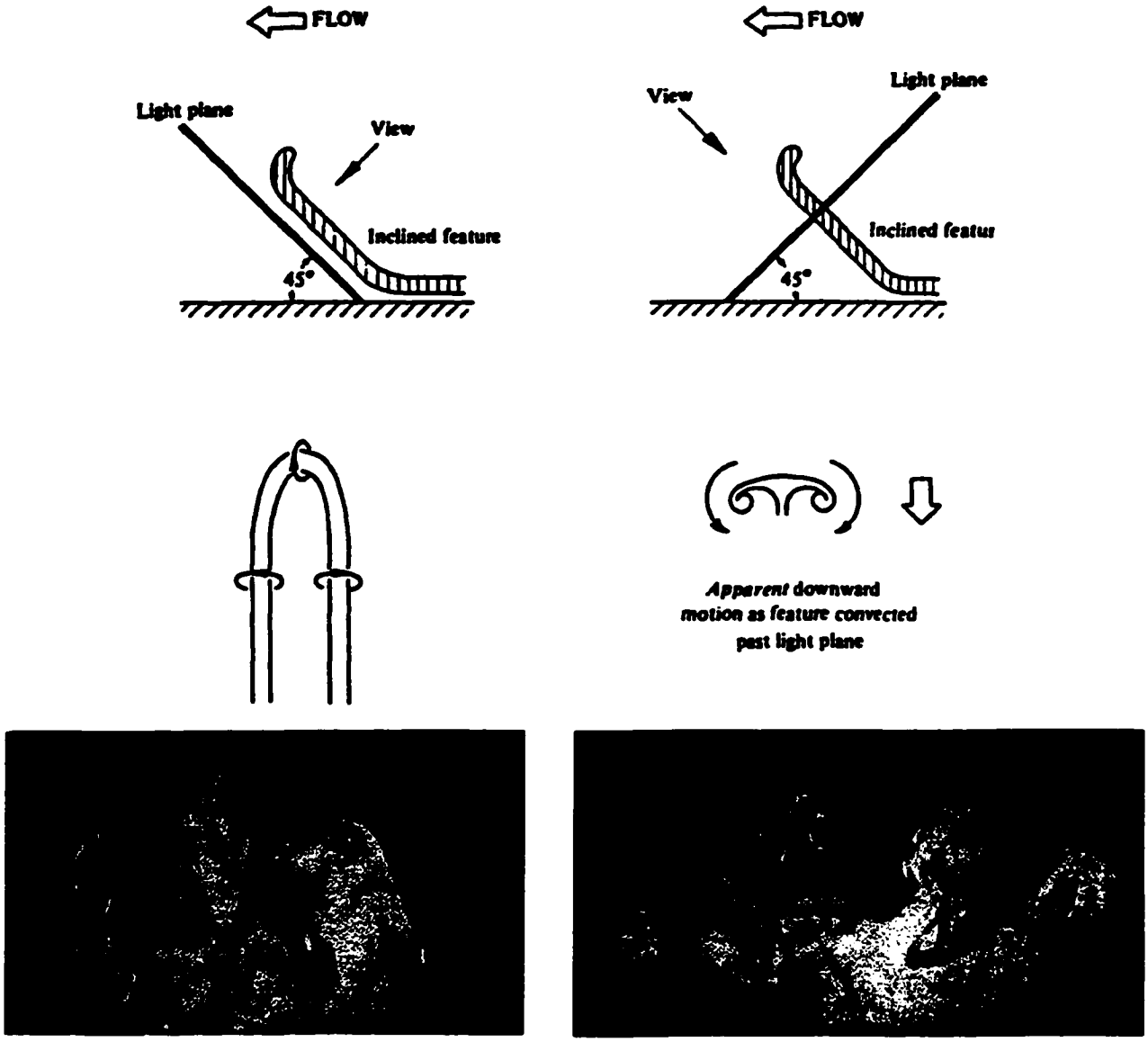

Figure 3.2 Sketch of hairpin-type vortex viewed with an inclined laser sheet and actual results. (Head and Bandyopadhyay, 1981)

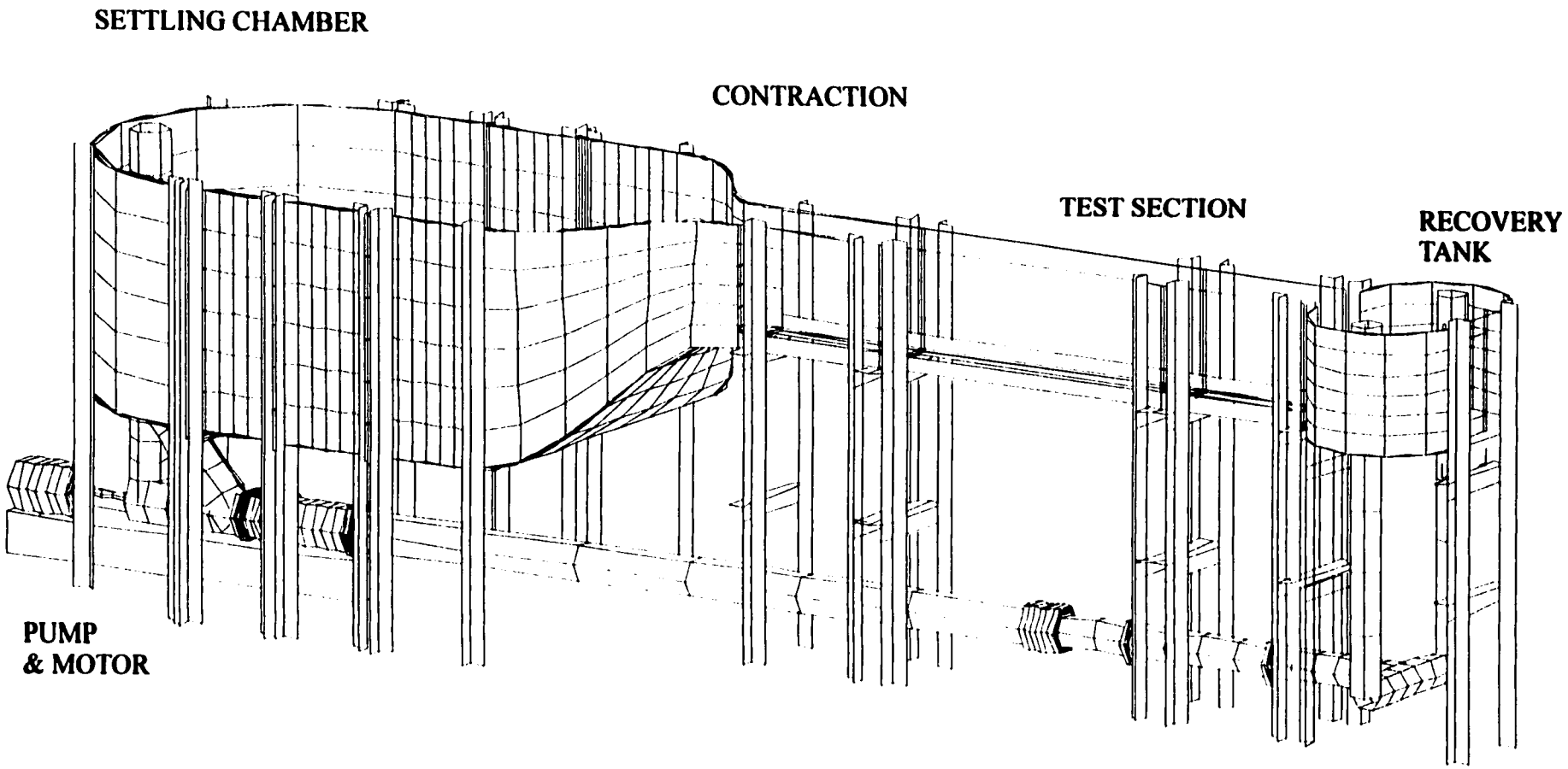

Figure 4.1 Sketch of the water tunnel facility.

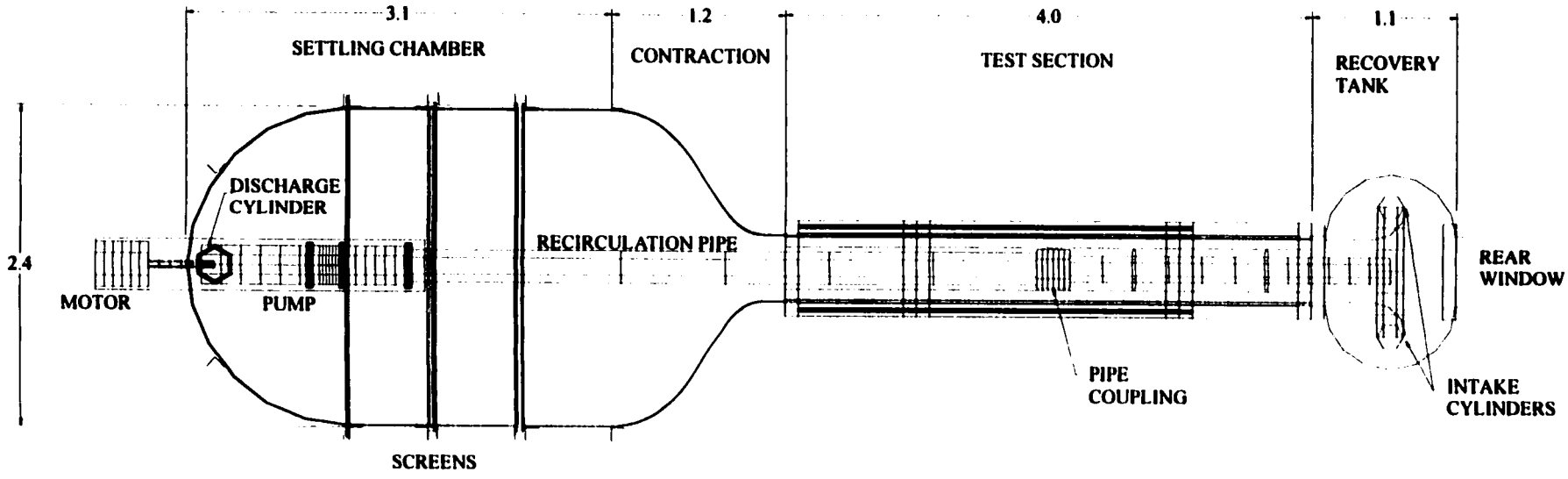

Figure 4.2 Water tunnel facility, top view

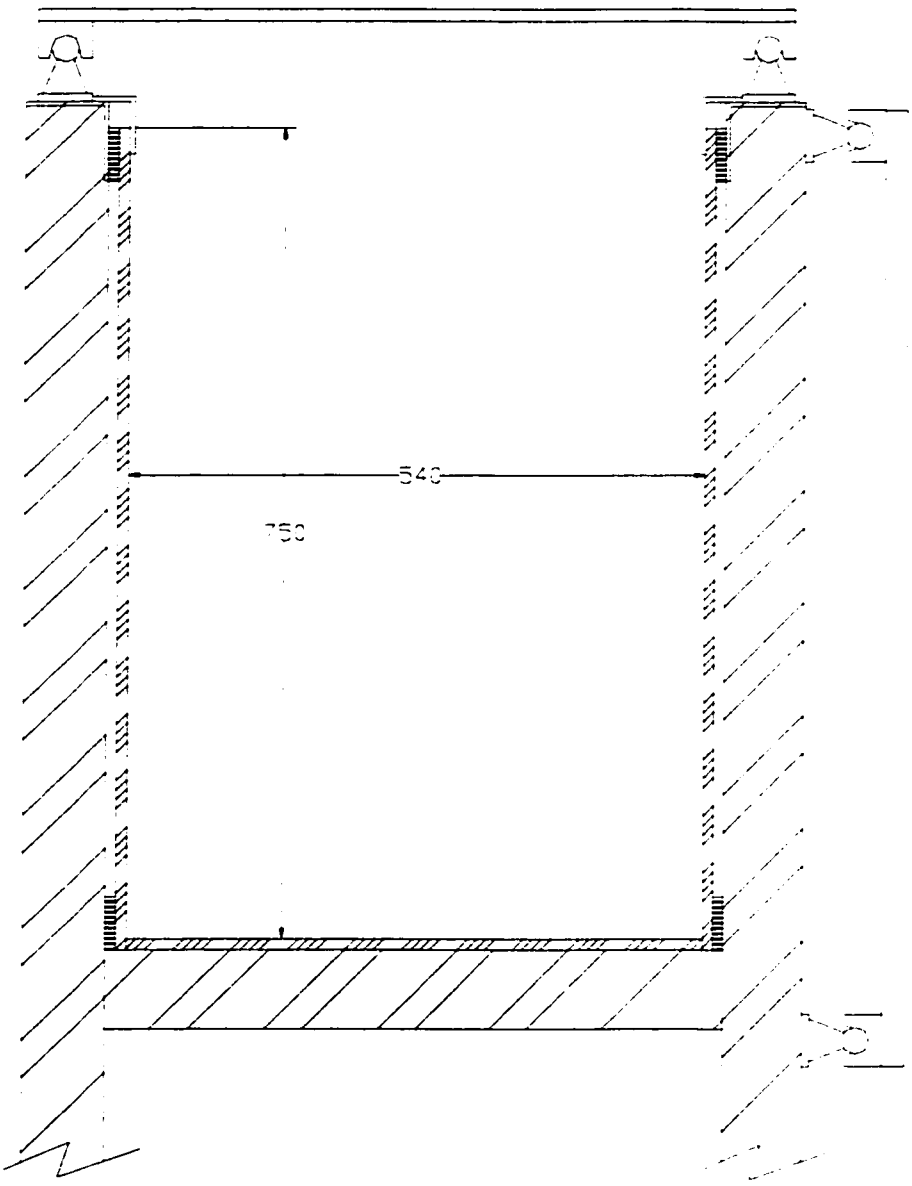

all dimensions in mm

Figure 4.3 Test section cross-section.

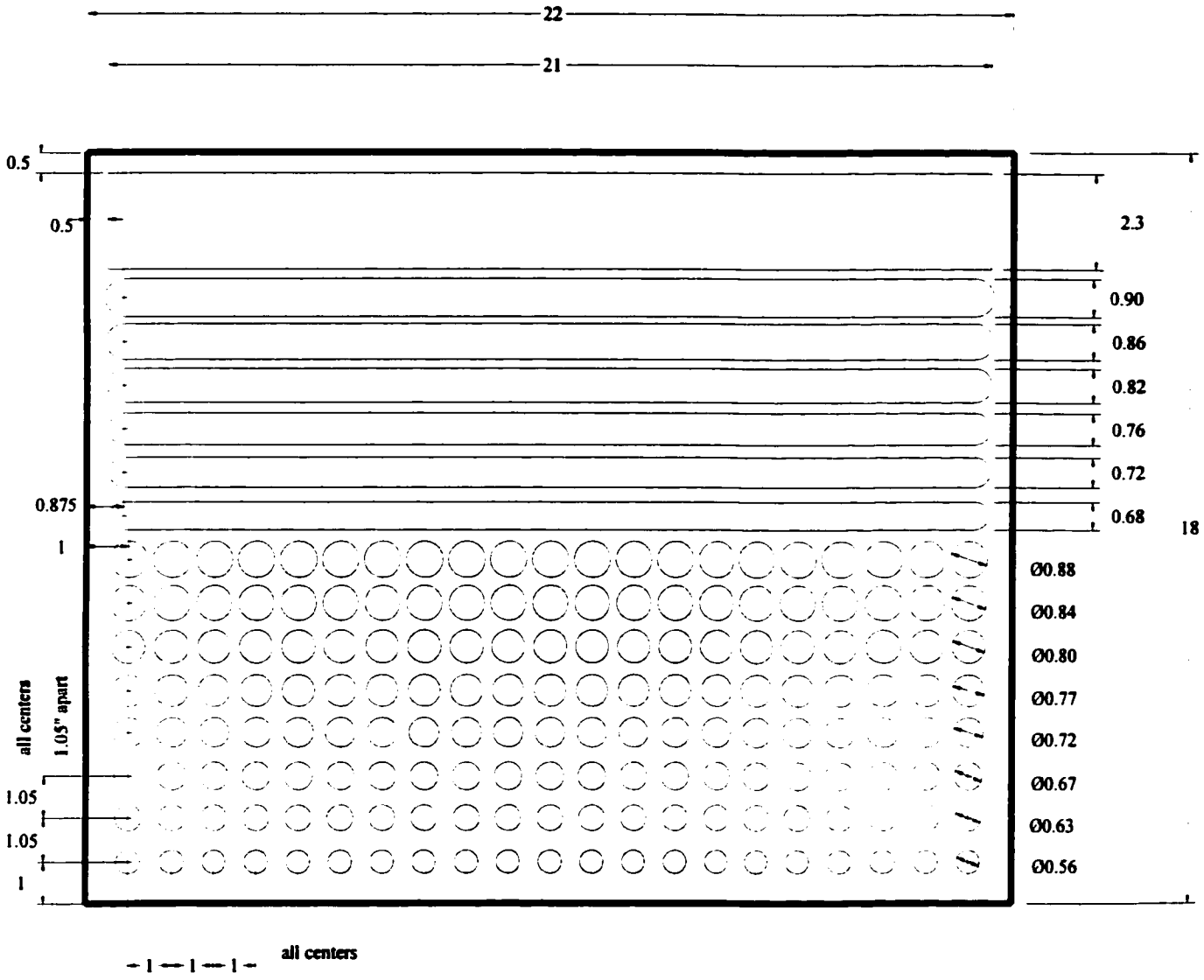

all dimensions in inches

Figure 4.4 Shear generator plate

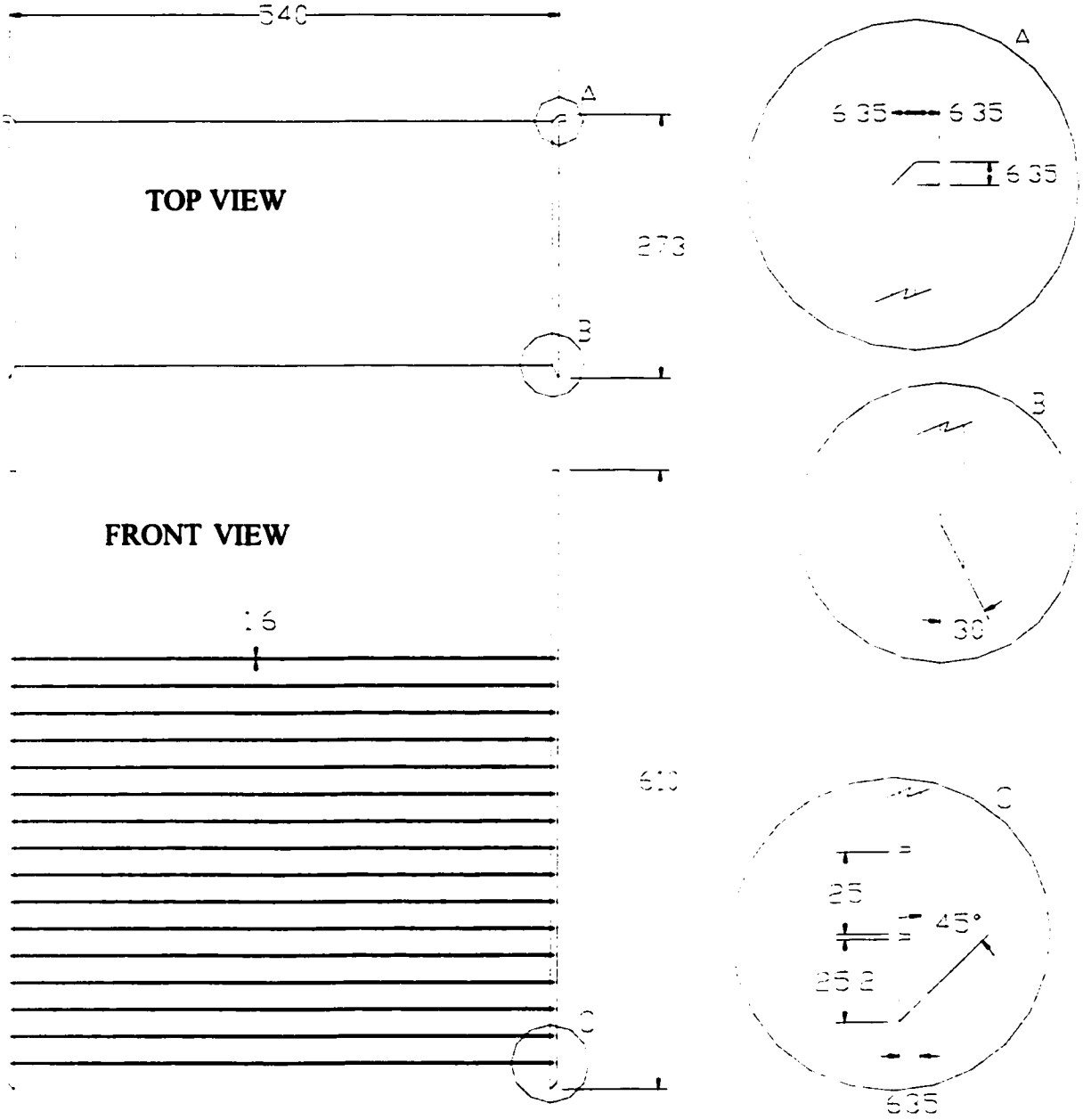

all dimensions in mm

Figure 4.5 Flow separator

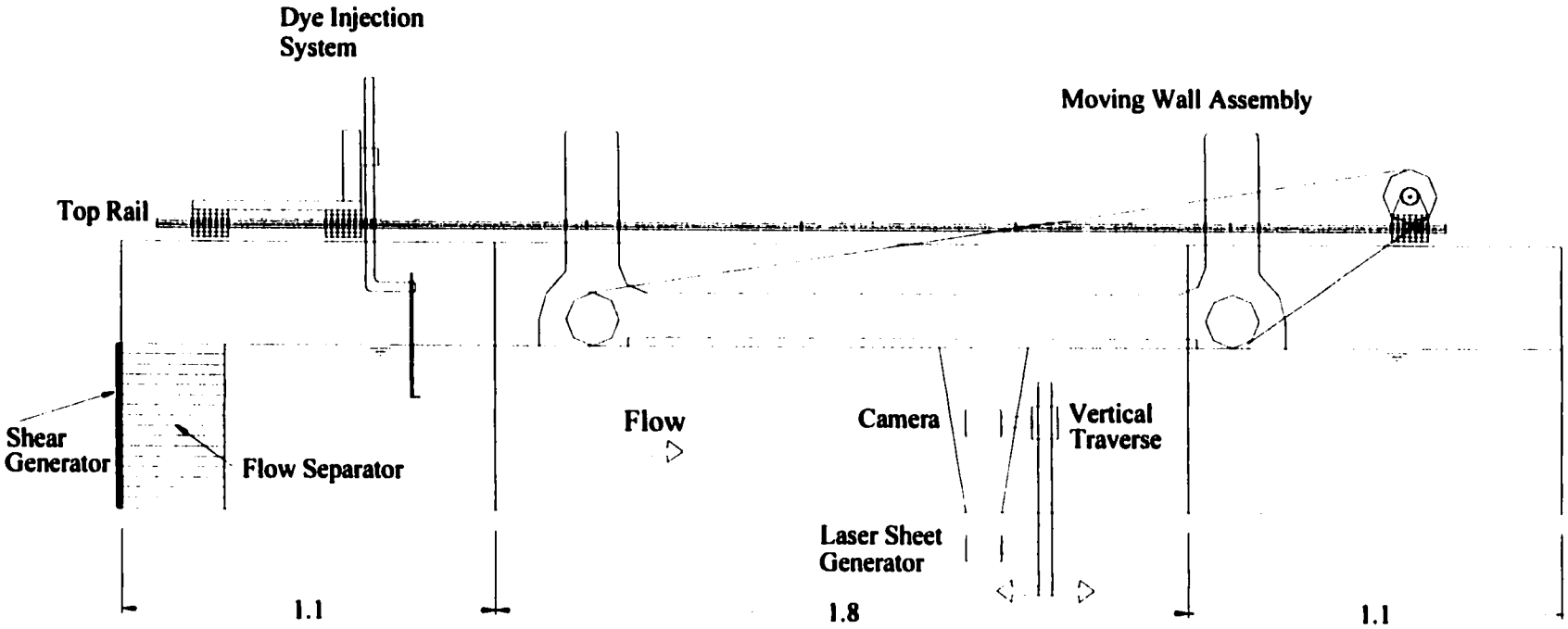

Figure 4.6 Test section side view with equipment locations

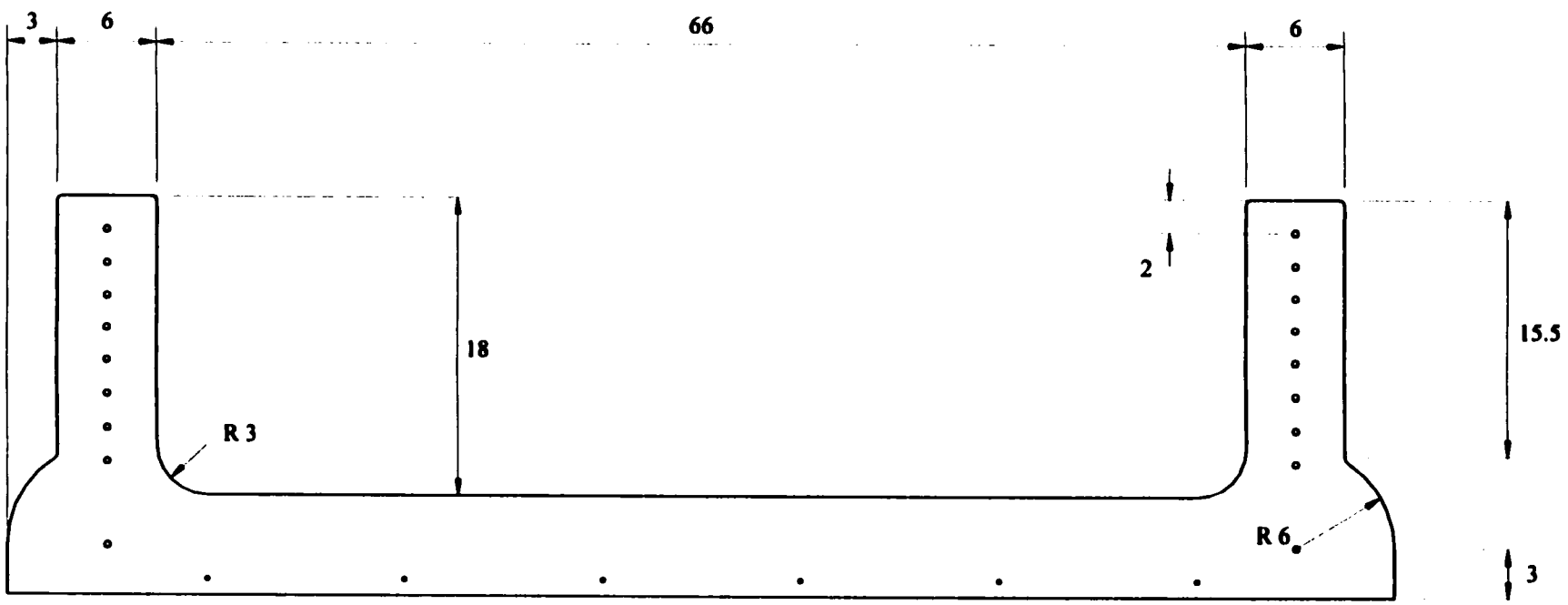

all dimensions in inches

Figure 4.7 Moving wall frame

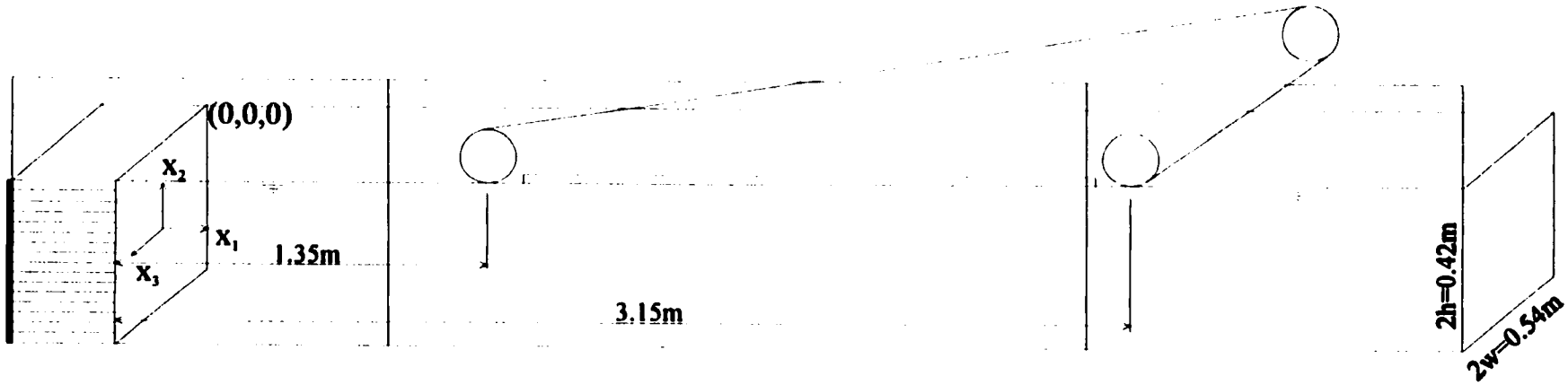

Figure 5.1 Coordinate system used for USF studies.

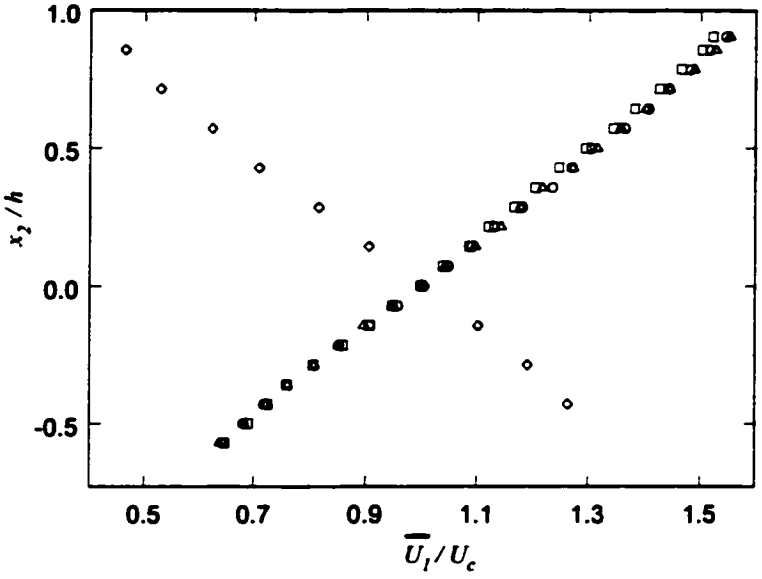

Figure 5.2 USF - Mean streamwise velocity profile for the high speed case at $\tau = 5.4(\circ)$, $7.9(\square)$ and $9.7(\triangle)$ and the low speed case at $\tau = 15(\diamond)$.

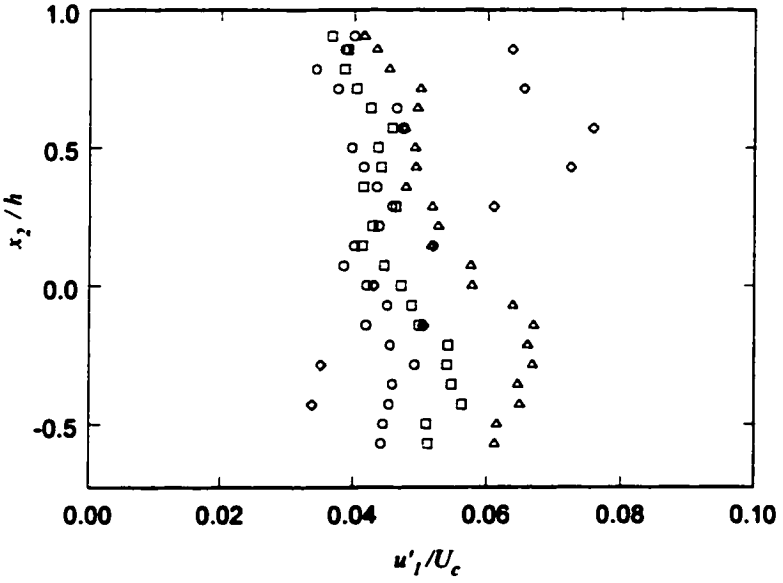

Figure 5.3 USF - Transverse profiles of the streamwise rms turbulence fluctuations for the high speed case at $\tau = 5.4(\circ)$, $7.9(\square)$ and $9.7(\triangle)$ and the low speed case at $\tau = 15(\diamond)$.

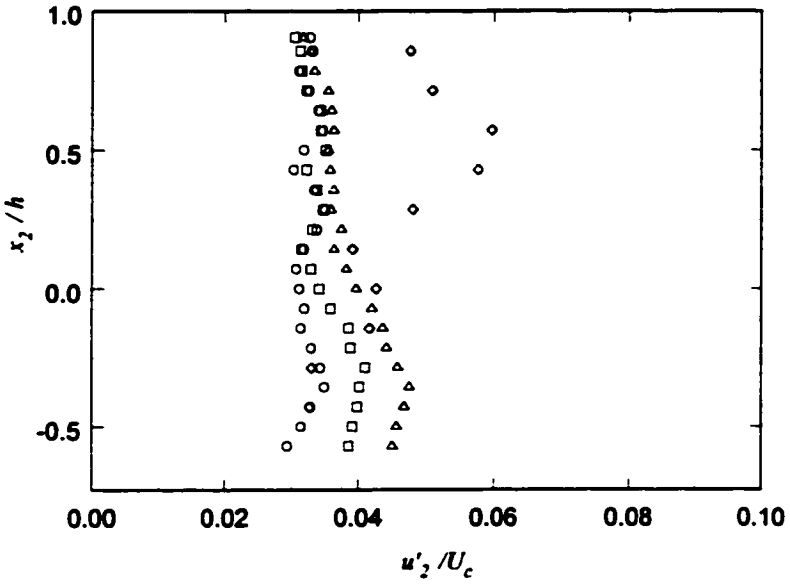

Figure 5.4 USF - Transverse variation of the transverse rms turbulence fluctuations for the high speed case at $\tau = 5.4(\circ)$, $7.9(\square)$ and $9.7(\triangle)$ and the low speed case at $\tau = 15(\diamond)$.

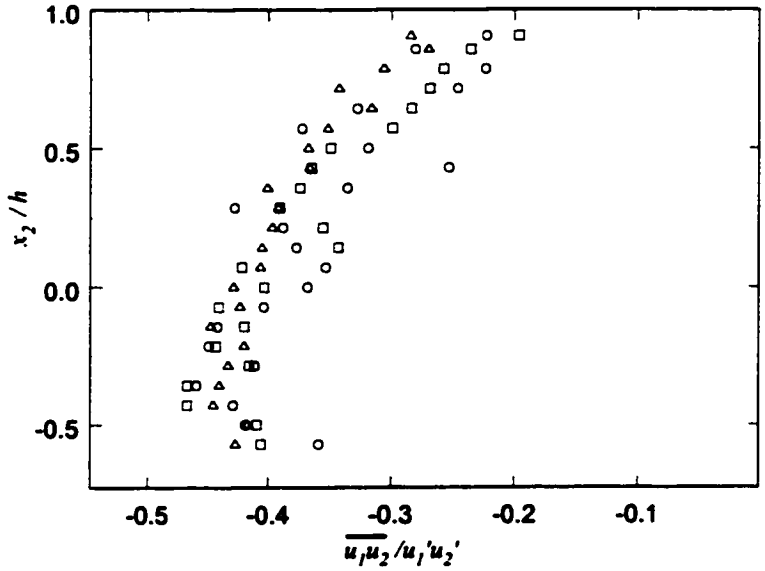

Figure 5.5 USF - Transverse profile of the shear stress correlation coefficient, $\overline{u_1 u_2}/u_1' u_2'$ for the high speed case at $\tau = 5.4(\circ)$, $7.9(\square)$ and $9.7(\triangle)$.

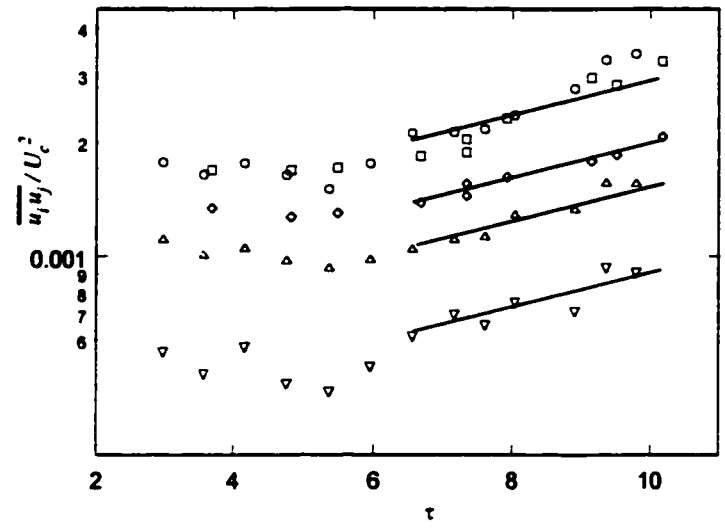

Figure 5.6 USF - Streamwise evolution of turbulent stresses along the water tunnel centreline for the high speed case: data from U_1 and U_2 LDV: $u_1'^2/U_c^2$(o), $u_2'^2/U_c^2$ (Δ), - $\overline{u_1 u_2}/U_c^2$ (∇); data from U_1 and U_3 LDV: $u_1'^2/U_c^2$($\Box$), $u_3'^2/U_c^2$($\Diamond$). Straight lines represent fitted exponential expressions.

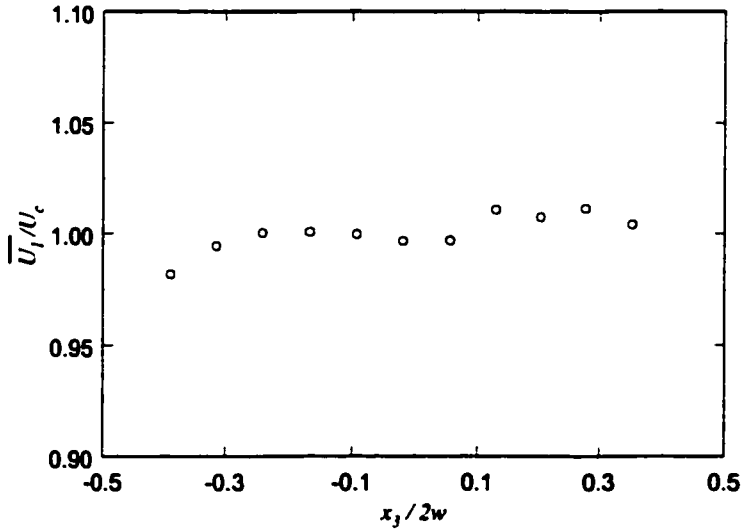

Figure 5.7 USF - Spanwise variation of mean streamwise velocity for the high speed case at $\tau = 7.9$.

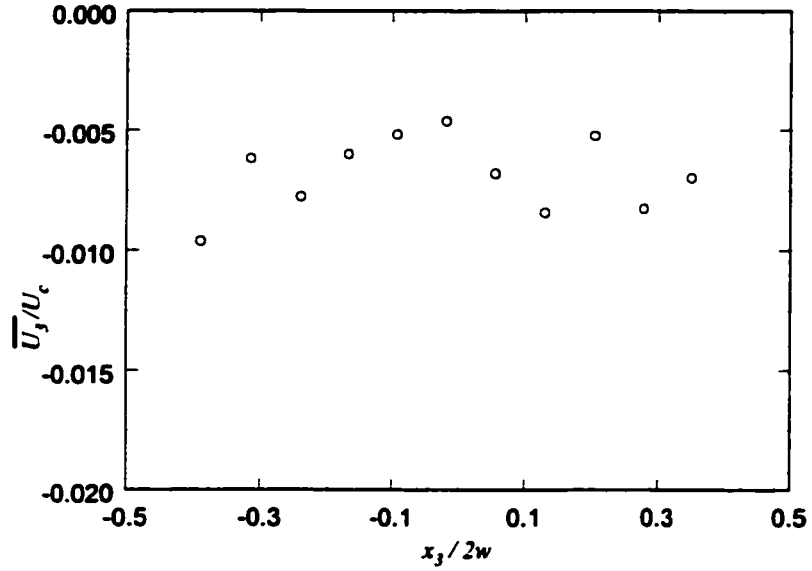

Figure 5.8. USF - Spanwise variation of mean spanwise velocity for the high speed case at $\tau = 7.9$, $y/h = 0$.

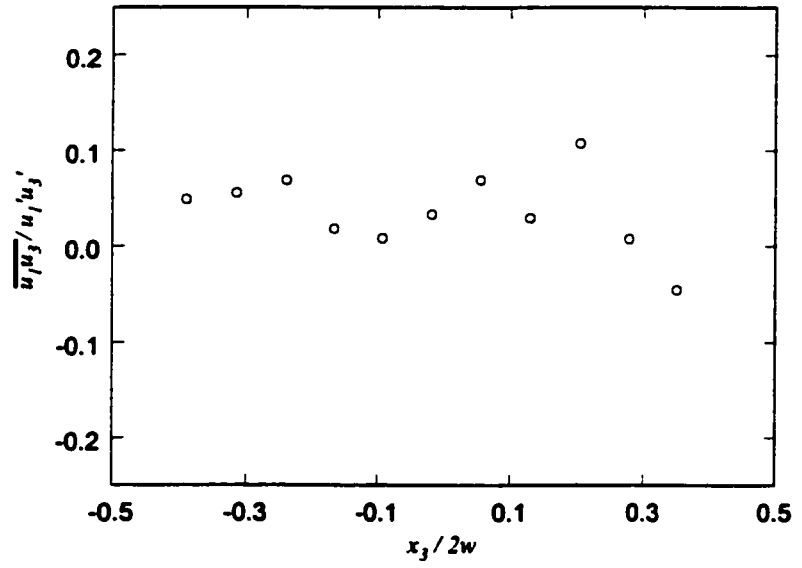

Figure 5.9. USF - Spanwise variation of the shear stress correlation coefficient, $\overline{u_1u_3}/u_1'u_3'$ for the high speed case at $\tau = 7.9$, $y/h = 0$.

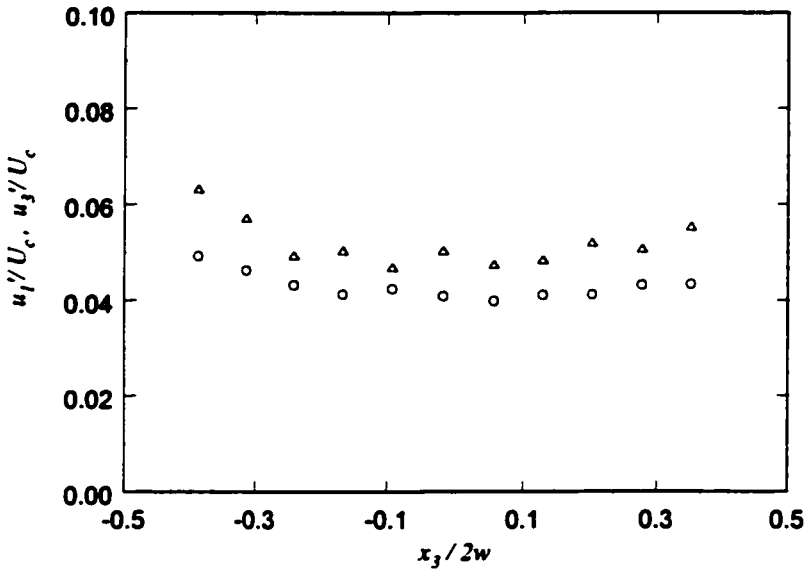

Figure 5.10 USF - Spanwise variation of rms turbulent fluctuations for the high speed case at $\tau = 7.9$, $y/h = 0$: $u_1'/U_c(\Delta)$, $u_3'/U_c(\circ)$.

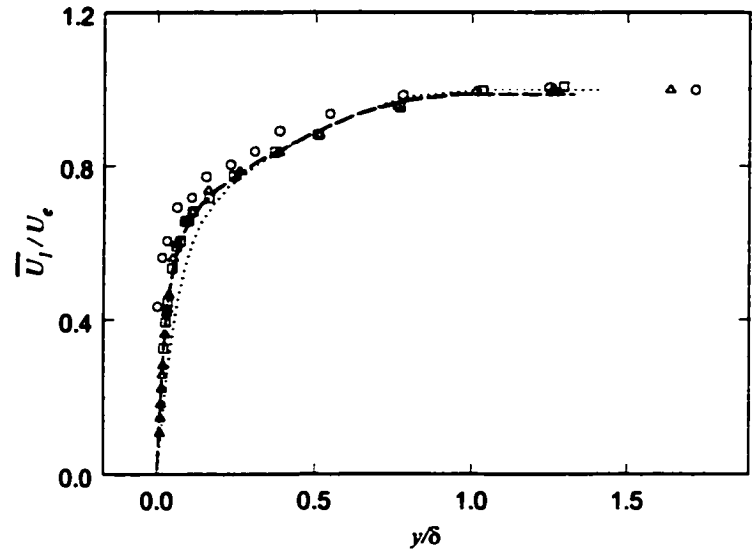

Figure 5.11 TBL - Mean streamwise velocity for low speed case (o) and high speed case: single component LDV (△) and two component LDV (□), at $x_1 = 2.6$ m. Data from Spalart, 1989 $\mathrm{Re}_\theta = 670(--)$, $Re_\theta = 300(\cdots)$.

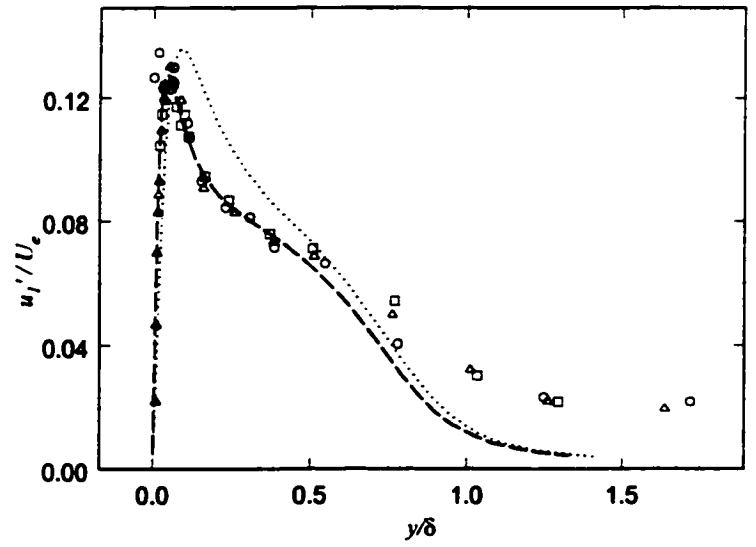

Figure 5.12 TBL - Streamwise velocity fluctuations at $x_1 = 2.6$ m. (for symbols see Figure 5.11)

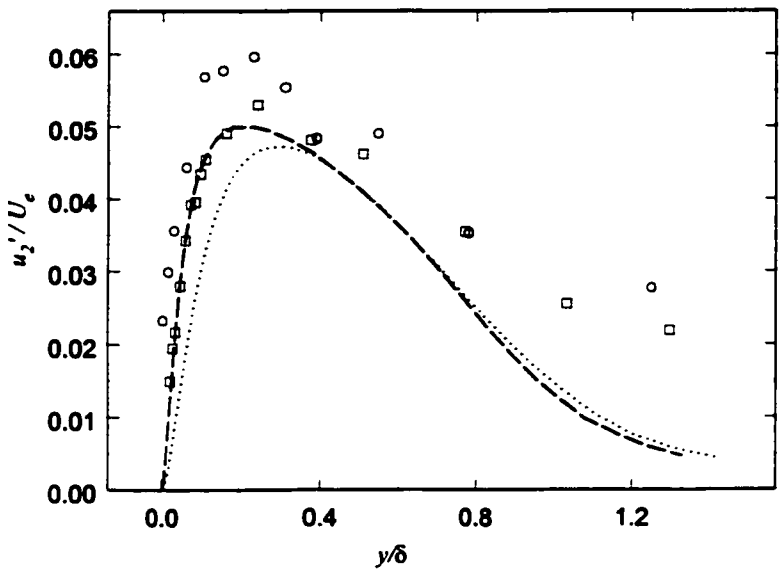

Figure 5.13 TBL - Normal velocity fluctuations at $x_1 = 2.6$ m. (for symbols see Figure 5.11)

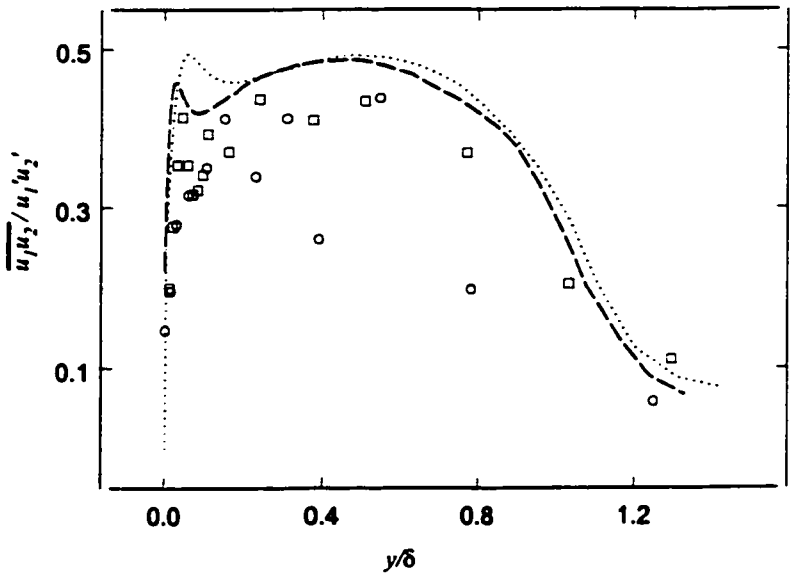

Figure 5.14 TBL - Shear stress correlation coefficient, $\overline{u_1u_2}/u_1'u_2'$ at $x_1 = 2.6$ m. (for symbols see Figure 5.11)

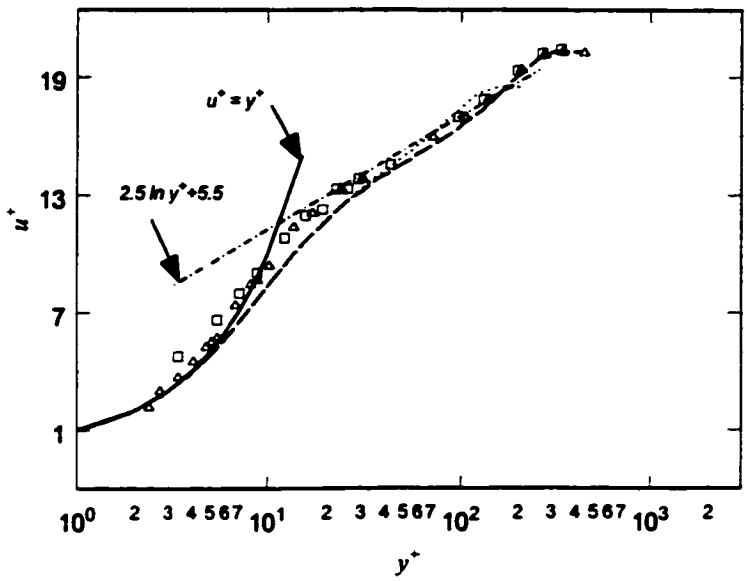

Figure 5.15 TBL - Logarithmic region of the boundary at $x_1 = 2.6$ m. (for symbols see Figure 5.11)

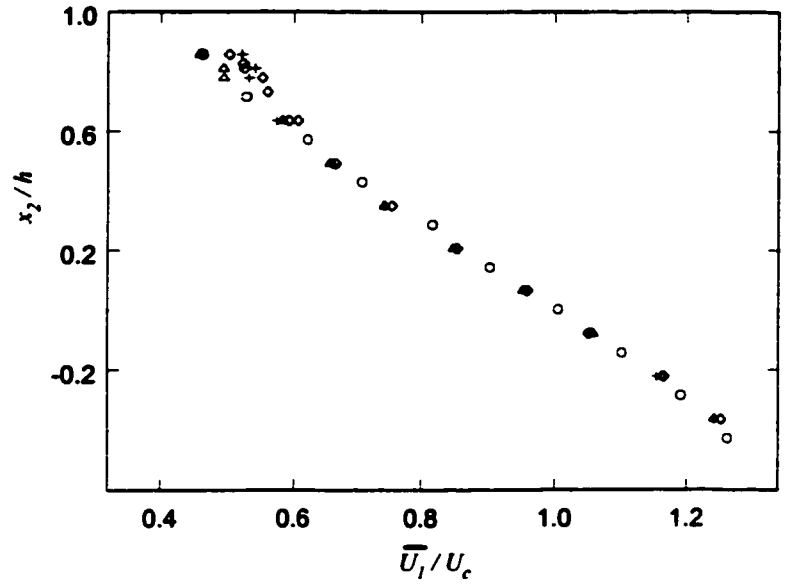

Figure 5.16 MW - Mean streamwise velocities in the core of the flow at $x_1 = 2.6\,\mathrm{m}$: MW0 (o), MWE (◇), MWN (△), MWP (+).

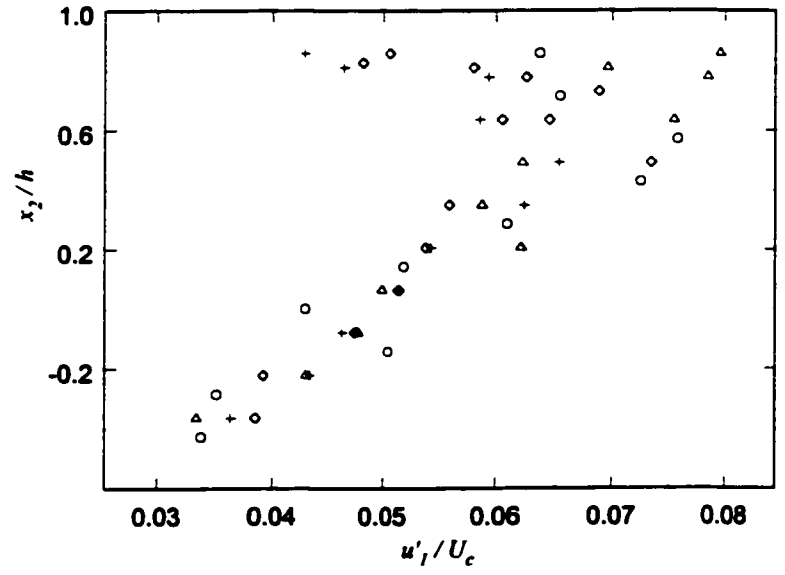

Figure 5.17 MW - Streamwise velocity fluctuations in the core of the flow at $x_1 = 2.6\,\mathrm{m}$: MW0 (o), MWE (◇), MWN (△), MWP (+).

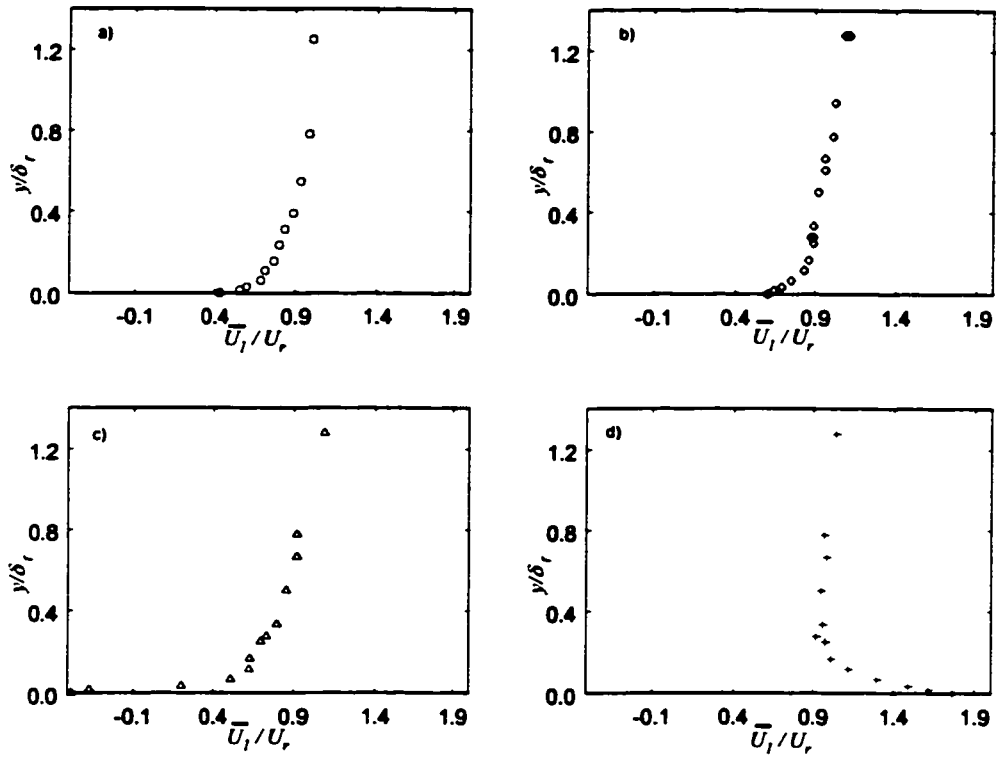

Figure 5.18 MW - Mean streamwise velocities near the wall at $x_1 = 2.6\,\mathrm{m}$: UF (o), MWE ($\diamond$), MWN (Δ), MWP (+).

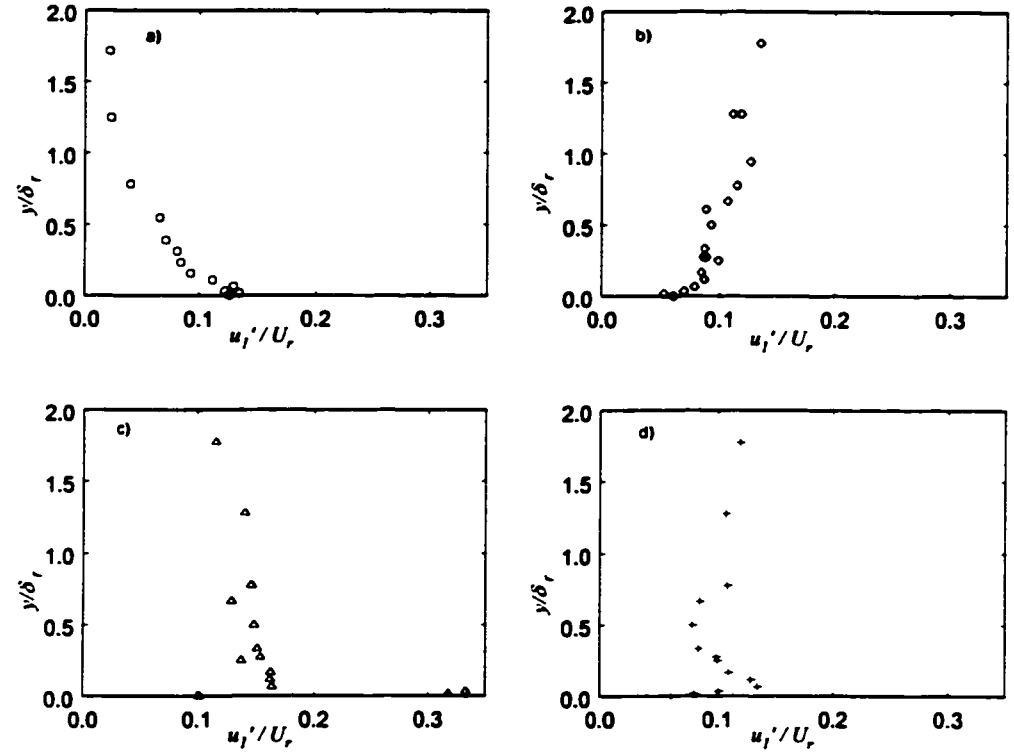

Figure 5.19 MW - Streamwise velocity fluctuations near the wall at $x_1 = 2.6\,\mathrm{m}$: UF (o), MWE ($\diamond$), MWN ($\triangle$), MWP (+).

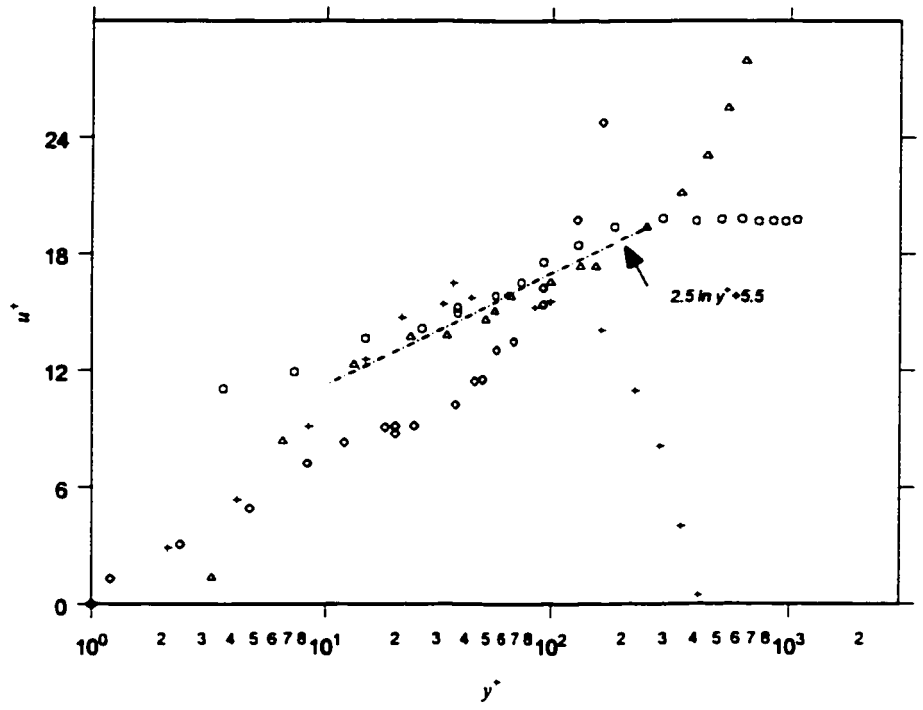

Figure 5.20 MW - Logarithmic region calculated for moving wall studies with $u^+ = \left|\overline{U}_1 - U_w\right| / u^*$ at $x_1 = 2.6\,\mathrm{m}$: UF (o),MWE (◇), MWN (△), MWP (+)

Frame sequence 6.1 - USF low speed case, core flow viewed from the side with camera moving downstream between approx $x_1 \approx 2.4$m and $x_1 \approx 2.6$m; a) t=0s, b) t=0.73s, c) t=1.6s, d) t=2.3s, e) t=2.9s (tape 2, 07:40)

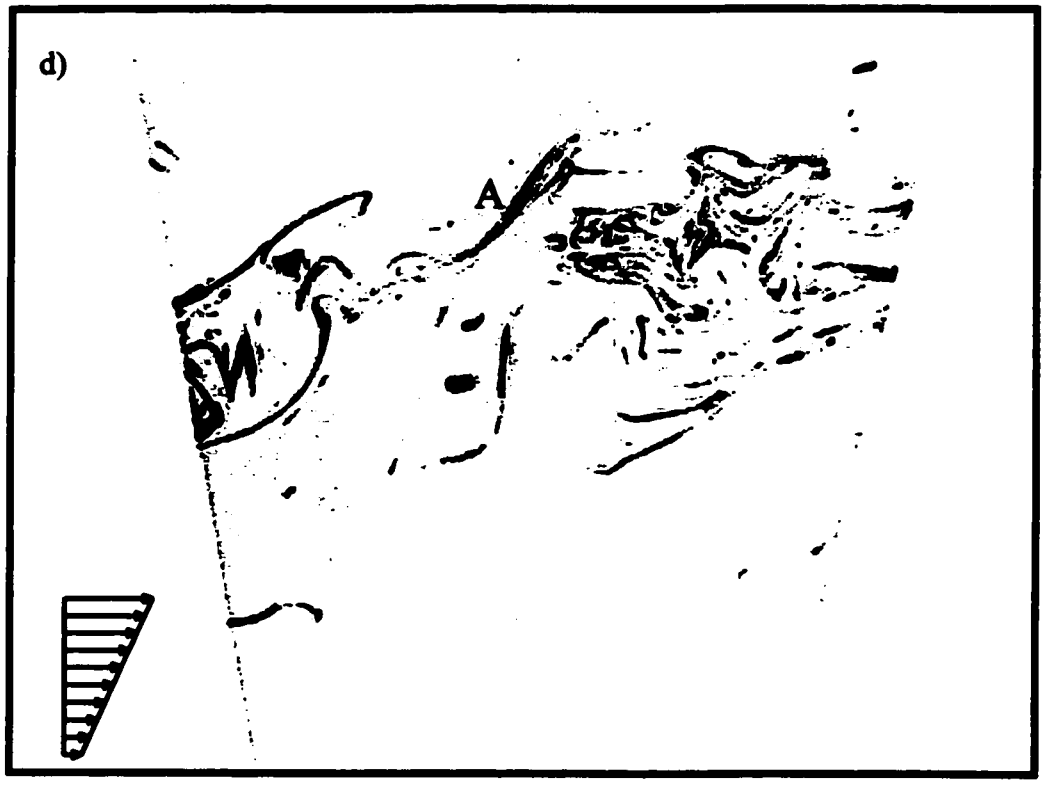

Frame sequence 6.1 (continued)

Frame sequence 6.1 (continued).

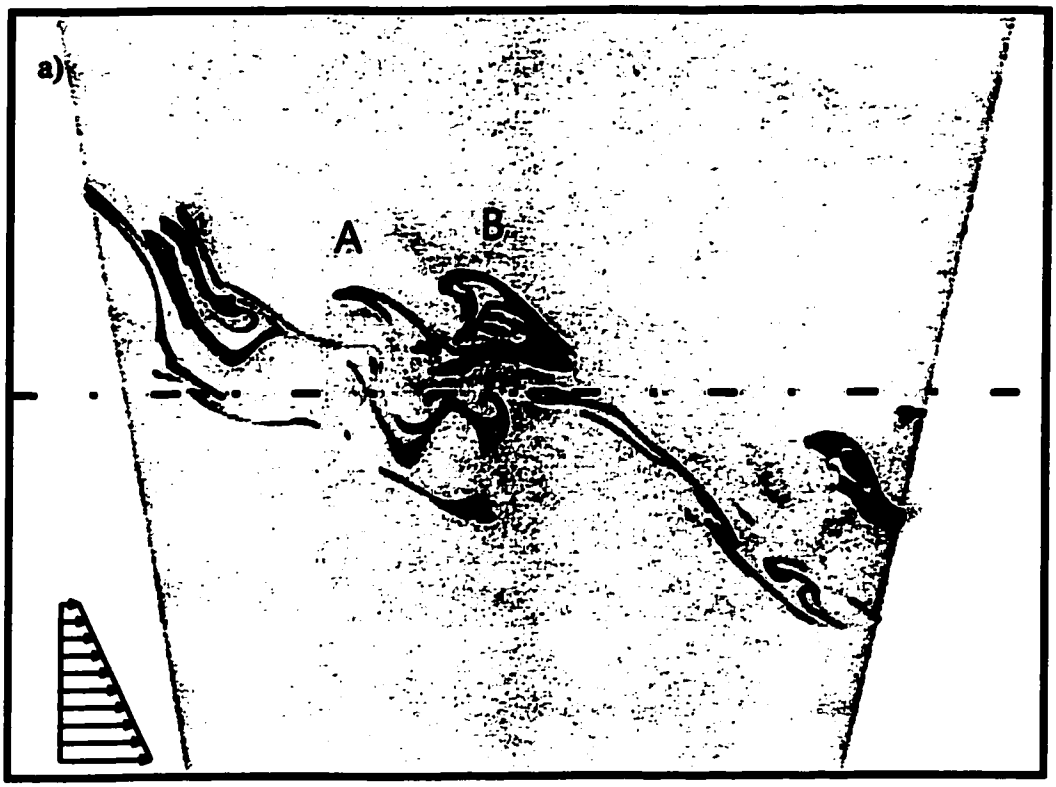

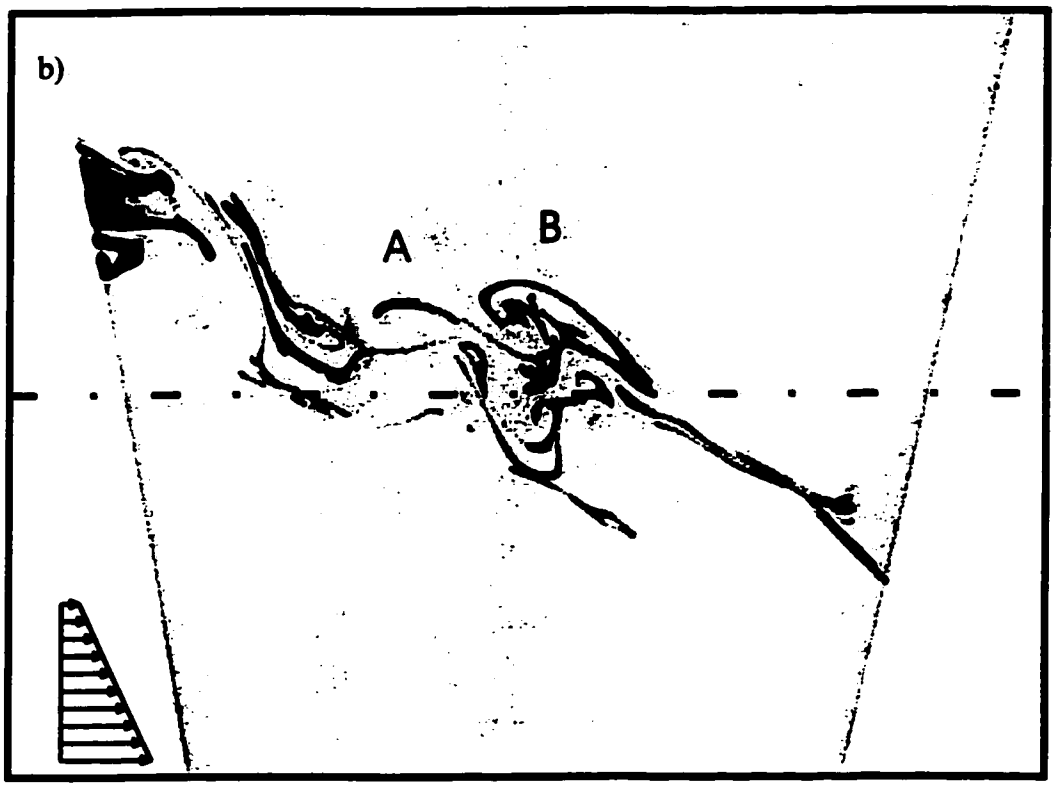

Frame sequence 6.2 - USF low speed case, core flow viewed from the side with camera moving downstream between approx $x_1 \approx 2.2$m and $x_1 \approx 2.6$m; a) t=0s, b) t=1.6s, c) t=3.5s, d) t=4.9s, e) t=6.1s (tape 2, 35:21)

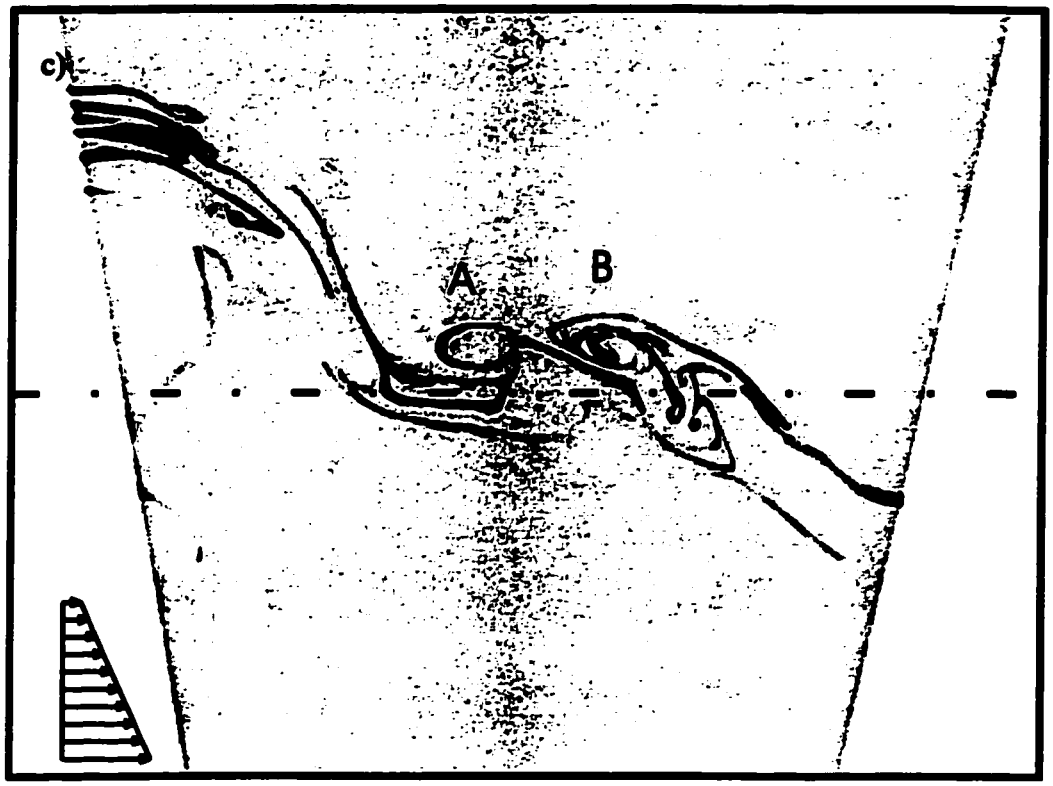

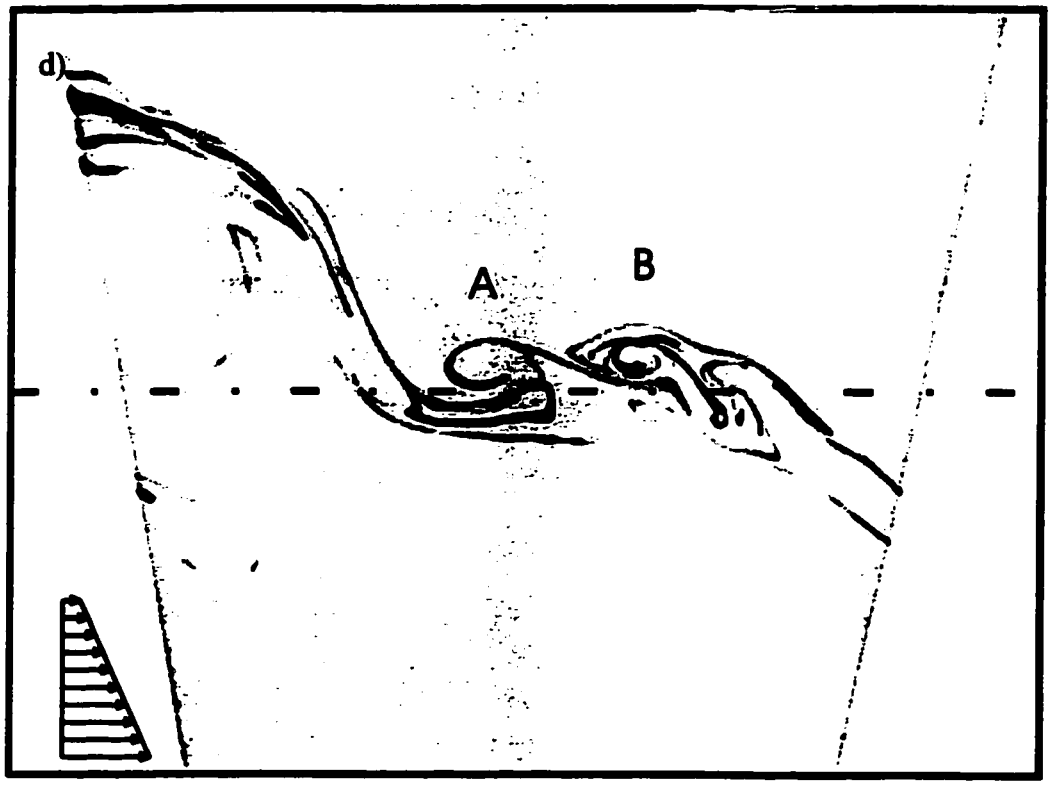

Frame sequence 6.2 (continued)

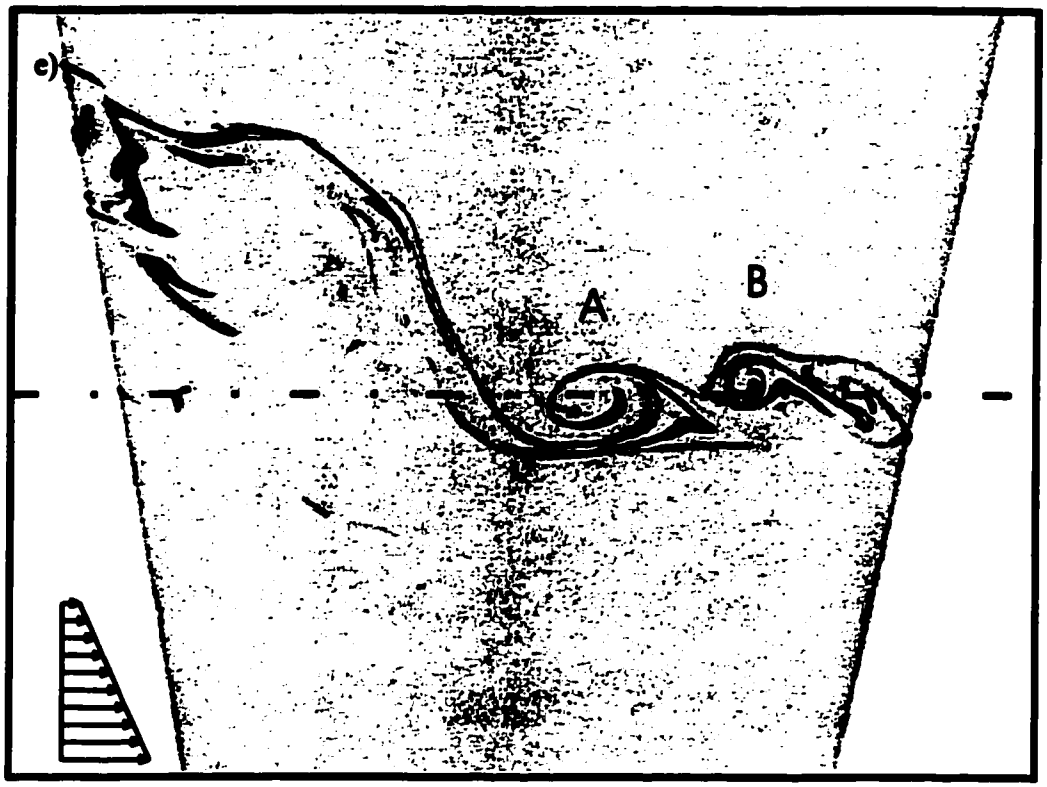

Frame sequence 6.2 (continued).

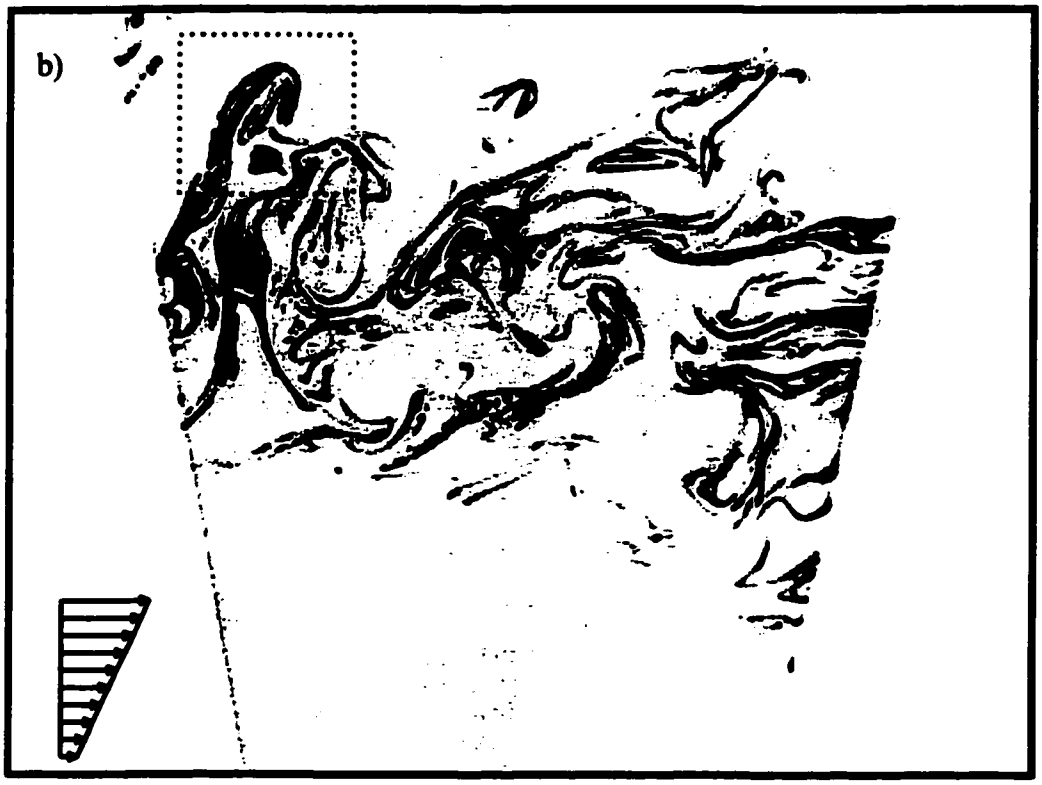

Frame sequence 6.3 - USF low speed case, core flow viewed from the side with camera moving downstream between approx $x_t \approx 2.4$m and $x_t \approx 2.6$m;; a) t=0s, b) t=1.0s, c) t=1.9s, d) t=3.0s (tape 2, 07:30)

Frame sequence 6.3 (continued).

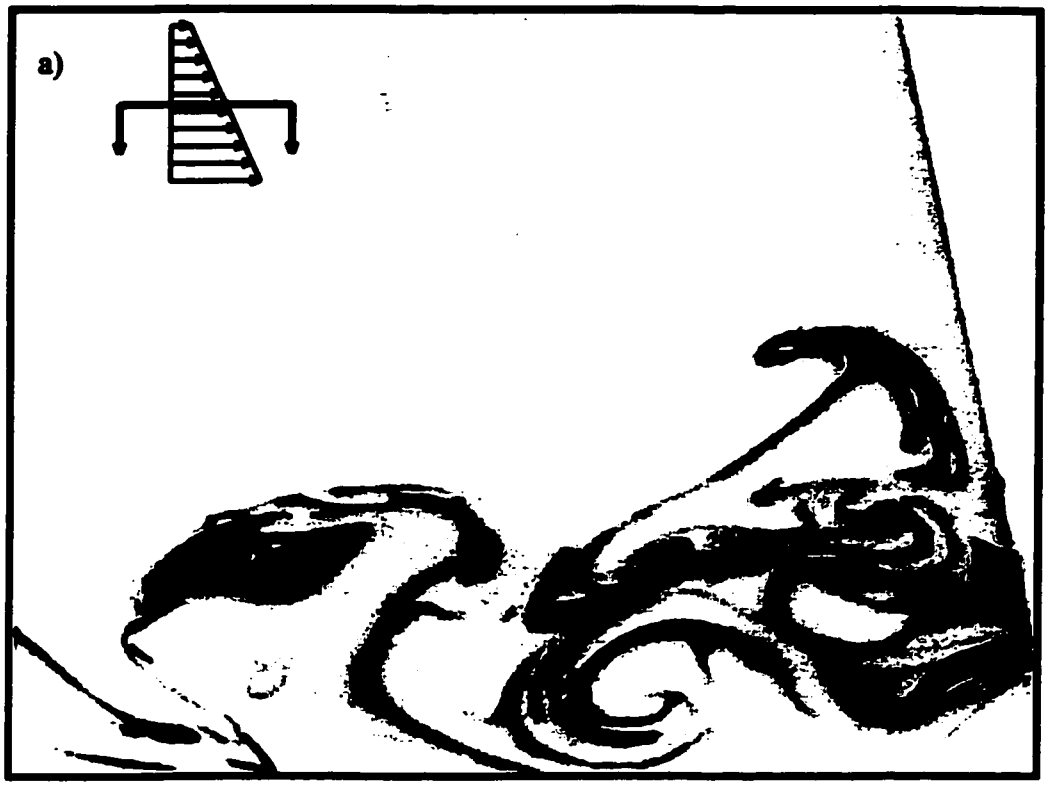

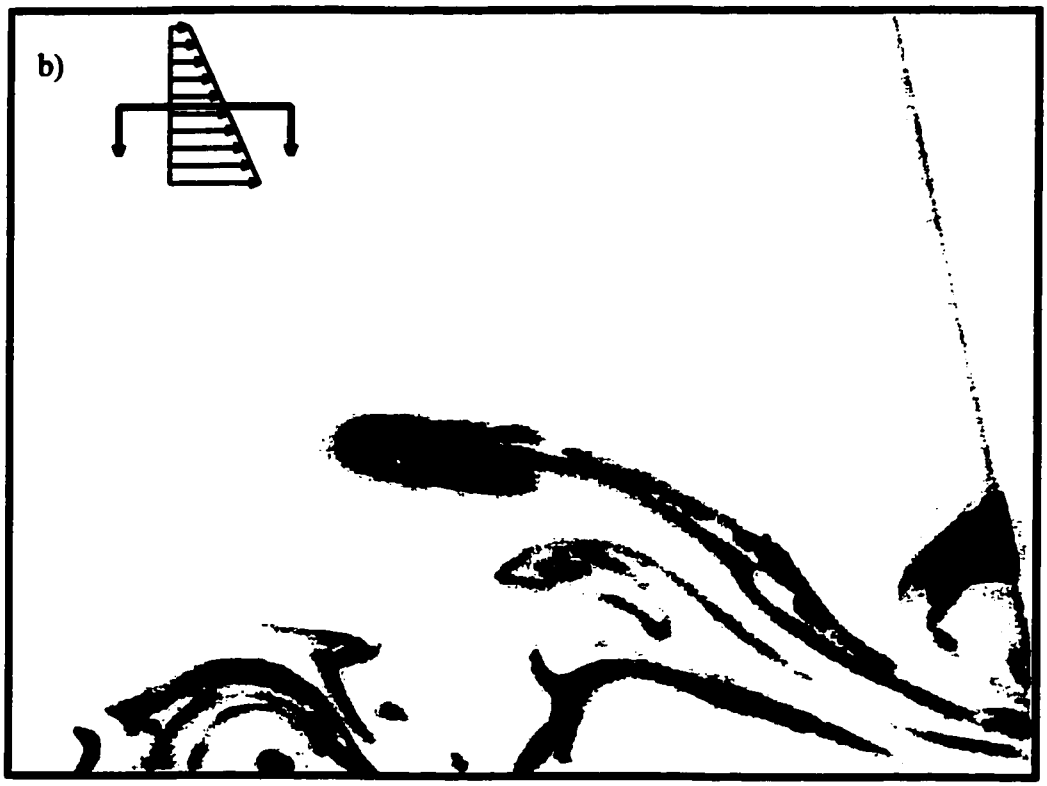

Frame sequence 6.4 - USF low speed case, core flow viewed from below; a) t=0s, b) t=0.38s, c) t=5.0s, d) t=13.3s (tape 2, 31:46)

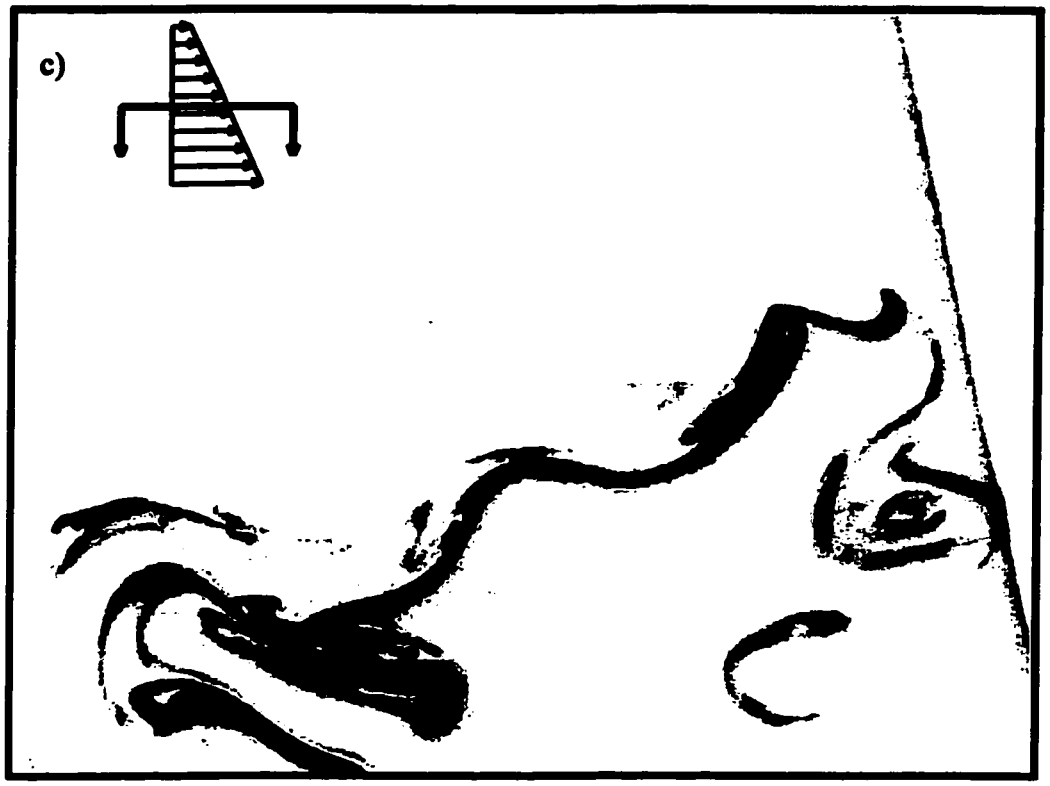

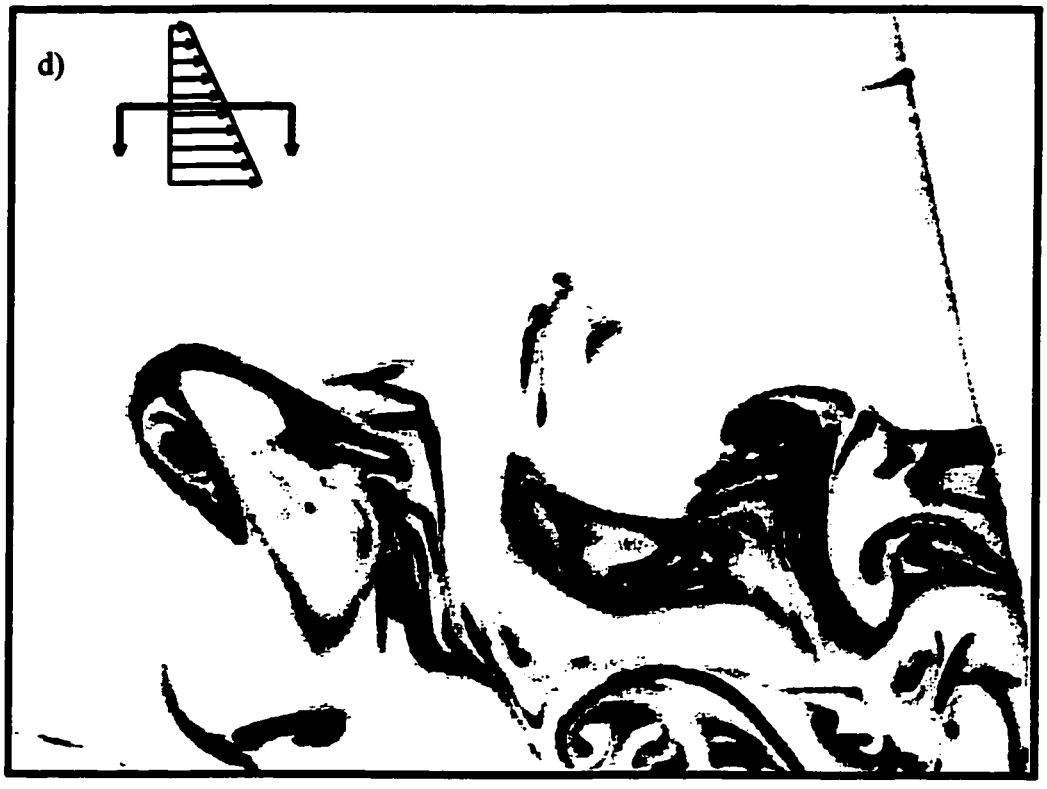

Frame sequence 6.4 (continued).

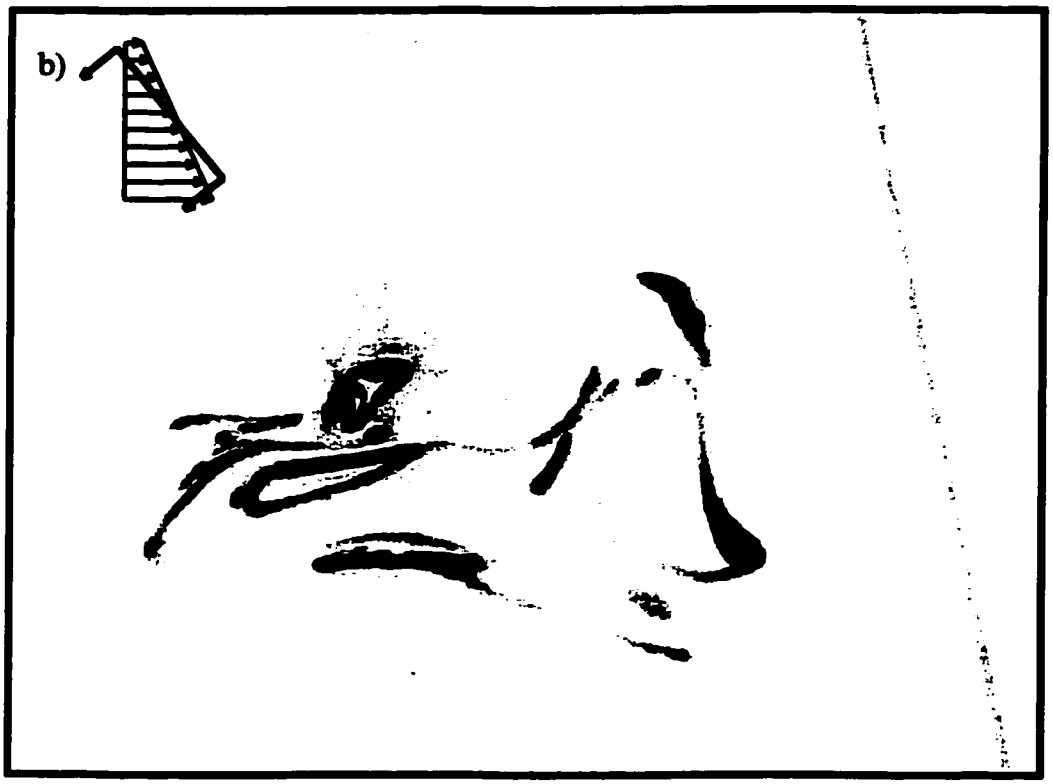

Frame sequence 6.5 - USF low speed case, core flow viewed from below with laser sheet at an angle; a) t=0s, b) t=0.67s, c) t=11.0s (tape 2, 32:15)

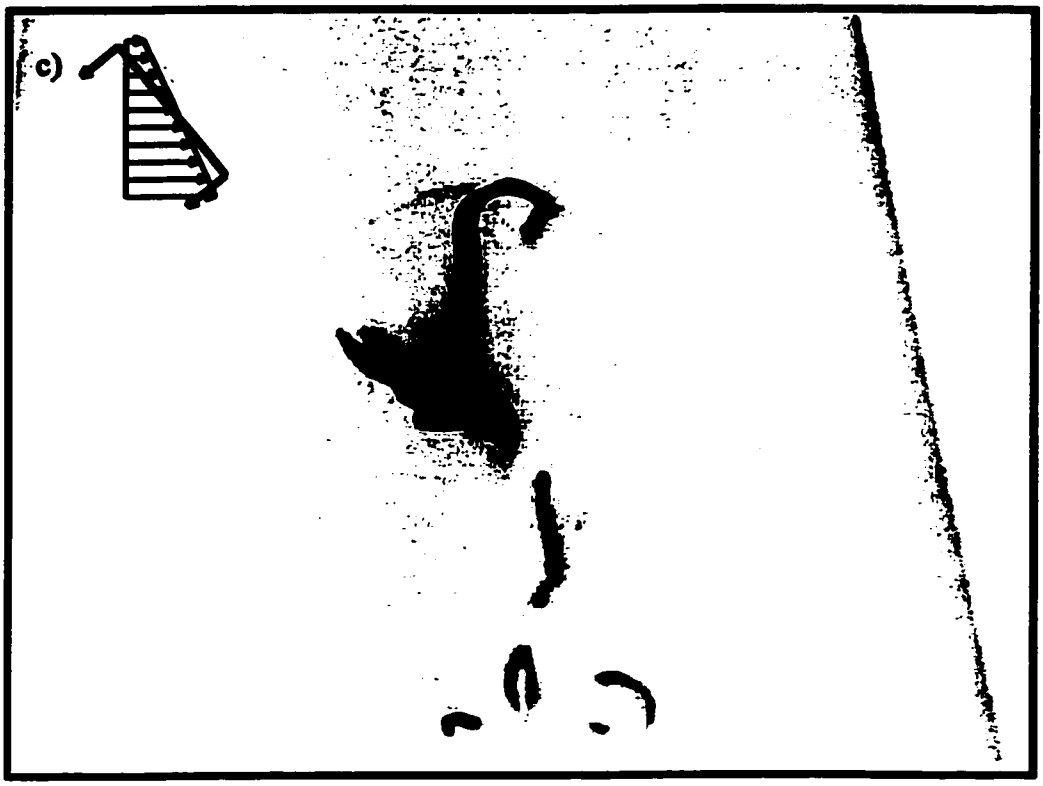

Frame sequence 6.5 (continued).

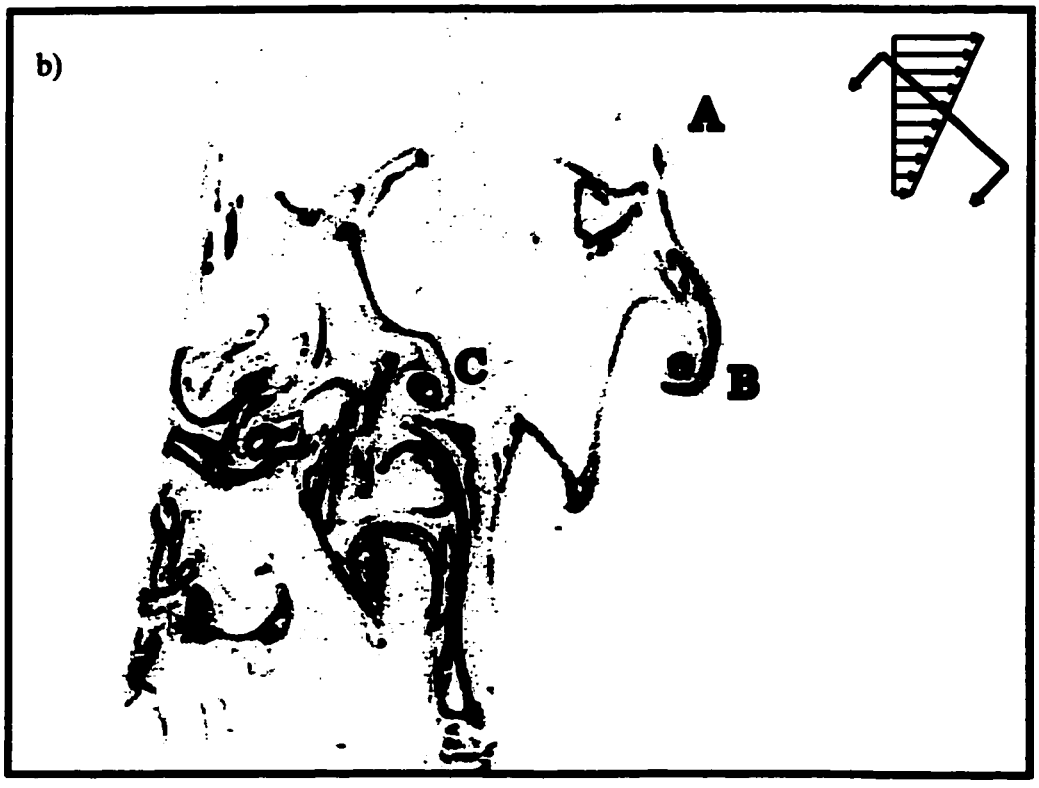

Frame sequence 6.6 - USF low speed case, core flow viewed from below with laser sheet at an angle; a) t=0s, b) t=0.10s, c) t=0.17s, d) t=0.23s, e) t=0.33s (tape 2, 09:42)

Frame sequence 6.6 (continued)

Frame sequence 6.6 (continued).

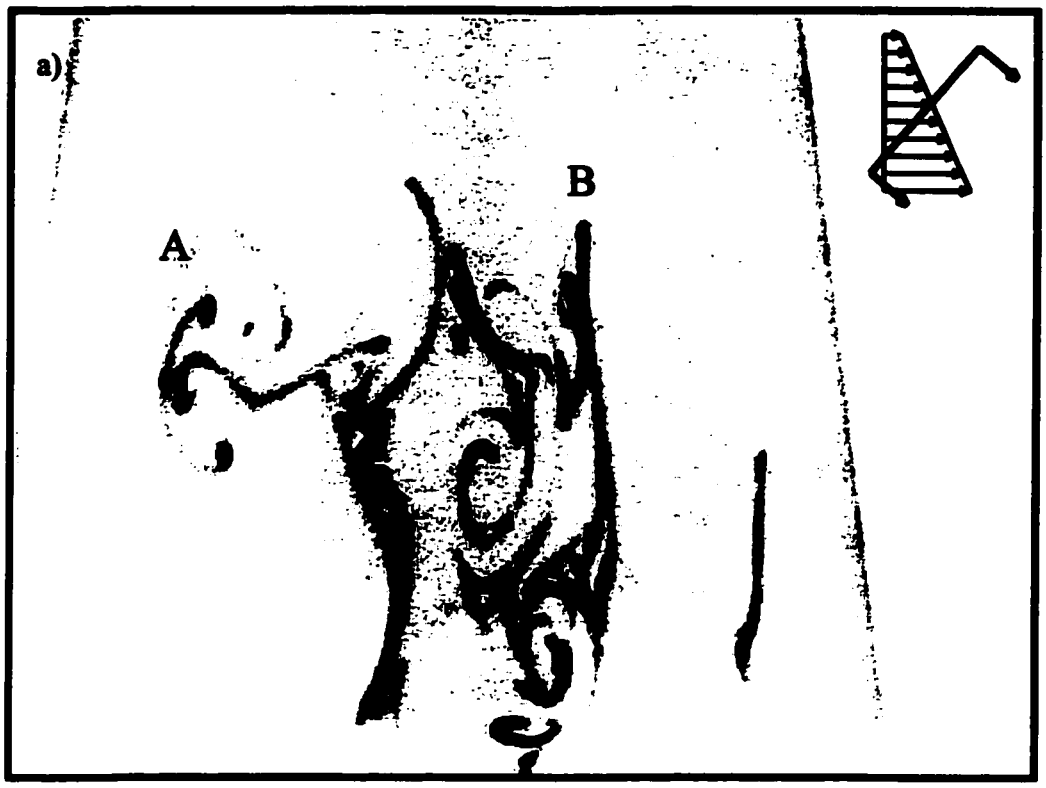

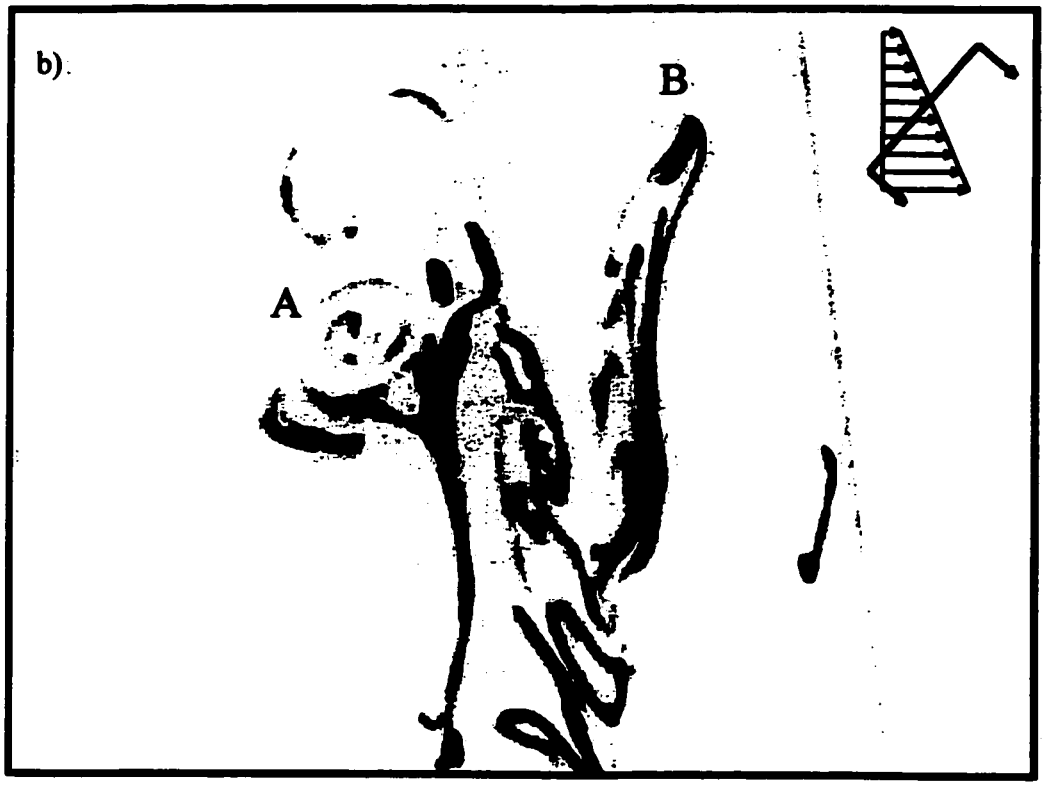

Frame sequence 6.7 - USF low speed case, core flow viewed from below with laser sheet at an angle; a) t=0s, b) t=0.17s, c) t=0.47s, d) t=0.63s (tape 2, 32:48)

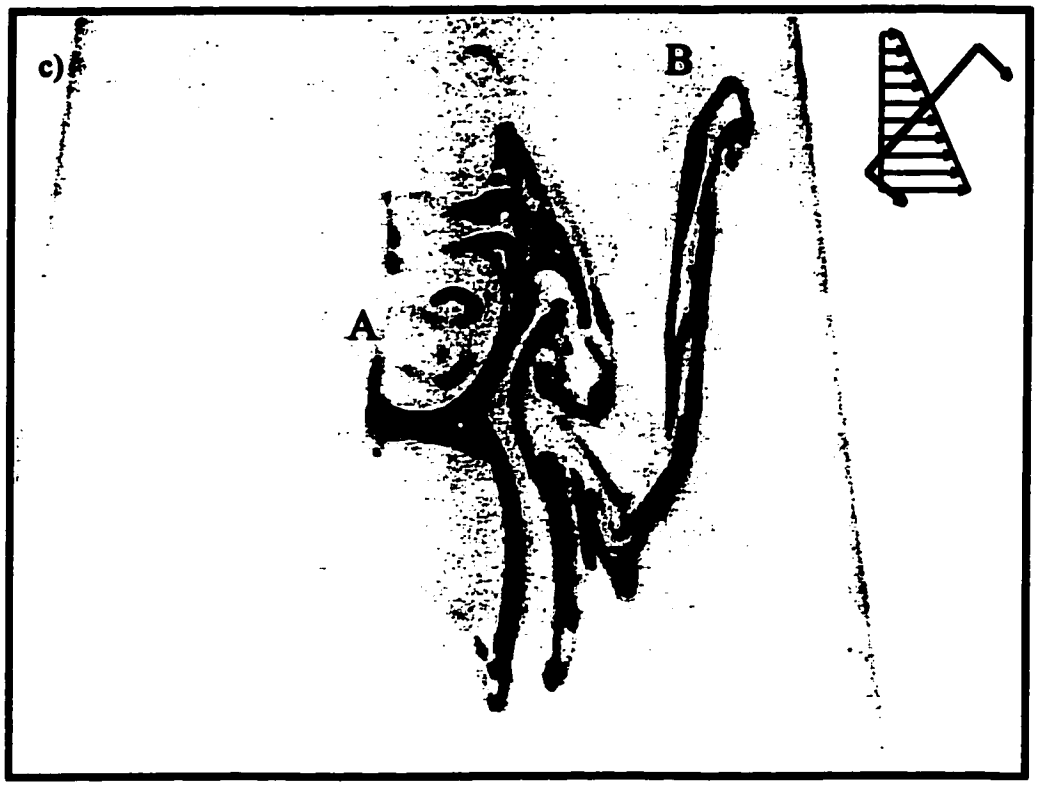

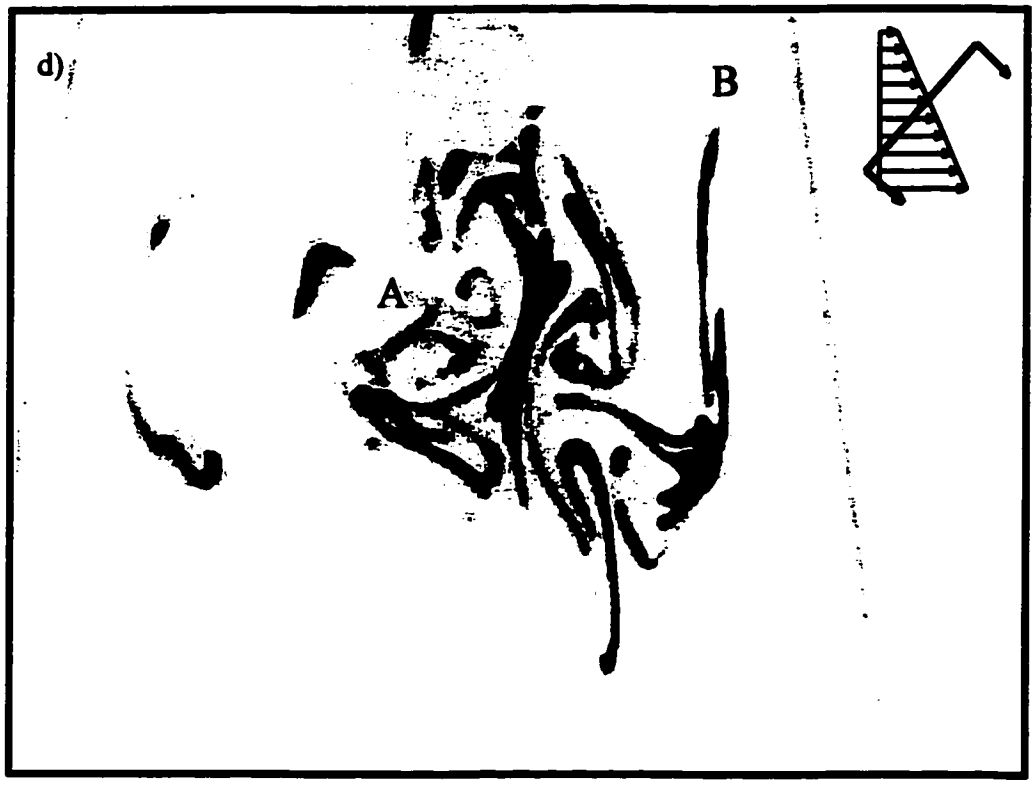

Frame sequence 6.7 (continued).

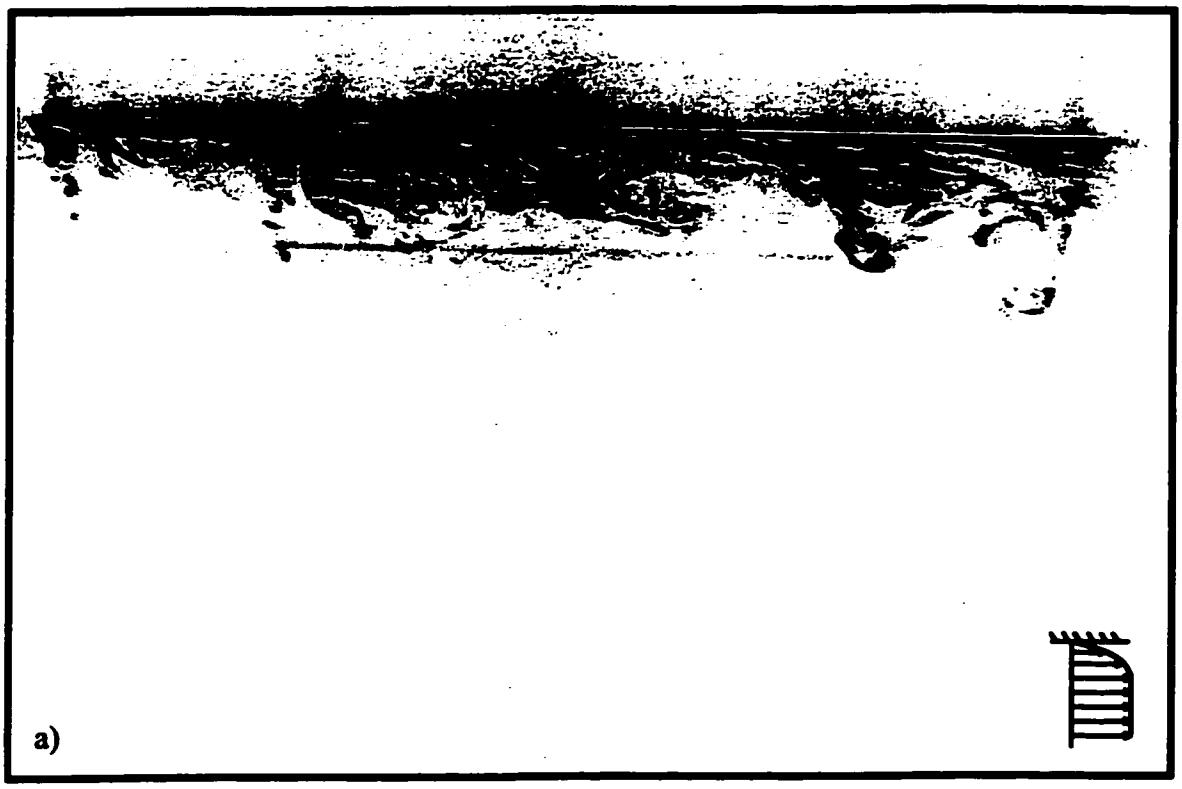

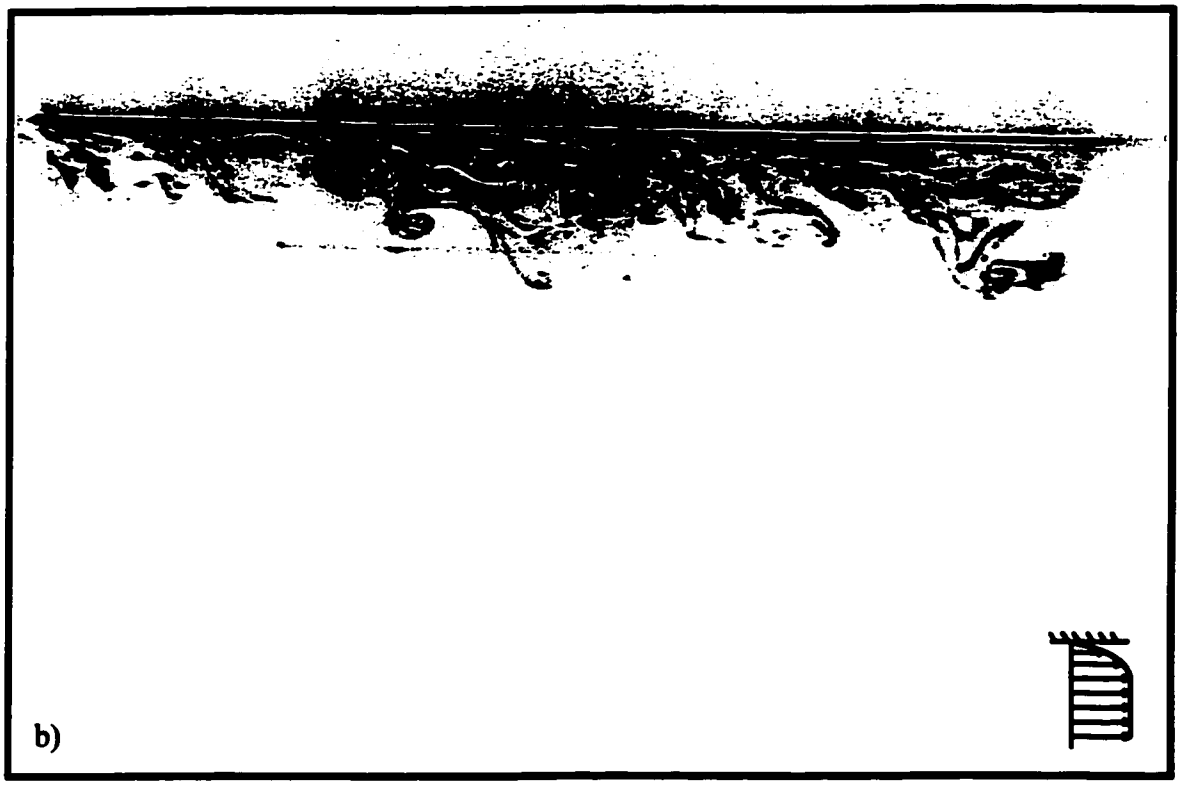

Frame sequence 6.8 - TBL in high speed Uniform Flow, wall flow viewed from the side with camera moving downstream between approx $x_t \approx 2.0$m and $x_t \approx 2.4$m, small dye tube at the wall; a) t=0s, b) t=0.70s, c) t=1.4s, d) t=2.0s, e) t=2.7s, f) t=3.2s (tape 2, 00:36)

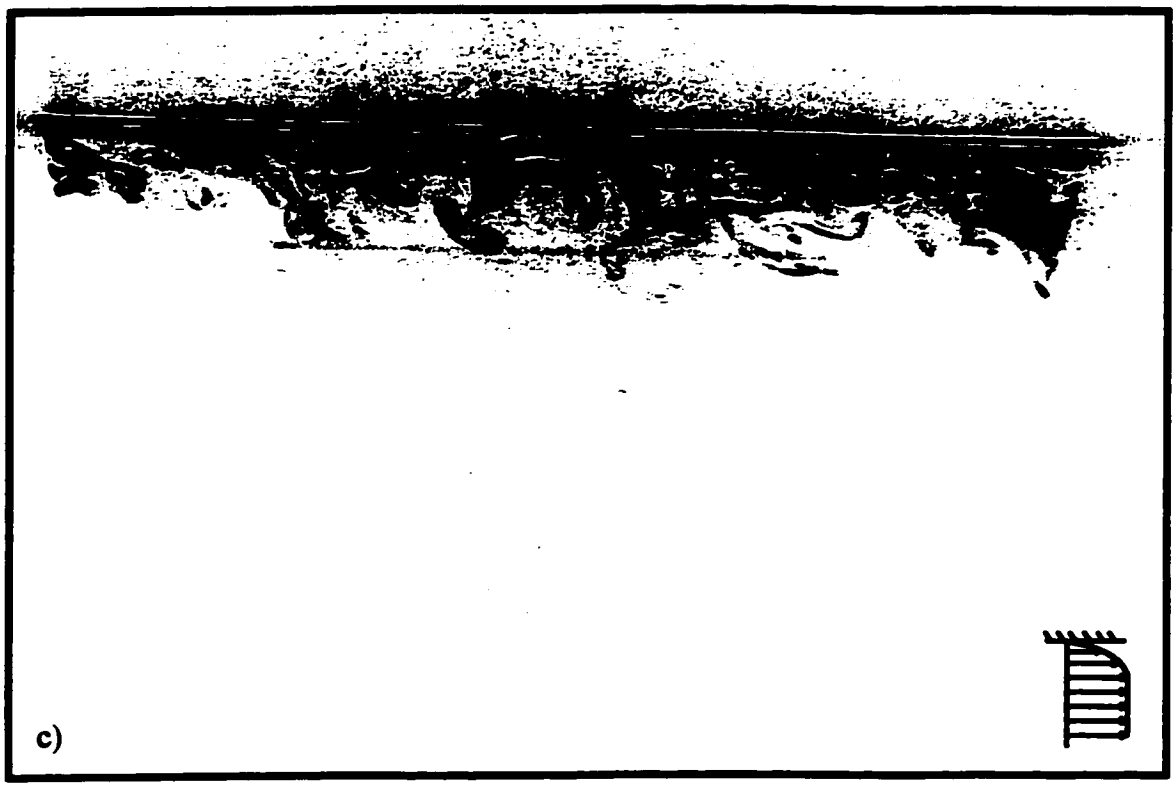

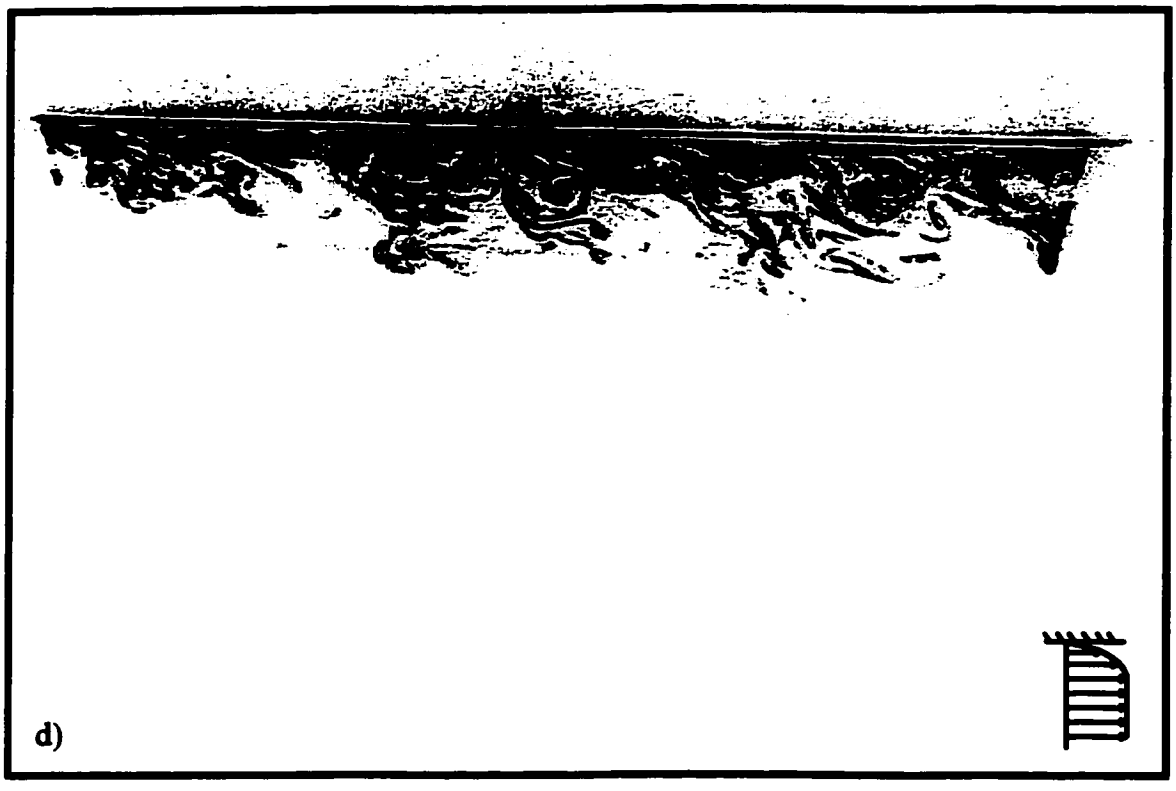

Frame sequence 6.8 (continued)

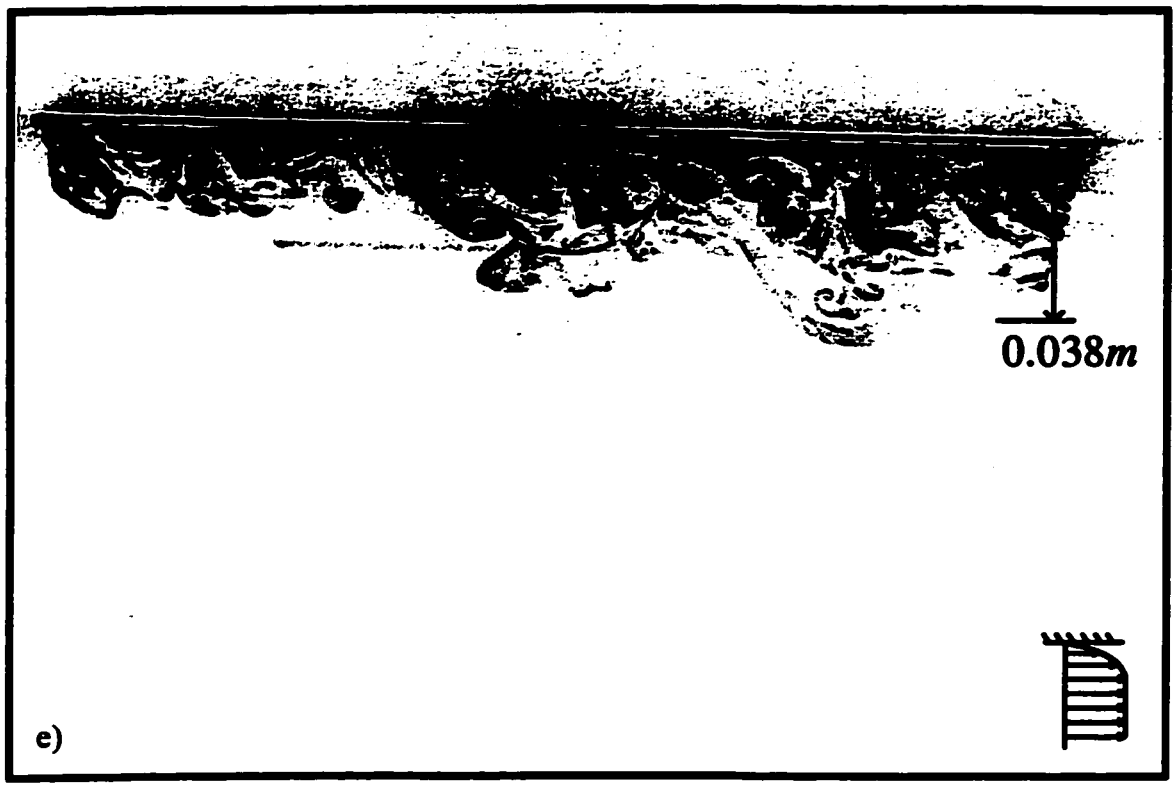

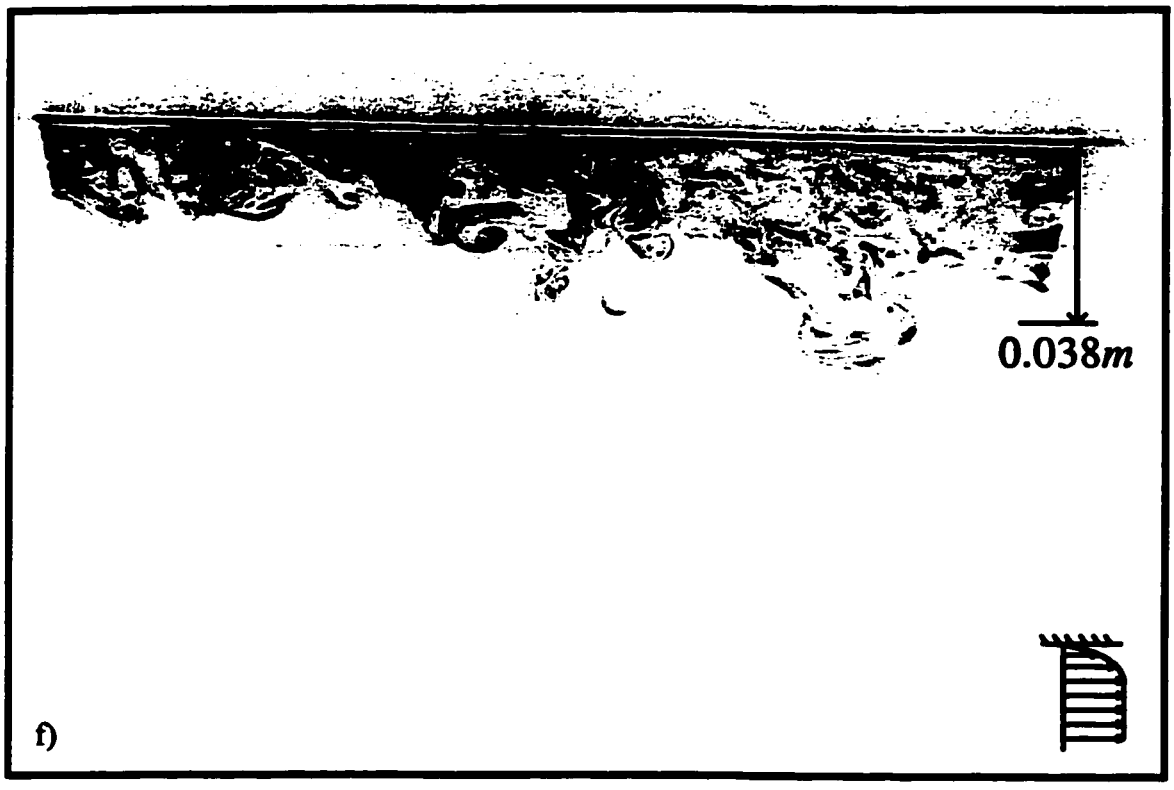

Frame sequence 6.8 (continued).

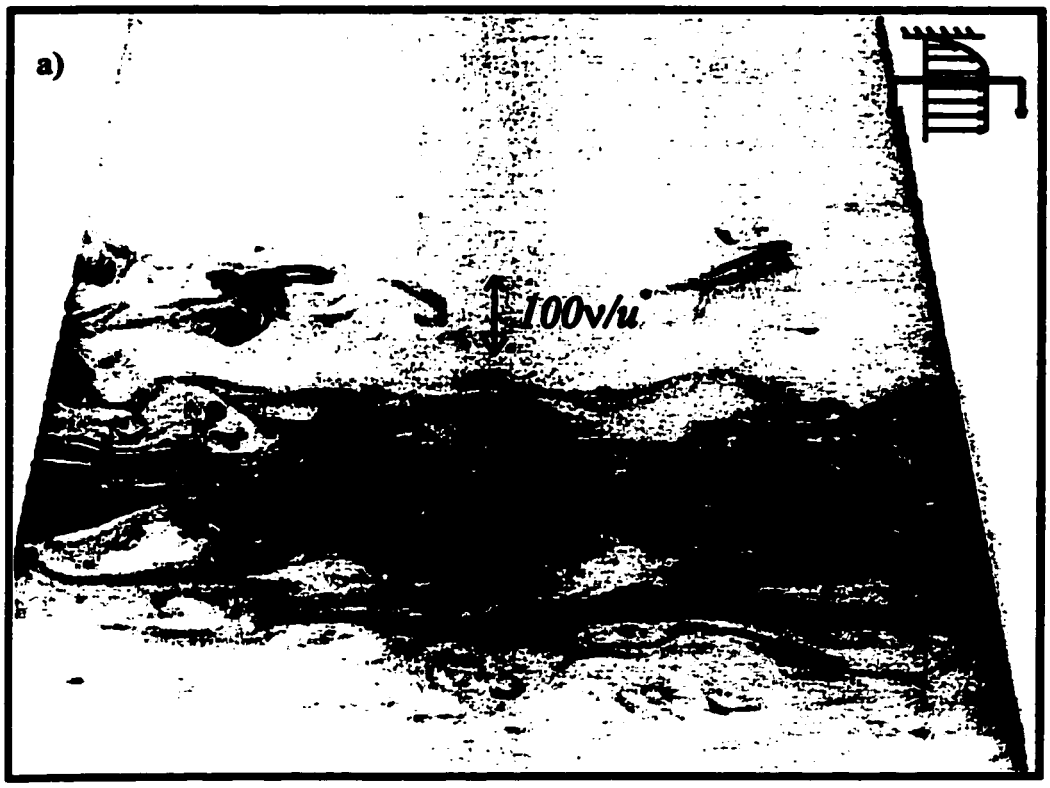

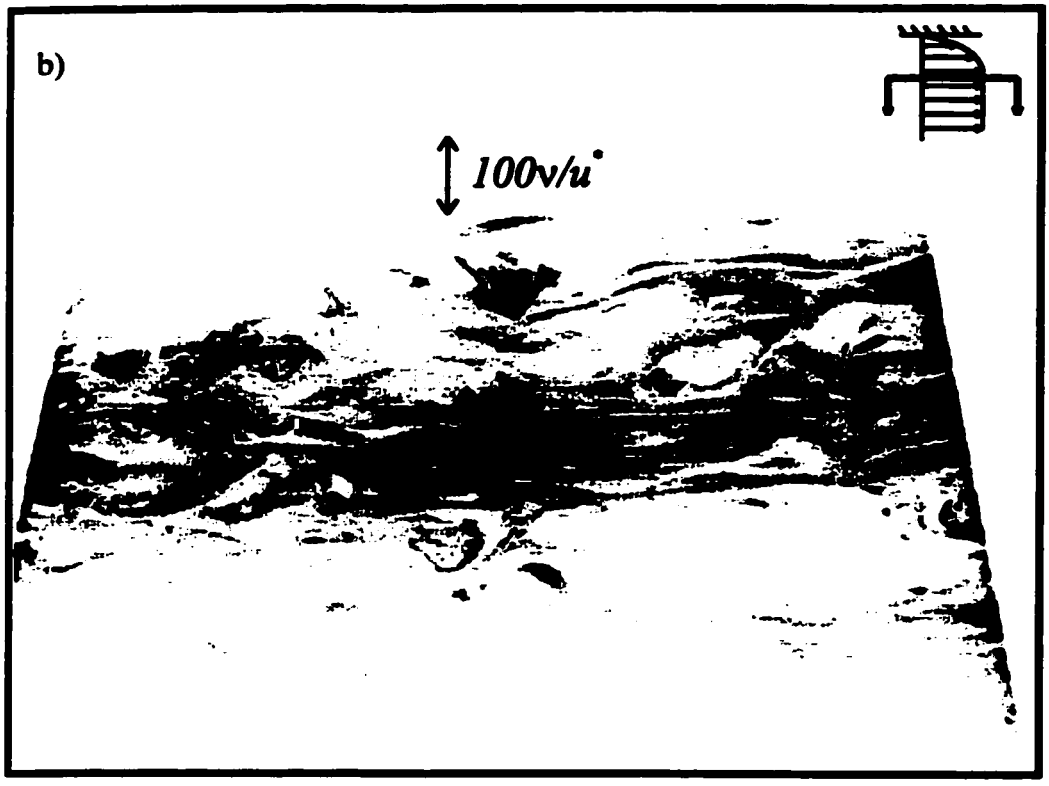

Frame sequence 6.9 - TBL in high speed Uniform Flow, wall flow viewed from below; a) $y^+=1$, b) $y^+=7$, c) $y^+=27$, d) $y^+=68$, e) $y^+=136$, f) $y/\delta=0.83$, g)-i) $y/\delta=1.1$ (tape 2. 16:00)

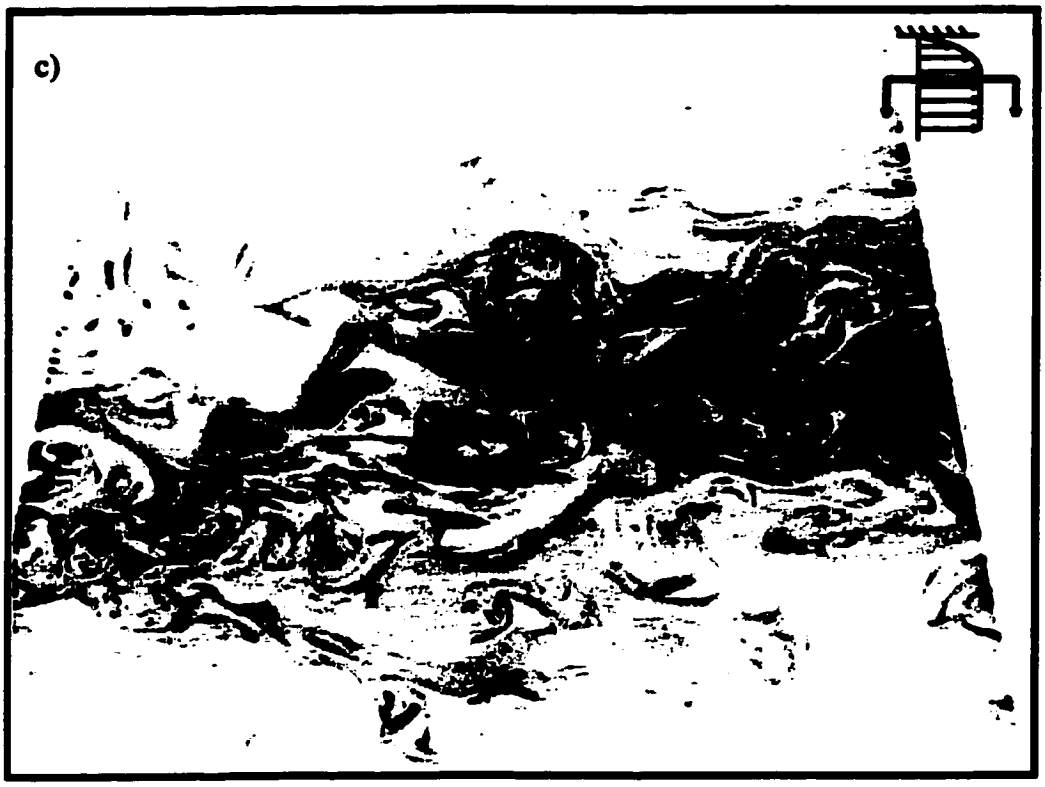

Frame sequence 6.9 (continued)

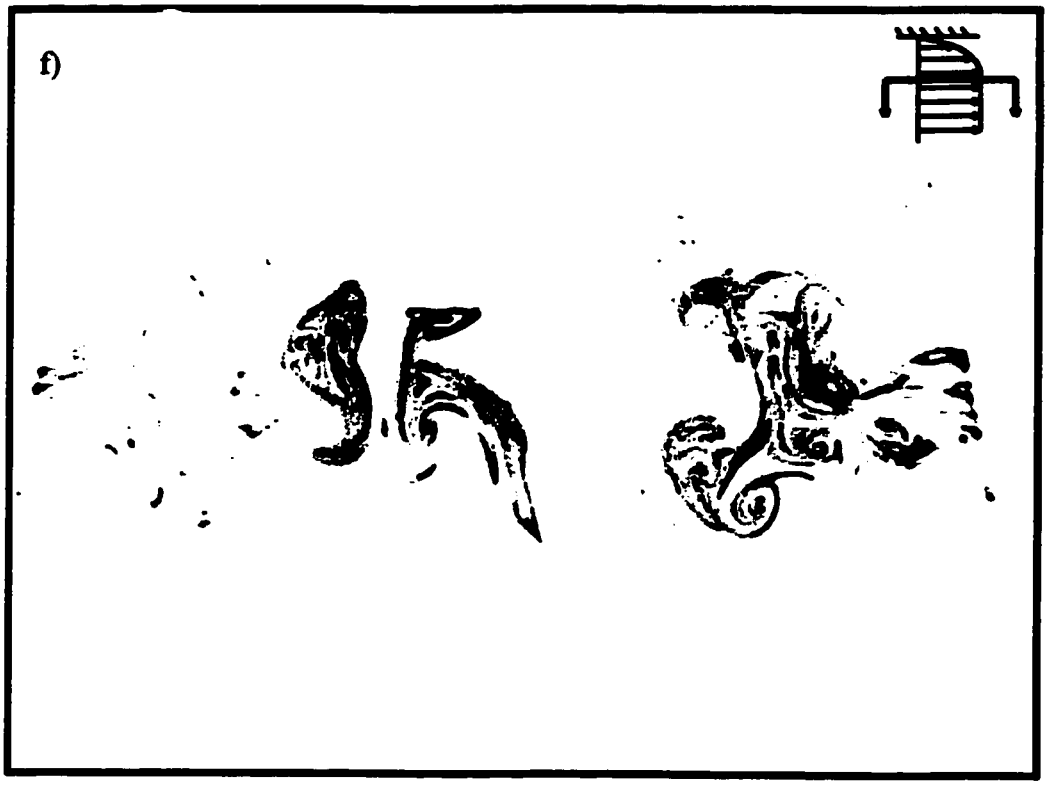

Frame sequence 6.9 (continued)

g)

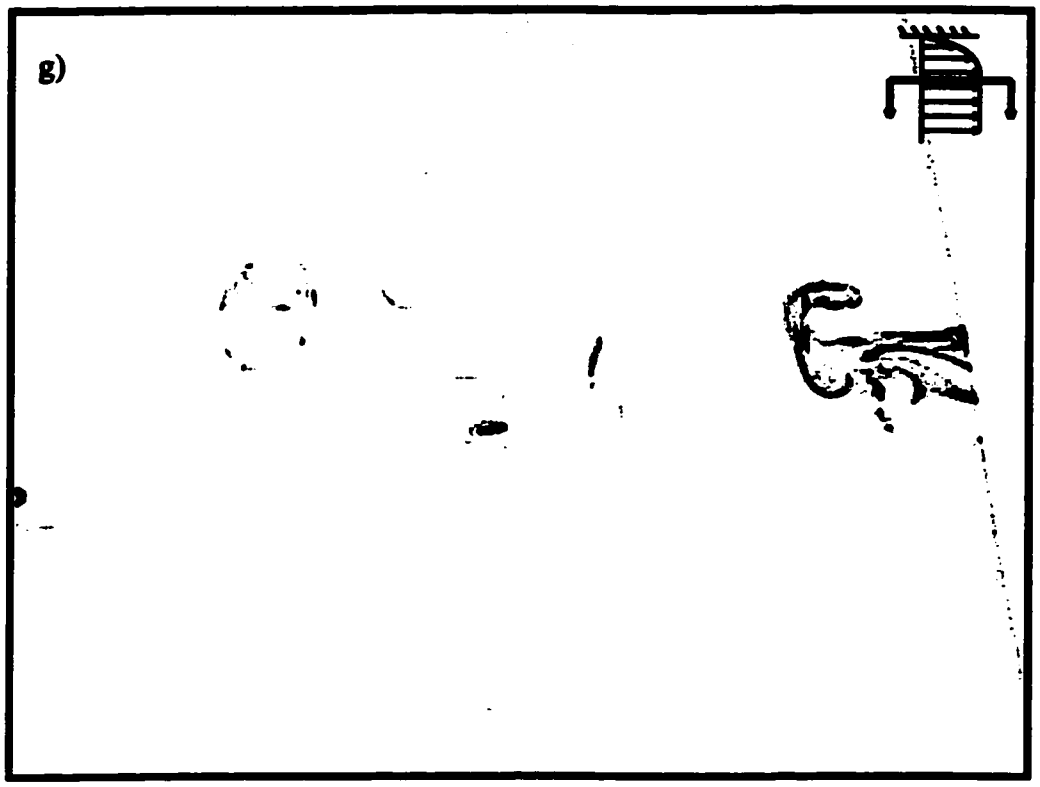

h)

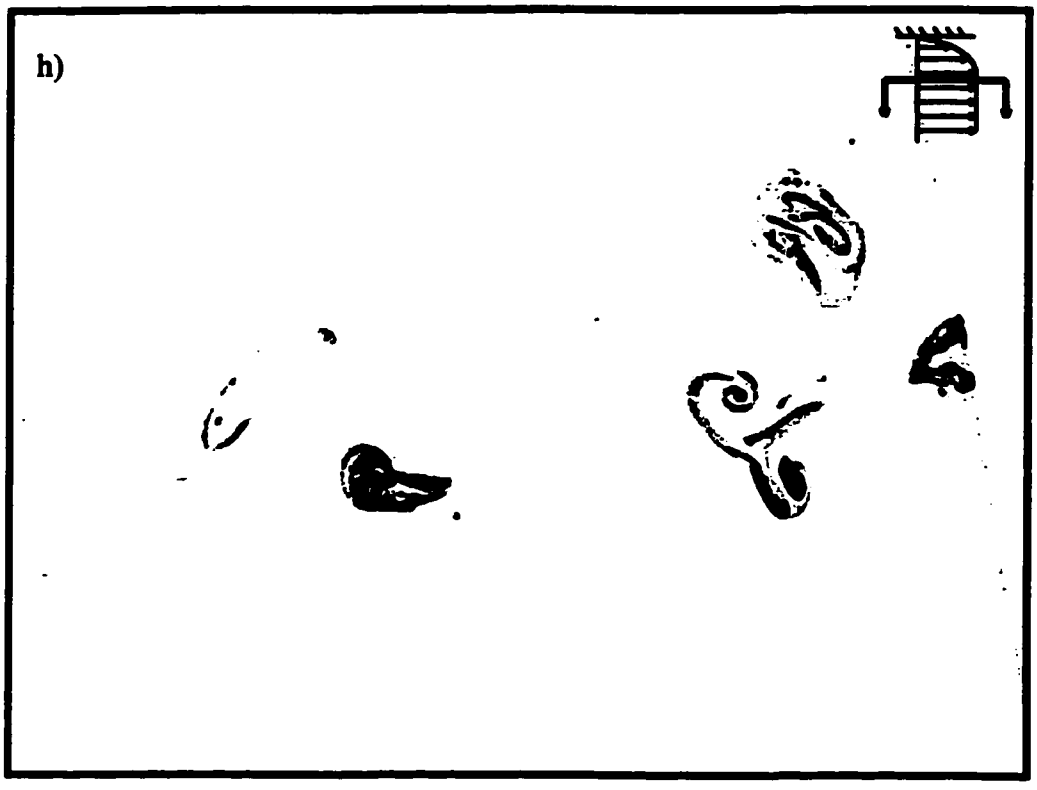

Frame sequence 6.9 (continued)

Frame sequence 6.9 (continued).

Frame sequence 6.10 - USF low speed case, moving wall stationary (MW0), flow viewed from the side; a) t=0s, b) t=1.0s, c) t=6.2s, d) t=8.0s, e) t=9.5s, f) t=10.8s, g) t=12.7s, h) t=14.3s, i) t=16.1s, j) t=18.9s (tape 3, 10:11)

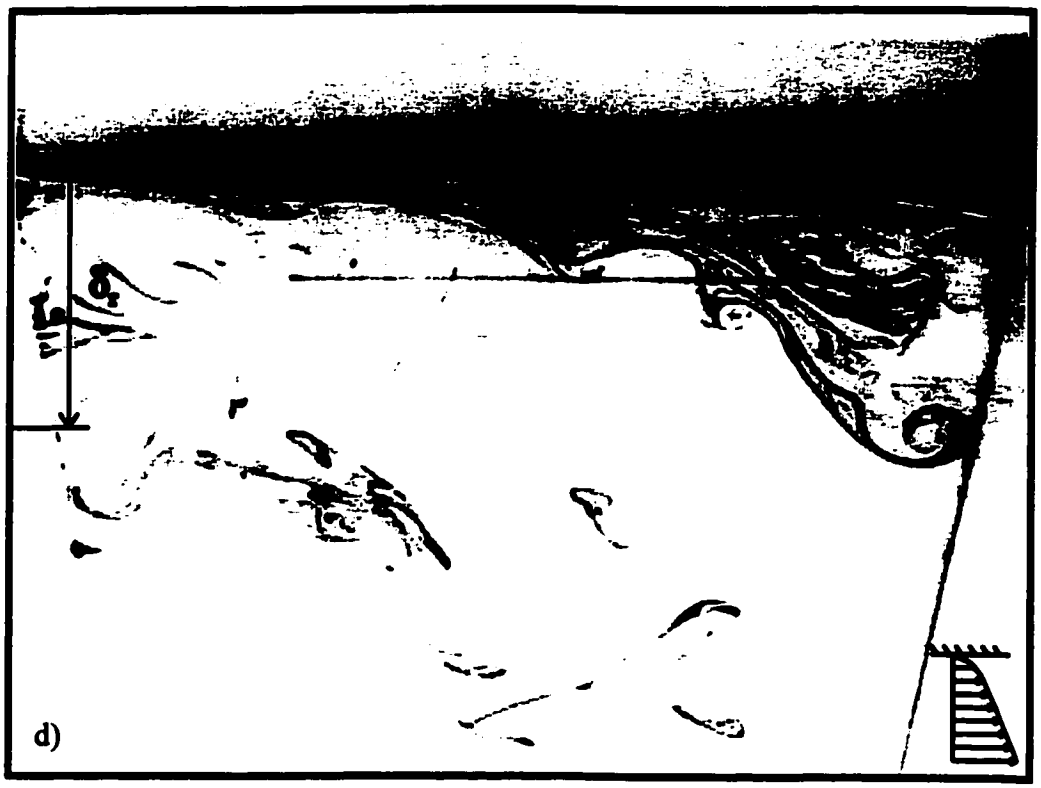

Frame sequence 6.10 (continued)

Frame sequence 6.10 (continued)

Frame sequence 6.10 (continued)

Frame sequence 6.10 (continued).

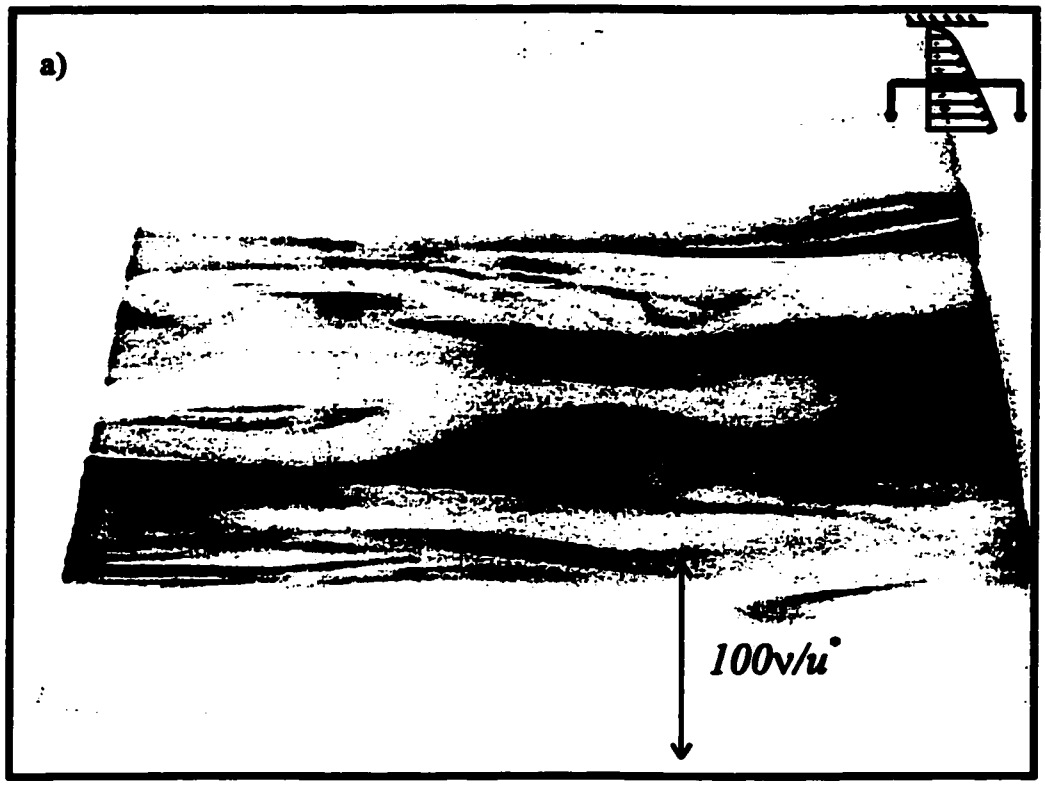

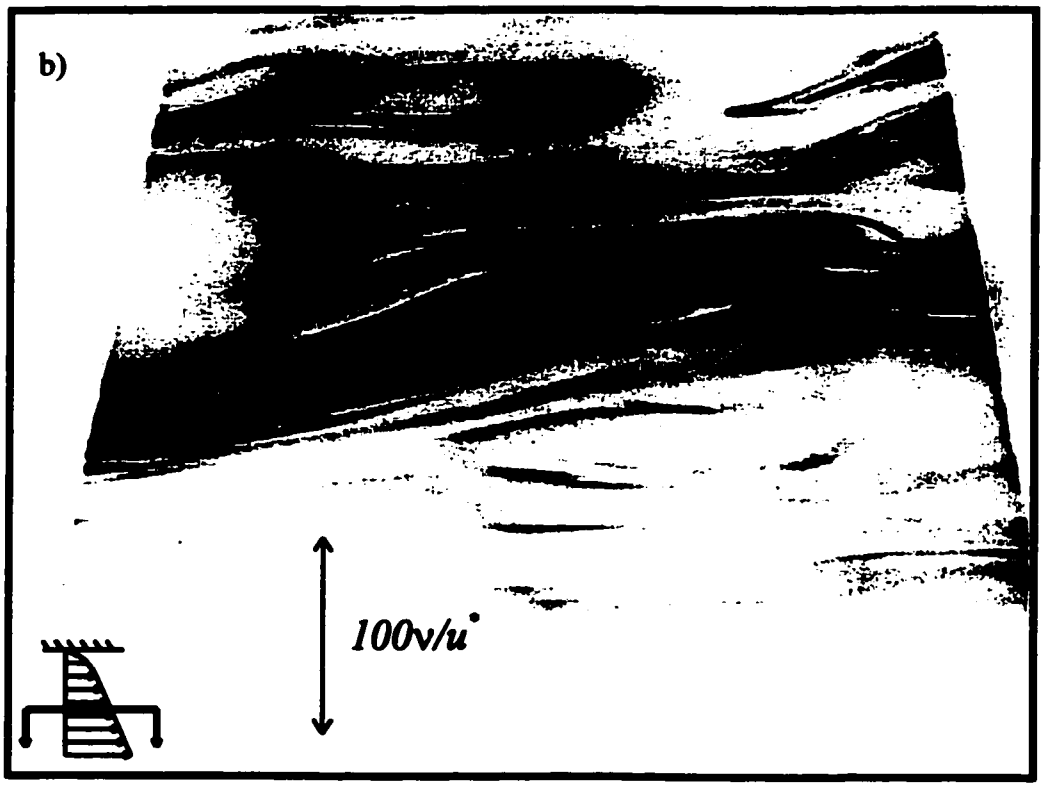

Frame sequence 6.11 - USF low speed case, moving wall stationary (MW0), flow viewed from below; a) *y=0.5mm*, b) *y=1mm*, c) *y=2mm*, d) *y=3mm*, e) *y=4mm*, f) *y=6mm*, g) *y=10mm*, h) *y=15mm*, i) *y=20mm* (tape 2, 13:09)

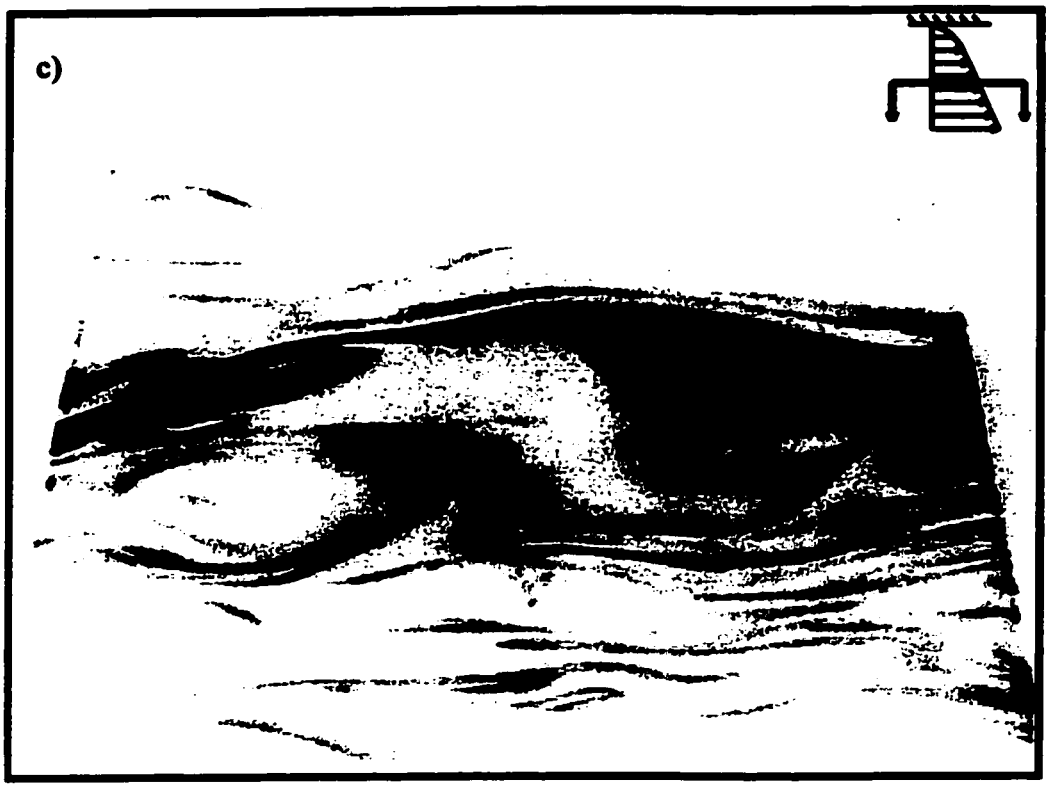

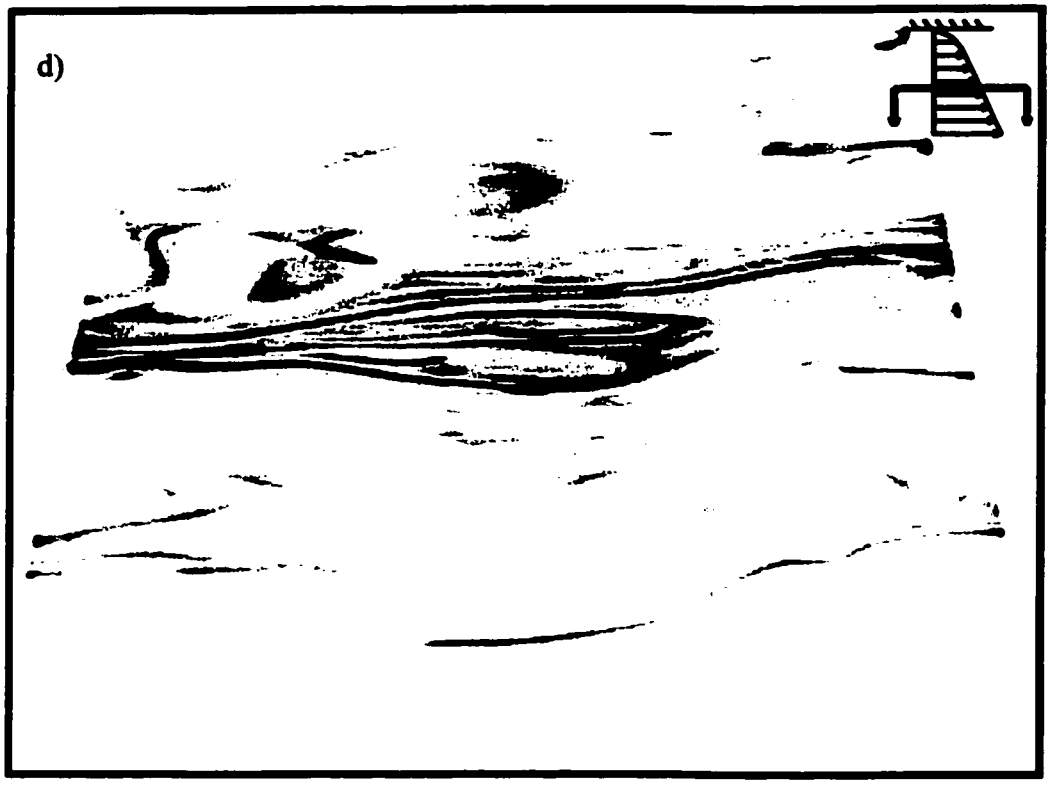

Frame sequence 6.11 (continued)

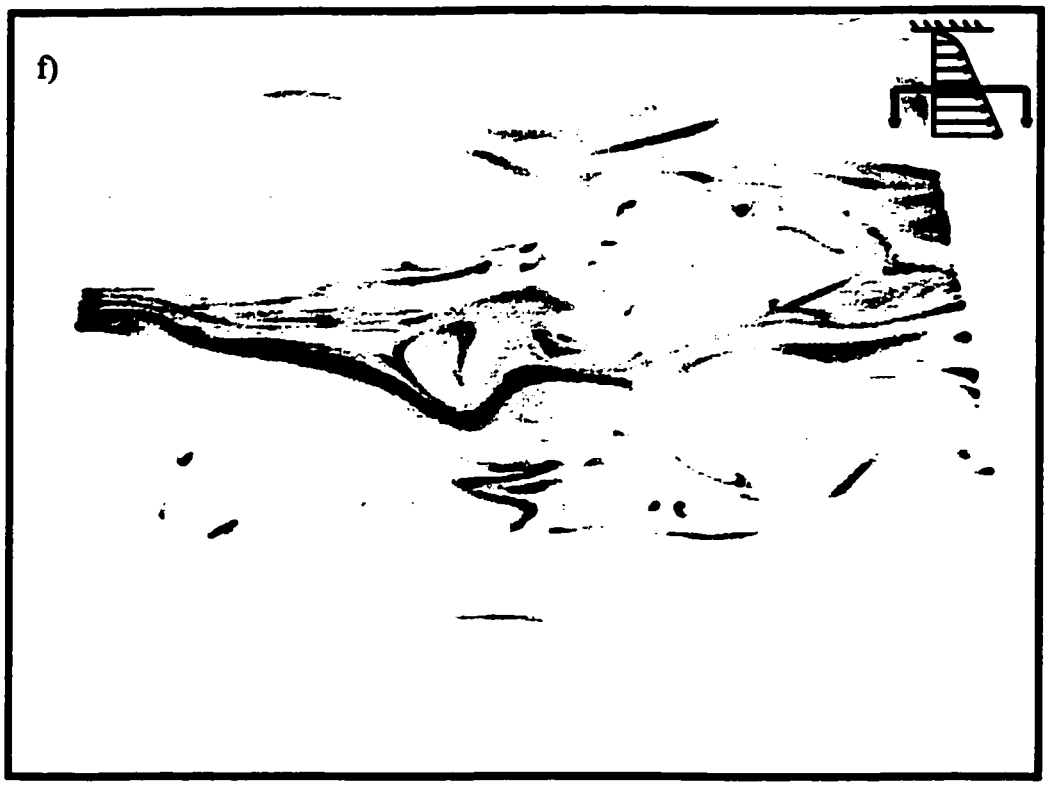

Frame sequence 6.11 (continued)

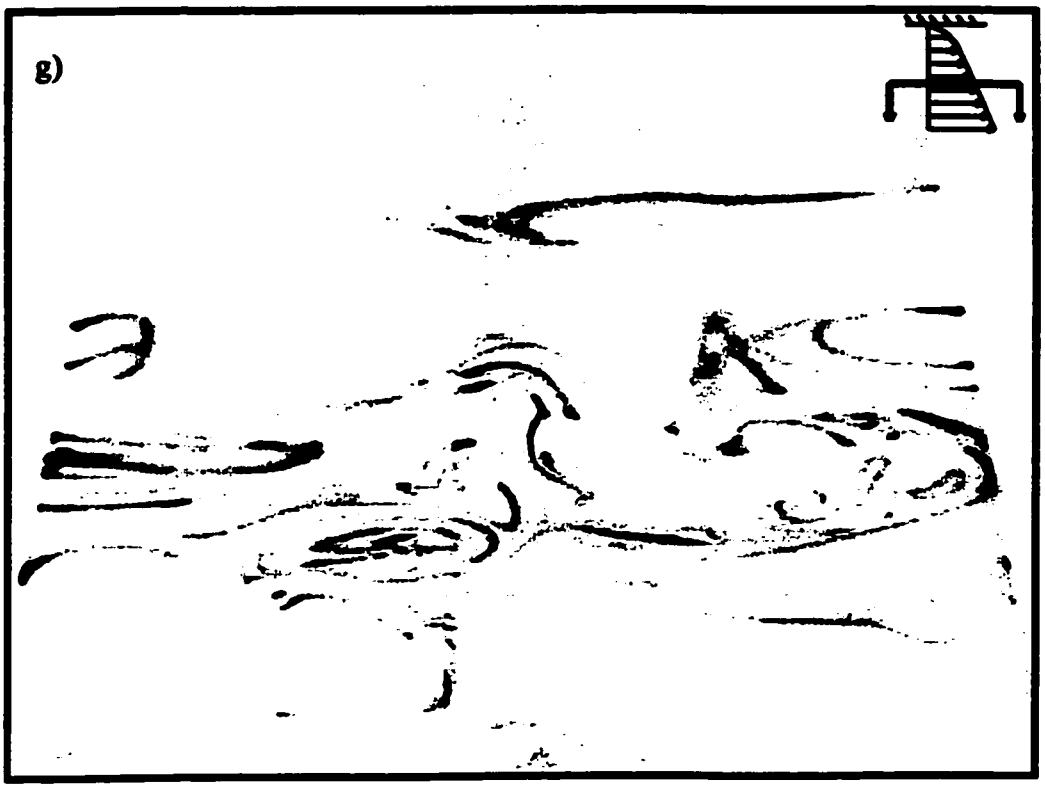

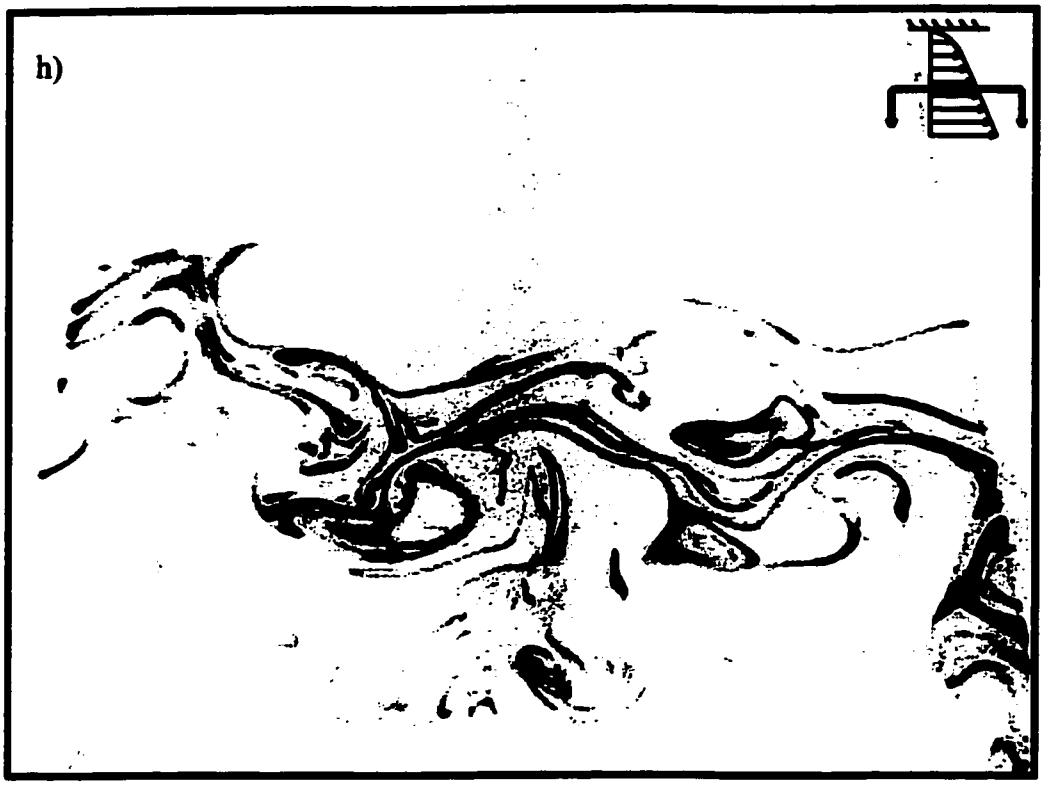

Frame sequence 6.11 (continued)

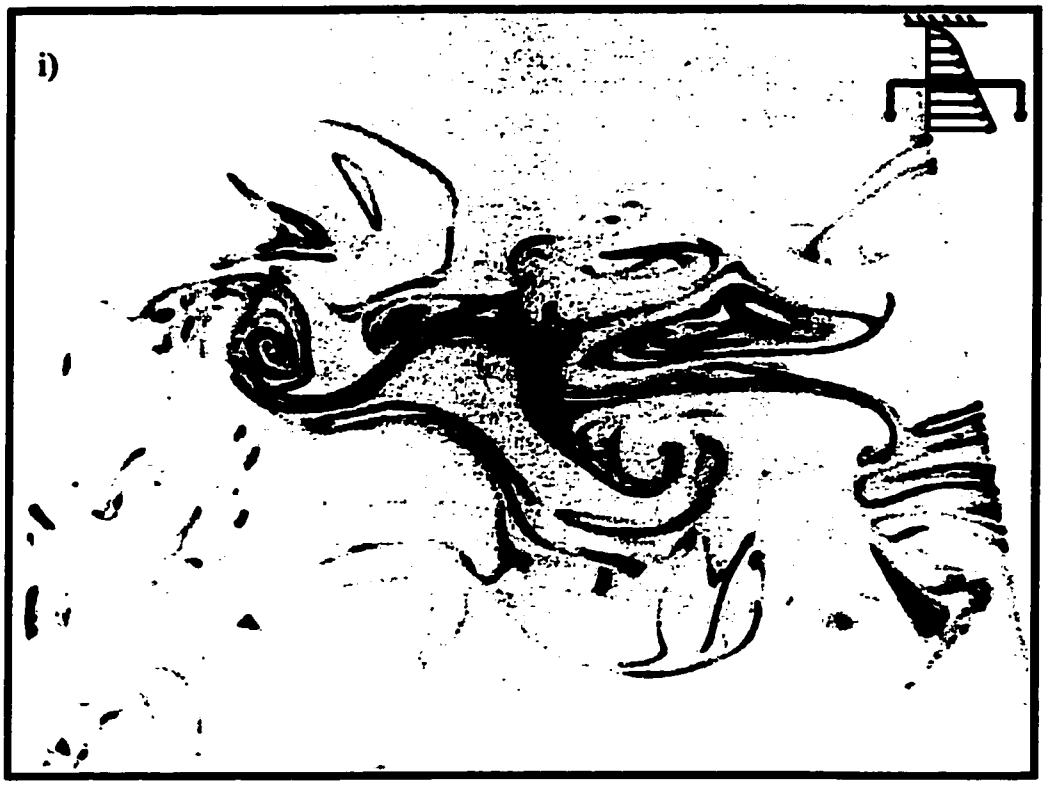

Frame sequence 6.11 (continued).

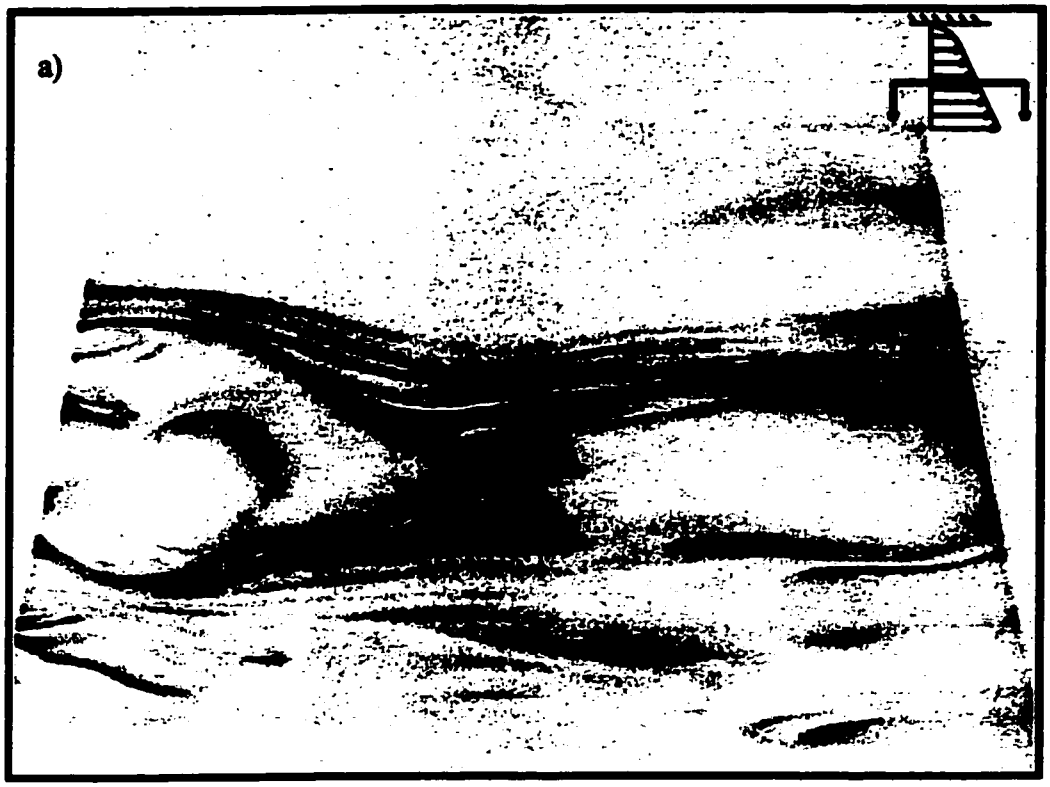

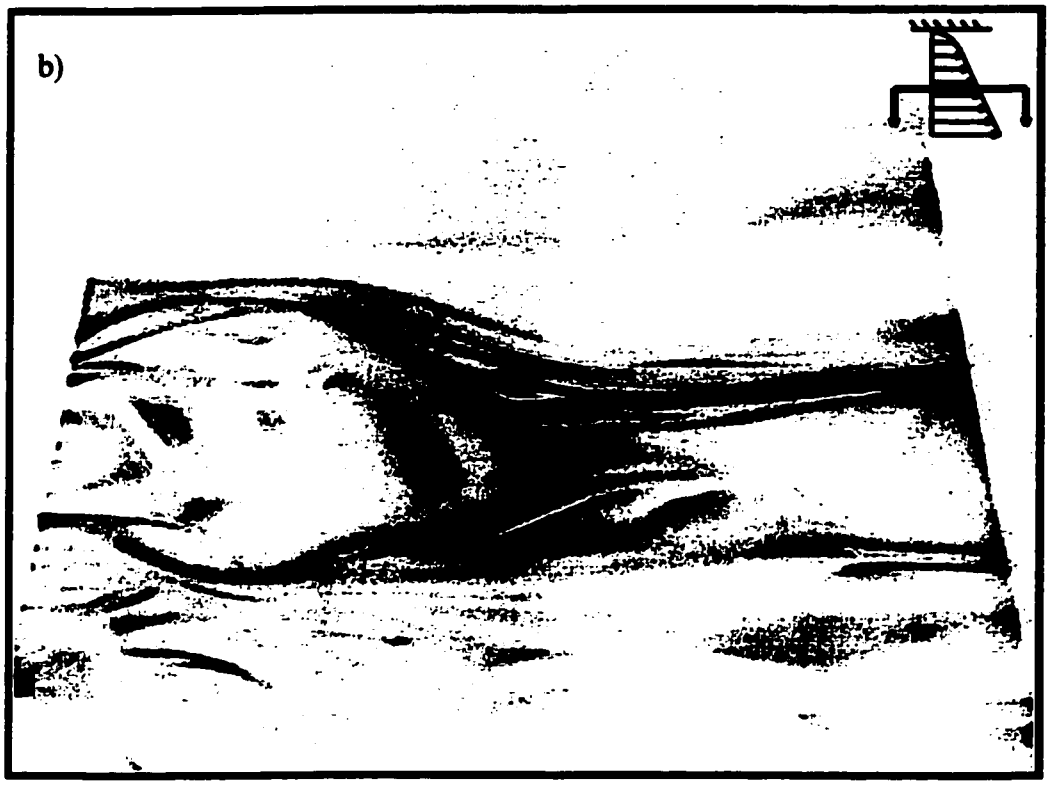

Frame sequence 6.12 - USF low speed case, mowing wall stationary (MW0), flow viewed from below at y=1mm; a) t=0s, b) t=1.0s, c) t=1.7s, d) t=2.4s, e) t=2.8s, f) t=3.9s (tape 2, 13:09)

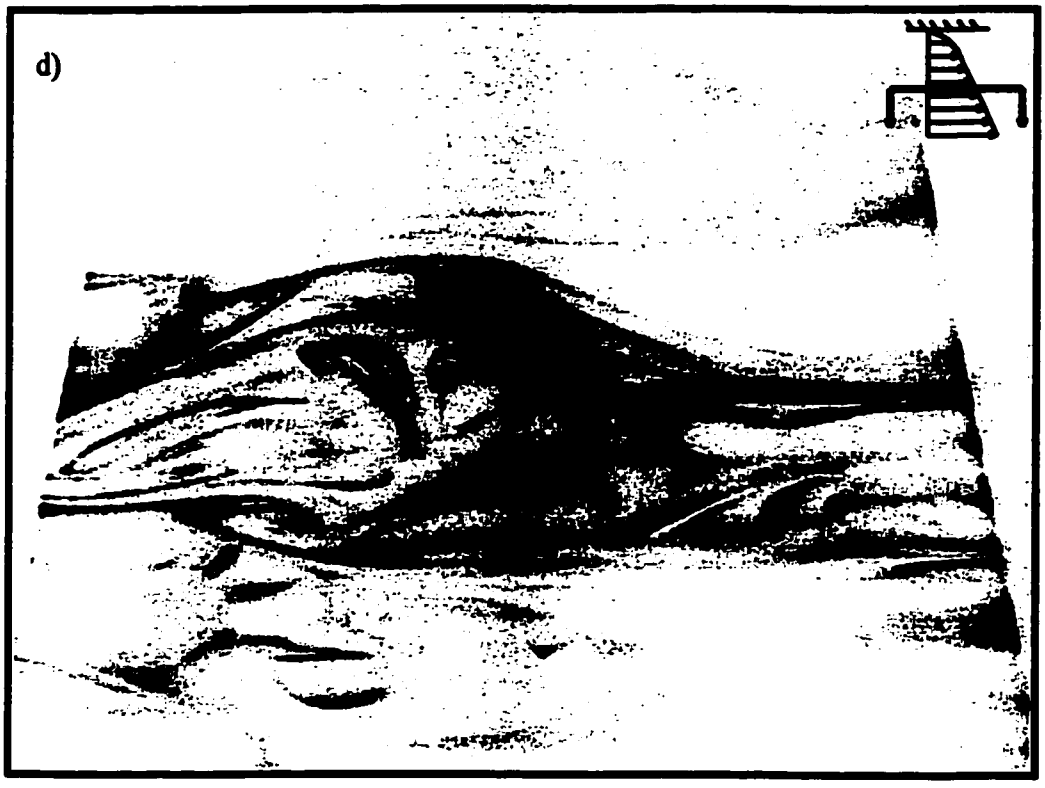

Frame sequence 6.12 (continued)

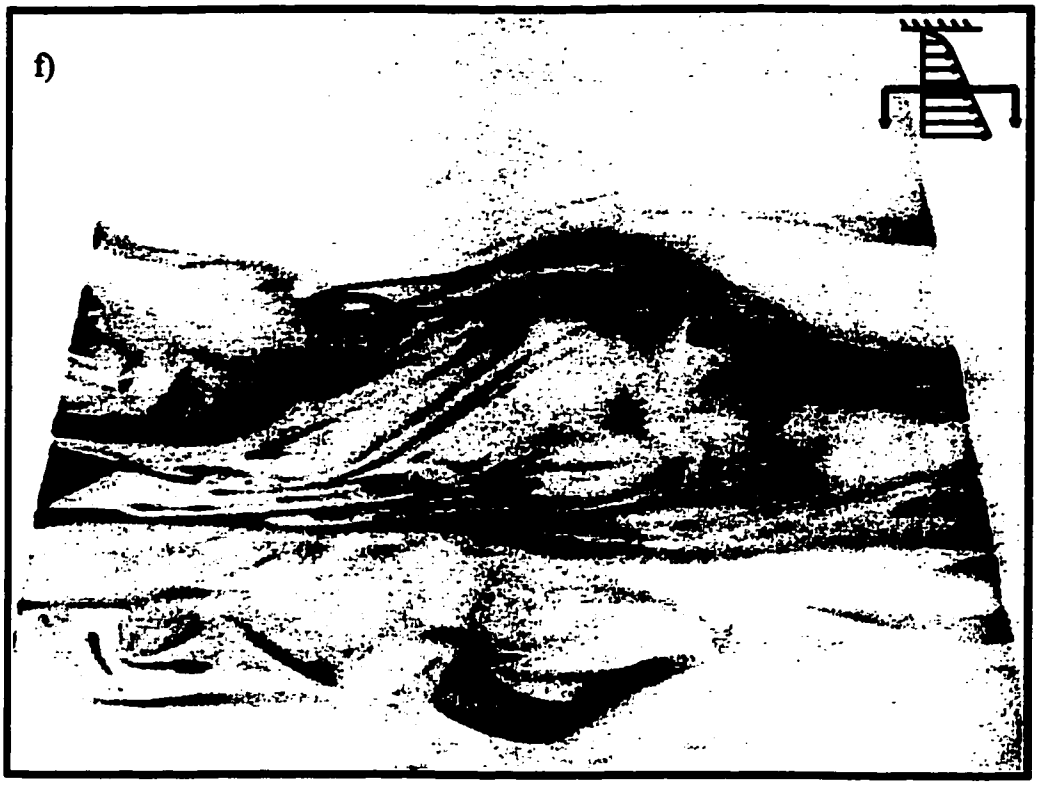

Frame sequence 6.12 (continued).

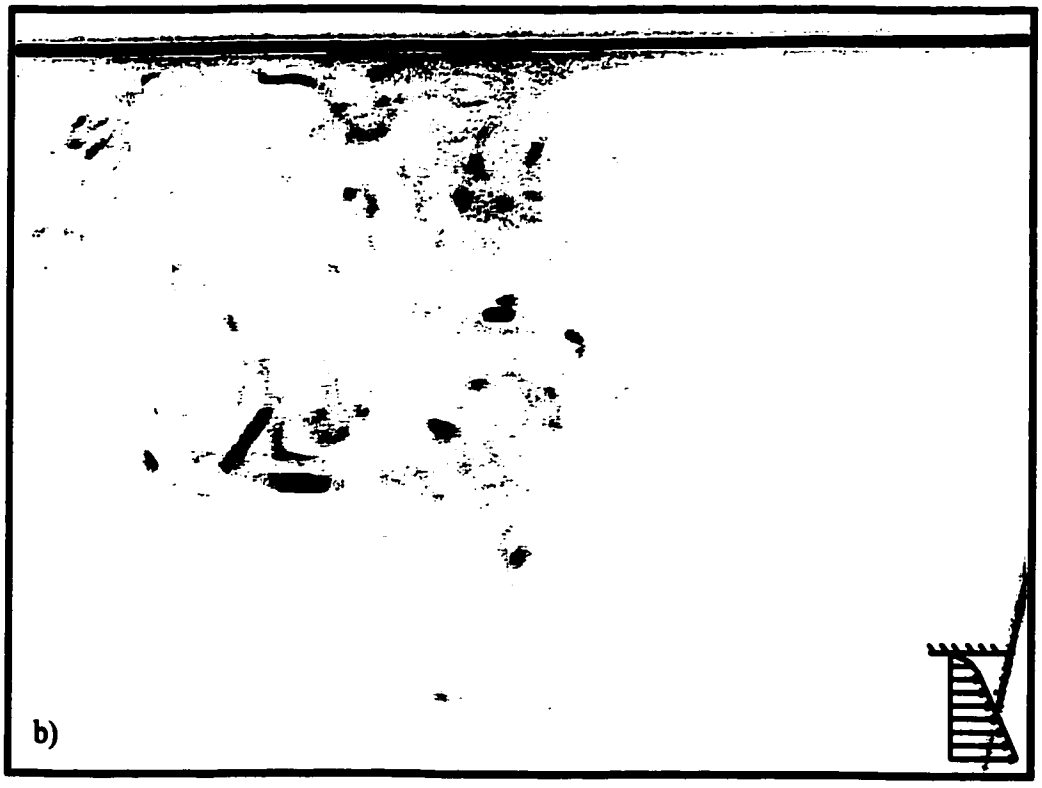

Frame sequence 6.13 - USF low speed case, mowing wall stationary (MW0), wall and core flow viewed from the rear. (Tape 3, 23:55)

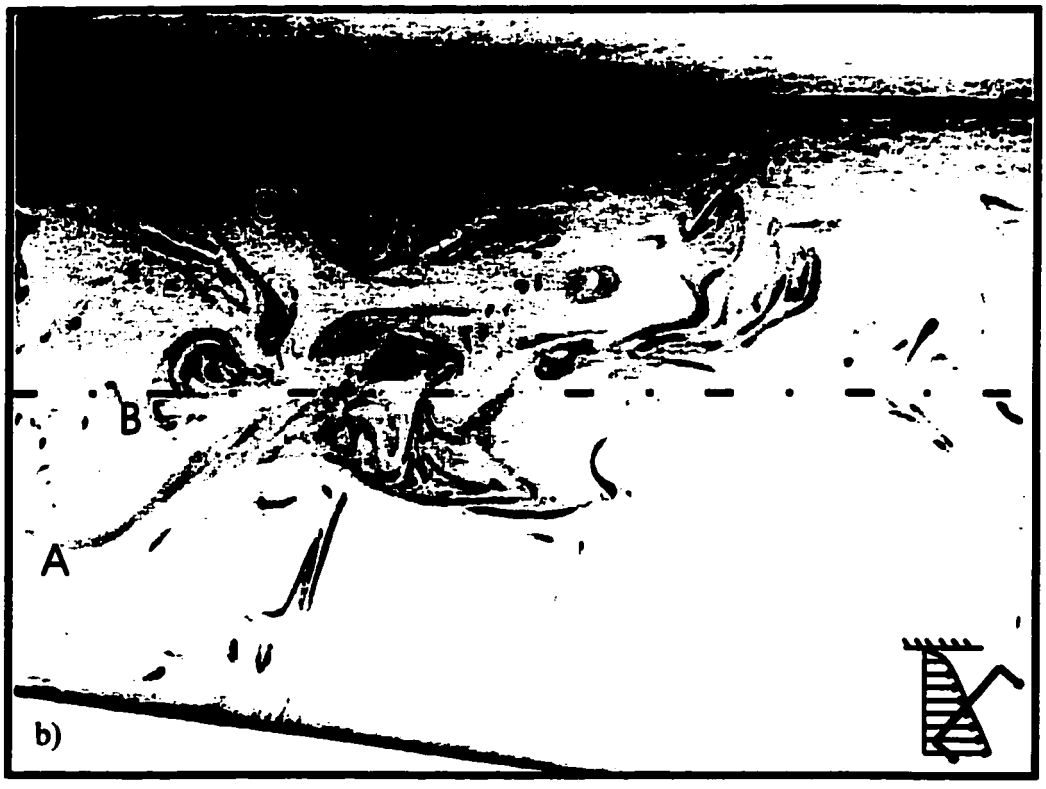

Frame sequence 6.14 - USF low speed case, mowing wall stationary (MW0), flow viewed from below with laser sheet at an angle; a) t=0s, b) t=0.20s, c) t=0.40s, d) t=0.60s (tape 3, 30:49)

Frame sequence 6.14 (continued).

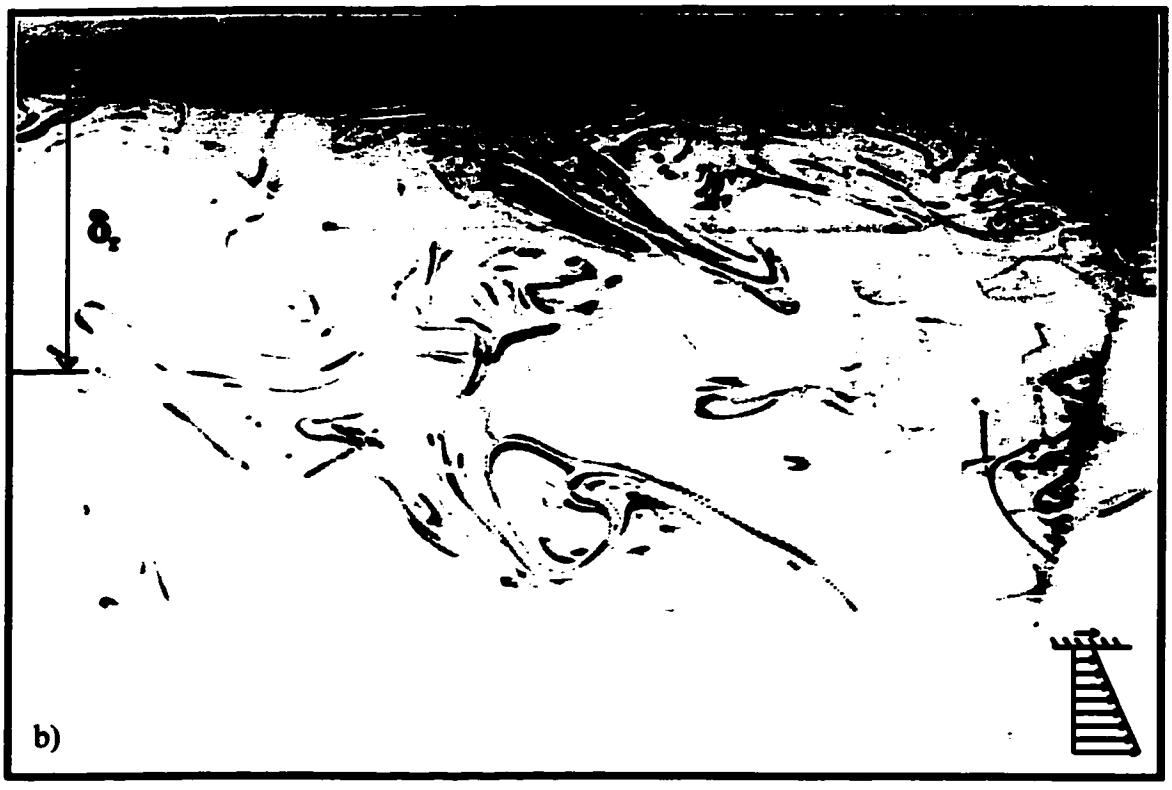

Frame sequence 6.15 - USF low speed case, moving wall equal to local velocity (MWE), flow viewed from the side with camera moving downstream between approx $x_i \approx 1.9$m and $x_i \approx 2.65$m; a) t=0s, b) t=2.1s, c) t=4.3s, d) t=7.1s, e) t=9.4s, f) t=11.0s (tape 3, 01:00)

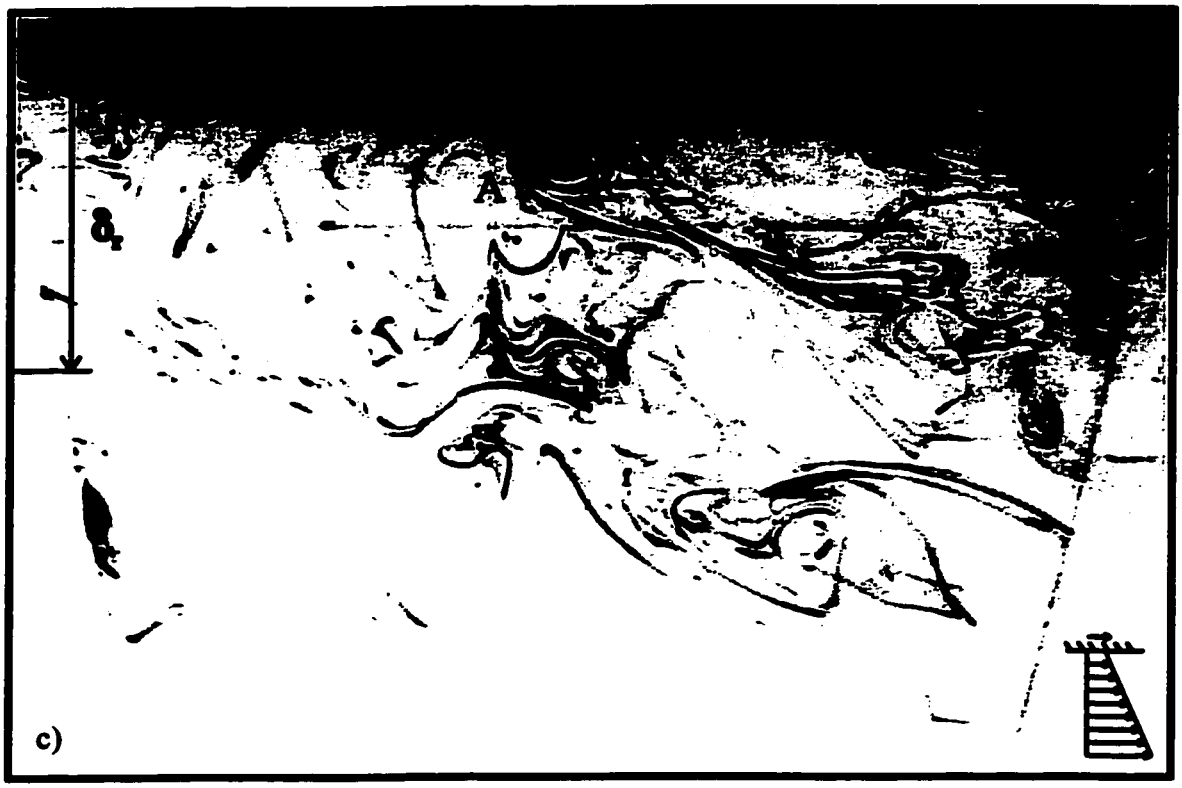

Frame sequence 6.15 (continued)

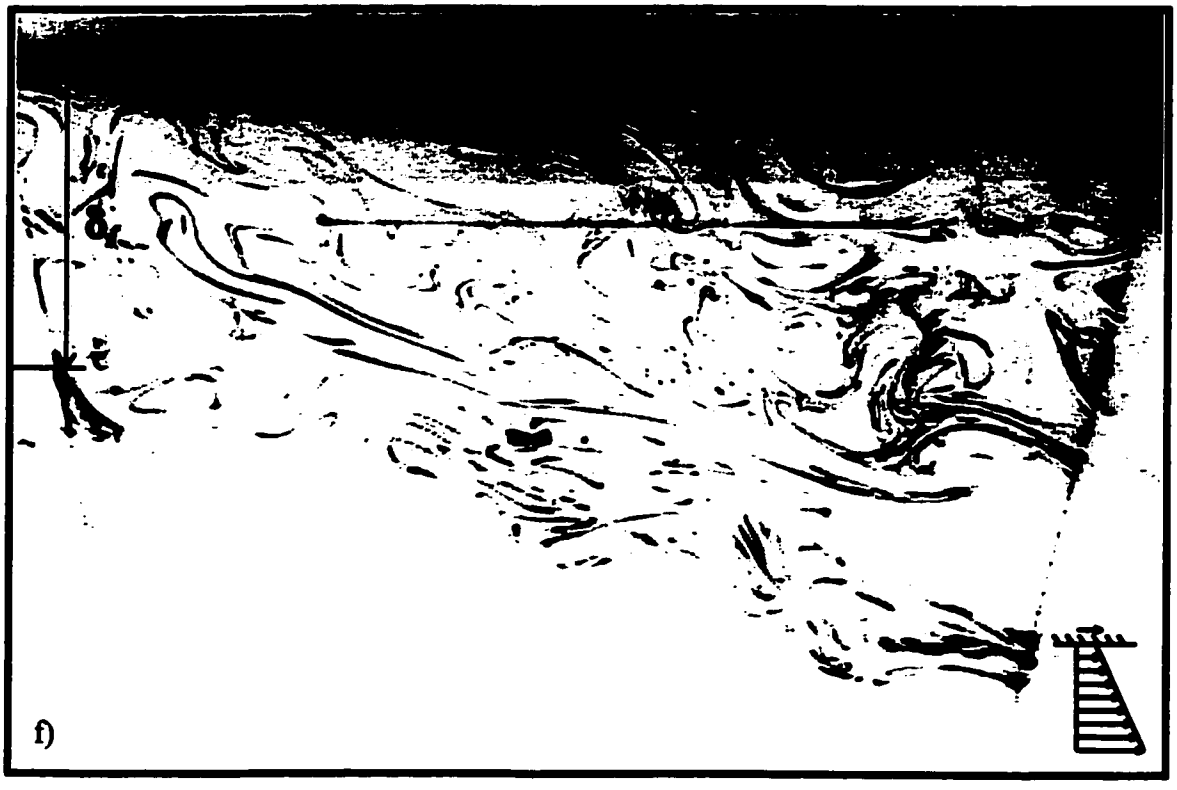

Frame sequence 6.15 (continued).

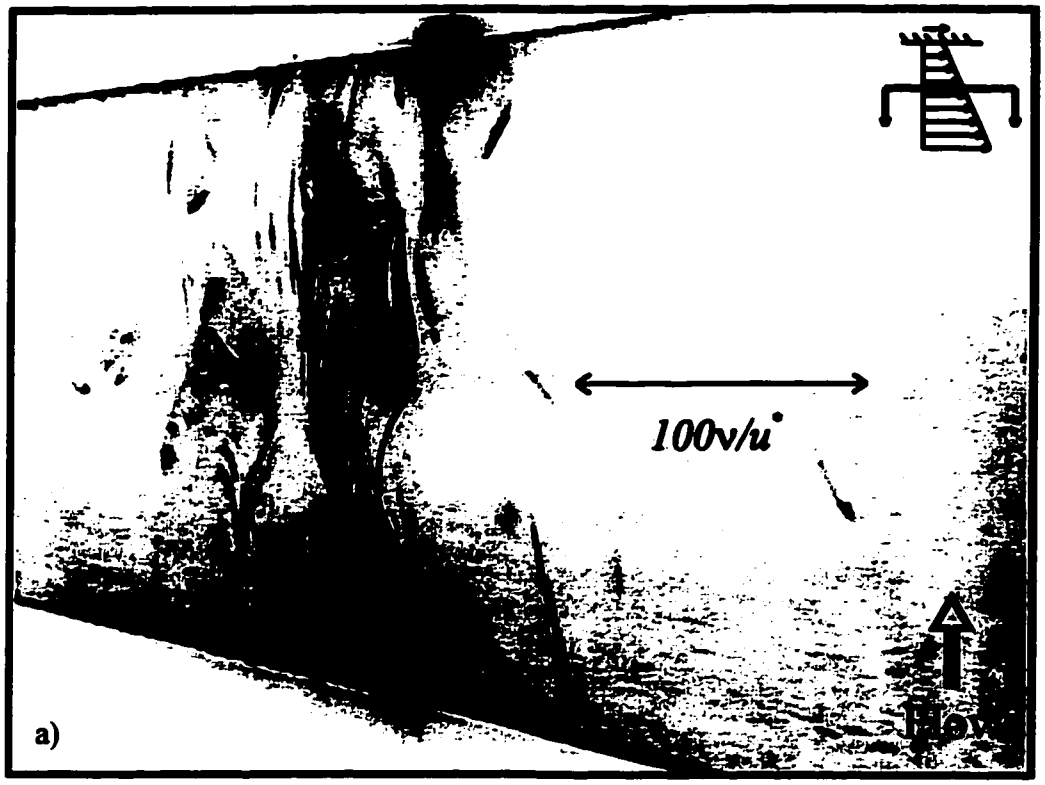

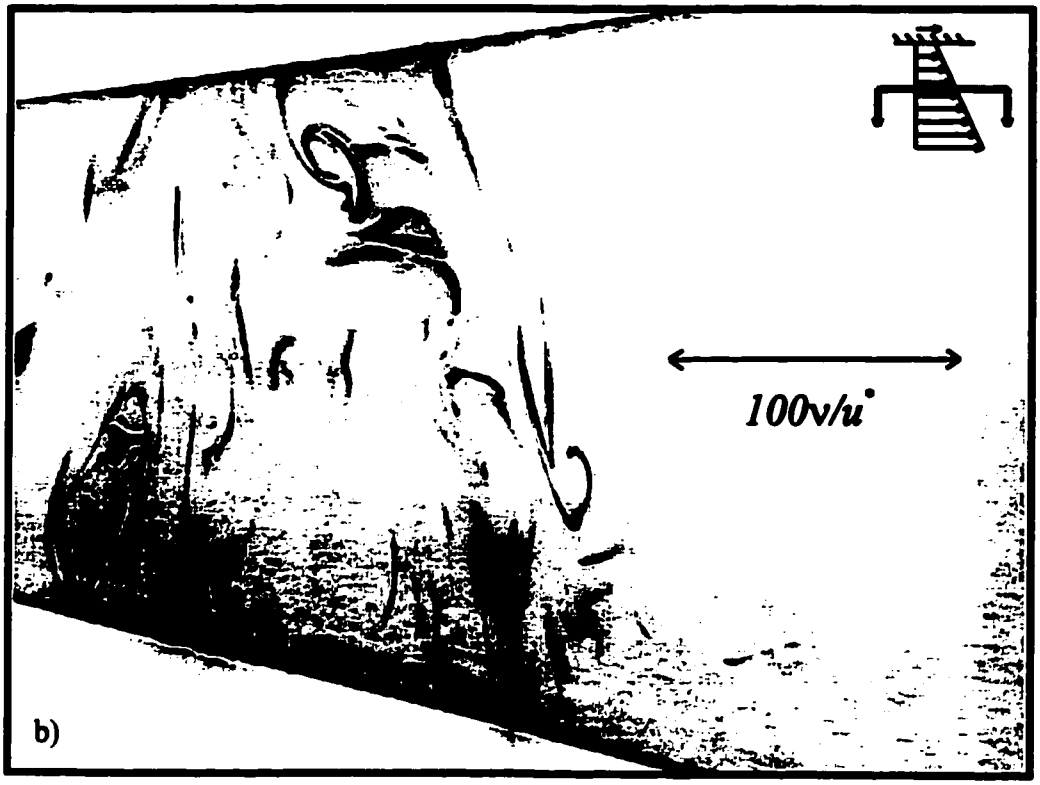

Frame sequence 6.16 - USF low speed case, moving wall equal to local velocity (MWE), flow viewed from below; a) *y=0mm*, b) *y=1mm*, c) *y=8mm*, d) *y=18mm*, e) *y=28mm*, f) *y=38mm*. (tape 3, 25:10)

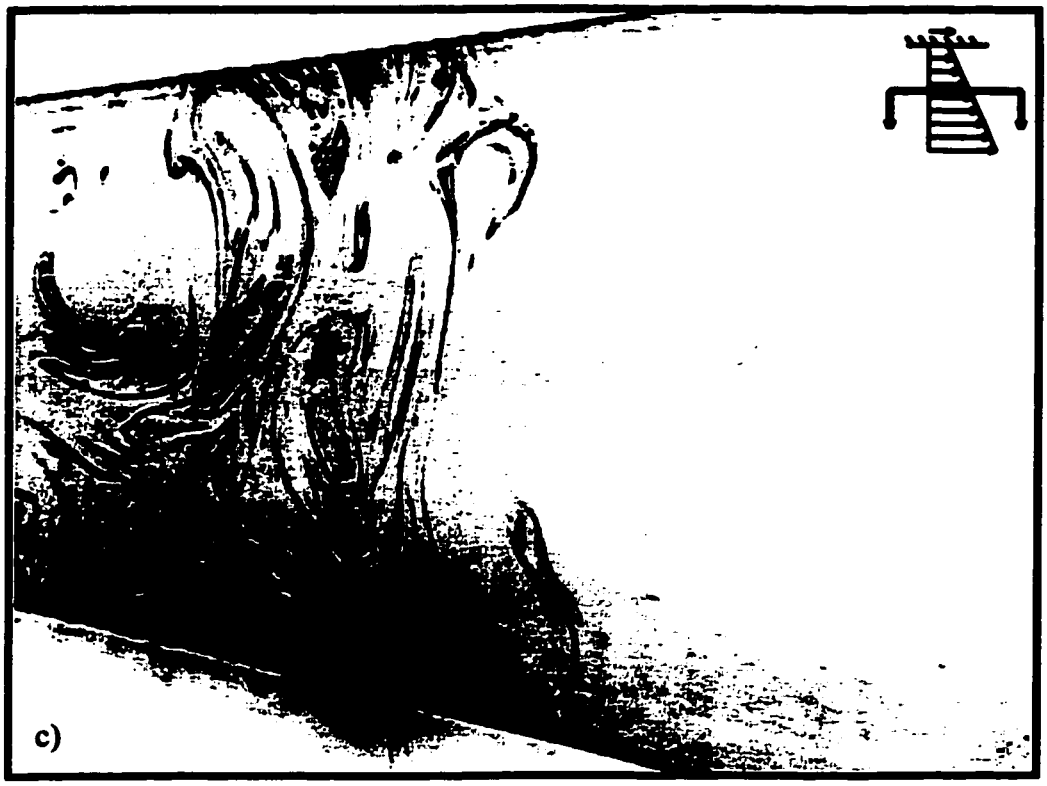

Frame sequence 6.16 (continued)

Frame sequence 6.16 (continued).

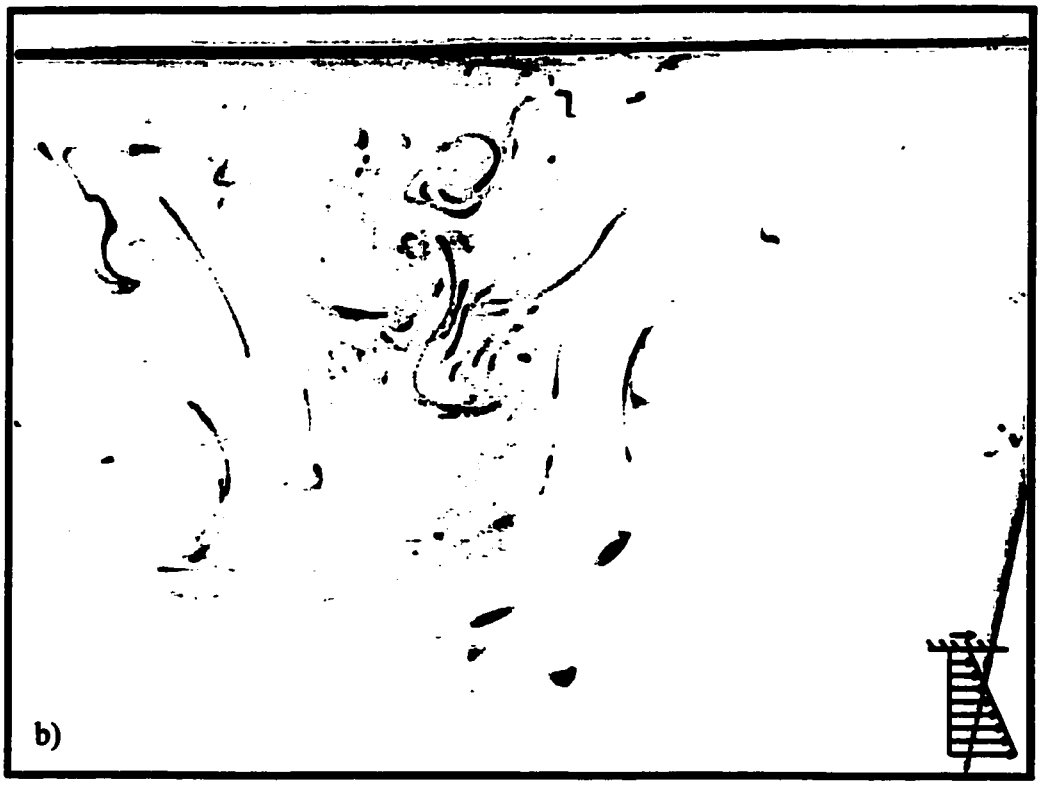

Frame sequence 6.17 - USF low speed case, moving wall equal to local velocity (MWE), wall and core flow viewed from the rear. (Tape 3, 23:55)

Frame sequence 6.18 - USF low speed case, moving wall equal to local velocity (MWE), flow viewed from below with laser sheet at an angle; a) t=0s, b) t=0.20s, c) t=0.40s, d) t=0.60s (tape 3, 31:23)

Frame sequence 6.18 (continued).

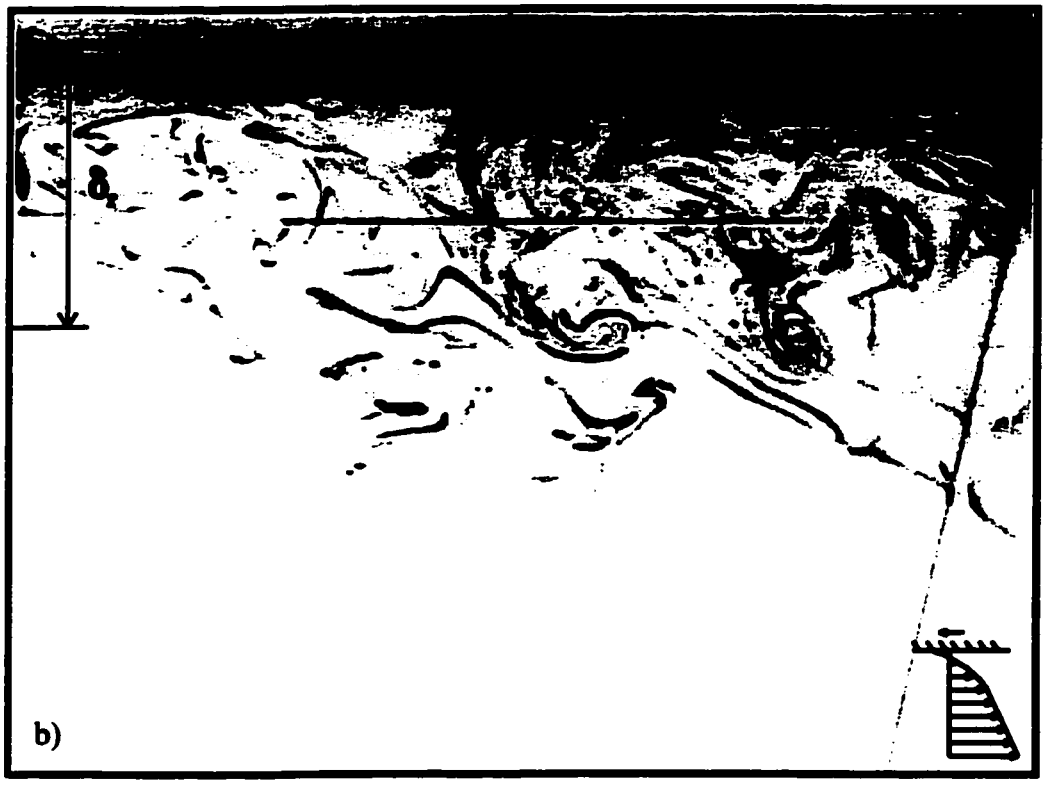

Frame sequence 6.19 - USF low speed case, moving wall opposite flow velocity (MWN), flow viewed from the side with camera moving downstream between approx $x_i \approx 1.6$m and $x_i \approx 2.6$m; a) t=0s, b) t=2.1s, c) t=3.7s, d) t=6.2s, e) t=7.3s, f) t=9.4s, g) t=11.8s, h) t=14.3s (tape 3, 04:02)

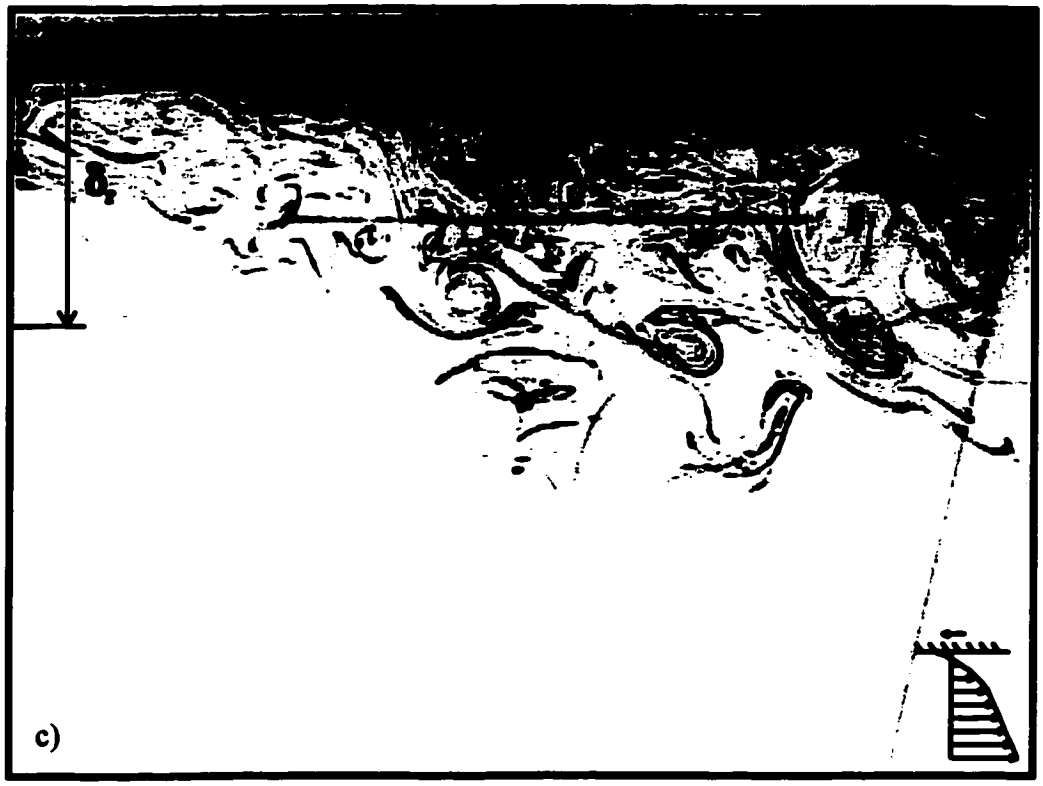

Frame sequence 6.19 (continued)

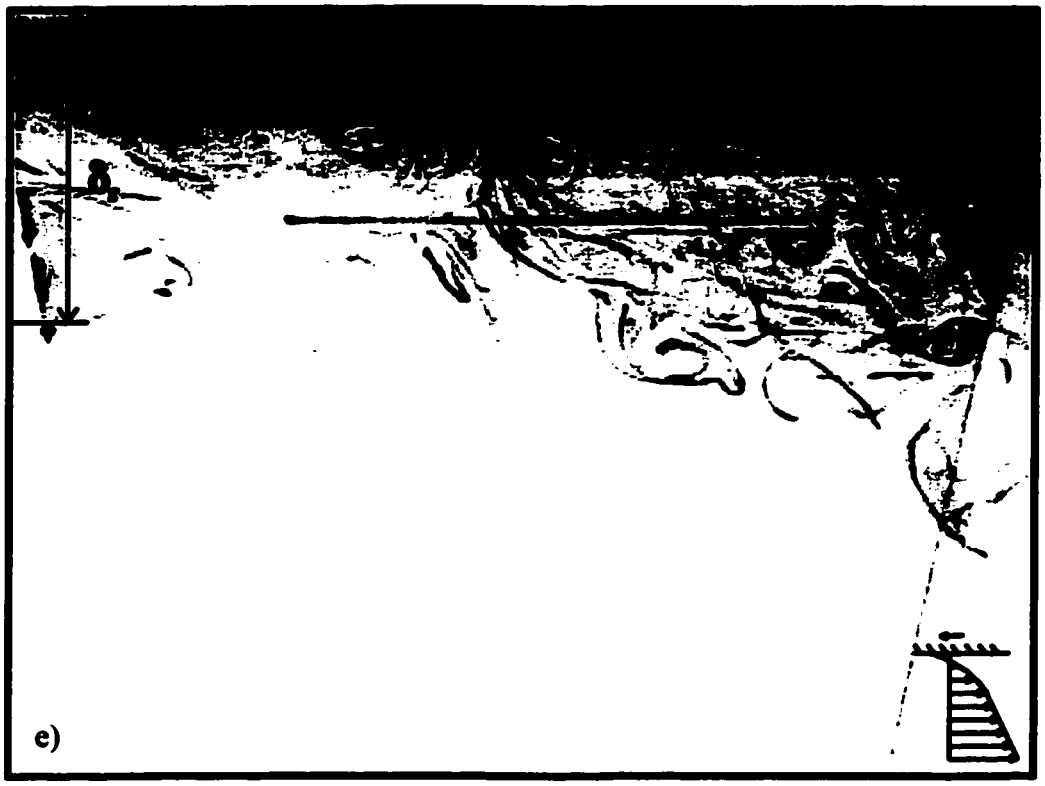

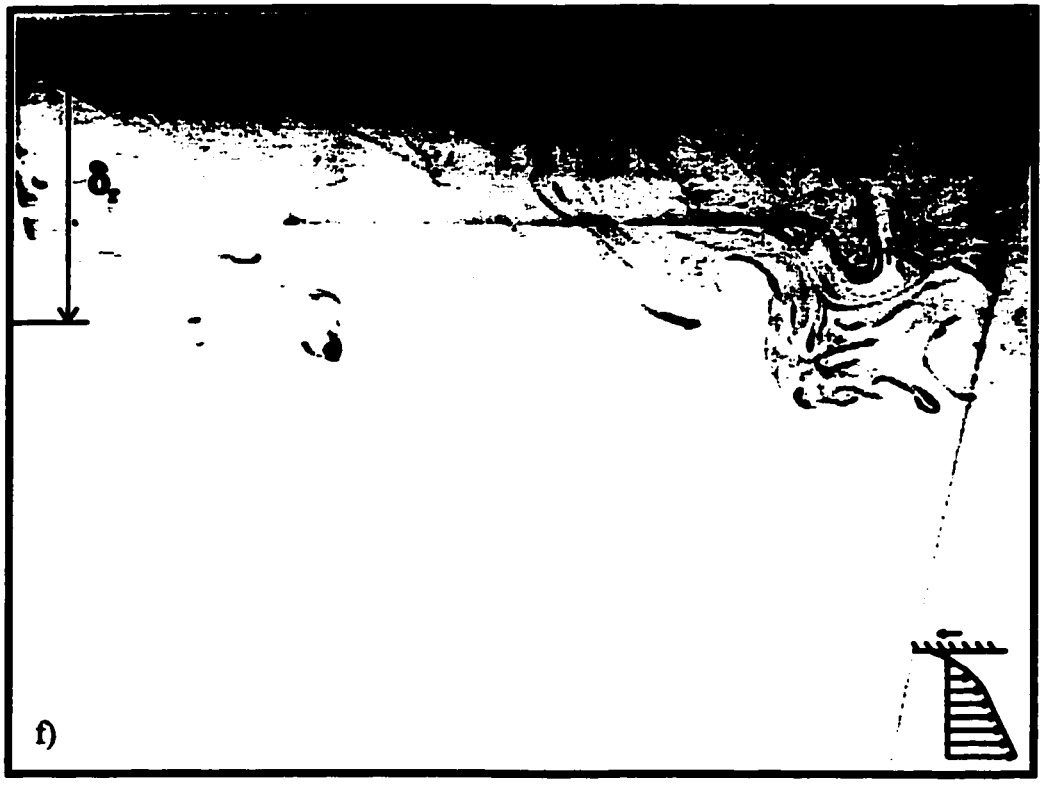

Frame sequence 6.19 (continued)

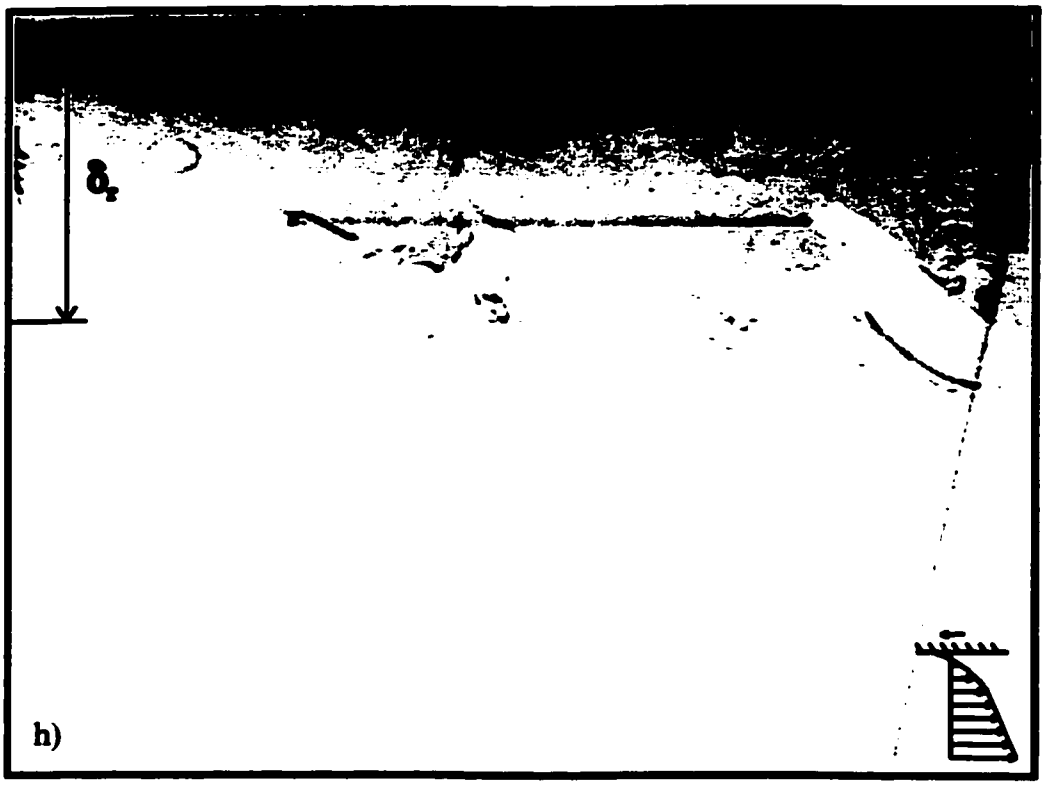

Frame sequence 6.19 (continued).

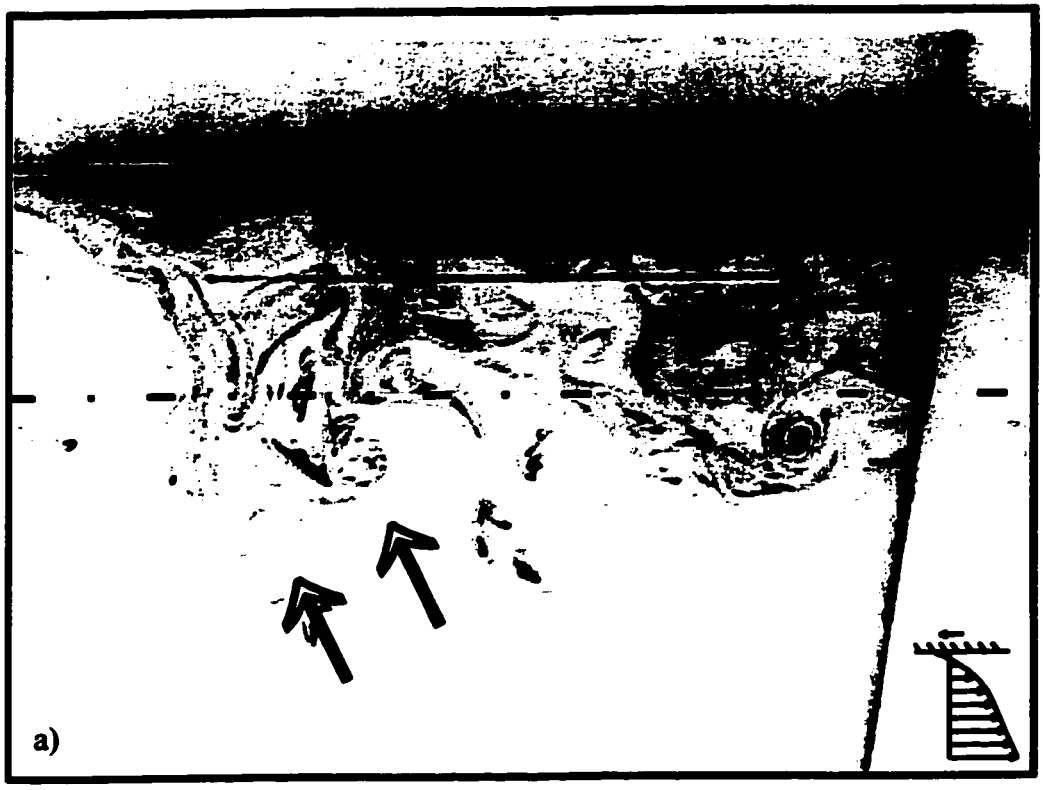

Frame sequence 6.20 - USF low speed case, moving wall opposite flow velocity (MWN), flow viewed from the side with the laser sheet moving in the spanwise plane a total distance of approximately 50mm; a) t=0s, b) t=0.1s, c) t=0.23s, d) t=0.37s, e) t=0.47s, f) t=0.6s, g) t=0.73s, h) t=0.87s (tape 3, 13:35)

Frame sequence 6.20 (continued)

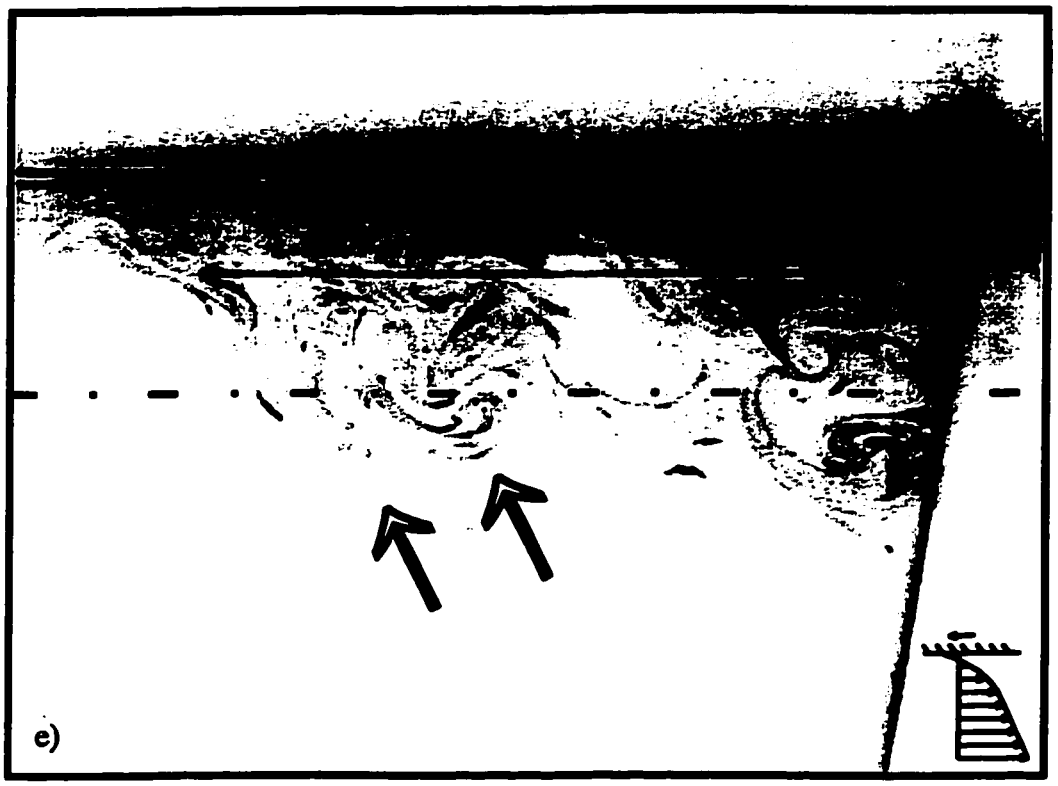

Frame sequence 6.20 (continued)

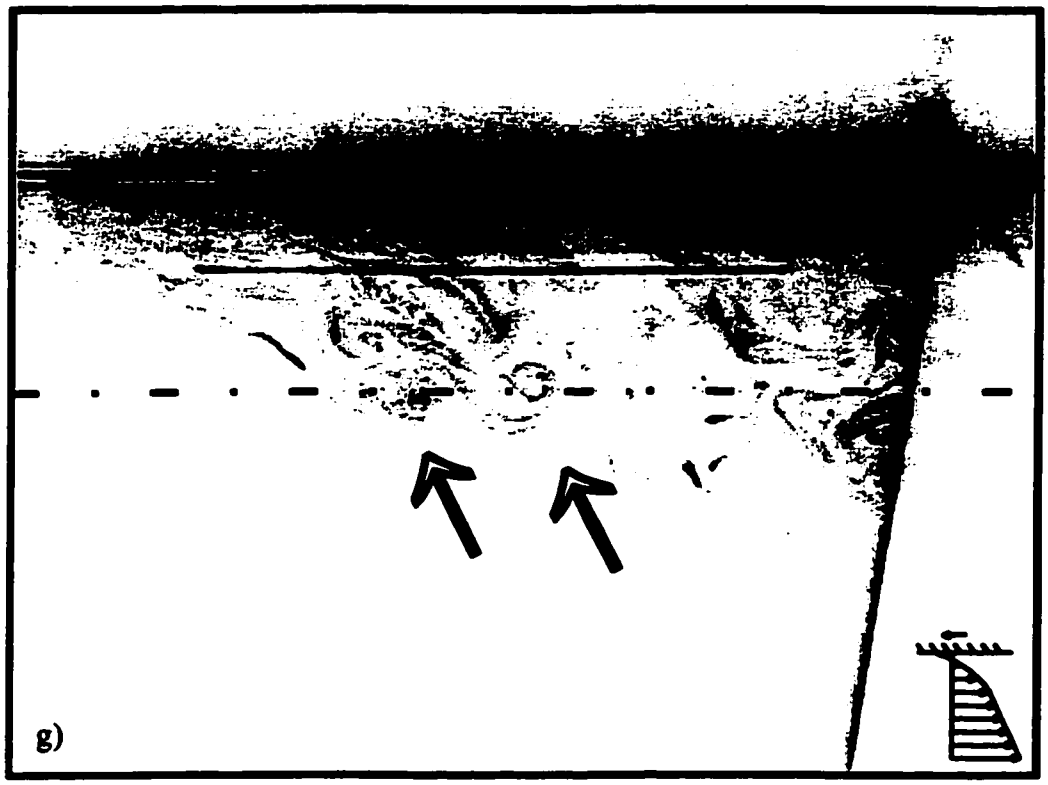

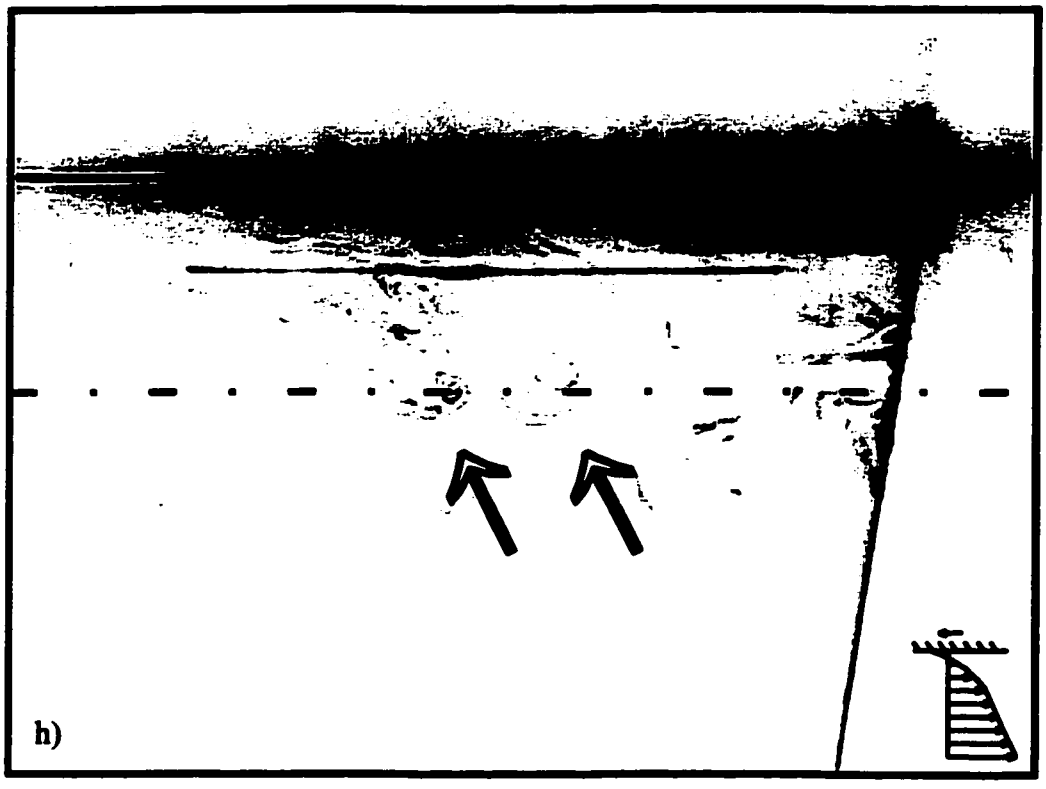

Frame sequence 6.20 (continued).

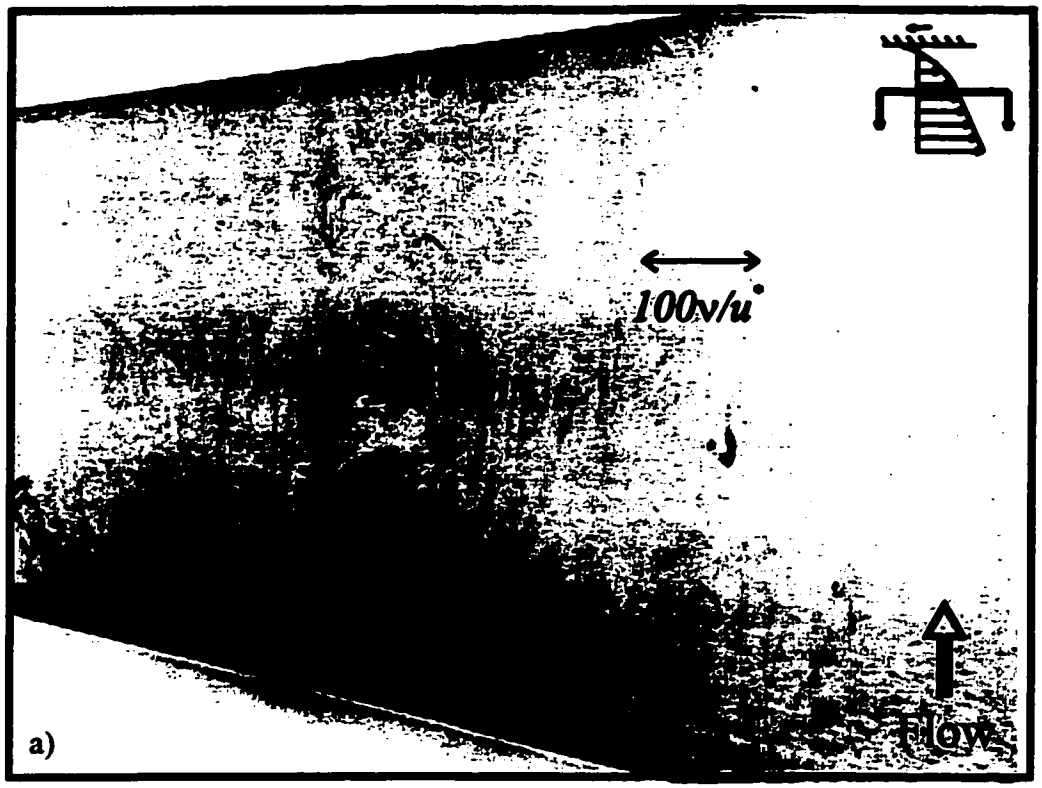

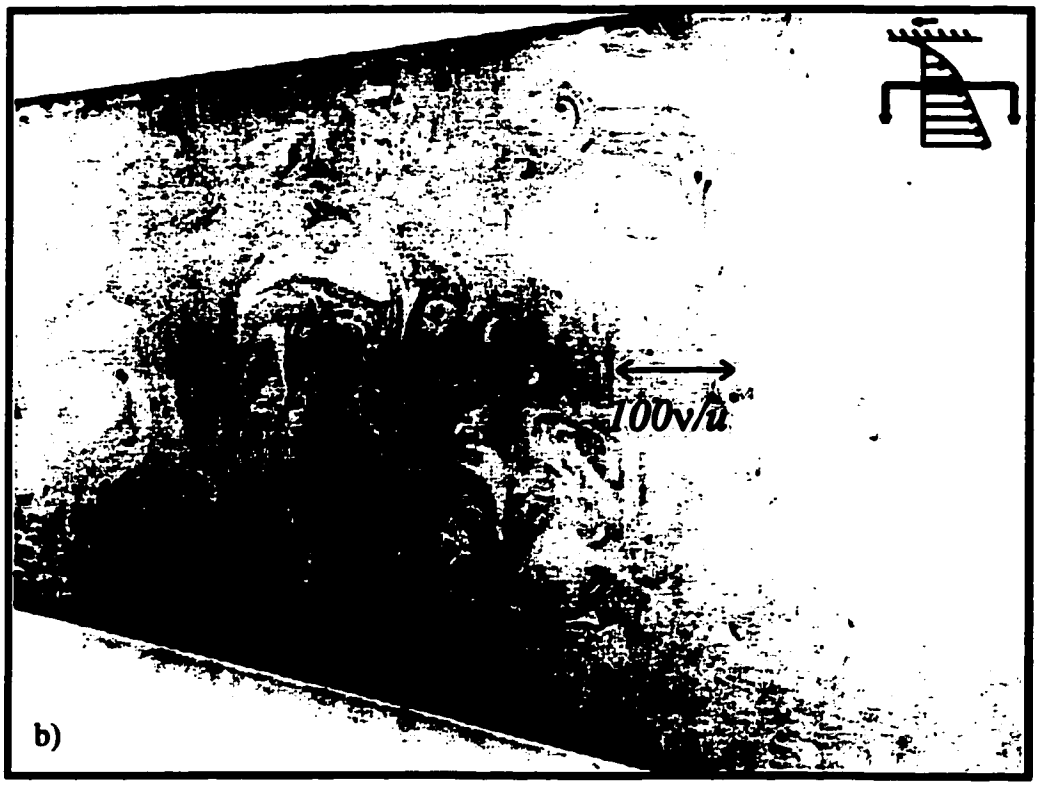

Frame sequence 6.21 - USF low speed case, moving wall opposite flow velocity (MWN), flow viewed from the below; a) *y=1mm*, b) *y=8mm*, c) *y=18mm*, d) *y=38mm*, e) *y=68mm* (tape 3, 28:21)

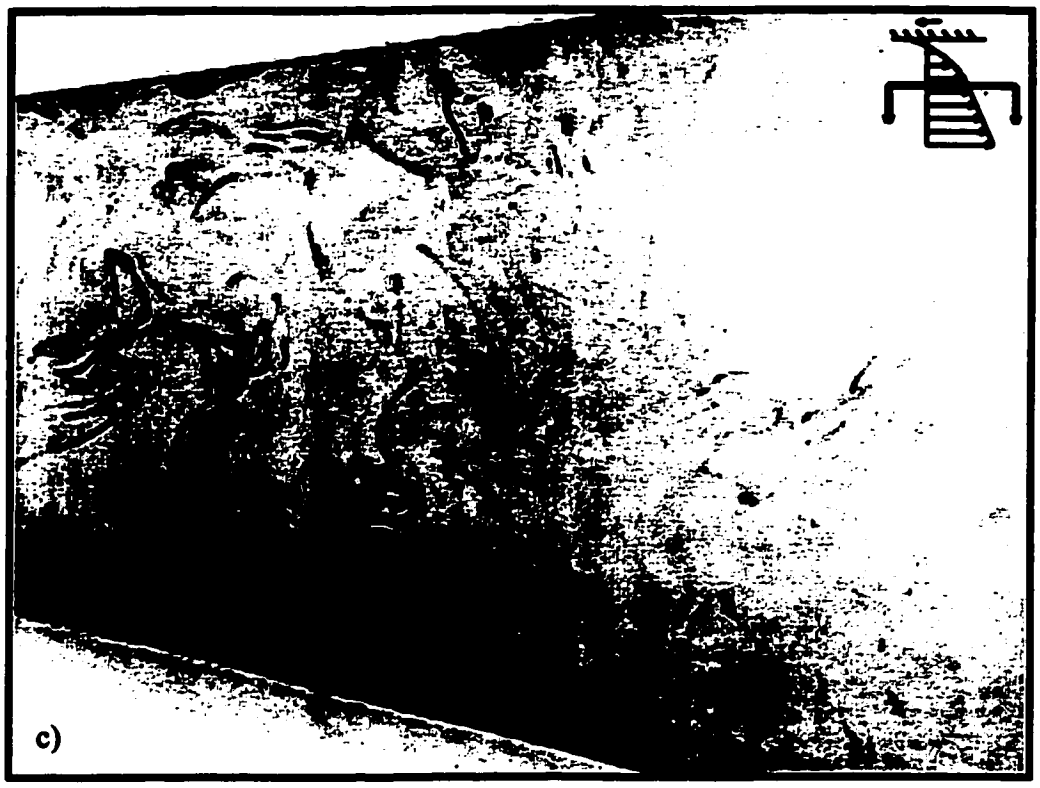

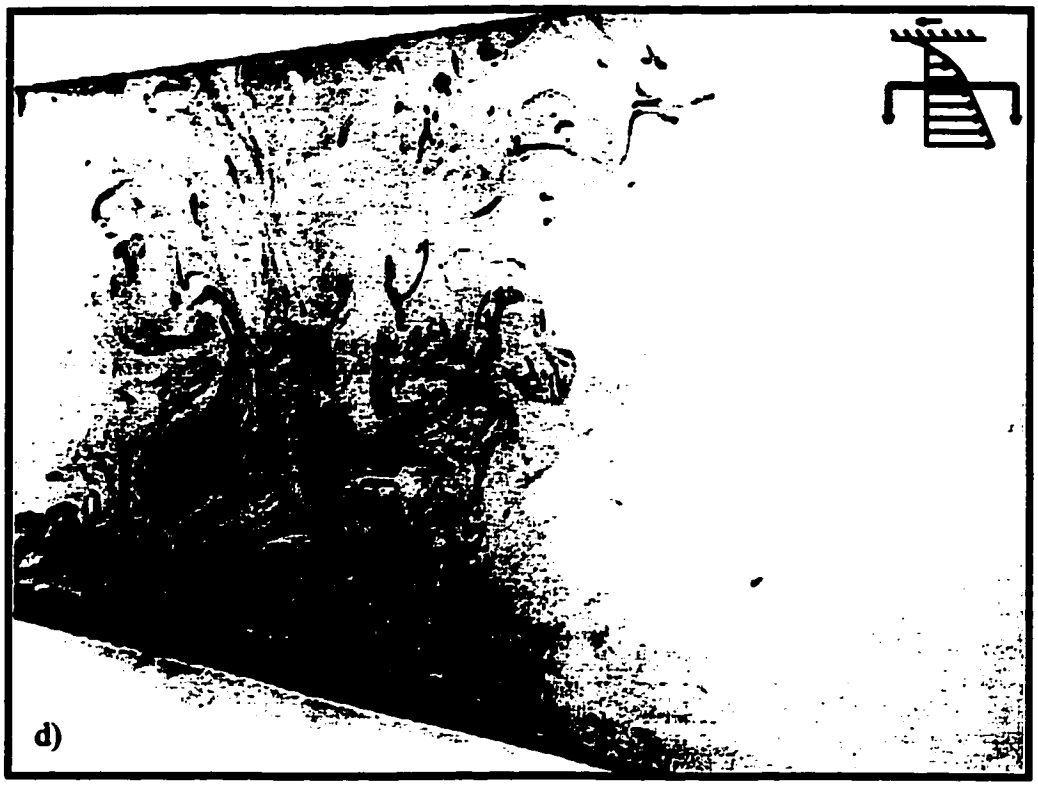

Frame sequence 6.21 (continued)

Frame sequence 6.21 (continued).

Frame sequence 6.22 - USF low speed case, moving wall opposite flow velocity (MWN), wall and core flow viewed from the rear. (Tape 3, 23:55)

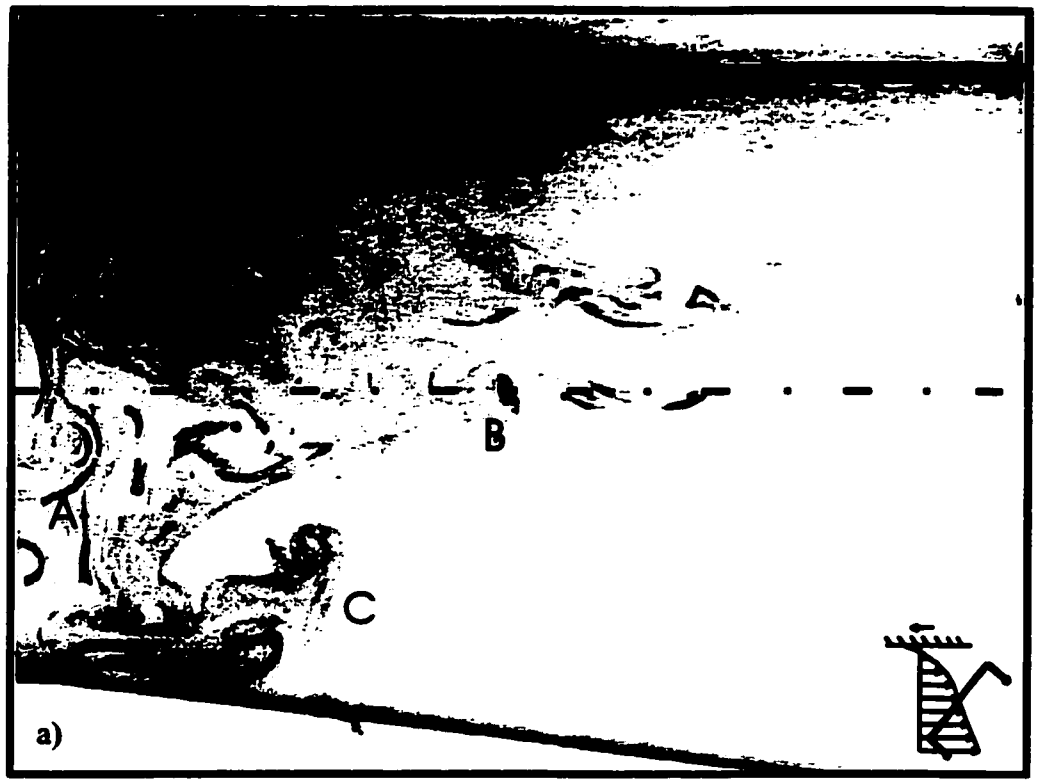

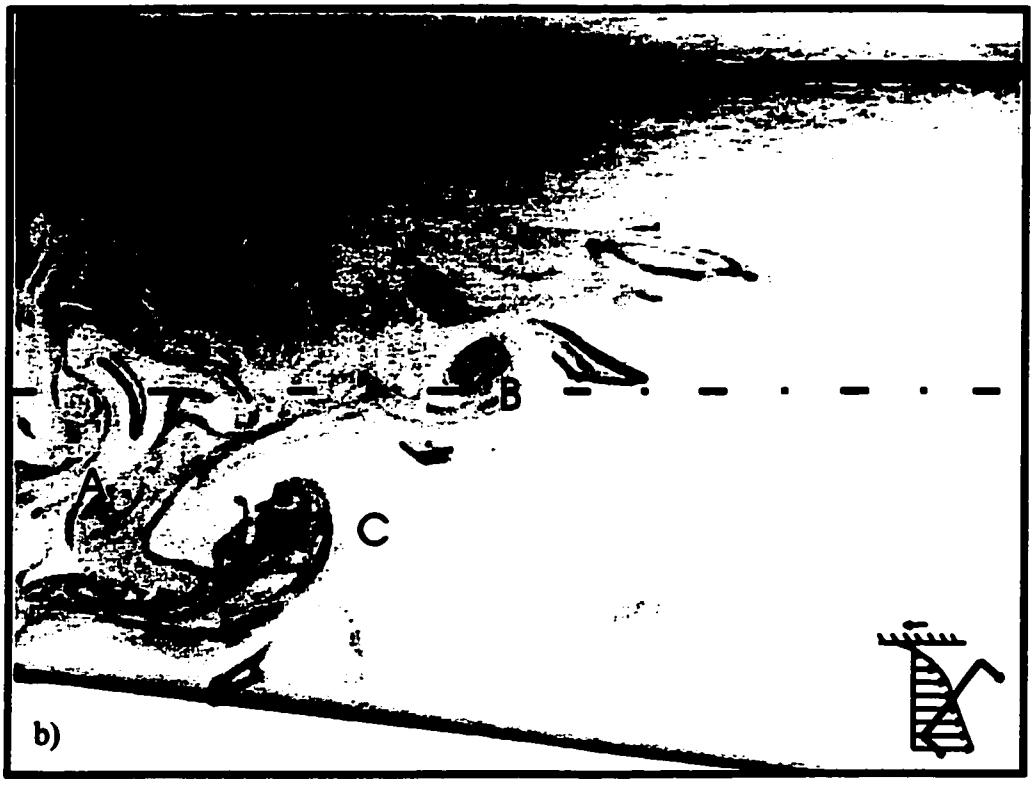

Frame sequence 6.23 - USF low speed case, moving wall opposite flow velocity (MWN), flow viewed from below with laser sheet at an angle; a) t=0s, b) t=0.20s, c) t=0.40s, d) t=0.60s (tape 3, 30:35)

Frame sequence 6.23 (continued).

Frame sequence 6.24 - USF low speed case, moving wall faster than local velocity (MWP), flow viewed from the side; a) t=0s, b) t=1.6s, c) t=3.7s, d) t=7.1s, e) t=9.3s, f) t=11.1s (tape 3, 04:46)

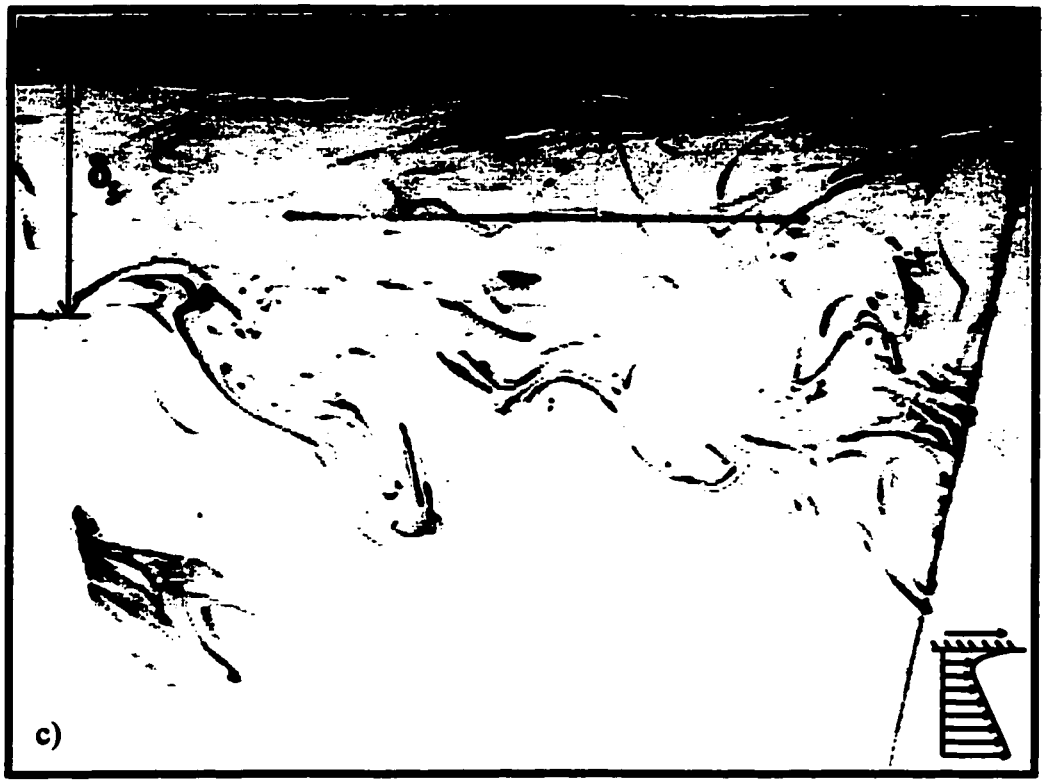

Frame sequence 6.24 (continued)

Frame sequence 6.24 (continued).

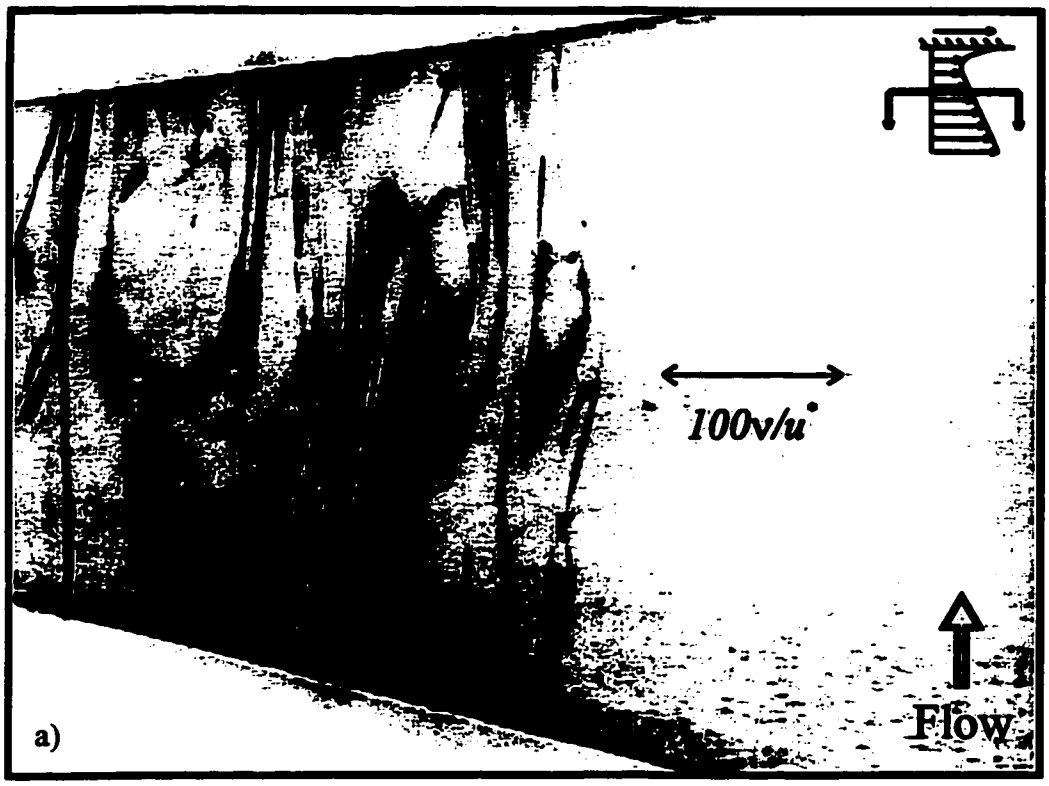

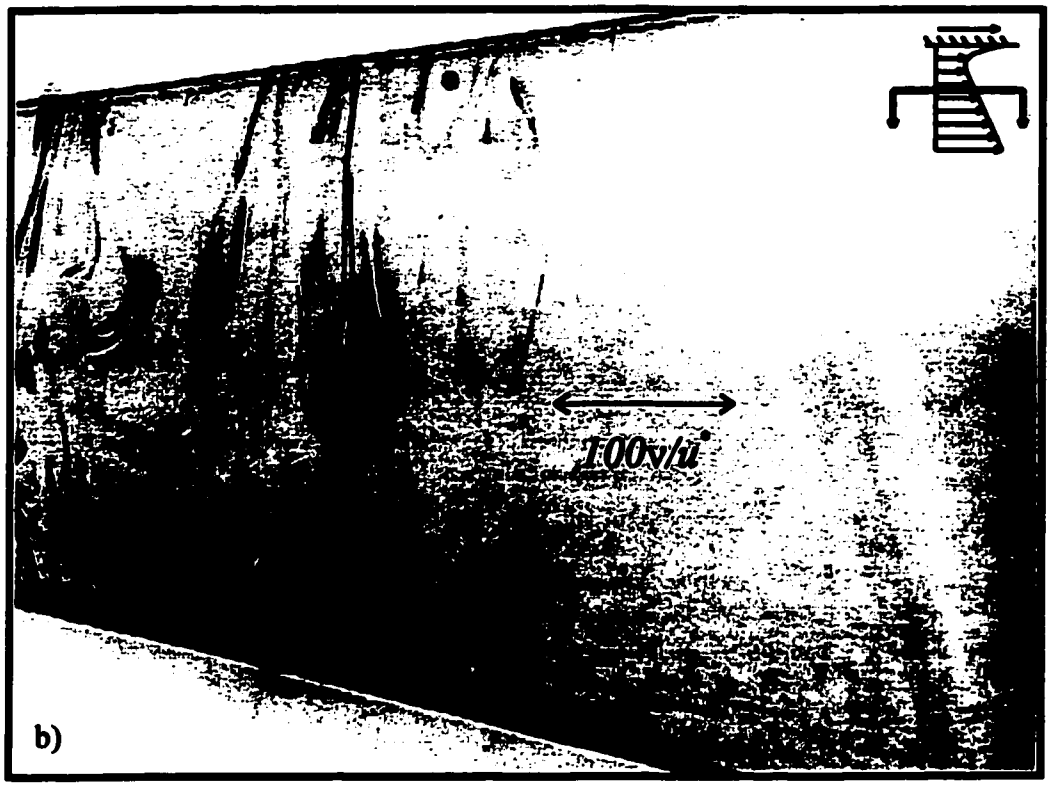

Frame sequence 6.25 - USF low speed case, moving wall faster than local velocity (MWP), flow viewed from below; a) y=1mm, b) y=3mm, c) y=8mm, d) y=38mm, e) y=48mm, f) y=68mm. (Tape 3, 26:10)

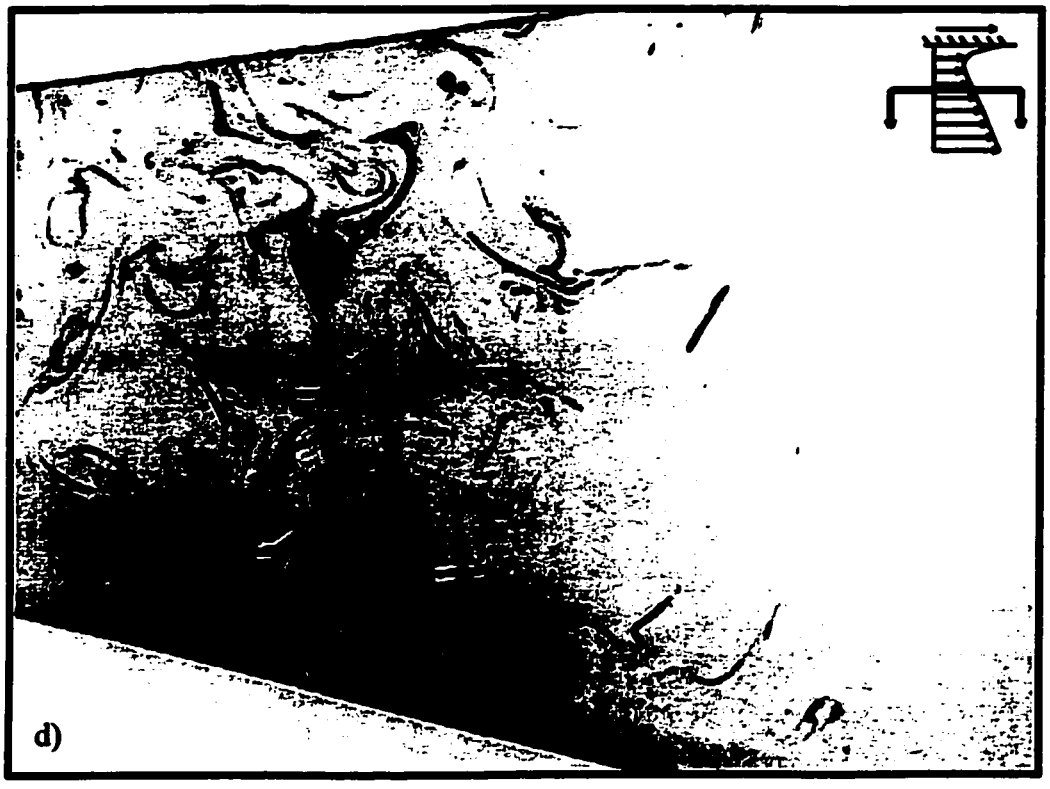

Frame sequence 6.25 (continued)

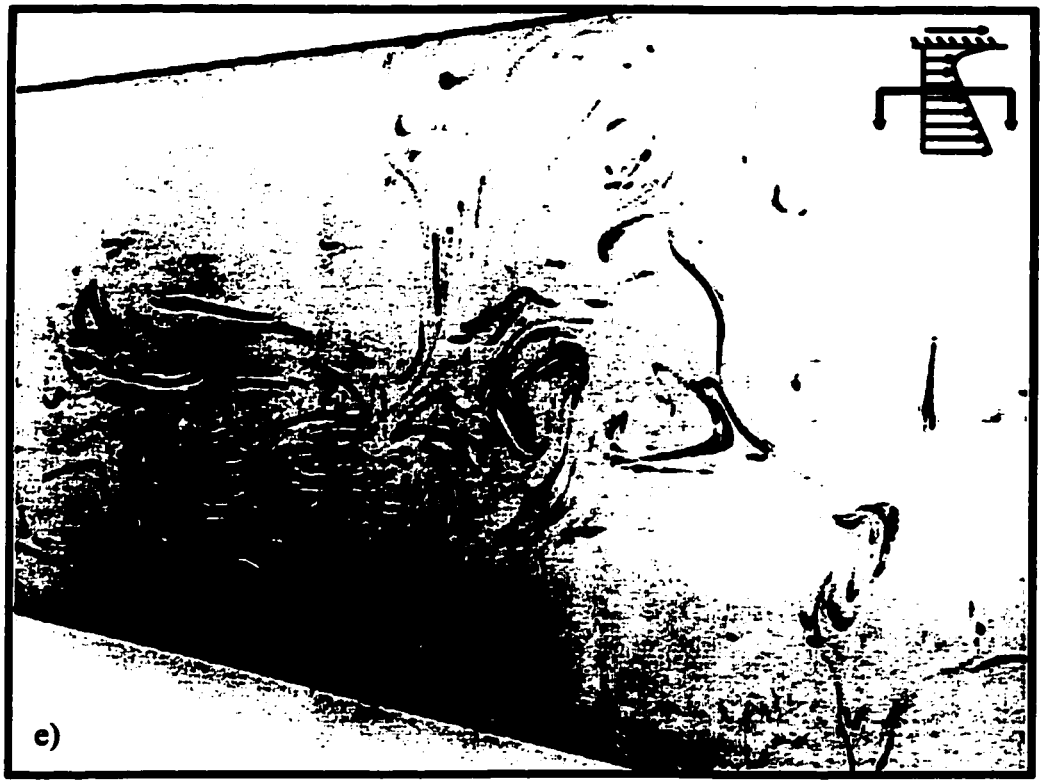

Frame sequence 6.25 (continued).

Frame sequence 6.26 - USF low speed case, moving wall faster than local velocity (MWP), wall and core flow viewed from the rear. (Tape 3, 23:55)

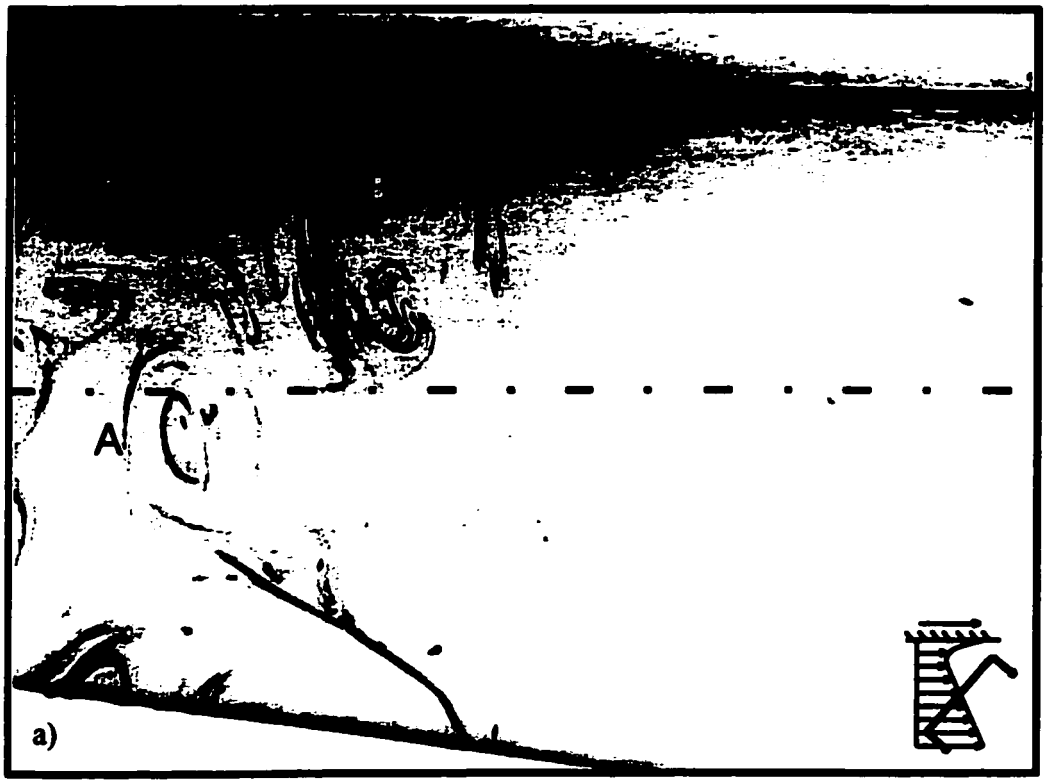

Frame sequence 6.27 - USF low speed case, moving wall faster than local velocity (MWP), flow viewed from below with laser sheet at an angle; a) t=0s, b) t=0.40s, c) t=0.80s, d) t=1.2s (tape 3, 31:47)

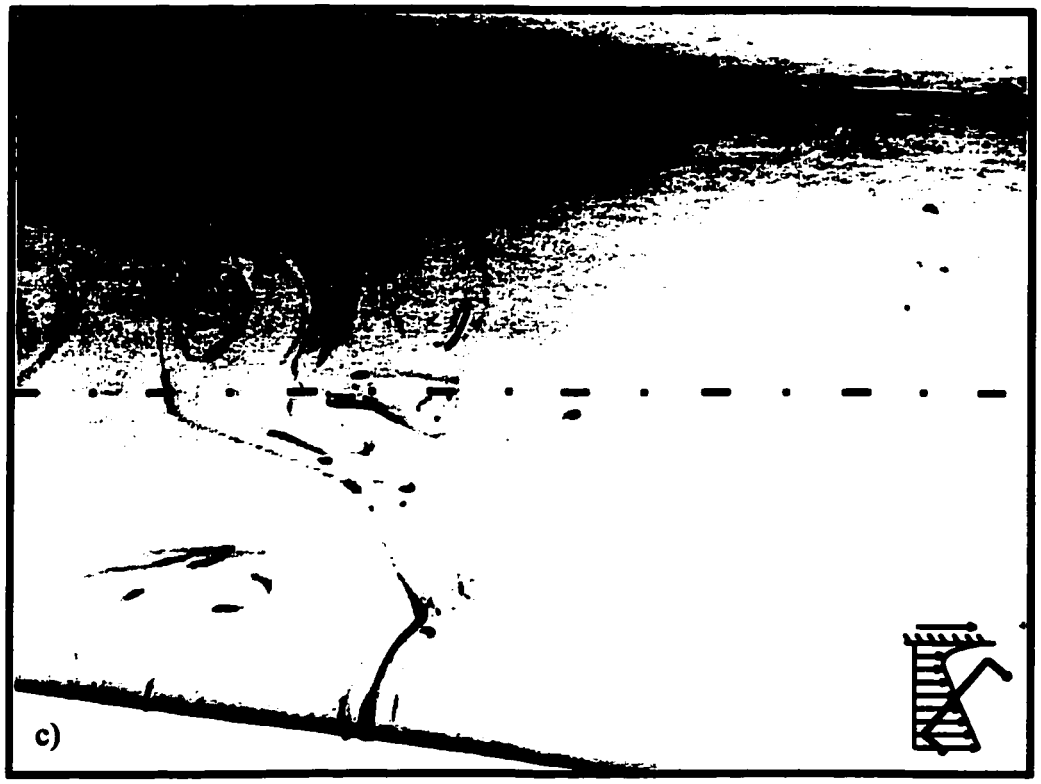

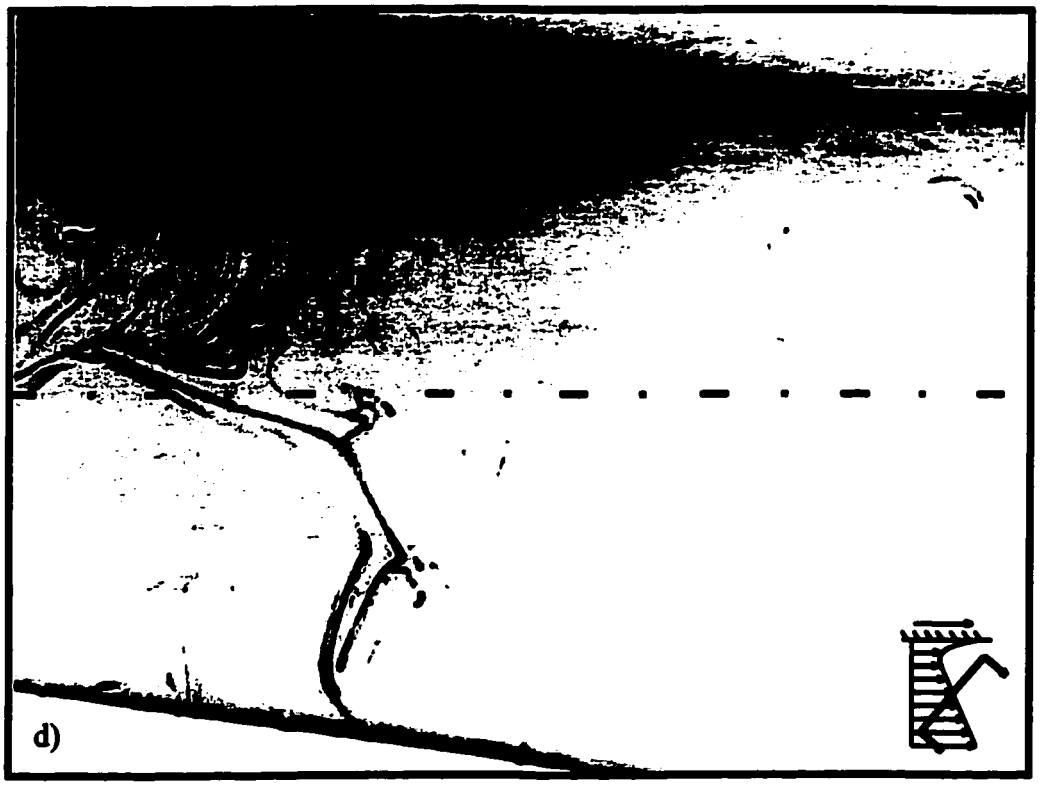

Frame sequence 6.27 (continued).

Appendix A

Water Tunnel Testing Facility

The water tunnel facility has been designed to provide a high quality flow for both visual and quantitative studies for a wide variety of possible experiments. It has been designed in large part by the author. The construction and assembly was completed primarily by the technical staff in the Mechanical Engineering machine shop at the University of Ottawa, with the fabrication of the larger stainless steel components contracted out to Alexander Metal Products Inc. of Ottawa.

The facility is a closed loop system recirculating a fixed mass of water, which can be varied to provide different water levels in the test section. The facility requires about 15 minutes for the flow to stabilize after start-up or change in speed, and can run for a full day, or presumably longer, without any variation in the flow rate. The flow rate was found to be reproducible from day to day. The water is kept clean using a filtration and chlorination system, and remains very clear for visual studies yet provides enough natural seeding for Laser-Doppler Velocimetry measurements. A small quantity of additional seeding particles,

mostly silicon carbide, have been used to provide higher data rates for LDV while still leaving the flow very clear. The facility is kept full of water, and is only emptied if work is to be performed on the tunnel, or if the water needs to be changed due to excessive concentration of dye. Vibration from the pump is minimal and does not disturb the flow, but sudden shocks to the facility do temporarily distort the flow (witnessed using a dye streak) and create waves if a free surface is being used. Surrounding noise in the laboratory is minimal and does not affect the flow. The temperature of the water follows that of the room, and should be allowed to stabilize when fresh water is added. Slight heating of the water during operation is unavoidable, with an increase of 1 K over 4 hours in most situations.

The features that make this a high quality facility include the following: a large contraction ratio and flow conditioning screens which provide low turbulence levels and a uniform velocity profile across the test section entrance; a relatively large test section, 0.54 m wide, 0.75 m high and 4.0 m long, which permits the insertion of reasonably large models and allows good development of the flow ; viewing accessibility on all sides of the test section, including from the rear, thus allowing visual and optical studies along nearly any plane; a variable top-surface for the test section permits many types of studies including a free surface channel or an enclosed tunnel, with the possibility of using differently shaped walls, including a moving wall; three sets of two-dimensional traversing systems, top and side, with the side traverse motorized in the vertical direction and the third traversing system under the test section that was added to the system after this research was completed; these traversing systems allowed ease of use of instrumentation and tracking of the flow in

a convected frame, as well as possible use of the tunnel as a towing tank.

The design of the water tunnel is largely based on features found in many other water testing facilities reviewed by Erickson et al (1986). The general layout of the water tunnel is similar to a commercially available water tunnel for visual studies (Eidetics, no date), but contains several significant improvements, including a larger contraction ratio, a longer test section and a removable top surface. A boundary layer removal system, similar to the one used by Humphries (1995), was also included to this facility to curtail flow distortion by boundary layer growth in the downstream half of the test section. The design of the moving wall equipment is similar to those of Uzkan & Reynolds (1967) and Thomas & Hancock (1977) with the additional benefit of a smooth transition of the flow to the wall by using the free surface. The use of screens and honeycombs for flow conditioning has been studied extensively, for example, by Groth & Johansson (1988) and Farell & Youssef (1996), and two screens and several layers of porous foam are successfully used in this facility. Screens used to generate shear have been discussed by Karnik & Tavoularis (1987) and a slight adaptation has been used to create the perforated plate shear generator. Designing a contraction is done as much by trial and error as it is by design, but helpful references can be found in Whitehead, Wu & Waters (1951) and the actual design follows recommendations by Mikhail & Rainbird (1978). Further details on the different components that make up the water tunnel facility follow below.

A.1 Pump

The circulation of the water is provided by a Cascade, 305 mm in diameter, axial flow pump located directly under the settling chamber. Water flows horizontally into the 254 mm in diameter suction inlet and the 254 mm in diameter discharge issues vertically into the settling chamber. The flow is driven by an impeller whose shaft exits at the 90°elbow and is coupled to the shaft of the 5.6 kW (7.5 hp) GE motor. The pump is rated at a maximum head of 2.13 m at 126 rad/s (1200 rpm). The motor is driven by a Siemens Relcon Q2000 controller. The flow rate can be adjusted, by adjusting the motor speed, from 0.003 to 0.1875 m^3/s. This corresponds to velocities in the test section up to roughly 0.3 m/s for nearly full tunnel, or higher for a partially filled test section. The pump is constructed of cast iron with a stainless steel shaft and bronze impeller. The inside and outside have been coated with a protective enamel to prevent corrosion. The entire pump is mounted on a single frame which is bolted to the floor, with rubber dampeners to minimize vibrations.

A.2 Settling Chamber

The settling chamber consists of three sections with total dimensions 1.52 m high by 2.44 m wide by 2.13 m long, leading to the contraction. It is constructed of 3.2 mm thick stainless steel sheet rolled and welded to shape. The first section is semi-parabolic and receives the water from a perforated PVC cylinder with a diameter of 254 mm, aligned with a hole on the tunnel floor. The water exits the cylinder in all directions horizontally. The cylinder is capped by an adjustable plunger to control the pressure of the water and

is wrapped with mesh screens to obtain a smoother discharge of the water out the holes. The open end of this section mates with the next two identical rectangular sections of the settling chamber, which lead to the large end of the contraction. The top of the settling chamber is open, allowing the water to have a free surface, and is braced by structural steel bars to keep the walls square. The sections of the settling chamber are connected together using several standard 75 mm clamps, with a clamp located every 150 mm on the sides and every 75 mm underneath. The settling chamber is raised 0.61 m above the ground to allow room for the pump and piping underneath. Its top is covered by a plastic cover sheet to prevent dirt and debris from contaminating the water. Between each pair of sections there is a slot for insertion of a screen or honeycomb. Two flow-conditioning screens have been installed. They have solidities of 0.42 and 0.40 and characteristic opening sizes of 4.8 mm diameter and 1.6 mm square, respectively. Several sheets of foam have also been installed with undetermined solidity.

A.3 Contraction

The contraction accelerates the flow from the settling chamber to the test section, reducing flow non-uniformity and turbulence. The contraction used follows the design method described by Mikhail and Rainbird (1978). It is constructed of 3.2 mm stainless thick steel and reduces an area of 1.52 m by 2.44 m to an area of 0.54 m by 0.75 m over a 1.52 m length. A straight section with a length of 0.305 m is included upstream of the contraction to allow decay of the turbulence produced by the last screen before the flow enters the contraction. It is symmetrical horizontally, with a contraction ratio of 4.5:1, but

not vertically, where the bottom half raises 2:1 and the top is simply the free surface of the water. Stainless steel was used instead of aluminum for higher strength and corrosion resistance. For any metal component that can come in contact with the water, stainless steel was preferentially used to prevent the formation of electric potential differences caused by dissimilar metals.

A.4 Test Section

The water leaves the contraction and enters the test section that is 540 mm wide by 750 mm high and 4.0 m long. It is composed of three steel frames, padded with rubber, that hold the 9 mm tempered glass side walls and bottom in place. The three sections provide large viewing areas of 1.07 m, 1.80 m and 1.07 m downstream of the contraction. Flow adjusting devices such as a grid or shear generator can be inserted in the first section and held in place using a slot provided between the contraction and the first section. The glass walls and bottom are formed by three separate pieces, one for each section, and are joined together with boundary layer bleeding slots installed between the individual frames, that is, 1.07 m and 2.93 m downstream of the contraction. The bleeding slots are 0.8 mm wide, machined into plexiglass and connected by tubing and valves to the auxiliary pump. These can be regulated to control the amount of water drawn away from the walls, thus reducing the size of the boundary layer. The glass and plexiglass sections are sealed with silicon caulking and rubber gaskets throughout the test section. The top of the test section can either be left open as a free surface or covered with five plexiglass sections forming a top wall. The plexiglass top can be positioned at any height it the test section. The top can

also be replaced in the middle viewing section by a moving wall assembly described later. The test section is equipped with traversing rail systems on top and on one side, to allow for mounting and traversing instrumentation. The top rails can also be used with a carriage system turning the water tunnel into a towing tank, and the beams that support the rails are used to support other equipment, such as a fully adjustable model sting mount. The walls of the test section are square along the entire length of the test section, in alignment with the two traversing rails. The test section is raised 1.37 m off the ground to allow for underside viewing. A walkway and ladder are mounted alongside the test section to allow easy access from the top of the tunnel.

A.5 Shear Generator and Flow Separator

A shear generator is used to achieve a uniformly sheared velocity distribution in the flow with high levels of turbulence. This is accomplished using a 3.175 mm thick aluminum plate perforated with holes and slots in a pattern that creates a linearly increasing solidity over the vertical height. This is done over 16 levels spaced 26.6 mm apart with solidity decreasing by 5% at each level, from 75 % to 0%, with the two top levels both being at 0%. The shear generator is inserted in the slot just after the contraction at the beginning of the test section. The flow will then pass through a flow separator, which is an array of 16 flat plates of glass, with a thickness of 1.6 mm, evenly spaced 26.6 mm apart. The glass sheets are held on the sides by two plates of PVC machined with appropriate grooves for the sheets of glass. This device prevents the different regions of different velocities to mix immediately after the shear generator and makes turbulence scales more uniform. A series

of 4.8 mm stainless steel rods can be added at the end of the flow separator, one rod in the centre of each channel, to further increase turbulence levels in the flow, with a side effect of reducing the shear in the flow. At the end of the flow separator, a uniformly sheared flow is achieved with turbulence characteristics which are similar over the entire height.

A.6 Water Recovery Tank

The water leaving the test section enters the 1 m long, 1.2 m wide by 0.75 m high water recovery tank and is collected by two 203 mm diameter perforated PVC cylinders, each located on either side of the tank. The cylinders lead to holes in the bottom of the tank which connect to a single pipe that returns the water to the main pump. Screens in the cylinders prevent any large objects from entering the piping and possibly damaging the pump. A plunger is installed in the cylinders to control the water level and prevent the formation of sink vortices that could draw air into the piping. The tank has a rear window to allow viewing of the test section from the downstream position. The possible reflection of waves at the back wall, which could affect the flow in the test section, has been found to be negligible. This tank is made of 3.2 mm stainless steel rolled to shape and connects to the test section with a plexiglass adapter that includes a slot for insertion of a screen or plate.

A.7 Piping and Valves

The water recovery tank is connected to the pump through a 203 mm diameter PVC pipe which is increased to 254 mm before it enters the main pump. The piping runs

along the centre of the tunnel. A drain and air release valve have been installed to allow for complete draining and to remove any air that may accumulate in the pipes. A second piping system connects the settling chamber to the water recovery tank. This is made of 76 mm PVC pipe isolated with valves, and leads to a 25.4 mm flexible piping system connected to a small centrifugal pump, driven by a 124 W (1/6 hp) motor. This system is used for the water filtration and chlorination systems as well as the boundary layer bleeding, and can be easily expanded for use with other systems. An additional loop is installed for possible degassing of the water using a venturi tube.

A.8 Moving Wall Apparatus

The top of the 1.8 m main viewing section of the test section can be replaced by a moving wall apparatus. This comprises a rubber belt, 530 mm wide, turning on three 152 mm diameter PVC drums. Two drums are mounted 1.8 m apart on aluminum shafts, using sealed 6304-2RSR stainless steel bearings, between two 3 mm aluminum side walls that can be lowered to various heights in the test section. The third drum is driven by a 93 W (1/8 hp) DC motor, controlled so that the speed of the belt can be varied in the forward or reverse directions. It is mounted on a carriage so that tension can be adjusted along the rails so that the belt runs true, and is cross-knurled so that slippage of the belt is minimized. Felt padding is installed near the drums to wipe any water droplets off the belt. A UHMW polyethylene sheet serves as a backplate for the belt, ensuring that the belt runs level.

A.9 Water Filtration System

A water filtration and chlorination system is used to maintain a clean water supply for viewing and to control particle size in the water. This is done using a cartridge type water filter and a chlorinator in the secondary flow loop, driven by the auxiliary pump. Test strips are used to determine pH levels, chlorine levels and alkalinity. Chlorine pucks or algaecide are added as needed. Filtration is first conducted using a 30 μm reusable filter to remove large particles when first filling the tunnel. Particle size can then be controlled by using a 15, 5 or 1 μm filter. A vacuum hose and soft brush are used with the filtration system to clean any dirt that may deposit on the bottom of the tank and to clean the walls of the test section. All these measures provide sufficient control of particle size for proper LDV measurements, but seeding of particles in the flow can also be achieved. The larger opening filters should be used when larger particle sizes are desired in the flow for flow visualization or PIV measurements.

A.10 Water Tunnel Initial Testing and Calibration

A.10.1 Visual Testing

The water tunnel was first tested using visual inspection with dyes injected through small tubes, tufts of cotton on rods, and hydrogen bubbles. These tests were first implemented to determine if regular operation of the tunnel provided a low-turbulence, uniform velocity profile in the test section. Initially, problems were observed due to strong recirculation of the flow near the flow outlet pipe in the settling chamber. This caused vertical

vortices to form in the settling chamber, which tilted with the flow as it passed through the contraction creating twin vortices down the test section. These were especially observed at high flow rates when air bubbles in the flow were observed to form together down the center of these vortices. A possible correction to this problem would have been to insert a large honeycomb device, but a simpler and probably more effective solution was to greatly increase the solidity of the screen immediately after the flow outlet from the pump. This created what would be a first settling chamber with a large enough pressure drop to evenly distribute the flow passed through the first screen to a rather uniform velocity profile. After passing the later screens and finally the contraction, the flow was tested to be uniform and vortex free in the test section.

Hydrogen bubble experiments were later performed in the test section to view the development of the flow in the core region and near the boundaries. Results obtained indicated that a low turbulence, uniform flow was being generated in the test section, with boundary layers growing on the three walls.

A.10.2 Shear Generator

When the shear generator was first tested in the water tunnel, a first problem was quickly observed in the form of waves on the free surface. This was due to the water level of the flow being very close to the top holes and the jet action from the large holes at the top of the shear generator. Adjusting the water level to match a solid section of the shear generator solved this problem but the free surface was always observed behind the shear generator to ensure a smooth flow hereafter.

The use of a perforated plate with linearly varying solidity was very good in pro-

ducing a uniformly sheared flow, but some fine adjustments of the shear generator were necessary to get the flow to be as close to uniform as possible over most of the height of the flow. This was accomplished by adding strands of fishing line over different rows of the generator to increase the pressure drop for each height. Adjusting one row however would impact all the other rows because flow that was reduced at one height would increase the flow at other height, so several iterations were required to get an acceptable flow.

A.10.3 Flow Separator

Further studies indicated that repeatability of results was not exact and that the original flow separator, which was removed and installed each day to prevent corrosion along the welds of the stainless steel sheets, did not have all channels with equal and uniform height. The first flow separator was manufactured of stainless steel sheets spot welded together with small tabs. Only one tab was inserted between each sheet, offset between the front and the back on alternate levels, to minimize the flow disturbance. Problems arose however due to the lack of strength in the tabs and the inaccurate production of spot-welded components. The channels of the flow separator ended up being of varying height over the width of each channel, and between different channels. This caused problems in the variation of the velocity in each channel. A new flow separator was implemented using thin sheets of glass with enough stiffness to avoid bending across the span of the tunnel. This provided very even channel heights with little disturbance to the flow, was lighter in weight making it easier to install, and could be kept in the tunnel indefinitely without corrosion problems. Recalibration of the shear generator was then necessary and only two small wires across two different rows were finally needed. Tests were thereafter reliably repeatable.

A.10.4 Moving Wall Apparatus

The use of a moving wall apparatus required proper consideration to be applied correctly for this research. The sudden insertion of a moving wall into a flow has been an issue of concern for researchers attempting this type of experiment, mainly due to the desire to remove an existing boundary layer before the moving wall is approached, contrasted with the desire not to have the moving wall inserted into a flow so as to reduce the channel cross-section and increase the flow velocity. By using the free surface of the water tunnel, this was not necessarily easier, but did seem to cause little disturbance to the flow, providing a smooth transition to a moving wall boundary. To enhance turbulence levels in the boundary layer along the moving wall, tripping of the boundary layer was performed near the front of the moving wall using a thick gauge strand of fishing wire.

Definition of a boundary layer in USF does not truly exist and no study for comparison was available. Matching wall and flow speed exactly was very difficult because of the multiple effects that the wall motion has on the flow. As the wall speed changes, the velocity defect near the wall changes, which causes velocity changes along the entire height of the flow. To match the wall speed exactly to that of the USF flow at the wall would require that the shear generator be slightly modified for each wall speed, and thus the USF would be different for each study. Because the purpose of this research was to study the different effects of the moving wall on coherent structures and the production of turbulence in sheared flows, it was deemed more important to keep the same initial shear generator configuration, and only change wall speed, whether or not a smooth USF velocity profile was achievable throughout the channel height and all the way to the wall.

The physical effects of the moving wall must also be considered during operation. Insertion of the apparatus caused a minor displacement of the water level, which had to be adjusted appropriately. The motor speed must be kept constant and no slipping of the belt on the drive drum can be allowed. Sagging in the belt must be kept to a minimum by applying tension and having a solid back wall for the belt to run against. Spanwise curvature of the belt must also be kept at a minimum. Vibration from the motor and pump were sufficiently dampened to prevent vibrations in the belt or variation in the belt tension or speed.

During tests of the high speed case, it was noted that the tension in the belt varied at specific intervals, which in turn caused sagging in the belt as well as changes in motor speed. The belt is formed of a single piece of material with a joining seam. When the seam was close to one of the drums, the belt tension would be high, whereas when the seam reached the center of the bottom span, the belt tension would decrease causing extra sagging in the belt. With the lower speed case, greater tension could be applied to the belt without creating excessive torque on the motor. The higher tension in the belt also aided in minimizing spanwise curvature. The achieved curvature had a negligible effect on the flow, but limited the access of the laser sheet and beams for visualization and LDV measurements. These could be compensated for by slightly adjusting the laser head, but had to be accounted for in the study.

For the low speed case, with the tension in the belt very high, the motor and controller were capable of maintaining a constant speed even with minor variations in the tension of the belt. The sag in the belt was at its maximum about 3 mm at the midpoint of

a span of 1.5 m. The radius of curvature this created is vastly greater than the boundary layer thickness and should have little effect on the flow. The belt speed was measured by timing a known displacement of a reference point on the belt. This was performed 5 times for every LDV run to ensure that the belt speed remained constant throughout the experiment.

Another problem that was noticed in earlier trials was the entrainment of air bubbles. This was most noticeable in reverse operation in which case bubbles were entrained from the back end of the belt toward the front. This limited the maximum reverse speed. This problem occurred in forward operation of the belt as well, but only at much higher speeds.

Appendix B

Measurements of Energy Spectra and Integral Lengthscales

Measurements of energy spectra are presented here (Figure B.1) only for the core USF case, in which the data rates obtained were relatively high, as well as one could estimate the dissipation rate from the downstream growth of turbulent kinetic energy. The available software was able to process the LDV data directly to obtain the frequency spectra of the flow. From the one-dimensional frequency spectra, the one-dimensional wave number spectra was obtained based on Taylor's "frozen flow" approximation, which should be valid, if one considers the relatively low turbulence intensity in the present USF. Raw plots of the spectra showed considerable scatter, indicating that the data records were not sufficiently long. The plots shown here have been smoothed using moving-average-type filtering. Normalization by Kolmogorov scales was performed and the value of the dissipation rate was adjusted slightly to make the inertial ranges as closely aligned as possible for the four cases

chosen. From Figure B.1, it can be seen that the turbulent kinetic energy, represented by the area under the curves, increased with downstream distance, consistently with the previous measurements. A line representing Kolmogorov's -5/3 law has also been drawn in the same figure. Comparison of the measurements with this line indicate the formation of a very narrow, if any at all, inertial range, in conformity with wind-tunnel USF results at comparable R_λ (Ferchichi & Tavoularis, 2000).

Another subject of interest to this flow is the integral lengthscales, which represent the average size of the energy containing eddies. In Figure B.2, integral lengthscales are presented along the centreline of the core USF and are shown to increase exponentially in the downstream direction. Estimates based on the empirical expression $L_{11} = 0.24q^3/\varepsilon$ as well as estimates based on the low-frequency intercept of the ordinate in the spectral plots have been presented and are in reasonable agreement.

The ability of the present LDV system to provide energy spectra data and integral lengthscales has been shown, however the accuracy of these needs improvement for the data to be reliable. The use of a higher resolution, 16-bit LDV system will hopefully allow for higher precision. Longer run times and higher data rates would also be required. Such measurements should be considered as future extensions of this research.

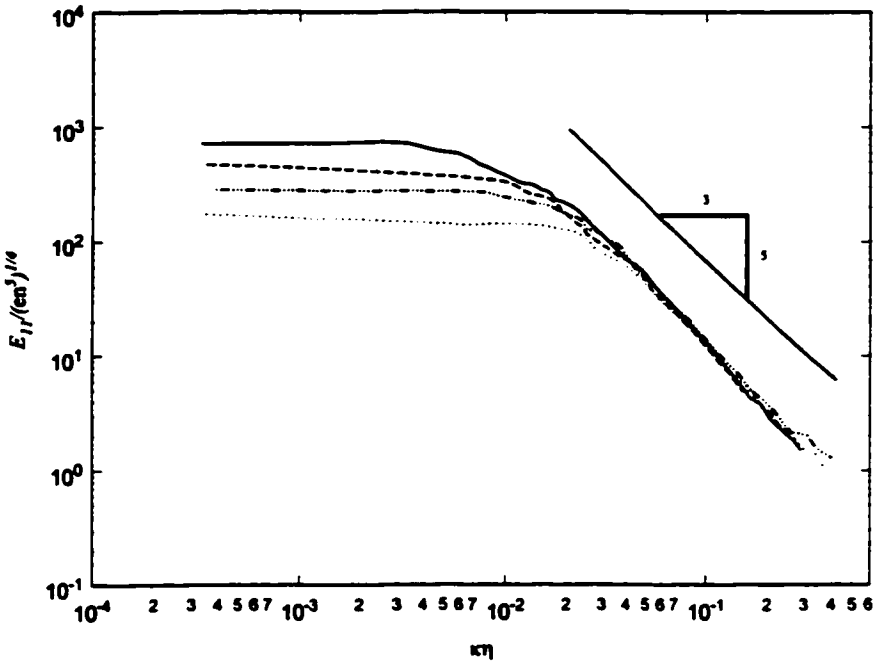

Figure B.1 USF - Wave number energy spectrum along centreline of tunnel for high speed case; starting from bottom line $\tau = 3.6$, 6.0, 8.0 and 9.8.

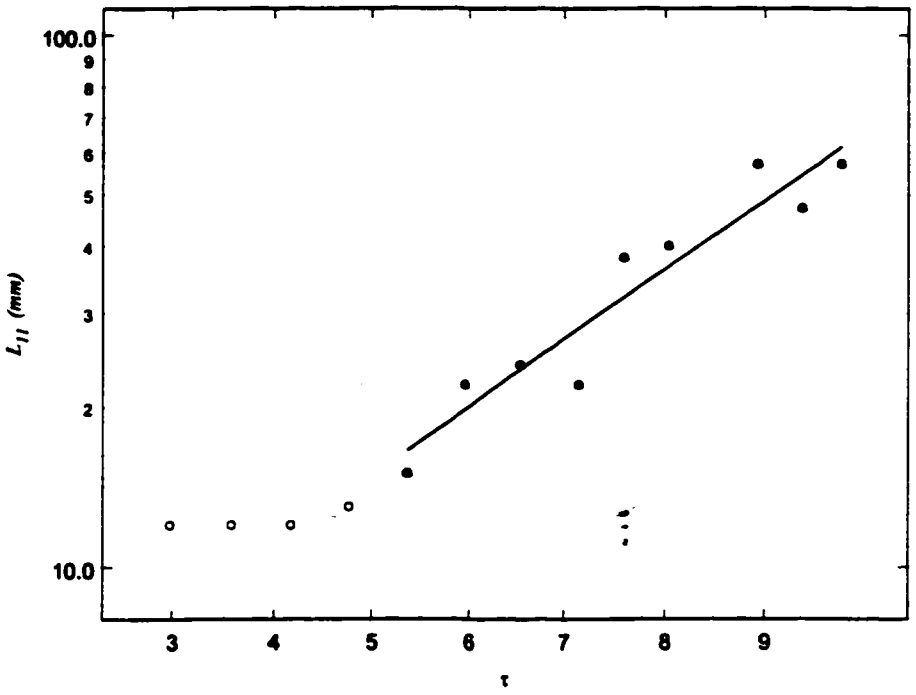

Figure B.2 USF - Integral lengthscale along centreline of tunnel for high speed case.